UNIVERSITÀ
DEGLI STUDI
DI PADOVA

Host Istitution: Università degli Studi di Padova

Dipartimento di Geoscienze

DOCTORAL COURSE IN EARTH SCIENCES
SERIES XXIX

TIDAL CHANNEL PATTERNS: FIELD INVESTIGATIONS, NUMERICAL MODELLING AND LABORATORY EXPERIMENTS

This PhD Thesis has been founded by SHELL International Exploration and Production project titled ”Tidal vs. tidally-influenced fluvial point bars: facies distribution and implications for reservoirs production development”

Coordinator: Prof. Fabrizio Nestola
Supervisor: Prof. Andrea D’Alpaos
Co-Supervisor: Prof. Massimiliano Ghinassi
Prof. Luca Carniello

PhD candidate : Alvise Finotello

Università degli Studi di Padova
Department of Geosciences

Ph.D. School in Earth Sciences

Tidal Channel Patterns: Field Observations, Numerical Modelling and Laboratory Experiments

Ph.D. Candidate:
Alvise Finotello
Matricola 1084751

Thesis advisor:
Prof. Andrea D'Alpaos

Thesis co-advisors:
Prof. Massimiliano Ghinassi
Prof. Luca Carniello

November 2016

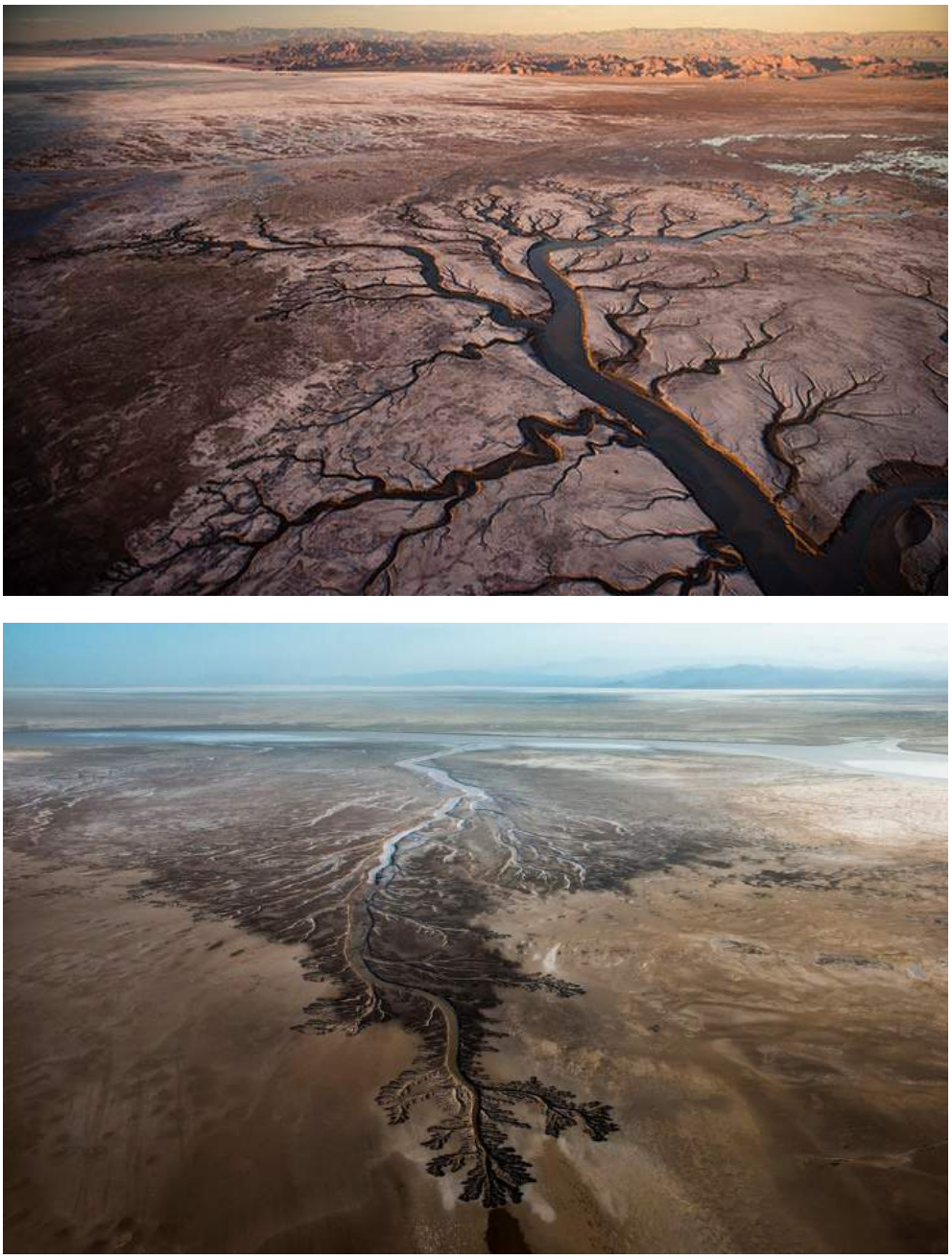

Tidal Channels in Gulf of California (MEX) *(Photo Credits: nature.org)*

The very thing about tide
is that,
eventually,
it changes.

Dedicated to my wife.

CONTENTS

LIST OF FIGURES

LIST OF TABLES

ABSTRACT

Tidal meandering channels are ubiquitous features of tidal landscapes and play a fundamental role on the eco-morphodynamic evolution of these environments. However, only a handful of papers provide details on tidal meander planimetric shape, morphometric characteristics and morphodynamic evolution, and the internal achitecture of tidal meanders has not been explored in detail. Moreover, the morphodynamic evolution of tidal meanders and the related sedimentary products have often been interpreted on the basis of the well developed models and theories existing for their fluvial counterparts, despite a number of differences were *a priori* identifiable. Toward the goal of improving current understanding of the morphodynamic evolution of tidal meanders, five main issues have been investigated in the present work: i) rates of migration and evolutionary dynamics of tidal meanders; ii) assessment and quantification of differences and analogies existing between the planform features of tidal and fluvial meanders; iii) variations of tidal meander hydrodynamics in response to different tidal phases, and the role that these variations exert on tidal meander sedimentary products; iv) role played by bidirectional flows, tidal asymmetries and lateral tributaries; v) assessment of influence of tide amplitude, basin slope and initial shoreline configuration on tidal channel network ontogeny and evolution via laboratory experiment. A multidisciplinary approach has been adopted, with different methodologies encompassing remote sensing techniques, field observations, numerical modelling and physical-laboratory experiments. Activities have been carried out in parallel with sedimentological studies, in order to provide a comprehensive framework.

The main results from this work highlighted that: I) once conveniently scaled with channel width, tidal meander migration rates are very similar to those displayed by fluvial meanders, thus challenging the paradigm of tidal meanders as a stable landscape features; II) differences and analogies between tidal and fluvial meander planforms can be addressed in a quantitative way, and different metrics exist thta allow one to successfully quantify these differences; III) strong asymmetries exist between different tidal phases, exerting a crucial role on the depositional patterns of tidal meanders; IV) under certain conditions, lateral tributaries can strongly influence the evolution of bends modifying local mechanisms of flow and sediment distribution; V) tidal channel network features evolve differently in response to different tidal ranges, basin slopes and relative sea level changes, whereas the number of breaches along the initial shoreline seems to have little effect on the evolution of the network itself.

SOMMARIO

Le reti di canali meandriformi costituiscono una delle principali componenti dei sistemi mareali, e giocano un ruolo di fondamentale importanza nell'evoluzione eco-morfodinamica di questi ambienti. Tuttavia, solo un numero limitato di studi scientifici ne ha analizzato le configurazioni planimetriche, le caratteristiche morfometriche e l'evoluzione morfodinamica. Inoltre, l'evoluzione morfodinamica e i prodotti sedimentari dei meandri a marea sono spesso stati interpretati sulla base di teorie e modelli sviluppati per i loro omologhi fluviali, nonostante numerose differenze tra le due tipologie siano identificabili a priori. Nell'intento di comprendere più approfonditamente l'evoluzione morfodinamica dei meandri a marea, nel presente lavoro sono stati studiati 5 differenti argomenti: i) tassi di migrazione e dinamiche evolutiove dei meandri a marea; ii) stima e quantificazione delle differenze planimetriche esistenti tra meandri fluviali e tidali; iii) variazioni dell'idrodinamica dei meandri a marea in risposta all'alternanza delle fasi mareali, e influenza di queste variazioni sui prodotti sedimentari propri dei meandri a marea; iv) ruolo della bidirezionalità del flusso, delle asimmetrie mareali e dei tributari laterali; v) stima dell'influenza dell'ampiezza di marea, delle pendenze topografiche del bacino tidale e della configurazione iniziale della linea di costa sulla nascita ed evoluzione morfologica delle reti di canali a marea. Nelle suddette analisi é stato utilizzato un approccio di tipo multidisciplinare, combinando metodologie quali remote-sensing, osservazioni *in situ*, modellazione numerica ed esperimenti su modelli fisici. Le attività sono state condotte in parallelo con studi sedimentologici, così da fornire un quadro che fosse il più esaustivo possibile.

I principali risultati ottenuti evidenziano che: I) se convenientemente normnalizzati con la larghezza del canale, i tassi di migrazione dei meandri a marea sono molto simili a quelli dei loro corrispettivi fluviali, inficiando così il paradigma che vede i meandri tidali come un'entità morfologica essenzialmente stabile; II) le differenze tra meandri tidali e fluvali non sono solo qualitative, e diverse sono le metriche che possono essere utilizzate per quantificare queste differenze; III) le asimmetrie tra le diverse fasi di marea sono significative, e influenzano i patterns deposizionali in modo determinante; IV) gli affluenti laterali possono influenzare fortemente l'evoluzione dei meandri, modificando i meccanismi locali di distrubuzione dei flussi e dei sedimenti; V) le reti di canali a marea evolvono in modo diverso in risposta a differenti ampiezze di marea, pendenze del bacino tidale e cambiamenti del livello relativo del medio mare, mentre la configurazione iniziale della linea di costa non sembra avere effetti significativi sull'evoluzione della rete stessa.

The lowest ebb is the turn of the tide

— Henry Wadsworth Longfellow

ACKNOWLEDGMENTS

Firstly, I would like to express my sincere gratitude to my advisors Prof. Andrea D'Alpaos and Prof. Massimiliano Ghinassi, for the continuous support of my Ph.D study and related research, for their patience, motivation, and immense knowledge. Their guidance helped me in all the time of research and writing of this thesis.

I would also like to deeply thank my other advisor, Prof. Luca Carniello, the person who first proposed me to attend a Ph.D. degree. Thanks for having always been willing to discuss scientific problems with me and share his knowledge, but above all thanks for having unconditionally support me even though I refused to tackle this Ph.D. journey with him.

Besides my advisor, I would like to thank my colleagues and co-author, particularly Dr.ssa Marcella Roner, Dr.ssa Lara Brivio and Dr.ssa Laura Tommasini. Besides having assisted me during the writing of this thesis, revising the initial drafts and providing meaningful suggestion for improve this manuscript, they have made this Ph.D. experience worthy, stimulating and above all funny day by day. I would also like to mention Dr.ssa Valeria Bianchi, Dr.ssa Benedetta Andreucci and Dr.ssa Ada Castelluccio, with whom I have had the privilege to share convivial moments.

My sincere thanks also goes to Prof. Chris Paola, who provided me an incredible opportunity to join his team at the St. Anthony Falls Laboratory as visiting student, in one of the most exciting and fruitful experience of my life. A deep thanksgiving goes also to Dr. Chris Ellis: without his assistance and technical expertise, the experiments contained in this dissertation would not have been possible. Finally, I would like to thank Dr. Nathan Lentsch, who strongly helped me in carrying out the experiments and analyzing the results. Thank for the sleepless nights we were working together before deadlines, and for all the fun we have had in Delta Basin 2.

I would like to thank my family: my parents and my sister, as well as my parents in law, for supporting me spiritually throughout writing this thesis and my life in general. Thanks to all my friends, for their constant friendship and support in spite of my tendency to disappear into the deep recesses of research for months. Thanks to my best men, Nicola and Andrea, for being such a cool guys and for having always been on my side.

Last but not the least, I want to thank, from the bottom of my hearth, my beloved wife Martina, for her constant support, her endless patience, and above all for making me a better person day by day. Nothing in the world could make me as happy as you do.

A. F.

1 INTRODUCTION

1.1 OVERVIEW

This study deals with tidal-channel patterns and aims at investigating the morphodynamic evolution of tidal channels, paying specific attention to their meandering behavior. The morphodynamic evolution of tidal meanders was analyzed through a multidisciplinary approach, that couples remote sensing techniques, field investigations and both numerical and physical modelling. Activities were carried out in parallel with sedimentological studies, in order to provide a comprehensive framework.

(a) Meandering tidal channel network near Banjul, Banjul Region (WAG) ©2016 Google, DigitalGlobe

(b) Dendritic tidal channel network near Derby, Kimberly Region (AUS) ©2016 Google, CNES/Astrium

Figure 1.1: Different examples of tidal channel networks

1.2 RELEVANCE OF THE PROBLEM

Tidal landscapes are commonly dissected by networks of tidal channels that exert a strong control on the ecomorphodynamic evolution of these environments, facilitating the exchange of water, sediments and nutrients (e.g. D'Alpaos et al., 2005; Hughes, 2012; Coco et al., 2013). Channel evolution chiefly depends on a number of factors, related to both the physical and biological features of the landscapes they dissect (e.g., bank erodibility, presence and type of vegetation, bioturbation), as well as to local hydrodynamics (e.g., water and solid discharges), in a fashion that is generally not easily comprehensible because of the mutual relationships and interactions

among the above recalled features and processes. As an example, channel cross-sectional dimensions are related to the flowing tidal prism[1], that in turn depends on both the tidal range[2] and the area drained or feeded by the channel, as well as on the morphology of the adjacent platform and channels which affect tidal propagation. These parameters determine sediment entrainment, transport and deposition that feedback on channel morphology, thus governing the evolution of the whole tidal environment.

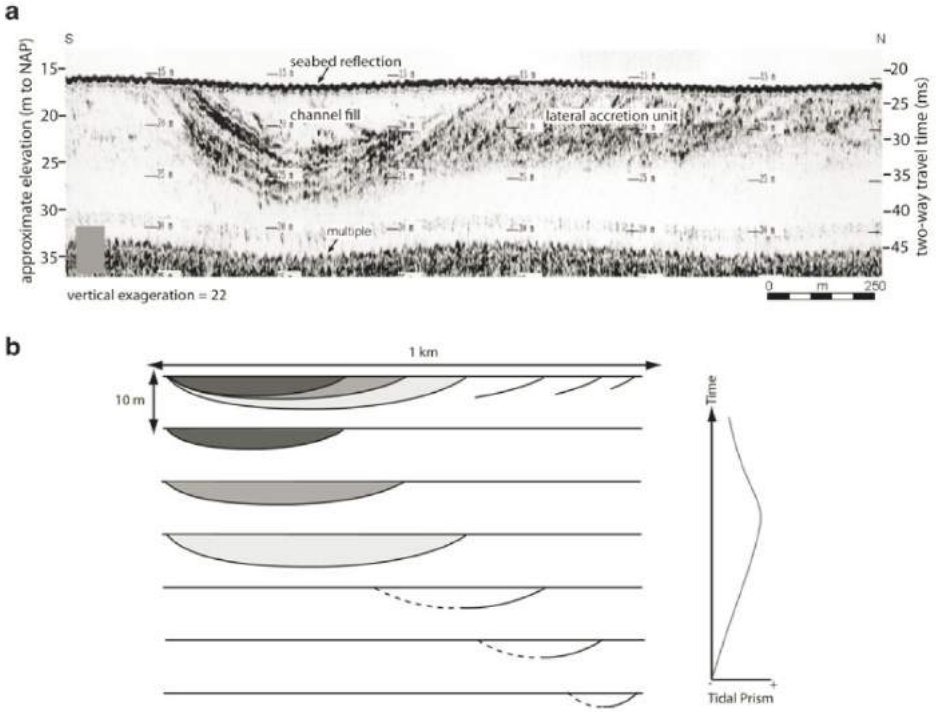

Figure 1.2: a) Shallow seismic records of cut-and-fill deposits of a tidal channel preserved offshore. A region of lateral accretion is clearly visible to the north of a channel, determined to be a main channel close to the tidal inlet; b) Schematic evolution of a channel with the inferred change in tidal prism responsible for the growth, lateral accretion and eventual infilling (Hughes (2012), adapted from Rieu et al. (2005))

A secondary, yet deeply important process in tidal network evolution is the meandering behaviour of tidal channels and the resulting point bar formation (Hughes, 2012). Besides influencing the planform evolution of the network, this phenomenon has a strong relevance on the stratigraphy of intertidal areas, especially in terms of preservation potential. In fact, tidal channels are typically preserved in the fossil record through lateral accretion, which occurs mostly at meander bends, and through channel infilling as the tidal prism decreases when the channel is partially abandoned *via* either avulsion or meander cut-off (Figure 1.2).

1 Tidal prism is defined as the volume of water flowing through a given cross section during either flood or ebb phase.

2 The tidal range is the vertical difference between the high tide and the succeeding low tide.

In spite of their prominence and wide occurrence, the characteristics and dynamics of meanders shaped by the periodically reversing tidal flows lack the detailed inspection that has been devoted to their fluvial relatives (e.g. Leopold and Wolman, 1960; Ikeda and Parker, 1989; Seminara, 2006; Zolezzi et al., 2012; Hooke, 2013). Moreover, the depositional architecture of tidal meander bends has also been somewhat neglected (Choi and Jo, 2015) compared to the attention devoted to the fluvial realm (e.g. Allen, 1965; Bridge et al., 1986) and has mainly been approached using facies models (Barwis, 1978; de Mowbray, 1983; Choi et al., 2004; Choi, 2011) which assume the stratal geometries of tidal deposits to show marked similarities with those of their fluvial counterparts (Jackson, 1976; Brierley, 1991). Nevertheless, the forcefulness of this assumption is challenged by the observation that several different processes sculpt tidal and fluvial meander and channel network morphology. Hence, one might expect tidal channels to display different morphologies and dynamics, thus leading to a relevant question, with theoretical and practical implications, that is whether (and to what extent) or not tidal and fluvial meanders are similar, and therefore if morphodynamic and architectural models mediated from the study of fluvial meanders, can be applied to their tidal counterparts.

In this chapter, we firstly review the literature on both fluvial and tidal meanders, then summarize the peculiar features belonging to tidal channels, particularly when compared to their fluvial fellows. An outline of the research questions addressed by the present study is finally presented.

1.3 LITERATURE REVIEW

Questions concerning possible analogies and differences between tidal and fluvial meander bends can hardly be seen as new ones, since the first questions on this very issue date back to the late Twenties (see Bain, 2014), when Campbell (1927) claimed that a stream flowing at and below tide-level "*has no inclination to form meanders and none to cut off meanders already formed*", concluding that meanders in such streams are indicative of relative sea-level rise along existing river meanders. Barton (1928) however demonstrated how a near-shoreline meander of the Brazos River, Texas, had been able to shift hundreds of meters in about fifty years. Likewise, Johnson (1929) challanged Campbell's theory because of its questionable terminology, stating that new analyses were necessary which included different rivers such as the Indus, where meandering is stronger and occasional oxbow lakes are present (Figure 1.3-a). During the following years, however, the general interest on meandering streams kept mainly focused on riverine meanders, a tendency that was initially driven by the problems related with the active meander migration in the lower Mississippi River.

(a) Scroll bars and oxbow lakes represents watertight signs of meander migration in the Indus River Delta area (PK).
©2016 Google, DigitalGlobe

(b) An area rich in meander neck cut-offs within the Pagliaga salt marsh, Venice Lagoon (IT)
©2016 Google, Landsat

Figure 1.3: Tidal meander dynamism highlighted by different fluvial-like migration features.

1.3.1 Fluvial Meanders

Tiffany and Nelson (1939) first recreated real-like sinuous stream in a laboratory experiment, with scour near bend apexes alternated with shallower areas between adjacent bends ("pools and riffles" pattern), and observed that an increase in sediment load accelerated the evolution of meander bends.
Matthes (1941) gasped that the fundamental mechanism leading to meander migration was the methodical transfer of sediment from the eroding concave-outer bank to the first downstream inner-convex bank. Sediment load was then identified as a chief factor for meander dynamics, together with valley slope, discharge and bed resistance. The role of floodplain heterogeneity in modifying meander evolution was also highlighted, particularly with respect to the influence exerted by abandoned meanders ("oxbow lakes") and secondary channels. In fact, after having been abandoned, a reach is partially reactivated during the major floods, which carry fine suspended silt-particles that settle down due to the reduced velocities, compact and progressively form highly resistant silt-bodies named "clay plugs". Such plugs can reduce normal erosion rates, thus promoting distorsion of the meandering patterns and shaping irregular bends.
Quraishy (1944) observed, in a initially straight flume, the formation of uniformely-spaced alternate bars which finally caused the stream to assume a sinuous course.
Friedkin (1945) carried out a laboratory study to investigate the influence of different factors, such as slope and discharges, on meander dynamics. Painting channel banks with different colors, he demonstrated that sediments eroded from the outer bank were deposited along the first downstream convex bank, as gasped by Matthes (1941).

According to Hooke (2013) however, the major era of quantitative research on river meanders started in the late Fifties, when the foundations of the modern fluvial geomorphology were laid with the fundamental work of Leopold and Wolman (1957), Leopold and Wolman (1960), Schumm (1963), Leopold et al. (1964), and Leopold and Langbein (1966). Scientific research started being dominated by morphometric analyses, that for instance clarified how the presence of fine sediments promotes sinuosity, whereas large width-depth ratios discourages it. Variations in sediment load proved to influence meander features and dynamics, although meandering was observed to occur even in the absence of sediment load (e.g., meanders in glaciers). More importantly, the empirical observation that mutual distance between riffles in straight channels equals the distance between inflection points in meandering streams of the same width, led to the hypothesis that the same mechanism that shapes meanders also operates in straight channels. According to Solari et al. (2002), this *de facto* set the basis for the modern *Bar Theory*[3], although meander evolution was still considered a transient condition, with bends tending to an equilibrium form over long timescales. Most of the geomorphologists agreed upon the hypothesis that such a form fitted a sine-generated curve[4] (see for example Kinoshita, 1961; Leopold and Langbein, 1966).

The long-term equilibrium hypothesis began to be challenged since the 1970s, when numerous studies, based on field-work and historical evidence, demonstrated how meander evolution took place also on short time-scales (few years), potentially producing complex transient morphologies (Daniel, 1971; Lewin, 1972; Brice, 1974; Hickin, 1974; Hickin and Nanson, 1975; Lewin, 1976; Hooke, 1979; Dietrich et al., 1979). At the same time, researchers started focusing on bar sedimentology (e.g., Jackson, 1976), and the relationship between straight, braided and meandering river became clearer (e.g., Fredsoe, 1978). Particularly, Parker (1976) first tried to treat meandering and braiding as effects produced by the same flow instability phenomenon, caused by sediment transport and friction, that finally leads to the formation of bars. Parker concluded that *"(...) most streams have a tendency to form bars even though they are in a graded state. If the slope and the width-depth ratio at formative discharges are sufficiently low, meandering is favored. If the slope and the width-depth are sufficiently high, braiding is favored"*.

During the 1980s and 1990s, some new empirical field-based and geomorphological studies were carried out, mostly focused on objective bend identification (O'Neill and Abrahams, 1986) and meander characterization (Howard and Hemberger, 1991; Stolum, 1996), as well as on bank erosion and me-

3 Bar theory *"essentially assumes that alternate bars, i.e. free migrating modes excited by a bottom instability, are precursors of meanders: in other words the presence of alternate bars in the originally straight channel would be the triggering mechanism which forces bank erosion, hence meander wavelength would coincide with bar wavelength."*(Solari et al., 2002)

4 According to Hathout (2015), sine-generated curves belong to a class of intrinsic functions which describe a curve by specifying its "direction angle". The curve is determined by ω, the maximum angle which the curve makes with the horizontal, and the fact that the direction angle changes in a sinusoidal fashion along the path.

ander migration dynamics (Hooke, 1980; Hooke, 1984; Hickin and Nanson, 1984; O'Neill and Abrahams, 1986; Nanson and Hickin, 1986; Williams, 1986; Furbish, 1988; Thorne, 1991; Stolum, 1998; Hudson and Kessel, 2000). The major finding of these studies was that meander-migration rates increase with channel curvature, reach a maximum when bend radius divided by channel width is about 3, and then decrease for sharper bends. However, this period was predominantly characterized by a number of theoretical and modeling studies on river meanders. Even though worth mentioning are the realistic meandering pattern obtained by Howard and Knutson (1984) and Johannesson and Parker (1985)'s models, as well as the theoretical contributions on flow in meandering streams (Kitanidis and Kennedy, 1984; Smith and Mclean, 1984; Johannesson and Parker, 1989) and meander time-development (Parker, 1986), the major contribution in understanding meander dynamics came from the fundamental work of Ikeda et al. (1981) and Parker et al. (1982) who proposed the so called *Bend theory*. Contrary to the *Bar theory*, the *"Bend theory assumes that bank erosion originates from steady flow perturbations induced by channel curvature, i.e. from forced modes rather than from migrating free alternate bar modes, hence the wavelength selected by the process of meandering initiation should be such as to maximize curvature-induced flow and topography perturbations"* (Solari et al., 2002). The two theories were finally unified by Blondeaux and Seminara (1985), who demonstrated that the *Bend theory* is just a particular case, for which bars neither grow nor migrate downstream, of the more general *Bar theory*. It is important to highlight that both the bend and the bar theory were originally obtained by using linear stability analysis, thus providing a linear model for solving flow field and bottom topography. Even though the theory and its solution were further improved, including non-linearities (e.g., Seminara and Tubino, 1992; Pittaluga et al., 2009), width variations (e.g., Luchi et al., 2011) and studying how flow-field perturbation might propagate upstream or downstream (Zolezzi and Seminara, 2001; Seminara et al., 2001), the main conclusion of this research path has been summarized by Seminara (2006) as follows: "*any small random perturbation of channel alignment eventually grows, leading to a meandering pattern as shown by bend instability theory*". Such a conclusion does not however suffice to explain meander in non-alluvial settings (e.g., glacial meanders), a problem that has been recently undertaken by Lazarus and Constantine (2013) who suggested that channel sinuosity would be dependent on the ratio between flow resistance and slope, with highly sinuous channels occurring in resistance-dominated environments.

If, on the one hand, the number of theoretical studies on meanders has never declined over the last two decades (e.g., Lanzoni et al., 2006; Lauer and Parker, 2008; Frascati and Lanzoni, 2013; Eke et al., 2014), on the other hand the new millennium has seen a resurgence of empirical and modelling studies, mainly driven by new technologies which improved the accuracy and speed of both measurement and numerical models. Among the major research topics undertaken during the last decades, worth mentioning are local hydrodynamics (e.g., Ferguson et al., 2003; Parsons et al., 2004), par-

ticularly along tight bends (Nanson, 2010) and cut-offs (Le Coz et al., 2010), meander migration and dynamics (Lagasse et al., 2004; Hooke, 2007; Frascati and Lanzoni, 2009; Frascati and Lanzoni, 2010) and its mutual interaction with planform heterogeneity (Constantine and Dunne, 2008; Guneralp and Rhoads, 2011), and the influence of bank failure on meander dynamics (Motta et al., 2014; Hackney et al., 2015).

It is finally worth recalling how research advances and new technologies had caused laboratory-based experiments to regain favor. Smith (1998) succeeded in modeling high sinuosity meanders in a small flume (see also Parker et al., 1998) by using a mixture of cohesive material (including kaolinite clay), thus preventing channel braiding. Channel stabilization has also been obtained by means of vegetation (e.g., Tal and Paola, 2007), as well as by employing flumes with rigid walls and mobile bed (e.g., Termini, 2004; Blanckaert, 2011)

1.3.2 Tidal meanders

In the tidal realm, the research had been initially focused on either estuarine meanders (Ahnert, 1960; Myrick and Leopold, 1963) or tidal channels as a whole (Dury, 1971), rather than on single tidal meanders, with seminal works mainly including measurements of morphometric and hydraulic features of channels, such as width-to-depth ratio and discharges.
In the last four decades a wide literature was developed, describing the hydrodynamics and consequences of tidal currents and asymmetries on sediment dynamics and other morphological characteristics of tidal channels (e.g., Boon, 1975; Bayliss-Smith et al., 1979; Pethick, 1980; Schuttelaars and De Swart, 1997; Lanzoni and Seminara, 1998; Friedrichs and Perry, 2001; Fagherazzi and Furbish, 2001; Lanzoni and Seminara, 2002; Fagherazzi et al., 2003; Lawrence et al., 2004; Friedrichs, 2012; Lanzoni and D'Alpaos, 2015; Sullivan et al., 2015), morphometric features of tidal networks (e.g., Pestrong, 1965; Pestrong, 1972; Leopold et al., 1993; Fagherazzi et al., 1999; Rinaldo et al., 1999a; Rinaldo et al., 1999b; Marani et al., 2003), and the eco-morphodynamic evolution of salt marshes and related tidal channel networks (e.g., French and Spencer, 1993; Marani et al., 2004; D'Alpaos et al., 2005; Kirwan and Murray, 2007; Mudd et al., 2010; D'Alpaos et al., 2011; Fagherazzi et al., 2011). A smaller piece of attention was conversely paid to tidal meanders as single morphological features, whose role in the evolution of tidal landscapes has been either purposefully neglected or considered of secondary importance. A handful of papers, in fact, exists that analyzed the planimetric shape, morphometric characteristics, and morphodynamic evolution of tidal meanders.

MORPHOMETRIC AND FIELD-BASE STUDIES at first focused on the role of vegetation on tidal channel migration and morphology. Garofalo (1980) observed that vegetation influences channel morphology (especially sinuosity), and stated that *"under normal tidal conditions both saline and freshwater tidal*

channels migrate little, if any (...) It is believed that most stream channel migration in both saline and freshwater wetlands occurs as a result of increased forces due to storms". Reduced migration rates, in the order of 2.3-5.7 cm/year, were also found by Gabet (1998) for tidal channel in the San Francisco Bay. Responsible for such reduced migration rates was claimed to be the presence of failed bank material ("slump blocks") in the channel: *"The slump blocks induce sedimentation, protect the banks, and prevent further bank erosion"*. Kleinhans et al. (2009) investigated meanders on an intertidal mudflat in the Westerschelde estuary (NED), concluding that the presence of highly cohesive bank and bed sediment justifies the reduced and more localized dynamics observed in tidal meanders. Moreover, it was stated that:

> *"the high thresholds for bed sediment erosion and for bank failure lead to two processes, uncommon in larger rivers, that cause most of the morphological change. First, the beds of the channels are eroded by backward migrating steps under hydraulic jumps, while the remainder of the bed surface along the channel is hardly eroded. Second, channel banks erode i) where eroding steps locally cause undercutting of otherwise stable channel banks and ii) in very sharp bends where the flow separates from the inner-bend channel boundary and impinges directly on the bank on the opposite side of the channel"*.

Nevertheless, the role of flow separation on meander bends still has to be further clarified.
Fagherazzi et al. (2004) coupled field observations and numerical modelling to analyze the effects of bidirectional flows on meander planform configuration and migration, pointing out that flow dominance within a tidal channel may be inferred from meander geometry and evolution, whereas Hood (2010) highlighted the role of depositional rather than erosional processes on tidal meander formation, suggesting that hydrodynamics at channel confluences promotes sandbar and marsh-island growth.
It is finally worth recalling the work of Marani et al. (2002), who proposed an objective method, based on the mathematical computation of channel curvature along the intrinsic channel-axis coordinate, to identify tidal meanders. Studying the geometrical properties of tidal meanders, a number of recurrently constant features over different orders of magnitude were found, interpreted by the authors as local morphological adaptations to the chief-hydrodynamic landforming fluxes. The occurrence of non-negligible second harmonics in the curvature spectrum was also proposed as possible tidal meander distinctive feature.

MATHEMATICAL AND NUMERICAL MODELLING have been widely employed to analyze the evolution of tidal networks, describing the planimetric development of tidal channel networks coupled with the vertical accretion of the adjacent salt marshes and tidal flats as a consequence of tidal forcings, varying sediment inputs and relative sea level changes (e.g. D'Alpaos et al., 2005; Kirwan and Murray, 2007). However, thus far none of the proposed model have accounted for meander bend evolution, not even in a simplified

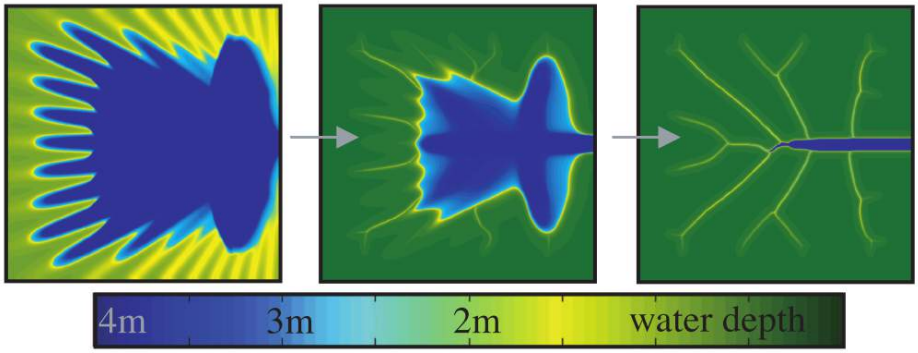

(a) Results of the model proposed by Kirwan and Murray (2007)

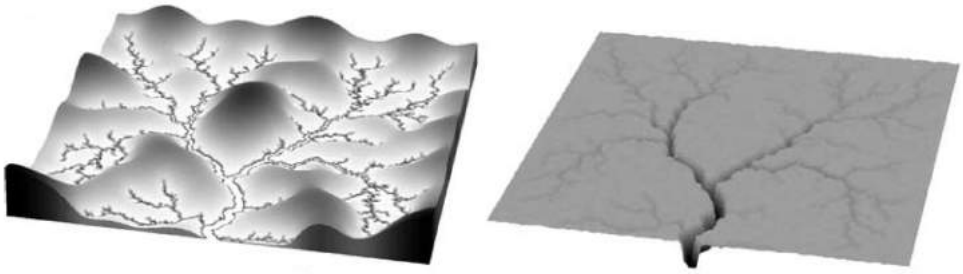

(b) Results of the model proposed by D'Alpaos et al. (2005)

Figure 1.4: Results of two different models simulating eco-morphodynamic evolution of tidal channel networks.

manner (see for example Figure 1.4).

Similarly, a number of theoretical and modelling studies have been developed to investigate the morphodynamic evolution and equilibrium morphology of tidal channels, but none of them included the presence of channel curvature. Some of these studies focused on the equilibrium longitudinal bed profile (e.g., Lanzoni and Seminara, 2002), even accounting for variations in longitudinal channel widths (e.g., Schuttelaars and de Swart, 2000; Seminara et al., 2010; Toffolon and Lanzoni, 2010). Less common are model in which channel shape is *a priori* unknown, and the channel is therefore left to freely evolve (e.g., Canestrelli et al., 2007; Lanzoni and D'Alpaos, 2015).

To the best of our knowledge, the only model capable to predict the flow field and bed topography in weakly meandering tidal channels was developed by Solari et al. (2002) by using linear theory. Solari et al. (2002) emphasized that similarly to fluvial meandering bend theory (Ikeda et al., 1981; Parker et al., 1982), a planimetric instability mechanism seems to be present that amplifies preferred wavelengths from the alternate-bar wavelengths (Blondeaux and Seminara, 1985), even though selected wavenumbers were smaller than those observed in nature. In addition, to overcome some of the simplifying assumptions embedded in their theoretical approach (e.g. constant channel width and cohesionless sediments), Solari et al. (2002) called for new modelling, field and laboratory insights on tidal meanders.

Garotta et al. (2006) investigated the role of overtides in promoting net migra-

tion of tidal free bars over a single tidal cycle, thus completing the seminal work of Seminara and Tubino (2001) and Solari et al. (2002) who had conversely observed no net tidal-bar migration employing a perfectly sinusoidal tide.

LABORATORY EXPERIMENTS have been mainly set up to investigate the initiation and evolution of tidal channel networks (Stefanon et al., 2010; Vlaswinkel and Cantelli, 2011; Stefanon et al., 2012; Kleinhans et al., 2015), even though the role of a number of factors and external forcings, such as initial shoreline configuration, basin slope and relative sea level changes, on the network evolution remains partially or completely unknown.
Thus far, the only physical experiment dealing with meandering tidal channel has been carried out by Garotta et al. (2007), who employed a sinuous flume with fixed walls and erodible bed, emphasizing along-channel changes in the relationship between bar–pool patterns and channel curvature.

1.3.3 A comparison between tidal and fluvial meanders

Several authors have identified a number of differences between tidal and fluvial meanders, leading Marani et al. (2002) to conclude that "*In any real case of fluvial versus tidal patterns, differences are the norm rather than the exception once carefully examined*". Among these differences, the existence of periodically reversing flows in tidal settings probably stands out most, as elegantly stated by Bridges and Leeder (1976):

> *Intertidal channels are different from other types because they serve as both arteries and veins: guiding semidiurnal flood tidal flows onto the moist tidal flats, and channeling the receding waters during the ebb tide. Thus the student of natural channels appreciates the fact that results based on tidal flat channels will not have complete applicability to non-tidal channels developed on similar substrates.*

Fagherazzi et al. (2004) also pointed out this fundamental discriminant factor ("*Bidirectional flow is thus a unique characteristic of tidal channels distinct from terrestrial rivers*"), whereas Whiting and Dietrich (1993) claimed that:

> *While the regularity of meandering channels might argue otherwise, there is no reason to expect that the same [wavelength] selection mechanism necessarily operates in all channels. Clearly, if bars are not present in the channel as in tidal marshes or mud flats, some mechanism other than bars must be operating.*

Behind experiencing a daily reversal of flows, tidal meanders are hydrodynamically characterized by a different discharge variability when compared to their fluvial counterparts. While rivers experience flood events characterized by high discharges which overlap to slowly varying discharges through the year, and high flow velocities can be maintained for relatively long periods of time during floods (days), tidal channels are characterized by highly

variable discharges during a tidal period (hours) but are generally shaped by water fluxes that vary in a well defined range of possible values. On the other hand, the spatial variability of the flowing discharge is higher than in the fluvial framework, thanks to the progressive landward reduction in tidal prism. Furthermore, the maximum discharges in tidal channels are typically observed for conditions different from, yet close to, the bankfull, which instead corresponds to both the peak and formative discharges in the riverine framework. It is also worth noting how the highest (lowest) tidal levels correspond to a "slack-water" condition (Figure 1.5-a). Also the role of the areas adjacent to the channels is quite different, with riverine alluvial plains that can be inundated only during exceptional floods, while salt marshes are subjected to periodical flooding. This difference is even more evident when considering subtidal channels, together with the adjacent tidal flats, which are almost constantly submerged. The hydrodynamics of such channels is extremely complex, since both minimum and maximum velocities of tidal currents are experienced when both the channel and related overbanks are flooded, and flow distribution within the channel can be influenced by currents developed in overbank areas.
Due to their alongshore position, tidal channels are also exposed to the action of storms and waves (Tornqvist et al., 2007; Howes et al., 2010; Priestas and Fagherazzi, 2011; Leonardi et al., 2015), and in wide shallow lagoons inter-channel areas can be affected by strong wind winnowing (Carniello et al., 2005; Carniello et al., 2011), which can influence sediment distribution along the channels.

FROM A NETWORK PERSPECTIVE it has been largely demonstrated (Fagherazzi et al., 1999; Rinaldo et al., 1999a; Marani et al., 2003) that tidal systems are scale-free morphological structures, conversely to their fluvial homologous which exhibit scale invariance at both meander and network scales (Leopold and Wolman, 1960; Rodriguez-Iturbe and Rinaldo, 1997). Hence, small tidal channels are often not a scaled version of the larger channels in a system (Hughes, 2012), possibly suggesting the existence of different chief landforming processes. Moreover, given the gentle bed slopes over which tidal networks are typically shaped, water flows in tidal environments are driven by water-surface, rather than topographic gradients (Rinaldo et al., 1999a; D'Alpaos et al., 2005; Coco et al., 2013). This occurrence was used by Fagherazzi (2008) to explain the presence of loops in tidal networks, in contrast to the dendritic, tree-like structure displayed by their fluvial relatives. Finally, Rinaldo et al. (1999a) found that in tidal systems typical geomorphic relationships derived for riverine systems do not hold, such as those relating the mainstream length of a channel (L) to watershed area (A) through the Hack (1957) law ($L = A^{0.57\pm0.03}$), with the area (A) being nearly proportional to the discharge (Q) that, in turn, can be inferred from channel width (B).

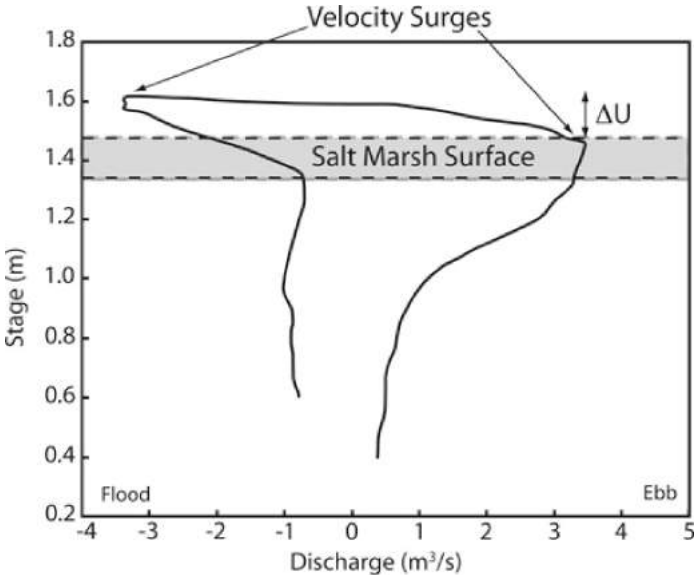

(a) The hysteresis observed in tidal velocity versus water depth (stage). Velocity is highly variable, but two distinct peaks are seen, one during the flood just above bankfull conditions when the water level is at the level of the marsh surface, and one during the ebb. In terms of symmetry around either high tide or the timing of bankfull conditions, the peak ebb velocities lag the flood transients, occurring later, at a lower stage of the tide, just below bankfull. ΔU indicates the difference in the height at which the peak velocity occurs (Hughes, 2012, from the observations of Bayliss-Smith et al. (1979), adapted from Fagherazzi (2008))

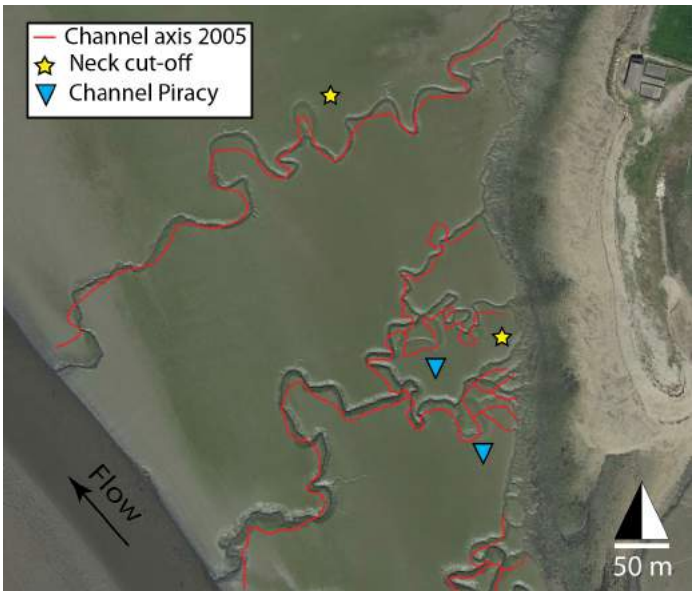

(b) Evolution of tidal channel wandering on muddy tidal flats in the Bay of Morlaix, Brittany (F). Background photos was take in 2014 (©2016 Google, DigitalGlobe), whereas red line stand for the channel axis configuration in 2004. The dynamism of the system may be inferred from 4 channel abandonments, two of which are meander neck-cutoffs (star-labelled), whereas other two (triangle-labelled) are determined by channel piracy, that is a contact of two channel branches of different order.

Figure 1.5: Hydrodynamics and evolution of tidal channels.

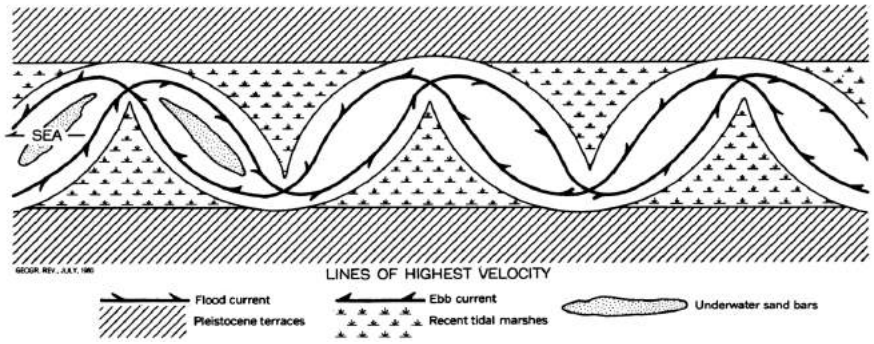

Figure 1.6: Schematic diagram of estuarine meanders (Ahnert, 1960)

AT THE CHANNEL–LENGTH SCALE the most remarkable differences between tidal and fluvial bends may be found from a planview perspective. The strong spatial gradients in channel width, which occur in shallow tidal channels of all orders, is arguably one of the key characteristics that distinguishes tidal systems from fluvial ones (Fagherazzi et al., 1999; Bain, 2014). Indeed, due to a progressive reduction in the tidal prism, tidal channels generally tend to narrow landward, displaying a characteristic funnel shape (Lanzoni and D'Alpaos, 2015). Moreover, intricate and complex networks generally formed by tidal channels include numerous low order tributaries that can interfere with the flow within the main channel.

AT THE MEANDER–LENGTH SCALE the mutually-evasive pathways of flood and ebb flows may also produce peculiar morphologies. The inner banks of many tidal meanders indeed display a unique, distinctive cuspate shape (Figure 1.7-a), a feature that has been attributed to the back-and-forth swinging of tidal currents caused by flow inertia, that displaces the ebb (flood) current toward the seaward (landward) edge of the channel (Ahnert, 1960; Fagherazzi et al., 2004; Dalrymple et al., 2010; Hughes, 2012 and see Figure 1.6).

The same phenomenon was suggested by the mathematical model proposed by Solari et al. (2002) as responsible for shifting the position of higher bed shear stresses from one bank to the opposite one, thus inhibiting meander migration. Another peculiar planform morphology of tidal meanders is the so called "box-shaped" meander (Dalrymple et al., 2010), that is a quasi-squared meander including two right-angle-like turns. The meander curvature signal displays two local curvature maxima, and Fagherazzi et al. (2004) claimed that in their study area many meanders were shaped in this way. The proposed explanation for the occurrence of these right-angle turns still lies in the bidirectional flow experienced by tidal meanders.
From the evolutionary dynamic point of view, expansion of tidal meanders is commonly associated with an increase in channel width, whereas the width of fluvial channels keeps almost constant during planform transformations (Brice, 1974). To the best of author knowledge, meander cutoff occurs in tidal channels only as consequence of meander neck narrowing (i.e. neck cutoff)

(Brivio et al., 2016), whereas in river meanders both chute and neck cutoffs can take place. However, the high spatial density of tidal channels makes channel piracies more frequent (Ghinassi et al., in rev. and see for example Figure 1.5-b).

SEDIMENTOLOGICAL CHARACTERISTICS of tidal meanders also highlight their distinctive traits. The architecture and sedimentary features of tidal point bars are relatively unexplored, and mainly based on studies focused on intertidal channels crossing through modern tidal flats (Barwis, 1978; de Mowbray, 1983; Choi et al., 2004; Choi, 2011; Hughes, 2012). In these settings in fact, the exposure of overbank areas during low tides allows the morphology of bars to be observed and easily investigated through trenching and coring. From these studies, an overall similarity between tidal and fluvial point bars emerged, highlighting the role of tidal currents in promoting inclined etherolithic strata in the point bar deposit. This led many authors to consider the basic architecture and facies models of tidal meander quite similar to those of fluvial bends (e.g. Díez-Canseco et al., 2014), assuming both the higher rate of mud accumulation and the degree of bioturbation, as well as bidirectional flows, as the key-distinctive features for the tidal case (Allen, 1982; Thomas et al., 1987). However, a recent detailed scrutiny of the internal architecture and sedimentary features of a tidal meander bend (Brivio et al., 2016) emphasized the existence of relevant differences imprinted in the sedimentary record, such as the absence of crevasse splay deposits, the development of elongated pool zones, the overall symmetric distribution of sediment grain size along the landward and seaward sides of the bend, and the observed spoon-shaped geometry of the bar-top mud, resulting from the coupled effects of lateral migration and vertical aggradation. Furthermore, it is known how, in subaqueous settings, water-saturation of point bar deposits decreases the intergranular friction, promoting collapses along the bar flanks (Bridges and Leeder, 1976; Choi et al., 2013).

The number of differences listed above suggests the existence of differences in the morphodynamic evolution of fluvial and tidal meanders, thus calling for new insights into the tidal members of the meander family, in order to set-up an evolutionary model for tidal meanders and related sedimentary products, as well as to define the key features allowing one to distinguish tidal meanders from their fluvial relatives. On one hand, this might contribute to increasing the efficiency of oil production processes thanks to a better knowledge of the point bar evolution and architecture (Willis and Tang, 2010). On the other hand, improving current understanding of meandering tidal channel patterns and their morphodynamic evolution might result crucial for the conservation and restoration of tidal environments, especially in the face of a climate-changing scenario.

(a) Cusp-shaped tidal meander in the Venice Lagoon (IT) ©2016 Google, Landsat

(b) Box-shaped tidal meander in Cobequid Bay, Salmon River estuary, Bay of Fundy (CAN) ©2016 Google

Figure 1.7: Examples of peculiar planform morphologies of tidal meanders

1.4 GOALS OF THE STUDY

Toward the goal of improving current understanding of the intertwined evolution of tidal channel networks and tidal meanders wandering through them, the present work investigates the morphodynamic evolution of meandering tidal channels and the chief factors controlling their evolution. A multidisciplinary approach was used, which combines i) remote sensing techniques; ii) field observations; iii) mathematical modelling; iv) physical modelling and v) sedimentary analyses. Focuses and research questions of this study are as follows:

i. Especially when compared to their fluvial relatives, tidal meanders have often been recognized as a quite stable landscape features, in spite of "*highly sinuous planforms, severely undercut banks, and high rates of bank erosion*" (Gabet, 1998). Furthermore, whether or not tidal meander evolution dynamics is similar to the fluvial one is still an open question.
Are the migration rates and evolutionary dynamics of tidal meanders similar to those of fluval bends?

ii. Despite many qualitative differences are *a priori* known and identifiable, it is surprising how few authors have quantitatively addressed the possible existence of differences in tidal and fluvial meander planform features.
Which, if any, are the quantitative differences between tidal and fluvial meander planforms? And which is the right metric to quantify them?

iii. Strong flow asymmetries between different tidal phases are known to play a role in the morphodynamic evolution of tidal meanders, although some aspects still remain unclear.
How do tidal asymmetries influence the morphodynamic evolution of different types of tidal meander bends, and the related sedimentary patterns?

iv. Tidal networks appear much more articulated and interconnected than fluvial networks, particularly because of a widespread number of low order tributaries that are extremely rare in fluvial settings.
Can minor tributaries influence the morphodynamic evolution of tidal channel bends?

v. Initiation and evolution of tidal channel networks have been investigated by a number of models, both mathematical and physical. However, in the first case none of the models accounts for meander bend evolution, whereas in the latter one many questions still have to be answered.
Is it true that higher tidal amplitudes increase the drainage density of tidal networks? What is the role of topographic slope and initial shoreline configuration in dictating the structure of tidal channel networks? How do tidal networks respond to an increase or to a reduction in the relative sea level?

1.5 THESIS OUTLINE

The present work is divided into three main chapters:

THE FIRST CHAPTER firstly describes, through remote-sensing observations and modelling interpretation, tidal meander migration rates and dynamics, a widely-examined issue in the fluvial landscape. Secondly, a statistical-comparative analysis between tidal and fluvial meander planform features is presented, based on a large worldwide database of meander morphometric variables that was specifically created.

THE SECOND CHAPTER investigates bottom profiles and velocity distributions, by means of an acoustic Doppler current profiler, over different typologies of tidal meander bends. Furthermore, the role of bidirectional flows, tidal asymmetries and lateral tributaries in shaping tidal meanders is investigated by means of 2D and 3D hydro- and morphodynamic numerical models. The analyses are integrated with parallel sedimentological studies on the same study-case bends, in order to provide a thorough framework.

THE THIRD CHAPTER focuses on the influence of basin slope, initial shoreline configuration and tide amplitude on tidal network ontogeny and evolution. The role of the mentioned forcings is assessed by analyzing geometric characteristics and evolution of tidal channel networks generated in different series of physical laboratory experiments.

A summary of the main results obtained from this thesis is finally traced in the fourth chapter.

The appendices A, B and C include three different works to which I contributed as co-author. In particular, in Appendix A a new methodology to determine meander migration rates in the absence of high-temporal resolution aerial photographs is proposed, based on the analysis of closely spaced sedimentary cores and the dating of significant sedimentary surfaces across the neck of an abandoned meander loop. Such work represents a paper currently under review in the journal *Marine and Petroleoum Geology*.

Appendix B and Appendix C embody two different papers, the first currently under review in the journal *Sedimentology* and the latter in preparation, dealing with the morphodynamic evolution of tidal meanders.

2 ANALYSIS OF TIDAL MEANDER PLANFORMS AND DYNAMICS

2.1 SUSTAINED MIGRATION RATES OF TIDAL MEANDERS CHALLENGE CONVENTIONAL VIEWS ON MORPHODYNAMICS

This chapter is a manuscript ready to be submitted to Proceeding of the National Academy of Science (PNAS) and focuses on the migration rates and evolution dynamics of tidal meanders. Meandering tidal channel networks play a central role in the eco-morphodynamic evolution of the landscapes they incise. In contrast to their ubiquitous presence and dynamical importance, few observations of tidal meander evolution exist, and we lack a theoretical understanding of the processes governing it. The quantitative analysis of aerial photos shows that tidal meanders, traditionally viewed as quite stable landscape features, display modes of migration and migration rates per unit width quite similar to those characterizing their fluvial counterparts. This result is of high value for the understanding of the evolution of coastal landscapes and their restoration, with important implications for the characterization of the related sedimentary products.

PAPER

Finotello, Alvise[1], Stefano Lanzoni[2], Massimiliano Ghinassi[1], Marco Marani[2,3], Andrea Rinaldo[2,4] and Andrea D'Alpaos[1]

[1]Dept. of Geosciences, University of Padova, via G.Gradenigo 6, Padova, PD I-35131, Italy

[2]Dept. ICEA, Univesrity of Padova, via Loredan 20, Padova, PD I-35131, Italy

[3]Nicholas School of Environment, Duke University, Durham, NC 27708

[4]Laboratory of Ecohydrology ECHO/IEE/ENAC, Ecole Polytechnique Federale Lausanne, 1015 Lausanne (CH)

2.1.1 Abstract

Meandering channels are ubiquitous features of waterscapes. Despite their critical role in driving landscape evolution, tidal meanders have received comparably less attention than their fluvial counterparts. A hitherto unanswered question is whether or not tidal meander evolution is driven by processes similar to those governing flu-

vial meander morphodynamics. Here, we quantify the typical time scales of tidal meander migration and evolution through observation and modelling interpretation applied to the Lagoon of Venice (Italy). Evidence from historical aerial photographs from more than 250 meander bends on 40 salt-marsh channels provides maximum and mean migration rates of about 2.00 m/yr and 0.17±0.19 m/yr, respectively. We show that tidal meander migration rates are strongly related to bend curvature through a fluvial-like non-linear relation. In addition, tidal meanders display migration rates per unit width which are of the same magnitude as those of their fluvial counterparts, thus challenging the view of tidal channels as either stable landscape features or landforms evolving on time scales much larger than those of the other landscape-forming processes. We also find that tidal channel migration dynamics, that we characterize through relations among meander migration rates, curvature-spectrum harmonics, and sinuosity, can be described through the theoretical framework developed for the fluvial setting. Our results imply that tidal meanders are much less stable than previously thought, with important consequences on the related stratal architecture, also in the face of changes in environmental conditions.

2.1.2 Introduction

Branching and meandering tidal-channel networks are common features of tidal landscapes that control water, sediment, and nutrient fluxes within these landscapes (D'Alpaos et al., 2005; Coco et al., 2013). Particularly, meandering exerts a prominent influence on both the dynamics of tidal channels and on the stratigraphy of the platforms they cut through, thus possibly leading to sedimentary patterns with complex stratal architectures (Barwis, 1978; Hughes, 2012). Despite their importance in landscape evolution and their ubiquity, tidal meanders have however received less attention than their fluvial counterparts (Leopold and Wolman, 1960; Ikeda et al., 1981; Parker et al., 1982; Blondeaux and Seminara, 1985; Seminara, 2006; Hooke, 2013). The large amount of studies on fluvial meanders is counterbalanced by quite a few papers which analyzed the geometrical properties of tidal meanders (Marani et al., 2002) and their dynamic evolution (Solari et al., 2002), accounting for the effects of bidirectional flow-field (Fagherazzi et al., 2004) and of bed and bank sediment cohesion (Kleinhans et al., 2009), on the basis of field observations (Marani et al., 2002; Kleinhans et al., 2009), numerical modeling (Solari et al., 2002; Fagherazzi et al., 2004), and laboratory experiments (Garotta et al., 2006). Moreover, the internal architecture of tidal meandering channels remains relatively unexplored (Barwis, 1978; Brivio et al., 2016) as well as their migration dynamics (Gabet, 1998), particularly if the large body of

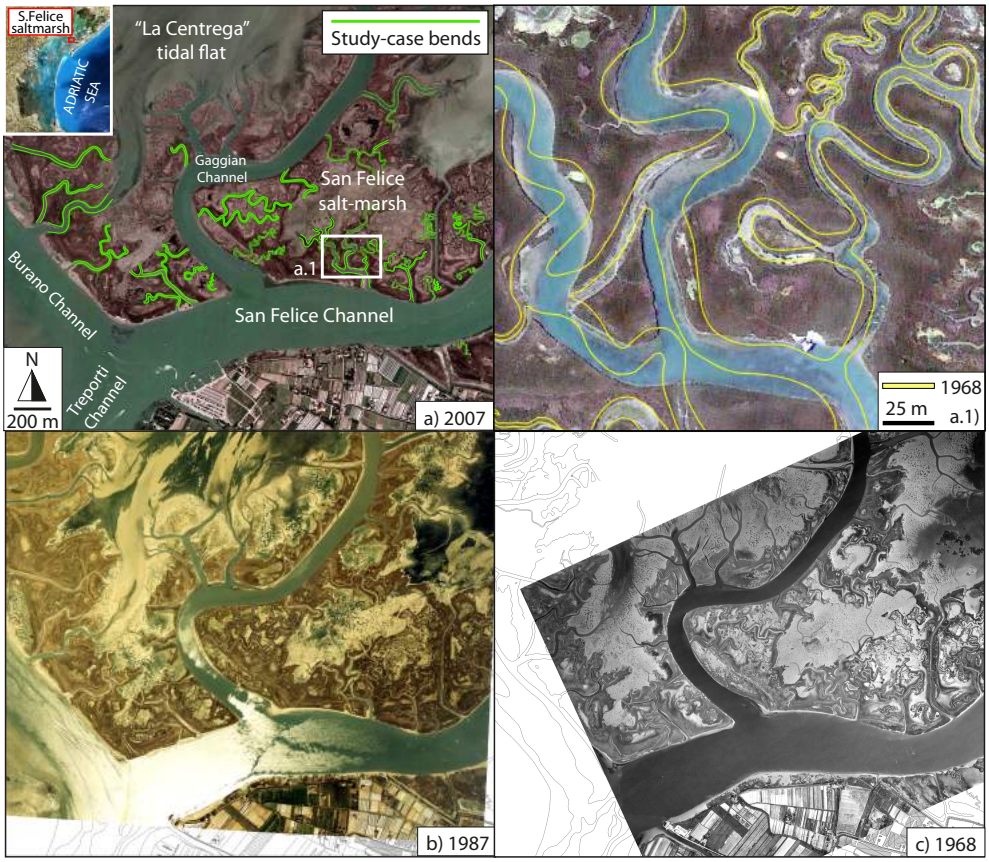

Figure 2.1: Aerial photographs of the study area. (Inset-a) Satellite image of the the Venice Lagoon. Characterized by an area of about 550 km^2, the Lagoon is connected to the Adriatic Sea through three inlets (Lido, Malamocco, and Chioggia) and is subjected to a semidiurnal tidal regime, with an average tidal range of about 1.0 m and peak tidal amplitudes of about 0.75 m around Mean Sea Level (MSL). The San Felice salt marsh, which is the study site for our analyses is highlighted. (a), (b) and (c): aerial photographs of the San Felice salt marsh and of the channel networks cutting through it. The San Felice salt marsh is located in the northern Venice Lagoon, which is one of the most naturally preserved portions of the Lagoon (Marani et al., 2003). Characterized by an average elevation of 0.26 m above MSL, it is mainly colonized by a mosaic of halophytic species, among which we find *Spartina maritima*, *Limonium narbonense*, *Sarcocornia fruticosa* and *Juncus maritimum* (Belluco et al., 2006). a.1) The analysis of the photos in 1968 and 2007 suggests that from 1968 to 2007 the channel-network configuration was almost preserved, despite watertight signs of meander evolution, such as channel avulsion and abandonment, as well as point-bar growth, meander migration and cut-off, are evident.

work on fluvial meanders is considered (Hickin and Nanson, 1975; Hickin and Nanson, 1984; Hooke, 1984; Nanson and Hickin, 1986; Thorne, 1991; Biedenharn et al., 1989; Lagasse et al., 2004).
This gap between the two bodies of literature calls for new insights on tidal meanders, which, besides displaying key morphodynamic differ-

ences compared to their fluvial counterparts (Brivio et al., 2016), are uniquely characterized by the constant, periodic reversal of the flow in response of tidal-phase variations. The mutually-balanced effect of bidirectional flows, together with the typical presence of highly cohesive bank and bed sediments, contributed to build tidal-meander reputation as quite stable features (Garofalo, 1980; Gabet, 1998), in spite of clear signs of both lateral erosion processes (e.g., bank undercutting, Gabet, 1998) fluvial-like migration dynamics (e.g., cut-offs Brivio et al., 2016). Improving our current understanding of tidal-meander dynamics is a fundamental step for disentangling the key role of tidal channels in the eco-morphodynamic evolution of lagoons and estuaries, with important consequences on the related stratal architecture and sedimentary products, as well as on wetland restoration. The present study aims at investigating tidal meander evolution, clarifying whether theories borrowed from the study of fluvial meanders can be applied to their tidal counterparts. The migration rates and dynamics of tidal meanders are investigated here by means of a sequence of high resolution orthophotos of the San Felice saltmarsh, in the Venice Lagoon (Figure 2.1). Two methods are applied to determine meander migration rates (see Methods): the Best Fitting Circle (BFC) (Lagasse et al., 2004) and the Homologous Points (HP) method. While the former represents a method widley employed in the literature of riverine meanders, the latter is a new procedure to objectively characterize meander displacements and planform features, such as width, curvature radius and sinuosity. Moreover, spectral properties of empirical channel curvature are extracted employing the Discrete Fourier Transforms, thus allowing for a comparative analysis with the theory of fluvial meanders (Ikeda et al., 1981; Parker et al., 1982; Blondeaux and Seminara, 1985; Seminara and Tubino, 1992; Seminara et al., 2001; Pittaluga et al., 2009).

2.1.3 Results and Discussion

We use the BFC method (Lagasse et al., 2004; Lagasse et al., 2001; Heo et al., 2009) (see Methods) to compute migration rates and express them as migration rates per unit width, $\zeta^* = \zeta/B$ [yr^{-1}] (Figure 2.4-a), as a function of the dimensionless ratio between radius of curvature and width, $R^* = R/B$ [-], for two periods of time, namely $1968-1987$ and $1987-2007$. Migration rates of tidal meanders are shown to be controlled by bend curvature: the ζ^* distribution in the $\{R^*;\zeta^*\}$ plane is enveloped by a bell-shaped curve that can be interpreted as the maximum-potential migration rate, as a function of bend curvature. Very poor correlations are observed between migration rates and channel-width variations (Figure 2.2), thus excluding that observed migration rates were due to channel broadening rather than

to real meander dynamics. The migration-rate curve reaches a maximum at $2 < R^* < 3$. As bend curvature decreases ($R^* < 2$), for a given channel width the highest potential for migration decreases rapidly, while it decreases more slowly for large values of the curvature radius ($R^* > 3$). The observed migration rates appear to be consistent for the two considered periods ($1968 - 1987$ and $1987 - 2007$). Although bends with $2 < R^* < 3$ are most likely to migrate at high rates, displaying the highest potential for erosion, data are generally clustered around relatively low values of both R^* and ζ^* and scatter widely for the considered range of R^*.

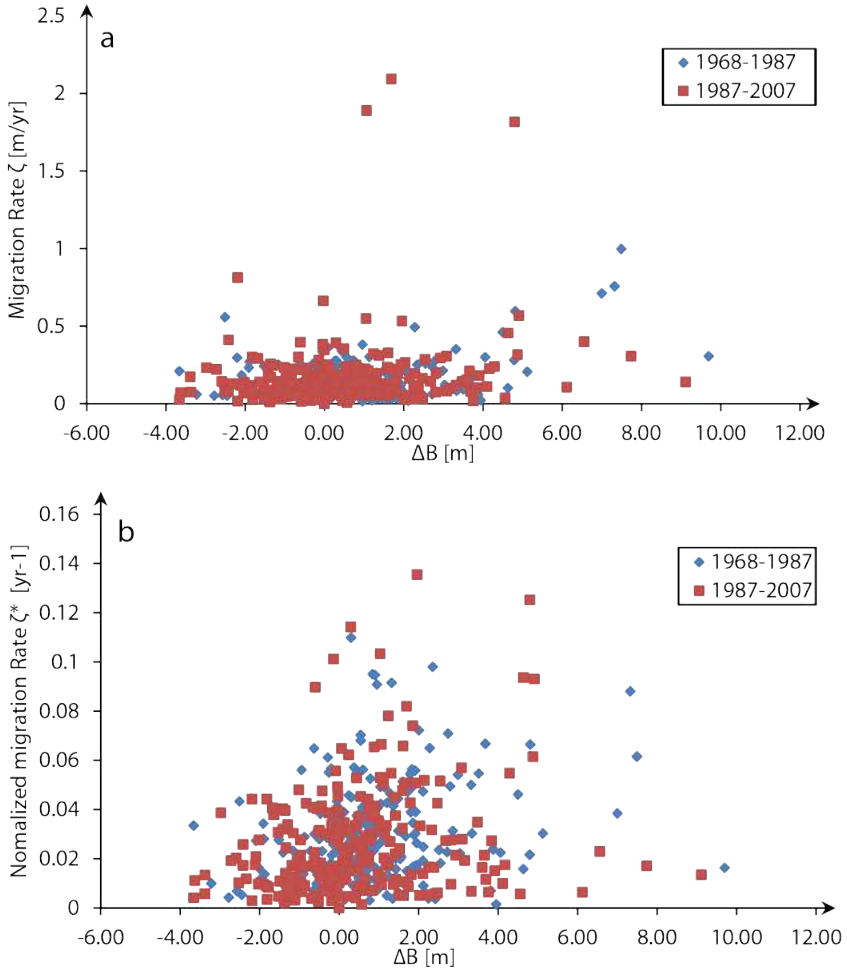

Figure 2.2: Tidal-Meander width variations are plotted against (a) dimensional and (b) width-normalized migration rates computed using the BFC method.

According to fluvial meander theories, the curvature-induced momentum redistribution and consequent secondary flow provide sufficient explanation for the control exerted by bend curvature on migration rates (Ikeda et al., 1981; Blondeaux and Seminara, 1985). Furthermore, the presence of a potential-migration peak at $2 < R^* < 4$ is a common feature of meandering rivers (Nanson and Hickin, 1986;

Hooke, 1987; Biedenharn et al., 1989; Lagasse et al., 2004). More interestingly, tidal data presented here agree with those by Lagasse et al. (Lagasse et al., 2004) observed from a total of 89 rivers (Figure 2.4-b). We find that the migration rates per unit width, ζ^*, of tidal meanders display the same maximum and median magnitude as those of fluvial ones (Figure 2.4-b 2.3). These results therefore suggest that, when scaled by channel width, tidal and fluvial meanders exhibit quite similar migration rates, furthermore challenging the reputation of tidal channels for being slowly evolving landscape features (Gabet, 1998). In the case of both tidal and fluvial meanders sharply curved bends ($R^* < 3$) are characterized by a large variance in migration rates per unit width. Possible explanations for such a variance in sharp bends are inner-bank flow separation, that excites secondary-flow induced erosion at the outer bank, and secondary flow saturation, which can conversely reduce outer-bank erosion (Blanckaert, 2011). In addition, such that scatter in Figure 2.4 can be interpreted as the manifestation of the presence of a whole family of curves (sensu Nanson and Hickin, 1986) characterized by different hydrodynamics and other local parameters, such as sediment characteristics and bank erodibility (Blanckaert, 2011). Finally, a comparison of channel migration rates per unit width versus curvature for a number of rivers (inset in Figure 2.4-b) shows that different datasets, independently of their fluvial or tidal origin, exhibit a maximum potential migration rate ζ^* at $2 < R^* < 3$ further emphasizing similarities between migration-rate magnitude and dynamics in fluvial and tidal landscapes.

The BFC method has doubtless proved to be an effective tool for characterizing meandering channel migration in a variety of environments, thanks to both its conceptual simplicity and relatively simple implementation. Nevertheless, this methodology suffers from some limitations, among which the most important are the subjective choice of the osculating circle and the fact that just the overall behaviour of a bend can be investigated. In order to overcome these limitations, we developed a new methodology, named Homologous Points (HP) method, which objectively identifies single meander bends and provides a spatially continuous characterization of local migration rates (see Methods for further details). Figure 2.5-a shows migration rates per unit width, ζ^*, as a function of the dimensionless radius, R^*, computed through the HP method, furthermore considering separately (inset in Figure 2.5-a) apex points and points other than the bend apexes. The resulting envelope curve has a shape similar to that obtained through the BFC method, with a peak in the potential migration rate for $2 < R^* < 3$ that is mainly determined by the migration rates of meander apical points (Figure 2.5-a). Nevertheless, the HP method provides estimate of the local migration rates, which can be

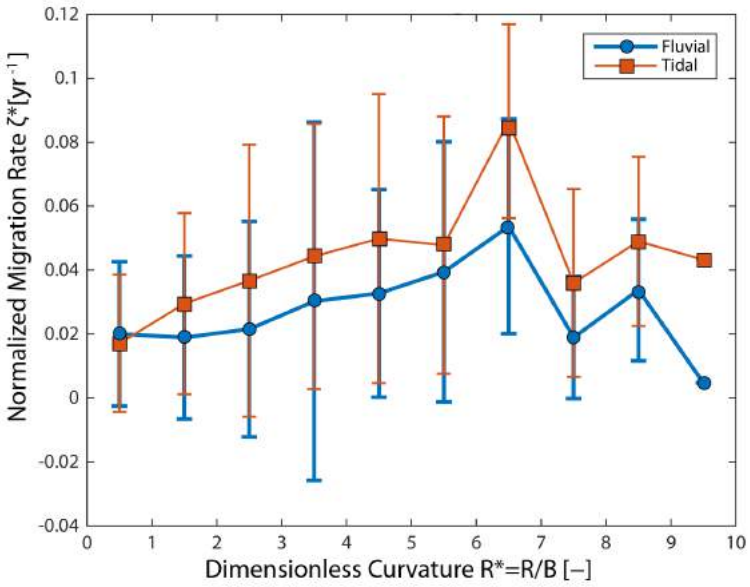

Figure 2.3: Comparison between binned-median values of the normalized migration rate for tidal (this study) and fluvial (Lagasse et al., 2004) meanders, computed with the BFC method. Bars represent 1 standard deviation.

up to two times larger than the meander-averaged migration rates obtained with the BFC method (apex points exhibit maximum and mean migration rates equal to $\zeta^*_{A\max} = 0.62$ yr^{-1} and $\bar{\zeta}^*_A = 0.35$ yr^{-1}, respectively). On the other hand, the distribution of migration rates of points other than the bend apexes is characterized by a relatively smoother peak in the range $5 < R^* < 6$ and a heavier tail (inset in Figure 2.5-a). Hence, also at the local scale, the potential migration rate is controlled by bend curvature, meaning that within a single meander points with higher curvature can potentially migrate faster. A lognormal function yielded the best fit to the binned maximum values of the migration rates. The highest correlation coefficient is found for the apex points ($r^2_A = 0.88$), while correlation coefficients obtained for every point other than the apexes ($r^2_O = 0.77$) and all the points ($r^2 = 0.67$) are smaller. The presence of local maximum in the distribution of a variable is usually dictated by two competing processes, that reduce (enhance) the considered variable (ζ^*) for small (great) values of the independent variable (R^*). It is known that strong channel curvature enhances both the secondary flow and the phase-lag between near bank velocity and the curvature itself (Parker et al., 1983; Seminara et al., 2001), thus resulting in more pronounced outer-bank erosion, and migration therefore. Nevertheless, in very sharp bends the increasing in curvature-induced secondary flow is limited by the growth of hydrodynamic nonlinearities (Blanckaert, 2009) that cause energy losses and reduce the erosion rates. These

phenomena, together with other site-specific factors such as bank-toe sediment grain-size (Nanson and Hickin, 1986) and abundance and type of vegetation(Garofalo, 1980), are crucial in determining actual meander migration rates, justifying both the peak and the large variance observed in ζ^* in the sharpest bends.
Although tidal meanders are uniquely shaped by bidirectional flows, potentially leading to planform features distinct from those of terrestrial rivers, no substantial differences between tidal and fluvial meander migration rates emerge. Therefore, some physical similarities between the two types of meander seem to be underlying. A possible explanation lies in the fact that in tidal landscapes either flood or, more commonly, ebb flows dominate the landscape formation processes, thus preferentially shaping meanders and their bars in a way similar to their fluvial counterparts.

The BFC method has doubtless proved to be an effective tool for characterizing meandering channel migration in a variety of environments, thanks to both its conceptual simplicity and relatively simple implementation. Nevertheless, this methodology suffers from some limitations, among which the most important are the subjective choice of the osculating circle and the fact that just the overall behaviour of a bend can be investigated. In order to overcome these limitations, we developed a new methodology, named Homologous Points (HP) method, which objectively identifies single meander bends and provides a spatially continuous characterization of local migration rates (see Methods for further details). Figure 2.5-a shows migration rates per unit width, ζ^*, as a function of the dimensionless radius, R^*, computed through the HP method, furthermore considering separately (inset in Figure 2.5-a) apex points and points other than the bend apexes. The resulting envelope curve has a shape similar to that obtained through the BFC method, with a peak in the potential migration rate for $2 < R^* < 3$ that is mainly determined by the migration rates of meander apical points (Figure 2.5-a). Nevertheless, the HP method provides estimate of the local migration rates, which can be up to two times larger than the meander-averaged migration rates obtained with the BFC method (apex points exhibit maximum and mean migration rates equal to $\zeta^*_{A\max} = 0.62\ \mathrm{yr}^{-1}$ and $\bar{\zeta}^*_A = 0.35\ \mathrm{yr}^{-1}$, respectively). On the other hand, the distribution of migration rates of points other than the bend apexes is characterized by a relatively smoother peak in the range $5 < R^* < 6$ and a heavier tail (inset in Figure 2.5-a). Hence, also at the local scale, the potential migration rate is controlled by bend curvature, meaning that within a single meander points with higher curvature can potentially migrate faster. A lognormal function yielded the best fit to the binned maximum values of the migration rates. The highest correlation coefficient is

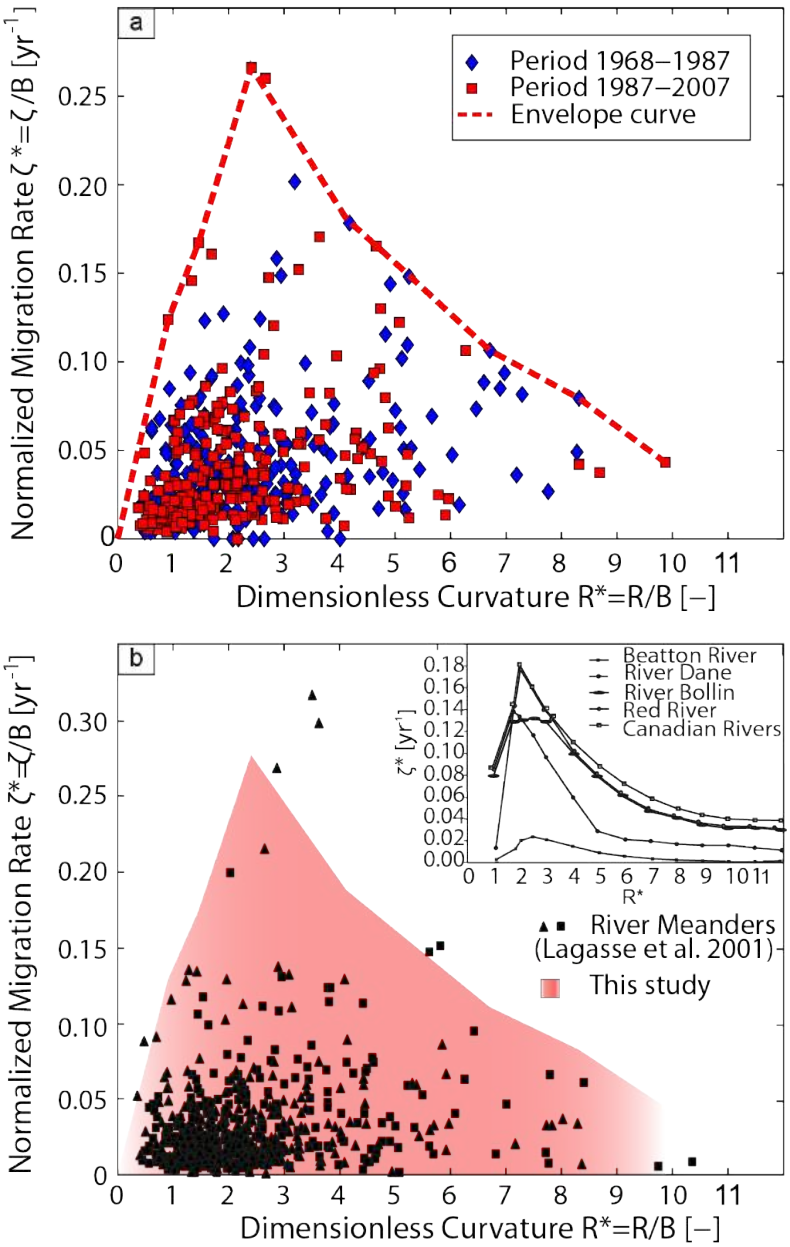

Figure 2.4: Migration rates as a function of bend curvature characterized through the BFC method. Migration rates per unit width, $\zeta^* = \zeta/B$ [yr^{-1}] are plotted versus the dimensionless radius of curvature, $R^* = R/B$ [–]. (a) Tidal meander data calculated in this study for the two considered periods, namely $1968 - 1987$ and $1987 - 2007$; red line represents the envelope of the data, computed as their shrinked convex hull. A $\xi = 0.1$ shrink factor was applied, where $\xi = 0$ provides the convex hull and $\xi = 1$ the concave hull, repectively. (b) Fluvial data derived from Lagasse et al. (Lagasse et al., 2001) are plotted, together with their envelope curve (green line, $\xi = 0.1$). The envelope curve calculated for tidal meanders is also shown. The inset shows data from the fluvial realm (adapted from Hooke, 2013).

found for the apex points ($r^2_A = 0.88$), while correlation coefficients obtained for every point other than the apexes ($r^2_O = 0.77$) and all the points ($r^2 = 0.67$) are smaller. The presence of local maximum in the distribution of a variable is usually dictated by two competing processes, that reduce (enhance) the considered variable (ζ^*) for small (great) values of the independent variable (R^*). It has known that strong channel curvature enhance both the secondary flow and the phase-lag between near bank velocity and the curvature itself (Parker et al., 1983; Seminara et al., 2001), thus resulting in more pronounced outer-bank erosion, and therefore migration. Nevertheless, in very sharp bends the increasing in curvature-induced secondary flow is limited by growth of hydrodynamic nonlinearities (Blanckaert, 2011) that cause energy losses and reduce the erosion rates. These phenomena, together with other site-specific factors such as bank-toe sediment grain-size (Nanson and Hickin, 1986) and abundance and type of vegetation (Garofalo, 1980), are crucial in determining actual meander migration rates, justifying both the peak and the large variance observed in ζ^* in the sharpest bends.

Although tidal meanders are shaped by bidirectional flows, potentially leading to planform features distinct from those of terrestrial rivers, no substantial differences between tidal and fluvial meander migration rates emerge. A possible explanation lies in the fact that either flood or, more commonly, ebb flows dominate the landscape formation processes, thus preferentially shaping meanders and their bars in a way similar to their fluvial counterparts.

The violin plot of the binned migration rates (Figure 2.5-b) provides information on the probability distribution of ζ^* for given intervals of bend-curvature values. Two peaks are observed for R^* in the ranges $2 < R^* < 3$ and $5 < R^* < 6$, representing the set of data relative to the apex points and all the other points, respectively. Both the mean and the median of the distributions slightly increase for values of R^* up to 4 and then attain an almost constant value around 0.05 yr^{-1} and 0.04 yr^{-1}, respectively (within every bin, the mean is constantly greater than the median as a consequence of right-skewed lognormal distributions). In agreement with the limited existing literature (Gabet, 1998), a value of $\bar{\zeta}^* = 0.45\%$ yr^{-1} has been found. Although potential migration rates (ζ^*)per unit width display quite similar values for tidal and fluvial environments, their dimensional counterparts (ζ) can generally be very different (Figure 2.5-c). In fact, a mean migration rate $\bar{\zeta} = 0.17 \pm 0.19$ m/yr (0.14 ± 0.17 m/yr with the BFC method) results for tidal meanders as compared to values ranging from a few meters to hundreds of meters per year that have been observed for alluvial rivers (Hickin and Nanson, 1975; Thorne, 1991; Hudson and Kessel, 2000). The values of dimensional migration rates computed here are in agreement to those obtained for the New Jersey

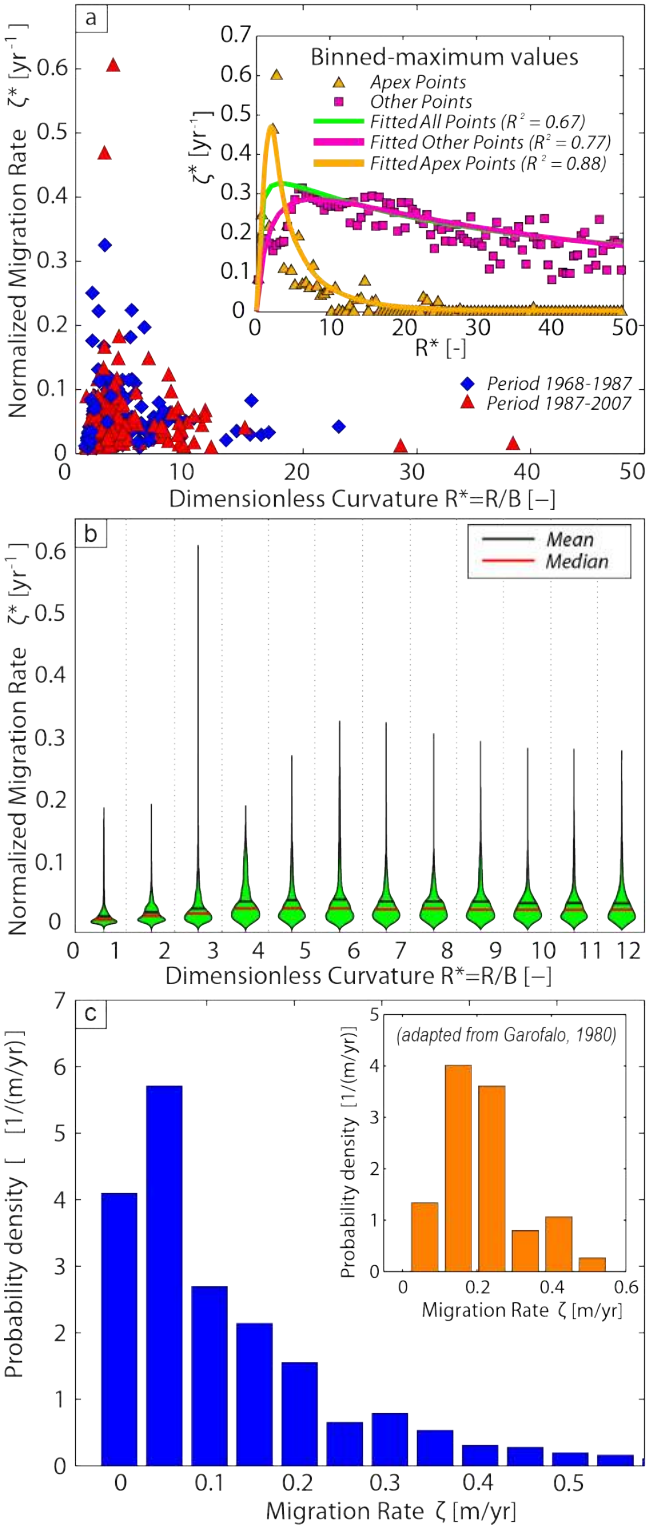

Figure 2.5: Continuous characterization of meander migration rates (on the basis of the HP method). (A) Normalized migration rate (ζ^*) vs. dimensionless curvature (R^*). For the sake of clarity, only results for apex points are entirely represented, whereas for both apex and all other points the maximum binned values are reported into the inset. (B) Violin plots of ζ^*-binned values. The mean (black lines) and the median (red line) of the distributions are also shown. (C) Probability density function of the migration rates (ζ). The inset shows the results obtained for New Jersey Wetlands by Garofalo et al. (Garofalo, 1980).

wetlands ($\bar{\zeta} = 0.23 \pm 0.2$ m/yr) (Garofalo, 1980), although the latter were referred to the migration of whole tidal channels rather than to single meanders. The relative frequency distribution of dimensional meander migration rates, ζ, appear to be right skewed (Skewness coefficient = 4.0) and can be fitted by a lognormal function.

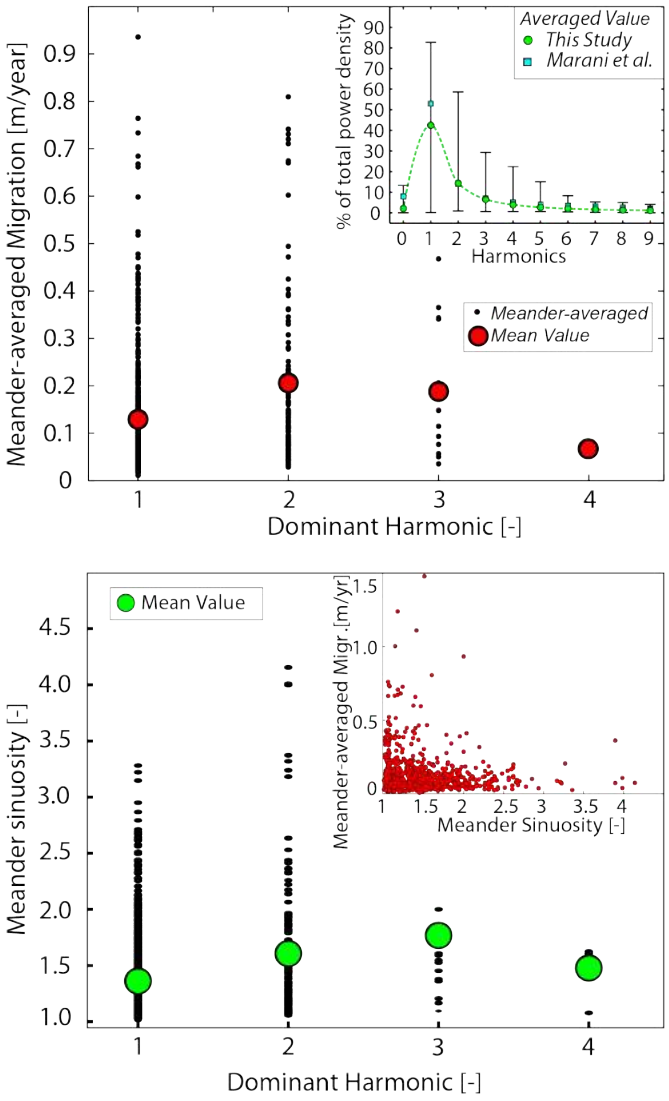

Figure 2.6: (a) Meander-averaged migration rates vs. meander dominant harmonics. Red dots represent the mean migration rate for each harmonic. The inset shows the curvature spectrum, together with average power density values obtained by Marani et al. (Marani et al., 2002). The vertical bars represent data range for the considered harmonics. (b) Meander sinuosity vs meander dominant harmonics. Green dots represent the mean sinuosity for each dominant harmonic. The inset shows meander-averaged migration rates vs. meander sinuosity.

Further comparisons between fluvial and tidal meandering patterns can be carried out by analyzing the spectral properties of the observed

channel patterns. A well established framework developed in the fluvial setting expresses meander curvature in terms of a sine-cosine generated curve (Kinoshita, 1961; Langbein and Leopold, 1966; Ikeda et al., 1981; Seminara et al., 2001). By analyzing, via Discrete Fourier Transforms, the curvature signal (Marani et al., 2002) the relationships between the various harmonics of the curvature spectrum, meander migration and sinuosity can be evalueted. On average, for a given meander bend, the first harmonic is found to dominate, although in some cases higher order harmonics prevail as suggested by the wide distribution ranges (inset in Figure 2.6-a). While the first order harmonic results in simple, sine-generated curve (Langbein and Leopold, 1966), its interaction with higher order harmonics causes the progressive "fattening" and skewing of the meander shape, increasing its planform sinuosity (Kinoshita, 1961; Seminara et al., 2001). High order harmonics are, in their turn, known to develop during meander evolution, their presence indicating a mature, highly sinuous meander indeed. However, such evolutionary pathway was not completely observable from our data, given the relative limitedness of the considered time span. We have therefore deducted the development stage of every individual meander by considering its dominant harmonic K, that is the harmonic containing the largest fraction of total power density. This provides us a rough, but nonetheless correct, first approximation of meander maturity, because the dominance of high order harmonics implies such harmonic to have non-negligible value, the latter being true for well-grown meanders. Our analysis indicates (Figure 2.6-a) that when the first harmonic is dominant the mean meander-averaged migration rate is about 0.13 m/yr. This value increases to a maximum close to 0.2 m/yr when the second harmonic becomes dominant, and it subsequently decreases for dominant harmonics of higher order. This observation agrees with nonlinear river meander models (Pittaluga et al., 2009), showing that bend-growth rate peaks at some intermediate harmonic value. A similar pattern is also observed when analyzing meander sinuosity σ as a function of the dominant harmonic, K: in this case σ reaches its maximum when the third harmonic dominates (Figure 2.6-b). Again, such a behaviour agrees with theories developed for fluvial meanders (Seminara et al., 2001), whereby the formation of the third harmonic in curvature spectrum is related to an increase in meander intrinsic wavelength, and therefore in meander sinuosity. Note that the meander-averaged migration rate decreases while meander sinuosity increases (inset of Figure 2.6-b), confirming that well-developed, sinuous meanders are in general more stable.

Our results therefore suggest a non-linear character in tidal meander evolution process, where an initial growth stage is followed by a decrease in the migration rate when meanders become more mature

(i.e., when sinuosity increases and higher order harmonics start to develop).

2.1.4 Conclusions

Even though many differences between fluvial and tidal meanders can be identified, particularly the occurrence of bidirectional flows shaping the latter, evidence from the analysis of aerial photos and modeling interpretation shows that if one considers the planform evolution of meander bends, differences are the exception rather than the rule. In fact, tidal meanders display modes of migration and dimensionless migration rates comparable to those characterizing their fluvial counterparts, thus challenging the notion that they are stable tidal landscape features. The non-linear relationship between maximum potential migration rates per unit width and dimensionless channel curvature, typically observed for fluvial patterns, is also characteristic of tidal ones: bend curvature crucially drives meander migration, both at the bend and local scale. The only relevant dissimilarity concerns values of absolute dimensional migration rates of tidal meanders, which are indeed orders of magnitudes smaller than those exhibited by their fluvial counterparts. However, this occurrence appears to be fully justifiable by the sheer difference in the sizes of the two systems. A similarity between tidal and fluvial meanders is also supported by the Discrete Fourier Transforms analysis of the curvature signal, which suggests that tidal meander dynamics displays strong analogies with the fluvial case, particularly evident in the increase in meander migration rates and sinuosity as the second and third harmonics, respectively, develop and become dominant. Besides challenging tidal-meander reputation of being quite stable morphological features, this result might implies that a similarity in physics exists between fluvial and tidal meanders, that outweighs the role exerted by bidirectional flows and leads to planform meander dynamics similar to terrestrial rivers. The dominance of either ebb or flood flow in tidal environments stands out as the most reasonable explanation for such a behaviour, even though the latter observation does not imply that the non-dominat flow has no effects, particularly in determining both sediment distribution within tidal point bars and peculiar morphologies observed in tidal meanders worldwide (e.g., channel funnelling, cusp- and box-shaped bends), which appear to be qualitatively different from those of fluvial meanders. These results can have important implications on our understanding of tidal channel shapes and dynamics, improving current methodologies adopted for wetland restoration and ecosystem-based coastal defence, even though it persists the dearth of a well developed prosody to quantitatively distinguish fluvial and tidal meanders from a planimetric point of view.

2.1.5 Methods

We use three sets of aerial photographs (Figure 2.1) acquired in 1968, 1987, and 2007, of tidal channels dissecting the San Felice salt marsh, in the Venice lagoon. All images were georeferenced to an accuracy of ± 0.1 m, and the two couples of images (1968−1987 and 1987−2007) were superimposed to obtain a map of the channel banks. We selected only bends which are included and clearly detectable in all of the photos, in order to prevent misleading results due to the incorrect identification of channel banks. Banks of chosen meanders were firstly digitized in a GIS environment: in the case a bifurcation of the network occurred, digitalization was continued only for the major reach, whereas a new digitalization was started for minor lateral tributaries.

Best Fitting Circle (BFC) method

Every meander bend is described by a series of delineation points, and the coordinates ($\{x_{c_B}, y_{c_B}\}$) and radius (R_B) of the best-fitting circle are computed by solving a linear system (Lagasse et al., 2004). The comparison of two different planar configurations at times t and $t + \Delta t$ allows us to calculate the rate of migration $\zeta_B = \sqrt{(\Delta x)^2 + (\Delta y)^2}/\Delta t$, where $\Delta x = x_{c_B}(t + \Delta t) - x_{c_B}(t)$ and $\Delta y = y_{c_B}(t + \Delta t) - y_{c_B}(t)$. Meander wavelength ($\ell_{xy}$), amplitude ($\mathcal{A}$), and width ($B$) are also measured. The main advantage of this method lies in its simplicity, although questions arise about its limitations, especially with respect to its arbitrariness. The radius of curvature, in fact, can be significantly different depending on how the circle is fit to the bend, especially for the smallest values of R_B. Furthermore, meander bends are rarely perfectly round with smooth bank lines. Hence, in many cases it is difficult to objectively identify where does a bend start and end. Finally, the actual meander migration is more complex than that identified by the BFC method: for example one part of the bend may be expanding or translating faster than another, resulting in changes in bend symmetry.

Homologous Points (HP) method

We apply a well-developed technique (Marani et al., 2002) to objectively identify and continuously characterize tidal meander geometry, which is based on a mathematical definition of the curve $\Gamma(s) = (x(s), y(s))$ where x and y are the Cartesian coordinates of the arbitrary axis point and s is its intrinsic coordinate, assumed to be pos-

itive if directed landward. The curvature $C(s)$ ($[L^{-1}]$) is therefore calculated as:

$$C = -\frac{d\theta}{ds} = \frac{\left[\frac{dx}{ds}\frac{d^2y}{ds^2} - \frac{dy}{ds}\frac{d^2x}{ds^2}\right]}{\left[\left(\frac{dx}{ds}\right)^2 + \left(\frac{dy}{ds}\right)^2\right]^{3/2}} \tag{2.1}$$

where θ is the angle between the tangent to the channel axis and the horizontal direction. A Savitzky-Golay low-pass filter is then applied to smooth noises in the curvature signal (Hamming, 1989; Fagherazzi et al., 2004). Inflexion (s_i) and apex (s_a) points, are identified as points of null ($C(s_i) = 0$) and local-maximum curvature ($C(s_a) = C_{MAX}$), respectively. A meander is then defined as a channel reach included between three consecutive inflection points. Geometrical features, such as channel width ($B(s)$), meander intrinsic wavelength (ℓ_s), are then computed along the intrinsic coordinate s, as well as the Cartesian wavelength (ℓ_{xy}), defined by the distance between the initial and the final section of the meander. Meander sinuosity is finally defined as $\sigma = \ell_s/\ell_{xy}$. In order to compute migration rates, every meander is firstly divided into a series of $\mathcal{N} = 100$ equally-spaced points, including the apex point. The landward (seaward) half-meander portion, which is the reach included between the apex and the most landward (seaward) inflexion point, is therefore divided into $(\mathcal{N}/2) - 1$ branches. After that, the displacement of the n^{th}-point (δ_n) is calculated as the homologous point distance between the initial (at time t) and final (at time $t + \Delta t$) channel planform configuration

$$\delta_n = \sqrt{[x_n(t + \Delta t) - x_n(t)]^2 + [y_n(t + \Delta t) - y_n(t)]^2} \tag{2.2}$$

The migration rate ζ_n of n^{th}-point is finally determined as

$$\zeta_n = \frac{\delta_n}{\Delta t} \tag{2.3}$$

The displacement could have been calculated along the direction perpendicular to the channel axis. However this method might have led to incorrect results, especially when bends are sharp and expansion is not the only chief migration way. Without loss of generality, the analyses were carried out considering every half-meander independently, in order to analyse every single channel bend, thus making possible a comparison with the results obtained with the first methodology.

2.2 THE DEGREE OF KINSHIP AMONG TIDAL AND FLUVIAL MEANDER PLANFORMS

This chapter is a manuscript in preparation for submission to Nature Geoscience and addresses the question of whether quantitative differences between tidal and fluvial meandering planforms exist, from meander- to reach-length scale. A quantitative objective analysis, employing statistical and spectral methods, of a suitable set of morphometric variables demonstrated that planform differences between tidal and fluvial meanders can be successfully detected and quantified. This analysis is valuable in that the results might allow one to distinguish tidal meanders and channels from their fluvial counterparts on the exclusive basis of their planimetric configuration.

PAPER

Finotello, Alvise[1], Manuel Bogoni[2], Andrea D'Alpaos[1], Massimiliano Ghinassi[1] and Stefano Lanzoni[2]

[1]Dept. of Geosciences, University of Padova, via G.Gradenigo 6, Padova, PD I-35131, Italy
[2]Dept. ICEA, Univesrity of Padova, via Loredan 20, Padova, PD I-35131, Italy

2.2.1 Abstract

Being shaped by fundamentally different chief-landforming processes, tidal and fluvial meandering channels are generally agreed to display different planform geometries (Bridges and Leeder, 1976; Fagherazzi et al., 2004). However, despite a number of qualitative dissimilarities exists (Barwis, 1978), prior studies did not achieve a consensus view oh whether or how tidal and fluvial planforms qualitatively differ. Here we present a series of statistical analyses, carried out on a dataset including several morphological variables for about 10000 meander bends over 98 tidal and fluvial channels worldwide. We find that, even though some morphological features are stastically different in themselves, an exhaustive and quantitative differentiation between the two typologies of channels may be achieved only by considering a suitable set of morphometric variables. Moreover, our results show that, at the single meander length-scale, tidal meander are less morphologically complex than their fluvial relatives. On the contrary, if a train of consecutive meanders is considered, fluvial streams appear to be more morphologically homogeneous, whereas in the tidal realm the planforms of a given meander are less similar

to those of other meanders belonging to the same reach. On the basis of these observations, we interpret the higher uniformity of tidal channels as a consequence of the regularity of their main landforming processes, as well as of the homogeneity of the basin substrate they typically cut through.

2.2.2 Introduction

Sinuous tidal channel networks represent one of the most fascinating patterns existing in nature. Shaped by cyclic tidal flooding of flat longshore areas (Knighton et al., 1992; Fagherazzi and Sun,2004; D'Alpaos et al., 2006; Vlaswinkel and Cantelli, 2011; Mariotti and Fagherazzi, 2013), or evolved along drowned fluvial channels when relative sea level rises (Gardner and Bohn, 1980), tidal channels are ubiquitous features of tidal landscapes. These widespread features play a fundamental role on the ecomorphodynamic evolution of coastal landscapes, serving as the main conduits through which tides propagate, sediments and nutrients are transported, and biota are exchanged with the open sea in tidal coastal landscapes (Hughes, 2012). A certain degree of parallelism between tidal and fluvial meandering channels has typically been assumed in the literature, given that well developed morphologies are at a glance similar in both realms. Particularly, planform geometries such as highly sinuous channels (Marani et al., 2002), the presence of cut-off meanders ('oxbow lakes', see Brivio et al., 2016) and signs of meander lateral migration ('scroll bars', see Hood, 2010) show marked similarities with those of their fluvial counterparts. Similar depositional architectures (Barwis, 1978; de Mowbray, 1983; Choi et al., 2004; Choi, 2011) seem to further support this analogy. However, a glaring gap exists in this morphologic and stratigraphic parallels, since several different hydrodynamic processes carve tidal and fluvial meander morphologies. Particularly, the periodic reversal of tidal flows certainly drives a wedge between the two families of meanders. As a consequence, in tidal channels highest discharges and velocities are typically observed for water levels different from, yet close to, the elevation of surrounding platform ('bankfull stage', see Bayliss-Smith et al., 1979; Hughes, 2012), which instead corresponds to the formative discharges in the riverine framework. Moreover, while rivers are characterized by flood events, with high velocity stages lasting for days/weeks, interspersed in low discharge periods through the year, tidal-channel discharges experience strong variations over a tidal period (hours) but are constrained in a well defined range of possible values. Furthermore, tidal and fluvial channels commonly differ in number of lateral tributaries, with the former exhibiting an higher spatial density than the latter. Finally, flow in river networks is typically driven by topographic gradients, whereas the water-surface driven

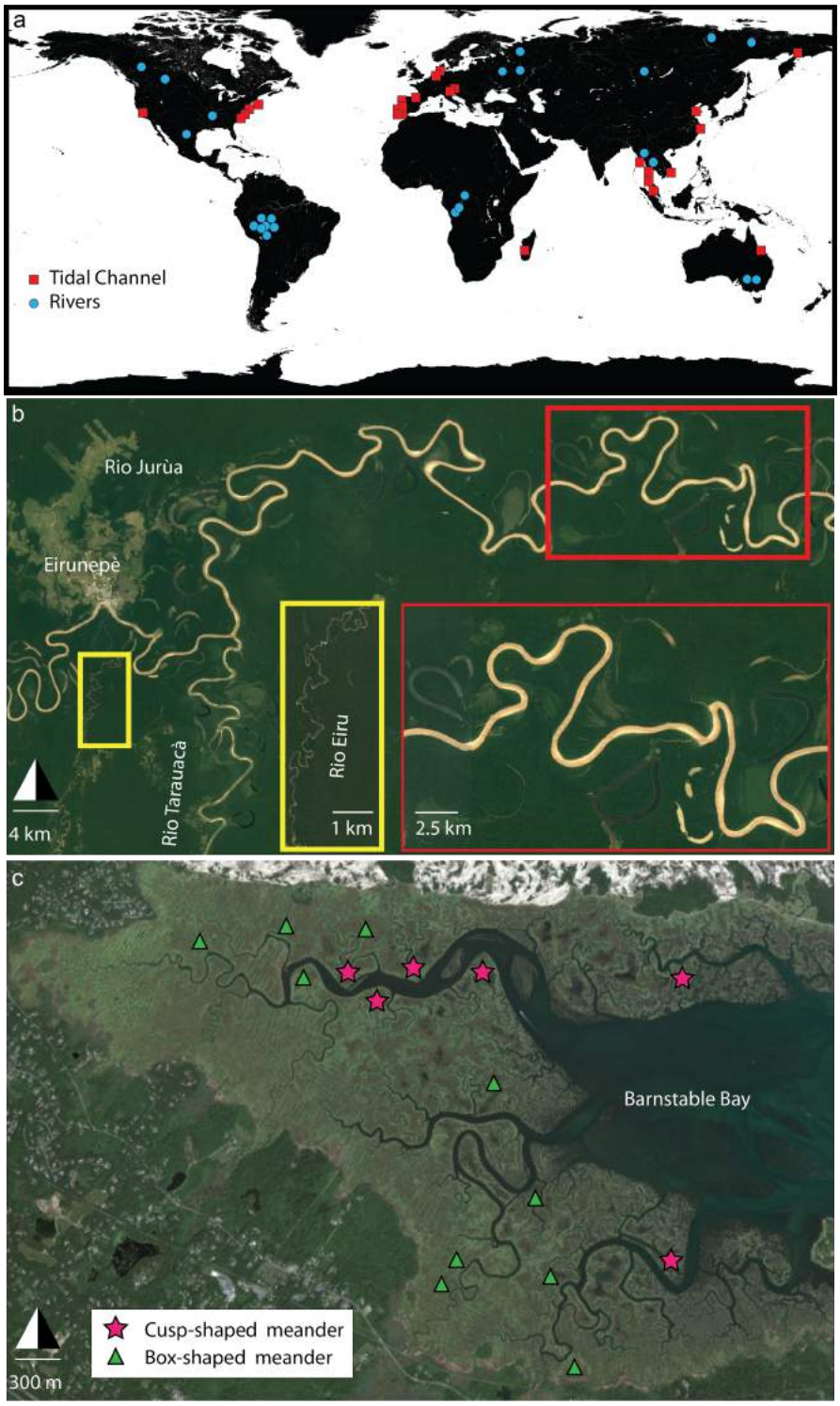

Figure 2.7: Tidal and Fluvial channels (a) Locations of tidal and fluvial channels considered in this study. (b) Confluence of R. Eiru and R.Tarauacá with R.Jurua, Amazonas (BR). All rivers freely meander for hundred of kilometers; yellow inset: a train of about 50 meander along R.Eiru; red inset: several oxbow lakes and scroll bars along R.Jurua (©Google, Landsat). (c) Tidal channel networks in Barnstable Bay (MA) displaying densely spaced lateral tributaries, width funneling and peculiar tidal meander morphologies.

flow in tidal channels promotes the formation of the channels (Rinaldo et al., 1999b; Fagherazzi, 2008; Coco et al., 2013), as topography is quite flat. The aforementioned differences, led by the mutually-evasive pathways of flood and ebb flows, are known to produce some peculiar qualitative morphologies belonging to the tidal meander dynasty. Certainly a strong landward decay in channel width ('funneling') is observed in tidal channels as a consequence of the reduction in tidal prism, and therefore in water discharges, moving landward (Lanzoni and D'Alpaos, 2015). Moreover, the back-and-forth swinging of tidal currents caused by flow inertia, that displaces the ebb (flood) current toward the seaward (landward) edge of the channel (Ahnert, 1960; Fagherazzi et al., 2004; Dalrymple et al., 2010; Hughes, 2012) is likely responsible for the distinctive cuspate shape displayed by the inner banks of many tidal meanders. The same phenomenon leads to the formation of the so called "box-shaped" meanders (Dalrymple et al., 2010), that is a quasi-square meander including two right-angle-like turns, classified as 'compound symmetrical' according to Brice (1974) classification. It is finally a matter of undisputed fact how tidal channel are shorter in length compared to their fluvial relatives, and that long meander trains are unlikely to occur (e.g., in Figure 2.7 the Rio Juruà is meandering along its 2414 km long course, whereas the longest tidal channel in Barnstable Bay contains about 60 meander bends and barely covers 5 km in length).

In spite of all these qualitative dissimilarities, the degree of kinship among the planform geometry of the two types of channels remains unclear. Few studies have in fact attempted to compare tidal and river channels at the meander- or reach-scale, providing empirical values for tidal meander geometric features, such as wavelengths, asymmetry index and sinuosity (Marani et al., 2002; Fagherazzi et al., 2004; Bain, 2014). However, a marked variability was observed for all the investigated features, and a consensus view on whether or how tidal and fluvial planforms quantitatively differ has still not been achieved.

Our goal is to understand whether the signatures of different processes sculpting tidal and fluvial meanders might be unraveled by the analysis of their planform configurations. Beside having direct implication for distinguishing tidal and fluvial channels from 3D seismic images, the importance of the careful observation of planar patterns in tidal wetlands is linked to the implications on the origin and long-term evolution of the complex morphological structures which characterize such environments, such as lagoons, deltas or estuaries (Marani et al., 2002). Therefore, we specifically developed a meander database, digitizing different aerial photos and extracting 39 different morphometric variables (Table 2.2) of 40 rivers and 58 tidal channels worldwide (Table 2.3), including as much as possible different environmental and geological contexts. As for tidal channels, we only considered

reaches containing at least 20 consecutive bends, in order to attain a close similarity with rivers where long trains of meanders are typically observed. The method we used to characterize meanders and reaches is based on the calculation of local curvature ($C[m^{-1}]$) along the intrinsic coordinate ($s[m]$, see Methods). All the dimensional variables are normalized with the mean half-channel width ($B_0[m]$), so that a direct comparison between the two groups is made possible.

2.2.3 Methods

Meander identification and characterization

We adopted the elegant procedure described in Marani et al. (2002) to objectively identify meanders and continuosly charcaterized their properties. We hereinafter report a brief summary of the aforementioned procedure, that is based on a mathematical definition of the curve $\Gamma(s) = \{(x(s), y(s)\}$, where x and y are the cartesian coordinates of the arbitrary axis point and s is its intrinsic coordinate.

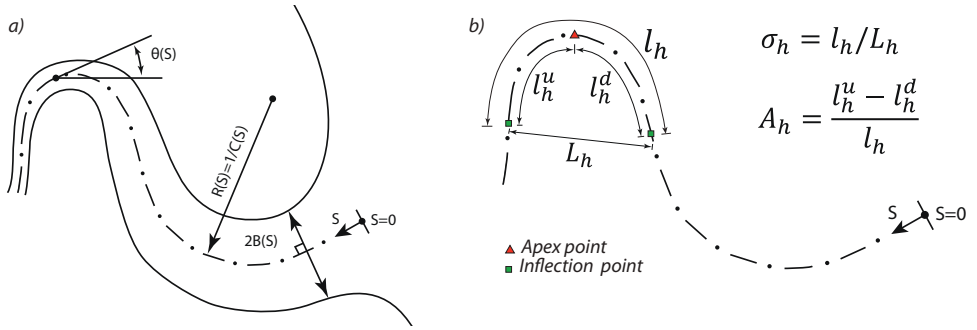

Figure 2.8: a) Sketch of a meander showing the parameters employed for describing the geometry of a meandering channel (adapted from Marani et al., 2002); b) Characterization of half-meander bend.

The geometry of the channel axis may be defined through its planar curvature $C(s)[m^{-1}]$, i.e., the inverse of the local radius of curvature. The characterization of planar curvature along the intrinsic coordinate s is based on the numerical determination of the functions $\theta(s)$ (i.e., the angle formed by the tangent to the axis and the horizontal direction, Figure 2.8) through the elementary relationship (Marani et al., 2002; Fagherazzi et al., 2004):

$$C(s) = -\frac{d\theta(s)}{ds} = \frac{\left[\frac{dx}{ds}\frac{d^2y}{ds^2} - \frac{dy}{ds}\frac{d^2x}{ds^2}\right]}{\left[\left(\frac{dx}{ds}\right)^2 + \left(\frac{dy}{ds}\right)^2\right]^{3/2}} \tag{2.4}$$

Important characteristics of a meander are also its intrinsic wavelength (l), computed along the s coordinate, and the cartesian wavelength, L, defined by the (cartesian) distance between the initial and the end sections of the meander. These sections are located in correspondence of the axis-inflection points, i.e., sites s_i where $C_{s_i} = 0$, and a full meander may be defined as any portion of the channel along s containing three such inflection points. On the contrary, half a meander is defined as a channel reach included between two consecutive inflection points. The planar characterization of a meandering channel is completed by its half width $B(s)[m]$, and by the coordinates s_a of the apexes, i.e., the points where the curvature has a local extreme, defined by $dC(S)/ds = 0$. The apex divides a meander into two different portion, namely the upstream and downstream portions, whose intrinsic lengths (l_u and l_d) allow one to define the meander asymmetry index:

$$A = \frac{l_u - l_d}{l}[-] \tag{2.5}$$

whereas the meander sinuosity is defined as the ratio between its intrinsic and cartesian wavelength:

$$\sigma = \frac{l}{L}[-] \tag{2.6}$$

All the definition may be indistinctly applied to both full and half meanders, once conveniently identified.

Fourier Analysis

In order to analyse the spectral properties of the observed full meanders, it is necassary to produce a representation of its axis $\{x(s); y(s)\}$ along a series of discrete points. The curvature signal is therefore resampled using a cubic spline interpolant, providing a signal known at N locations separated by sampling length Δs ($C_n = C(s_n)$ with $s_n = n \cdot \Delta s$, $n = 0, ..., N-1$). Note that $N \cdot \Delta s$ is equal to the meander intrinsic length l_F. The Discrete Fourier Transfrom yelds a set of N harmonic magnitudes, defined as such:

$$\hat{C_k} = \sum_{n=0}^{N-1} C_n e^{-i\frac{2\pi n}{N}k} \tag{2.7}$$

Here n is used to represent the space-domain ordinal, N is the length of the sequence to be transformed, and k is used to denote the harmonic (i.e., wavenumber) domain ordinal. Similar to the Δs-spacing samples of C_n in the space domain, wavenumber resolution between the components of $\hat{C_k}$ in the wavenumber domain reads:

$$\Delta k = \frac{1}{N\Delta s} = \frac{1}{l_F} \tag{2.8}$$

that is known as the fundamental wavenumber.

Since the operation treats the signal as if it was periodic of period l_s, the evaluation of $\hat{C}_k$ is carried out for the fundamental wavenumber and its harmonics (i.e., $k = 0, ..., N-1$). It is finally worth mentioning that every full meander in our dataset has been considered as a DC-free waveform, that is filtering out the mean value of the curvature signal ('DC component'). This operation produces curvature spectra with mean null power spectral density along the zero-order harmonic.

Singular Spectrum Analysis

Singular Spectrum Analysis (SSA) is a technique of time series analysis incorporating the elements of classical time series analysis, multivariate statistics, multivariate geometry, dynamical systems and signal processing. In particular, SSA provides adaptive filters associated with the dominant oscillations of the system, clarifying the characteristics of the possible noise affecting the data (Vautard and Ghil, 1989). The numerical procedure is here summarized, based on the work of Ghil et al. (2002).

The starting point is to embed a time (space) series X_i, $(i = 1, N)$ into a vector space of dimension M. The Singular Value Decomposition (SVD) of the $M \times M$ lag-covariance matrix $\mathbf{C_X}$ provides the M eigenvalues λ_k, taken in decreasing order of magnitude, and the corresponding eigenvectors $\mathbf{y}_k$ $(k = 1, M)$. Projecting the original time series into each eigenvector yields the corresponding principal components (PCs), and thus the reconstructed components (RCs) of the pristine signal. No information is lost in the reconstruction process, as the sum of all individual RCs reads back to the original signal. The choice of the window length M is based on a trade-off between the quantity of extracted information (large M) versus the degree of statistical confidence in that information (large N/M).

The singular values (SV), defined as the square roots of the eigenvalues, $\lambda_k^{1/2}$, lead to a possible separation between fundamental components of the signal and higher-order noise, therefore being an indicator of the signal complexity due to its splitting along the M components.

The Multivariate Singular Spectrum Analysis (or Multi-channel Singular Spectrum analysis, MSSA) is an extension of SSA to a multivariate input signal composed by L channels.

2.2.4 Results and discussions

We initally focus on a single morphometric variable at a time. Fluvial and tidal reaches exhibiting the highest and lowest value of half meander intrinsic length (l_{av_H}), asymmetry index (A_{av_H}) and sinuos-

Table 2.1: Results of Kolmogorv-Smirnov test on the selected morphometric variables. The significance level is constant ($\alpha = 0.05$).

Variable	Null Hyp. (H_0)	Alt. Hyp. (H_1)	Rejected H_0?	p-value
l_{av_H}	$cdf_{Tidal} = cdf_{fluvial}$	$cdf_{Tidal} \neq cdf_{fluvial}$	No	$1.70e^{-1}$
A_{av_H}	$cdf_{Tidal} = cdf_{fluvial}$	$cdf_{Tidal} \neq cdf_{fluvial}$	Yes	$8.60e^{-15}$
	$cdf_{Tidal} = cdf_{fluvial}$	$cdf_{Tidal} > cdf_{fluvial}$	No	$9.80e^{-1}$
	$cdf_{Tidal} = cdf_{fluvial}$	$cdf_{Tidal} < cdf_{fluvial}$	Yes	$4.30e^{-15}$
σ_{av_H}	$cdf_{Tidal} = cdf_{fluvial}$	$cdf_{Tidal} \neq cdf_{fluvial}$	Yes	$1.30e^{-2}$
	$cdf_{Tidal} = cdf_{fluvial}$	$cdf_{Tidal} > cdf_{fluvial}$	No	$1.00e^{0}$
	$cdf_{Tidal} = cdf_{fluvial}$	$cdf_{Tidal} < cdf_{fluvial}$	Yes	$6.43e^{-4}$
l_{av_F}	$cdf_{Tidal} = cdf_{fluvial}$	$cdf_{Tidal} \neq cdf_{fluvial}$	No	$1.84e^{-1}$
A_{av_F}	$cdf_{Tidal} = cdf_{fluvial}$	$cdf_{Tidal} \neq cdf_{fluvial}$	Yes	$4.95e^{-2}$
	$cdf_{Tidal} = cdf_{fluvial}$	$cdf_{Tidal} > cdf_{fluvial}$	Yes	$2.47e^{-2}$
σ_{av_F}	$cdf_{Tidal} = cdf_{fluvial}$	$cdf_{Tidal} \neq cdf_{fluvial}$	No	$3.72e^{-1}$
C_{av_T}	$cdf_{Tidal} = cdf_{fluvial}$	$cdf_{Tidal} \neq cdf_{fluvial}$	Yes	$2.13e^{-2}$
	$cdf_{Tidal} = cdf_{fluvial}$	$cdf_{Tidal} > cdf_{fluvial}$	Yes	$2.13e^{-2}$

ity (σ_{av_H}) are reported in Figure 2.9. At first, it is worth noting how the variability of normalized channel widths ($B^*(s) = B(s)/B_0[-]$, Figure 2.10-a) is higher in tidal channels. This is in accordance with empirical evidences, tidal channel displaying a characteristic "funneling" behaviour with channel widths progressively reducing landward. Employing the two-sample Kolmogorov-Smirnov test to evaluate whether a given morphological feature differs in tidal and fluvial meanders, we show that (Table 2.1), at a significance level of 5%, the averaged intrinsic length (i.e. computed along the intrinsic coordinate s) of both half ($l_{av_H}[-]$) and full ($l_{av_F}[-]$) meanders (Marani et al., 2002), as well as the average full meander sinuosity ($\sigma_{av_F}[-]$), are found to belong to the same distribution. On the contrary, the cumulative distribution function ('cdf') of the distribution of tidal variables is larger than the cdf of the distribution of fluvial variables with respect to reach averaged curvature ($C_{av_T}[-]$) and full meander average asymmetry index. An opposite behavior is instead observed considering half meander average sinuosity ($\sigma_{av_H}[-]$) and full meander average asymmetry index (A_{av_F}).

Of particular interest are the results concerning the asymmetry index. Many authors, in fact, ascribed the upstream ($A < 0$) or downstream ($A > 0$) skewing of tidal meanders to the relative dominance of the ebb or flood flow, respectively (Barwis, 1978; Fagherazzi et al., 2004; Burningham, 2008), since unidirectional flows are typically believed to skew river meanders in an upstream manner (Parker et al., 1983; Marani et al., 2002; Seminara, 2006) (Figure 2.10-c). However, recalling that river meander skewing depends on the value of meander wave number and width-depth ratio, and that super-resonant

conditions create upstream skewed meanders, whereas sub-resonant conditions promote the development of downstream skewed meanders (for further details see Zolezzi and Seminara, 2001; Blondeaux and Seminara, 1985), the characterization of ebb vs flood dominance as a function of the full meander average asymmetry index does not seem to be sufficiently supported. From our data indeed we do not observe a preferred skewing direction in tidal meanders, suggesting that the constant duel between ebb and flood flows often results in a final outcome which produces symmetric meanders. We further observed that peculiar cusp- or box-shaped tidal-meanders corresponds to quite symmetric planform configurations, an that in box-shaped meanders the occurrence of two local curvature maxima of about the same magnitude makes the skewness detection quite an unsteady procedure.

We have also employed spectral analysis methods for identifying periodicities and characterizing, if anything, the underlying regular dynamics in meander forms. The periodogram method is perhaps the most well known method to carry out spectral analysis. By Fourier analyzing (i.e., by discrete Fourier transformation) the curvature $C(s)$, periodic of period l_F (note that full meanders are considered), we derive the power spectra, normalized by the total power density, of all the considered meanders (Figure 2.11-a). For both the spectra the binned and average values of the dimensionless power density corresponding to each harmonics, indicate that the energy associated to the first three/four harmonics is dominant, although in some cases higher order harmonics prevail (Figure 2.11-a). A physical interpretation of our result may be provided considering the ideal fluvial model equation (Kinoshita, 1961; Leopold and Langbein, 1966; Ikeda et al., 1981; Seminara et al., 2001):

$$C(s) = C_0 \left[\frac{2\pi s}{l_F} - C_F cos3\frac{2\pi s}{l_F} - C_S sin3\frac{2\pi s}{l_F} \right] \tag{2.9}$$

where C_F and C_S are the fattening and skewing coefficients, respectively. The lack of even harmonics, particularly of the second one, in equation 2.9 is theoretically justified (Seminara et al., 2001) by the cubic geometric nonlinearity of the equation describing the planimetric-evolution of meanders. This occurrence led some authors (Marani et al., 2002) to propose that tidal meanders can be differentiated from fluvial meanders based on the presence of even harmonics in curvature spectra . However, our results do not support the latter hypothesis, the two types of bends displaying indeed almost identical power density along the second harmonic (Figure 2.11-a). Even though the spectral energy magnitude is similar, it is worth noting that tidal meanders display higher concentration along the first and second harmonics, followed by a decay of spectral energy toward higher modes.

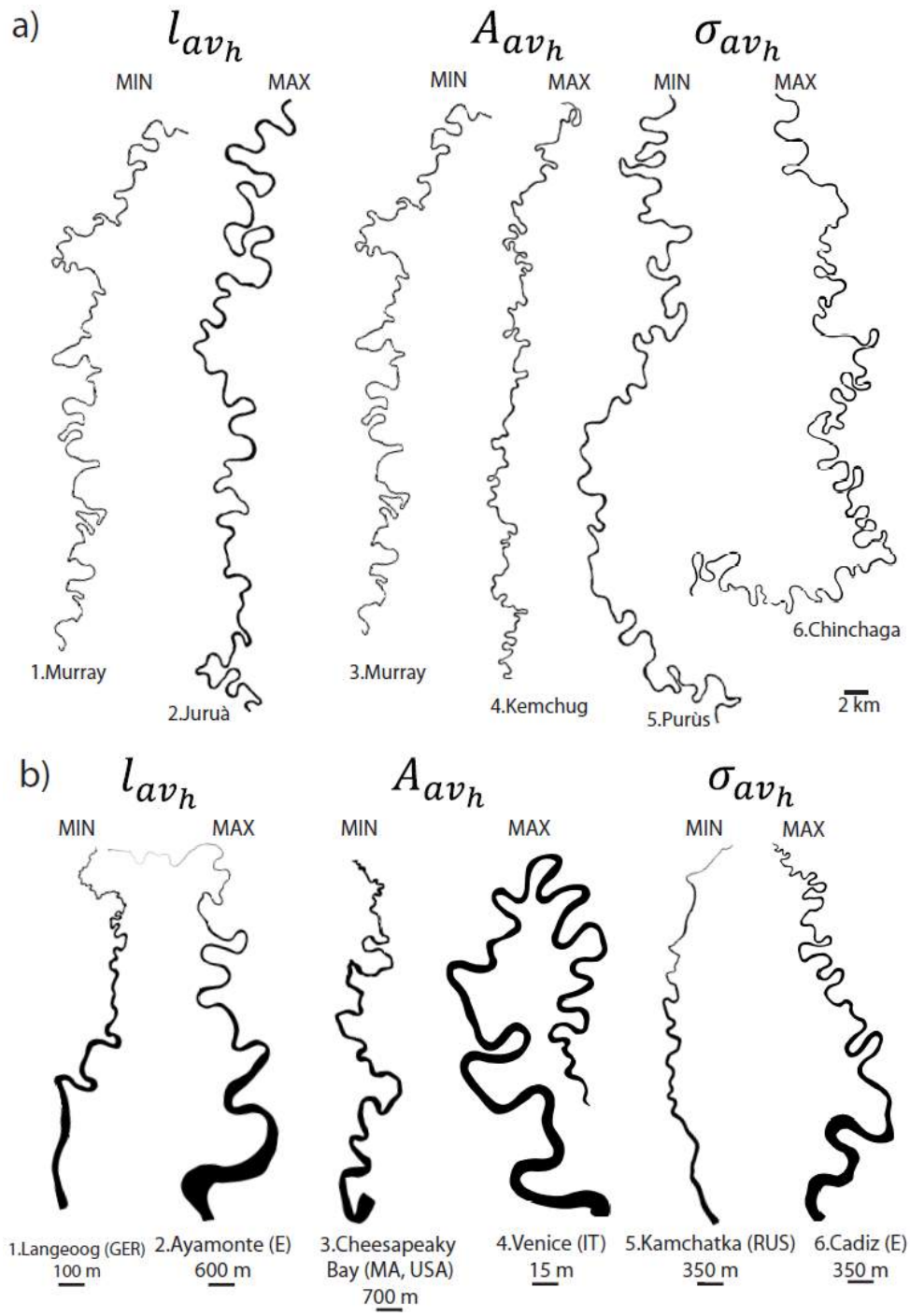

Figure 2.9: Fluvial (a) and tidal (b) reaches included in the dataset which exhibit the highest and lowest values of half-meander intrinsic wavelength, sinuosity and asymmetry index.
a.1) Murray River (AUS), $l_{av_H} = 12.19$; a.2) Juruà River (BR), $l_{av_H} = 30.59$; a.3) Murray River (AUS), $A_{av_H} = -0.20$; a.4) Kemchug River (RUS), $A_{av_H} = -0.02$; a.5) Purùs River (BRA), $\sigma_{av_H} = 1.12$; a.6) Chinchaga River (CAN), $\sigma_{av_H} = 1.56$;
Tidal channels in b.1) Langeoog (GER), $l_{av_H} = 9.40$; b.2) Ayamonte (E), $l_{av_H} = 104.126$; b.3) Cheesapeaky Bay (MA, USA), $A_{av_H} = -0.10$; b.4) Venice Lagoon (IT), $A_{av_H} = 0.24$; b.5) Kamchatka Peninsula (RUS), $\sigma_{av_H} = 1.3$; b.6) Cadiz Bay (E), $\sigma_{av_H} = 2.31$

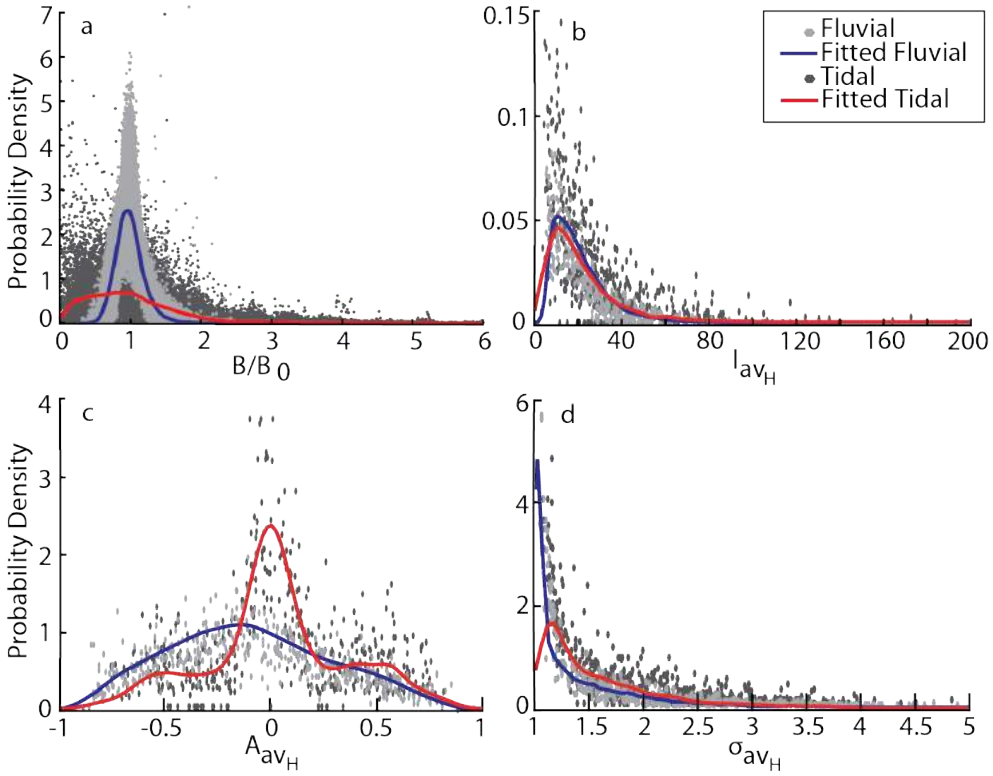

Figure 2.10: Probability density function for some of the considered morphometric variables considered in this study. Each dot represents individual reach data, whereas continuous lines stand for fitted distributions.(a) Normalized channel width along the intrinsic axis coordinate for the whole reach; (b) Mean meander intrinsic length along the whole reach; (c) Mean asymmetry index along the whole reach; (d) Mean meander sinuosity along the whole reach.

Hence, tidal meander planforms are more similar to a pure, neither fattened nor skewed, sinusoidal shape, whereas fluvial meanders exhibit more marked convolutive (nonlinear) interactions among modes. We therefore conclude that members of the tidal-meander family are somehow planimetrically simpler than their riverine kins (see also Figure 2.9).

Despite the periodogram could be computed in a straightforward way, it however suffers from severe deficiencies: it is an inconsistent estimator (it does not converge to the true spectral density as the sample size tends to infinity), it exhibits very high spectral leakage, and the estimate has a positive bias in the presence of additive noise (Hayes, 1996).

We therefore extended the Singular Spectrum Analysis method ("SSA", Ghil et al., 2002), originally designed to extract information from short and noisy time series, to full-meander curvature series ($C_F(s)$). Considering the curvature of each full meander as an independent signal, the intrinsic coordinate s was normalized by the full meander length

($s^* = s/l_F : 0 < s^* < 1$), and the signal was resampled using a constant number of points ($K = 1000$) in order to have homogeneous data. The obtained curvature series,

$$\{C(s_k^*) : k = 0, ..., K, s^* = 0, ..., 1\} \tag{2.10}$$

is then represented in a vector space of dimension M by a succession of overlapping "views" of the series through a sliding M-point window. From the SSA eigenvalue spectrum (Figure 2.11-b) the significance of the various components can be qualitatively judged by comparing the variance contributed by each SSA component relatively to the noise background. The latter includes components which lie in the flattish tail of the eigenvalue spectrum (i.e. components from about 5 to 20). Although a distinct break in the eigenvalue spectrum is hardly revealed, that usually corresponds to signal to noise (S/N) separation (Ghil et al., 2002), SSA seems to confirm the higher relative simplicity of the tidal meander signal. In fact, except for the first one, spectrum components constantly contribute to more variance in the fluvial case.

The multivariate extension of SSA, named multi-channel SSA (M-SSA), was instead employed to investigate the interplay among series of N'-adjacent half-meanders (i.e., a half meander and the following $N' - 1$ ones). Let $\{X_{l,n} : l = 1, ..., L; n = 1, ..., N\}$ be a series containing N data points for every L-variable in the dataset. For every reach, we consider a $L = 3$ dimensionality, making use of half meander sinuosity (σ_H), intrinsic length (l_H) and asymmetric index (A_H). In order to increase data homogeneity, a principal component analysis (PCA) is first applied to the $X_{L\times N}$ matrix of every reach. All the PCA components are then retained, thus producing a $G_{L\times N}$ matrix that is the projection of X along its covariance eigenvectors. As for the number of consecutive half meanders, we employ N' values equal to 2, 5 and 8 (i.e., 4 consecutive full meanders), thus leading to a covariance matrix of ranks $N' \times L$ euqal to 6, 15 and 18 respectively. Increasing the window length N' the eigenvalue spectra of river show, on the average, a progressively clearer break, standing for S/N separation, that is conversely absent in tidal channels (Figure 2.11-c). Nonetheless, the simulated tidal signal invariably shows a less heavy spectrum along higher M-SSA modes. Hence, we conclude that tidal meander trains are somehow more complex than their fluvial fellows, whose underlying dynamics is more regular and less structured. In other words, tidal meanders belonging to a series of consecutive bends are more likely to display morphological features different from each other, whereas in the fluvial settings the characteristics of a given individual meander are more similar to those of the neighbouring bends. The physical interpretation of this findings is likely related to the higher spatial variability of tidal channel features (e.g., funneling and presence of lateral tributaries), that perturbs meander train

dynamics in a crucial manner. Finally, our 39 statistic dataset (Table 2.3) has been analyzed through Principal Component Analysis (PCA), whose M-SSA is basically an extension. The goal of the PCA is to reduce the dimensionality of the data while retaining as much as possible of the variation present in the original dataset. The best lower-dimensional space can be determined keeping only the terms corresponding to the largest eigenvalues of the covariance matrix of the data (Lay, 2000; Frascati and Lanzoni, 2009). Employing the whole dataset, the first three principal components (i.e., the eigenvectors corresponding to the first three largest eigenvalues of the covariance matrix) barely account for 50% of the observed variance. We however know that some of variables are not strictly independent, and a selected suite of them has to be considered to increased the explained variance (Howard and Hemberger, 1991; Frascati and Lanzoni, 2009). We then consider a subset of variables including total sinuosity (σ_T), half-meander average sinuosity ($\sigma_{\alpha\nu_H}$), full- meander average sinuosity ($\sigma\alpha\nu_F$); mean, variance, skewness and kurtosis of half meander intrinsic wavelength ($l_{\alpha\nu_H}, l_{\nu a_H}, l_{sk_H}, l_{kr_H}$); variance ($C_{\nu a_T}$) and kurtosis ($C_{kr_T}$) of channel axis curvature; mean, kurtosis and 60-90 length percentile of half meander asymmetry index ($A_{\alpha\nu H}, A_{krH}, A_{60-90_H}$). The ensemble of these morphological features can quantitatively discriminate among different meandering patterns, showing two well clusterized groups (Figure 2.12-a). The first three principal components account for 66% of the observed variance, whereas the relative importance of higher order principal components decays exponentially (Figure 2.12-b). Furthermore, the loading plot (Figure 2.12-c) indicates that fluvial-meandering reaches are characterized by lower values of $A_{\alpha\nu_H}$ and stronger curvature variance ($C_{\nu a_T}$), thus confirming our previous suggestions about the occurrence of more complex and asymmetric meanders in the riverine framework. Our results show that, at the meander length scale, meandering in tidal streams produces patterns which are less complex than those of fluvial reaches; this occurence is instead overturned if a sequence of meanders is taken into account.

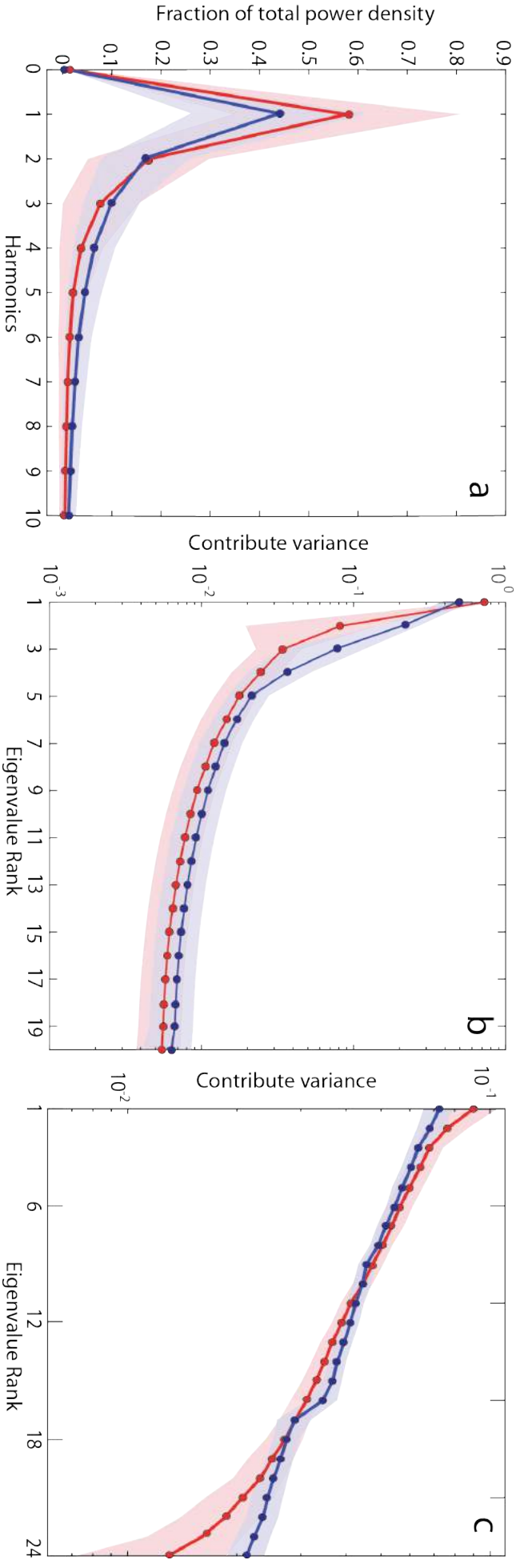

Figure 2.11: Results of spectral analysis methods. (a) Periodogram of $C(s)$; (b) Eigenvalue spectrum of SSA using a moving window of size 20. The units of abscissa are SSA component number (eigenvalue rank), and with the variance contributed by each SSA component on the ordinate; (c) Eigenvalue spectrum of M-SSA considering 8 consecutive half meanders. The units of abscissa are M-SSA component number (eigenvalue rank), with the variance contributed by each M-SSA component on the ordinate. In (a), (b) and (c) shades correspond to one standard deviation.

This might be a direct consequence of the different governing landforming processes, whose regularity in tidal environments is higher (lower) at the meander (reach) length scale than the regularity which characterized fluvial landscapes. As a matter of example, water discharges along a tidal bend constantly vary within a well defined range, i.e. between the maximum flood and ebb discharges, whereas in the riverine case high-discharge values are attained only during the major flood events, whose frequency is approximately annual. On the contrary, if a whole channel is considered, the flowing discharge in tidal realms constantly increased from the source to the channel outlet, receiving the contribution of surrounding salt-marsh and tidal-flat areas drained by the channel itself, whereas river discharges remain constant over long distances, since they can significantly vary only in correspondence of confluences which are indeed not so frequent. Furthermore, the substrates that tidal and fluvial channels typically cut through, display different rates of variability, with tidal ladscapes being in general characterized by a massive presence of fine sediment (from medium-fine sand to mud). This is partially due to the peculiar mechanisms of evolution that typifies salt-marshes, where channels migrate slowly because of their moderate width (see previous section in this chapter) and the periodic flooding of marshplains causes frequent deposition. As a consequence, the major part of marshplain is constituted of sediment deposited by overbank flows, whereas sedimentary products related to channel migration represent the majority of river floodplains (Howard, 1996; Fagherazzi et al., 2004).

Hence, within the great meander family, tidal and fluvial meander has to be treated more as cousins than as brothers, their planforms being quantitative different. Nonetheless, we have shown that their planform evolution does not exhibit such strong differences (see the previous chapter). This dualism therefore leaves an open question regarding whether a right metric exists, capable of accounting for peculiarities, if anything, in tidal meander planform evolution. Our results however represent a first key-step to bridge this gap in current knowledge.

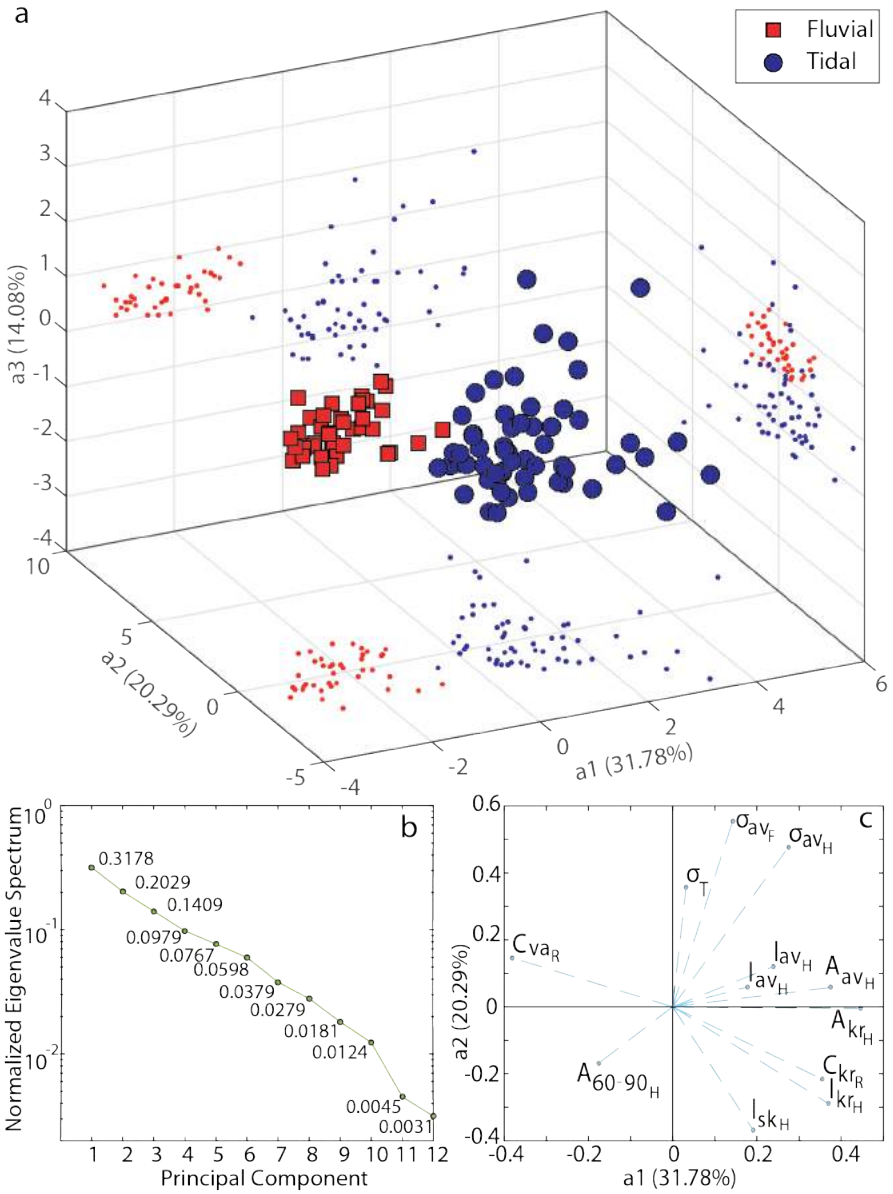

Figure 2.12: Results of Principal Component Analysis.(a) Scatterplot of the three principal component coefficients (the relative variance explained by each PC is represented along the axes); (b) Eigenvalue spectrum of PCA (the relative variance explained by each PC is represented near each points); (c) Loading plot for the first PC. Each of the 12 morphometric variables considered in the analysis is represented by a vector, and the direction and length of the vector indicate how each variable contributes to the two principal components in the plot.

Table 2.2: Suite of the Morphometric Variables Used to Objectively Characterize Planform Meandering Patterns mobile

Feature	Variable	Description
Sinuosity	σ_{av_H}	half meander average sinuosity
	σ_{va_H}	variance of half meander average sinuosity
	σ_{std_H}	stand. dev. of half meander average sinuosity
	σ_{sk_H}	skewness of half meander average sinuosity
	σ_{kr_H}	kurtosis of half meander average sinuosity
	σ_{av_F}	full meander average sinuosity
	σ_{va_F}	variance of full meander average sinuosity
	σ_{std_F}	stand. dev. of full meander average sinuosity
	σ_{sk_F}	skewness of full meander average sinuosity
	σ_{kr_F}	kurtosis of full meander average sinuosity
	σ_T	reach sinuosity (tortuosity)
Length	$ł_{av_H}$	half meander average intrinsic length
	$ł_{va_H}$	variance of half meander average intrinsic length
	$ł_{std_H}$	stand. dev. of half meander average intrinsic length
	$ł_{sk_H}$	skewness of half meander average intrinsic length
	$ł_{kr_H}$	kurtosis of half meander average intrinsic length
	$ł_{av_F}$	full meander average intrinsic length
	$ł_{va_F}$	variance of full meander average intrinsic length
	$ł_{std_F}$	stand. dev. of full meander average intrinsic length
	$ł_{sk_F}$	skewness of full meander average intrinsic length
	$ł_{kr_F}$	kurtosis of full meander average intrinsic length
Curvature	C_{av_T}	reach average local curvature
	C_{va_T}	variance of local curvature
	C_{std_T}	stand. dev. of local curvature
	C_{sk_T}	skweness of local curvature
	C_{kr_T}	kurtosis of local curvature
	E_{C_T}	$\int_0^{s_{tot}} C^2 ds$
Asymmetry	A_{av_H}	average half meander asymmetry coeff.
	A_{va_H}	variance of half meander asymmetry coeff
	A_{std_H}	stand. dev of half meander asymmetry index
	A_{sk_H}	skewness of half meander asymmetry index
	A_{kr_H}	kurtosis of hal meander asymmetry index
	A_{60-90_H}	60^{th} to 90^{th} percentile of half meander asymm. index
	A_{av_F}	average full meander asymmetry coeff.
	A_{va_F}	variance of full meander asymmetry coeff
	A_{std_F}	stand. dev of full meander asymmetry index
	A_{sk_F}	skewness of full meander asymmetry index
	A_{kr_F}	kurtosis of full meander asymmetry index
	A_{60-90_F}	60^{th} to 90^{th} percentile of full meander asymm. index

Table 2.3: List of reaches included in the dataset.

Type	Name	Location	Bends	Source
Tidal	Sindacale channel	Caorle (IT)	19	©WorldImagery-Microsoft
Tidal	Canal de Tavira	Santa Luzia, Faro (P)	20	©WorldImagery-Microsoft
Tidal	Tiang	Che Bilang (THA)	20	©WorldImagery-DigitalGlobe
Tidal	(unknown)	Dongying (CN)	21	©WorldImagery-CNES/AirbusDS
Tidal	(unknown)	Gulf du Morbihan (F)	21	©WorldImagery-Microsoft
Tidal	Rio de la Bota	Huelva (E)	21	©WorldImagery-IGN/CNIG
Tidal	(unknown)	Pagliaga, Venice (IT)	21	©WorldImagery-Microsoft
Tidal	(unknown)	Campalto, Venice (IT)	26	©WorldImagery-Microsoft
Tidal	(unknown)	Campalto, Venice (IT)	26	©WorldImagery-Microsoft
Tidal	(unknown)	Sant'Erasmo, Venice (IT)	26	©WorldImagery-Microsoft
Tidal	(unknown)	Long Hoa (VN)	21	©WorldImagery-DigitalGlobe
Tidal	Tha Taphao	Trat (THA)	22	©WorldImagery-DigitalGlobe
Tidal	Dei Lovi Channel (1)	Bibione (IT)	23	©WorldImagery-Microsoft
Tidal	Strait of Malacca	Perak (MAL)	23	©WorldImagery-DigitalGlobe
Tidal	(unknown)	Kamcatka (RUSS)	23	©WorldImagery-
Tidal	Marisma Isla Cristina	Ayamonte (E)	23	©WorldImagery-IGN/CNIG
Tidal	Song Dong Tranh	Long Hoa (VN)	23	©WorldImagery-DigitalGlobe
Tidal	Dei Lovi Channel (2)	Bibione (IT)	24	©WorldImagery-Microsoft
Tidal	(unknown)	Pagliaga, Venice (IT)	24	©WorldImagery-Microsoft
Tidal	(unknown)	Mourilyan Harbour (AUS)	25	©WorldImagery-DigitaGlobe
Tidal	(unknown)	Rade de Morlaix (F)	25	©WorldImagery-Microsoft
Tidal	Sungai Kerisek	Kota Juala Muda (MAL)	25	©WorldImagery-DigitalGlobe
Tidal	(unknown)	Makanbôn Kyun (MYA)	25	©WorldImagery-DigitalGlobe
Tidal	(unknown)	Hat Sai Ri (THA)	25	©WorldImagery-DigitalGlobe
Tidal	Rio de San Pedro	Cadiz (E)	26	©WorldImagery-IGN/CNIG
Tidal	(unknown)	Luoyuan Bay (CN)	27	©WorldImagery-CNES-AirbusDS

continued ...

... continued

Type	Name	Location	Bends	Source
Tidal	Stér el Istrec	Rivièr d'Etel (F)	27	©WorldImagery-Microsoft
Tidal	Stang	Baie Saint-Jean (F)	28	©WorldImagery-Microsoft
Tidal	Hai Lam	Ban Laem District (THA)	28	©WorldImagery-DigitalGlobe
Tidal	Tha Taphao	Trat (THA)	28	©WorldImagery-DigitalGlobe
Tidal	(unknown)	Tessera, Venice (IT)	29	©WorldImagery-Microsoft
Tidal	Etiere du Goilé	Baié de pont Maé (F)	30	©WorldImagery-Microsoft
Tidal	Sungai Santi	Johor (MAL)	30	©WorldImagery-DigitalGlobe
Tidal	(unknown)	Ayamonte (E)	30	©WorldImagery-IGN/CNIG
Tidal	(unknown)	Norderney (GER)	30	©WorldImagery-DigitalGlobe
Tidal	Riviere de l'Epinay	Le Tour du Parc (F)	31	©WorldImagery-Microsoft
Tidal	(unknown)	Ayeyarwady (MYA)	31	©WorldImagery-DigitalGlobe
Tidal	Monie Creek	Chesapeake Bay (MD, USA)	31	©WorldImagery-USDA FSA
Tidal	(unknown)	Tessera, Venice (IT)	31	©WorldImagery-Microsoft
Tidal	(unknown)	Blavand (DEN)	31	©WorldImagery-DenmarkImagery
Tidal	(unknown)	S.Francisco Bay (CA, USA)	32	©WorldImagery-SFEI - Quantum Spatial
Tidal	(unknown)	Tessera, Venice (IY)	32	©WorldImagery-Microsoft
Tidal	Rivier de Sarzeau	Le Tour du Parc (F)	34	©WorldImagery-Microsoft
Tidal	(unknown)	Ayeyarwady (MYA)	34	©WorldImagery-DigitalGlobe
Tidal	(unknown)	Santa Luzia, Faro (P)	20	©WorldImagery-Microsoft
Tidal	(unknown)	Mellum (GER)	35	©WorldImagery-Microsoft
Tidal	(unknown)	Blavand (DEN)	36	©WorldImagery-DenmarkImagery
Tidal	Ruisseau de Lizildry	Baie d'Enfer (F)	37	©WorldImagery-Microsoft
Tidal	(unknown)	S.Francisco Bay (CA, USA)	39	©WorldImagery-SFEI - Quantum Spatial
Tidal	(unknown)	Maintirano (MAD)	42	©WorldImagery-DigitalGlobe
Tidal	(unknown)	Gulf of Morbihan (F)	45	©WorldImagery-Microsoft
Tidal	Tuckahoe	Great Egg Harbor Bay (NJ, USA)	45	©WolrdImagery-USDA FSA

continued ...

... continued

Type	Name	Location	Bends	Source
Tidal	Lakes Creeks	Great Egg Harbor Bay (NJ, USA)	45	©WolrdImagery-USDA FSA
Tidal	Scorton Creek (1)	Barnstable (MA, USA)	50	©WorldImagery-USDA FSA
Tidal	(unknown)	Langeoog (GER)	51	©WorldImagery-USDA FSA
Tidal	Scorton Creek (2)	Barnstable (MA, USA)	61	©WorldImagery-USDA FSA
Tidal	Etiere de la Barre	Baié de Pont Maé (F)	102	©WorldImagery-Microsoft
Tidal	Chase Gardens Creek	Barnstable (MA, USA)	107	©WorldImagery-USDA FSA
Fluvial	Lungwebungu River(1)	Angola	243	©2016 Google, DigitalGlobe
Fluvial	Lungwebungu River(1)	Angola	65	©2016 Google, DigitalGlobe
Fluvial	Beaver River	Canada	65	©2016 Google, DigitalGlobe
Fluvial	Rio Bravo	Mexico	504	©2016 Google, DigitalGlobe
Fluvial	River Chet	South Norfolk (ENG)	78	©2016 Google, Getmapping plc
Fluvial	Chinchaga River	Alberta (CAN)	114	©2016 Google, Cnes/Spot Image
Fluvial	Chulym River	Krasnoyask (RUS)	354	©2016 Google, Cnes/Astrium
Fluvial	Curucà River (1)	Parà (BR)	208	©2016 Google, Cnes/Spot Image
Fluvial	Curucà River (2)	Parà (BR)	204	©2016 Google, Cnes/Spot Image
Fluvial	Darling River	New South Wales (AUS)	479	©2016 Google, Digital Globe
Fluvial	Dulgalakh River	Yakutia (RUS)	65	©2016 Google, Digital Globe
Fluvial	Rio Envira	Acre (BR)	153	©2016 Google, Digital Globe
Fluvial	Javary River	Ucayali (PE)	194	©2016 Google, Landsat/Copernicus
Fluvial	Jurua River (1)	Ucayali (PE) - Amazonas (BR)	210	©2016 Google, Landasat
Fluvial	Jurua River (2)	Ucayali (PE) - Amazonas (BR)	122	©2016 Google, Landsat
Fluvial	Jurua River (3)	Ucayali (PE) - Amazonas (BR)	223	©2016 Google, Landsat
Fluvial	Kemchug River (1)	Krasnoiarsk Krai (RUS)	151	©2016 Google, Digital Globe
Fluvial	Kemchug River (2)	Krasnoiarsk Krai (RUS)	148	©2016 Google, Digital Globe
Fluvial	Irtysh-Ob'	Kipo-Kulary (RUS)	242	©2016 Google, Digital Globe
Fluvial	Kwango River	Angola	98	©2016 Google, CNES/Astrium

continued ...

... continued

Type	Name	Location	Bends	Source
Fluvial	Sittang River	Bago (MYA)	166	©2016 Google, CNES/Astrium
Fluvial	Mississippi River (1)	USA	85	©2016 Google, Landsat/Copernicus
Fluvial	Mississippi River (2)	USA	113	©2016 Google, Landsat/Copernicus
Fluvial	Murray River (1)	Australia	342	©2016 Google, CNES/Astrium
Fluvial	Murray River (2)	Australia	230	©2016 Google, CNES/Astrium
Fluvial	Murray River (3)	Australia	104	©2016 Google, CNES/Astrium
Fluvial	Nan River	Thailand	111	©2016 Google, Digital Globe
Fluvial	Orthon River	Pando (BOL)	443	©2016 Google, CNES/Spot Image
Fluvial	Purus River (1)	Brazil - Perù	182	©2016 Google, Landsat/Copernicus
Fluvial	Purus River (2)	Brazil - Perù	133	©2016 Google, Landsat/Copernicus
Fluvial	Tarauacà River (1)	Amazonas and Acre (Brazil)	144	©2016 Google, Digital Globe
Fluvial	Tarauacà River (2)	Amazonas and Acre (Brazil)	144	©2016 Google, Landsat/Copernicus
Fluvial	Tarauacà River (3)	Amazonas and Acre (Brazil)	114	©2016 Google, Digital Globe
Fluvial	Tym River (1)	Krasnoiarsk Krai - Tomsk Oblast (RUS)	274	©2016 Google, Landsat/Copernicus
Fluvial	Tym River (2)	Krasnoiarsk Krai - Tomsk Oblast (RUS)	178	©2016 Google, Landsat/Copernicus
Fluvial	Tym River (3)	Krasnoiarsk Krai - Tomsk Oblast (RUS)	114	©2016 Google, Landsat/Copernicus
Fluvial	Tym River (4)	Krasnoiarsk Krai - Tomsk Oblast (RUS)	151	©2016 Google, Landsat/Copernicus
Fluvial	Tym River (5)	Krasnoiarsk Krai - Tomsk Oblast (RUS)	161	©2016 Google, Landsat/Copernicus
Fluvial	Vakh River	Khanty-Mansia (RUS)	202	©2016 Google, Landsat/Copernicus
Fluvial	Yana River	Sakha (RUS)	189	©2016 Google, Landsat/Copernicus

3 TIDAL MEANDER EVOLUTION: FIELD INVESTIGATIONS AND NUMERICAL MODELLING

3.1 LINKING HYDRODYNAMICS AND PLANFORM EVOLUTION OF TIDAL MEANDERS

This chapter is a manuscript in preparation, whose primary goal is to address how the periodically-reversing tidal flow influences the evolution of tidal meanders. A series of *in situ* measurements, carried out by means of an acoustic Doppler current profiler, shows strong flow-field differences along tidal meander bends of different typologies. Particularly, the occurrence of flow separation zones may, under certain conditions, shape tidal meander in an unusual way, leading also to the preservation of outer bank deposits. Moreover, in channels of limited depth, flow fields can be strongly altered by channel-bottom vegetation that might therefore play a role in the evolution of tidal meander bends. These results represent a first step for better understanding how the evolution of tidal meanders is contingent on the periodic mutual turnover of tidal flows, and might therefore constitute a benchmark to associate (or distance) fluvial-meander models to (from) tidal ones.

Part of the results derived from this study have been, and currently are, employed in sedimentological studies carried out on the same bends, on the basis of an integrated approach that allows us to obtain a better interpretation of the collected data. A first example of such an integrated approach is shown in Appendix B, which contains a manuscript currently under review in the journal Sedimentology.

PAPER

Finotello, Alvise[1], Massimiliano Ghinassi[1], Luca Carniello[2], Enrica Belluco[2], Mattia Pivato[2], Laura Tommasini[1] and Andrea D'Alpaos[1]

[1]Dept. of Geosciences, University of Padova, via G.Gradenigo 6, Padova, PD I-35131, Italy

[2]Dept. ICEA, Univesrity of Padova, via Loredan 20, Padova, PD I-35131, Italy

3.1.1 Abstract

Tidal flows represent the main erosional and depositional agents operating in tidal meanders. However, the paucity of quantitative data on the characteristics of such periodically-reversing tidal flows has so far undermined speculations about their geomorphic effects. Particularly, the effects of secondary flows occurring in tidal meander bends is poorly characterized. The present work aims at bonding morphodynamic evolution of tidal meanders with the observed 3D-velocity distributions, characterizing their hydrodynamic behavior. By means of an acoustic Doppler current profiler (ADCP), we have surveyed meander-flow fields over three different tidal channels in the San Felice salt marsh (northern Venice Lagoon). Measurements have been carried out along bends of three distinct types, based on different evolutionary dynamics, in order to highlight differences and analogies. In all of the study-case bends, our results highlight a strong asymmetry in depth-averaged velocity distributions between the flood and ebb phases. The shift in the position of velocity maximum is also responsible for the varying position, intensity and type of secondary circulations and flow-separation zones. In spite of the recurrency of fluvial-like morphologies dictated by the simultaneous erosion and deposition along meander outer and inner bank, respectively, we observed that under certain conditions the presence of flow-separation zones shape tidal meanders in an unusual way, resulting in both inner bank erosion and outer bank bar deposits with possible high preservation potential. In some cases, channel-bottom vegetation is shown to strongly affect the flow field within the channel, thus likely influencing its morphodynamic evolution.

3.1.2 Introduction

Tidal flows are the main erosional and depositional agents in salt marsh creeks, and control both creek morphology and the overall sediment and nutrient budgets of adjacent marshes (Bayliss-Smith et al., 1979; D'Alpaos et al., 2005; Kirwan and Murray, 2007; Mudd, 2011; Hughes, 2012). A number of existing studies have focused on the magnitude and frequency of such flows. Myrick and Leopold (1963) and Pestrong (1965) first measured discharges and current speeds over complete tidal cycles in salt-marsh channels, highlighting flow asymmetries over different tidal stages. These asymmetries are different from those observed in tidal-flat channels by Postma (1961), who demonstrated a flow asymmetry which is out of phase by half a tidal wavelength. An explanation for such differences was first proposed by Boon (1975) studying a salt marsh system in Virginia, and refined by Bayliss-Smith et al. (1979), and essentially lies on the relation be-

tween marsh height and high-tide level, i.e. on the storage capacity of marshplains sorrounding marsh channels. Indeed, the level of marsh surface provides a threshold ('marshfull') at which both velocities and discharges can increase shortly before and shortly after high tide (Bayliss-Smith et al., 1979). This leads to two distinct discharge peaks, which occur when tidal levels are just above (during the flood phase) or below (during ebb) the elevation of the marsh platform. This observation was further substantieted by Pethick (1980) who also studied the role of marsh channels in modifying tidal stages. Due to different roughness between channels and marshes, the marshfull stages and high water slack are attenuated (French and Stoddart, 1992), thus favouring generally greater ebb-flow velocity pulses (Bayliss-Smith et al., 1979; Healey et al., 1981; Leopold et al., 1993; Friedrichs and Perry, 2001), albeit the flood pulse occurs at higher stages and may become dominant under storm surge conditions (Bayliss-Smith et al., 1979; Dzwonkowski et al., 2014). Lawrence et al. (2004) characterized the role of tidal channels in delivering and removing material from salt-marsh platforms, and strong differences between flood and ebb pathways have been observed in overmarsh circulation as well (Sullivan et al., 2015). Attempts to link the morphodynamic evolution of tidal channels with the characteristics of the flow within them were carried out in a few studies, whose main focus was the effect of bidirectional, mutually evasive pathways of ebb and flood flows on both the channel-planform (Ahnert, 1960; Barwis, 1978; Solari et al., 2002; Fagherazzi et al., 2004) and channel-bottom morphologies (Solari et al., 2002; Garotta et al., 2006). Nonetheless, a gap in the body of knowledge still exists that links morphodynamic evolution of tidal meanders with quantitative data on the nature of tidal flows within them, particularly at the meander-length scale. In fact, the flow field along tidal meanders, together with its morphological implications, is currently poorly characterized. Moreover, morphological implications of flow distribution along tidal bends have been frequently overlooked given the suppposed similarity between tidal channels and river bends, where flow dynamics are well known (Prandtl, 1952; Rozovskii, 1957; Engelund, 1974) and have been addressed by a variety of both field (e.g., Dietrich et al., 1979; Frothingham and Rhoads, 2003; Dinehart and Burau, 2005a; Nanson, 2010) and laboratory studies (e.g., Blanckaert and Vriend, 2004; Blanckaert, 2011; Liaghat et al., 2014), as well as by means of numerical models (e.g., Bridge and Jarvis, 1982; Dietrich and Smith, 1983; Kawai and Julien, 1996; Blanckaert and Vriend, 2003; Ferguson et al., 2003; Ferguson and Parsons, 2004; Parsons et al., 2004; Abad and García, 2005). Hence, the unbalancing between the centrifugal force and lateral pressure gradient induced by free surface lateral slope, the latter increasing upwards while the former being vertically constant (Solari et al., 2002), is ulti-

mately assumed to play the same role in tidal and fluvial landscapes. While recognising the overall correctness of this assumption, we do believe that in tidal meanders such a mechanism, coupled with the periodic reversal of tidal flow, might lead to evolution paths which differ from those of fluvial meanders and therefore deserves a closer scrutinity. Particularly, a close investigation on the relationship between flow structures and different types of channels planform transformations, together with the related erosional and depositional patterns, is missing. In this paper, we consider this issue based on a series of field surveys of three-dimensional tidal-meander hydrodynamics. An acoustic Doppler current profiler has been employed for measuring tidal-current structures at spatial resolution that is otherwise unobtainable by conventional means. In order to highlight differences and analogies, the measurements have been carried out along meanders showing different planform shapes, based on different evolutionary dynamics, the latter having been inferred from historical images of the study case bends. Our main goal is to to analyze the relationship between the hydrodynamics of the study bends and their planform evolution. The role played by flow-field differences in determining meander evolution is discussed, together with possible implications for the formation of sediment deposits with high-preservation potential. Whilst not denying that it might have an influence on tidal meander evolution, in the present work the role played by storm surges is not taken into account, the main focus being on the more regular and frequent flows caused by astronomical tides.

3.1.3 Study cases

In this study we focused on three tidal channels located in the San Felice salt marsh area, in the northern part of the Venice Lagoon that has been recognized as the most naturally preserved part (Marani et al., 2003). The Venice Lagoon, formed over the last 7500 years, is the largest Mediterranean brackish water body, with an area of about 550 km^2. It is connected to the Adriatic Sea through three inlets (Lido, Malamocco and Chioggia) and is subjected to a semidiurnal microtidal regime, with an average tidal range of about 1.0 m and peak tidal amplitudes of about 0.75 m around Mean Sea Level (MSL). Over the last centuries, the Lagoon has experienced several hydraulic modifications, among which the stabilization of inlets through the building of jetties has induced the most important effects (Tambroni and Seminara, 2006; D'Alpaos, 2010) turning the system into a currently ebb-dominated system (Gatto and Carbognin, 1981; Stevenson et al., 2000; Ferrarin et al., 2015).
Characterized by an average elevation of 0.26 m above MSL, the San Felice salt marsh is mainly colonized by a mosaic of halophytic species,

among which we find *Spartina maritima, Limonium narbonense, Sarcocornia fruticosa* and *Juncus maritimum* (Belluco et al., 2006; Roner et al., 2016). Sediments range from medium-fine sand to mud, with shell fragments on the channel bottom (Brivio et al., 2016). Our first study case is represented by a symmetrical meander loop (*sensu* Brice, 1974, see Figure 3.1-a) belonging to a tidal channel displaying a E-W trend. The channel is about 11 m wide and up to 1.8 m deep. The analyzed meander bend displays an intrinsic length of 65 m and a mean radius of curvature of about 28 m. Over the last 50 years the bend showed and expasional behavior (*sensu* Daniel, 1971; Jackson, 1976), with the apex following a NE-SW trajectory. We hereinafter refer to this bend as bend "E" due to its expansional behaviour, characterized by a weak non-linearity with a more pronounced point-bar growth along the landward side of the inner bank.

The second and third study case bends are located close each other (Figure 3.1-b), and consist of two channels with similar sizes. Prior to 1968 the two channels were connected through a minor creek ("MFC" in Figure 3.1-b) that was abandoned and mud-infilled when the two main channels progressively merged southward into a single reach. The Eastern meander bend (labelled as "T" in Figure 3.1-b) shows a "simple asymmetric" planform (sensu Brice, 1974) and its axis trends ENE-WSW. It has a radius of curvature of ca. 17 m and varies in depth from 3 to 2 m in the channel pool and riffle zone, respectively. This channel exhibits a translational mode of planar transformation, keeping its sinuosity constant while the bend apex migrates seaward transverse to the channel-bend axis. On the contrary, the western channel (labelled as "C" in Figure 3.1-b) consists of two adjacent meanders with cuspate inner-banks, a planform that has often been recognized as peculiar of tidal channels (Ahnert, 1960; Fagherazzi et al., 2004; Dalrymple et al., 2012). Due to the different inner and outer bank shape, such a planform cannot be ascribed to any of the classes proposed by Brice (1974). Meander bends in channel "C" displayed quite an odd planar transformation. In fact, while meanders translate seaward, the sinuosity of the channel decreases progressively, thus leading to meanders that straighten and decrease their sinuosity. As a consequence, the mean curvature radius has increased from 20 m in 1968 to 35 m nowadays, while channel-mean width slightly increased from 15 m to 20 m. The current depth ranges from 1.5 to 3 meters along the channel thalweg.

3.1.4 Methods

Acoustic Doppler Current Profilers (ADCPs) represent the current standard for flow measurements in large-scale open water systems (Vermuelen et al., 2014) The use of such technology has increased

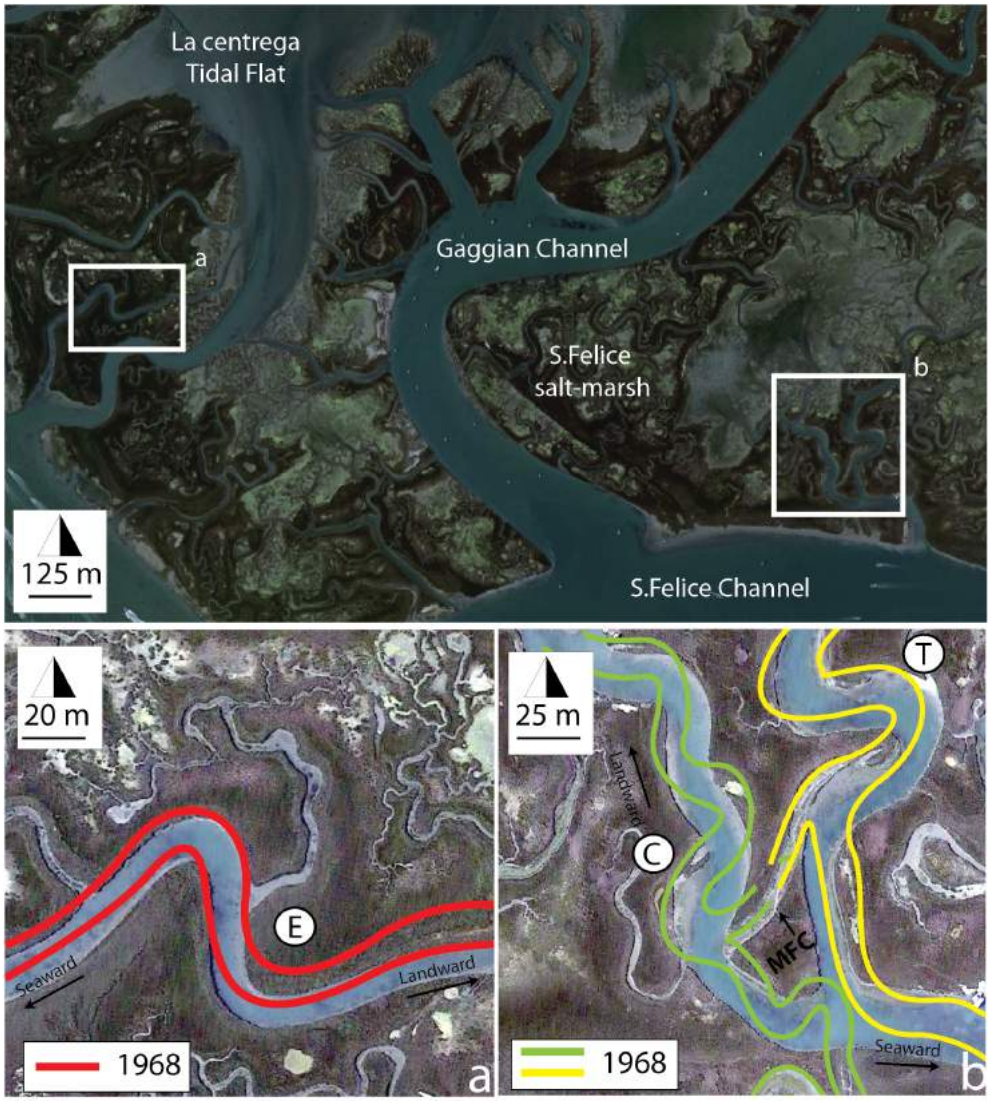

Figure 3.1: Study Case Bends. (Top) Overview of the San Felice area, Northern Venice Lagoon. (a) The first study case bend, namely the expansional meander. Red line stands for channel banks in 1968, as obtained from historical photos (©2016 Google, TerraMetrics). (b) The other study case bends, namely the translating (on the right) and the cusp-shaped (on the left) meanders. Continuous lines represent channel bank in 1968, as obtained from historical photos (©2016 Google, TerraMetrics).

rapidly in recent years primarily driven by advances in acoustic technology and signal processing (Parsons et al., 2013). Besides providing accurate river-discharge measurements (Le Coz et al., 2008; Nihei and Kimizu, 2008; Sassi et al., 2012; Lee et al., 2014), ADCPs have proved to be a useful mean in studies of complex geophysical surface flows (Thorne and Hanes, 2002; Kostaschuk et al., 2004; Hoitink and Hoekstra, 2005; Kostaschuk et al., 2005; Rennie et al., 2007; García et al., 2007; Czuba et al., 2011; Hackney et al., 2015), flow structures at bifurcations, junctions and near obstacles (Dinehart and Bu-

rau, 2005b; Lane et al., 2008; Jamieson et al., 2011; Le Coz et al., 2010; Sassi et al., 2012), and for investigating hydrodynamic flow field in meander bends (Frothingham and Rhoads, 2003; Jugaru Tiron et al., 2009; Zinger et al., 2013; Flener et al., 2015; Engel and Rhoads, 2016). In fact, ADCPs can provide refined views of secondary flows and sediment movement in large rivers, with cross-stream velocities that could be resolved by averaging ADCP surveys (Dinehart and Burau, 2005a). With regard to tidal environments, several authors have employed ADCPs for measuring velocities at inlets (Defendi et al., 2010), flow fields around complex morphologies such as headlands (Geyer and Signell, 1990), solid transport (Defendi et al., 2010; Ferrarin et al., 2010; Zarzuelo et al., 2015a; Zarzuelo et al., 2015b), residual current (Mancero-Mosquera et al., 2010), wave propagation on salt-marsh surface (Priestas and Fagherazzi, 2011), overmarsh circulation (Sullivan et al., 2015) and to determine freshwater budget (Onken and Riethmuller, 2010). However, to the best of our knowledge, no field studies have examined in detail the flow structure within tidal meander loops. Along our study case bends, we surveyed the flow field as well as the bathymetry employing a SonTek RiverSurveyor M9 ADCP mounted on a 'Hydroboard' floating platform. The M9 ADCP is a nine-beam system with two sets of four profiling beams which measure samples using different frequencies. Each sample is divided vertically into separate cells, also referred to as bins. The cell height is dynamically adjusted depending on depth and speed in order to optimize performance and resolution. An additional 0.5-MHz vertical acoustic beam (echo sounder) provides a precise bathymetric survey. The presence of an integrated Differential Global Positioning System (DGPS) ensures a sub meter precision in positioning data. The SonTek M9 ADCP has been recently tested and validated by the USGS Office of Surface Water (Boldt and Oberg, 2015).

In comparison to ADCP surveys in fluvial settings, additional operational limitations have to be overcome in tidal channels due to the flow unsteadiness. In order to obtain robust estimates of the mean velocity fields and turbulence-averaged velocity, several transects are usually needed. During a single survey, a minimum number of six transects at the same cross-section was estimated (Dinehart and Burau, 2005a) to be necessary for determining peak discharges in rivers, where however temporal variability of discharges is smaller and high velocity stages last for longer periods than in tidal channels. Dinehart and Burau (2005a), by way of example, reported that seven hours of boat time were required to obtain six crossings at each of eight sections, and to profile channel topography in a 1 km fluvial reach. However, the semidiurnal tidal regime characterizing the flow field in our study case bends does not allows for such long surveys. Furthermore, rather than obtaining precise and reliable measurements of

flowing discharges, we are more interested in investigating flow structures near the maximum velocity stages, when the flow structures themselves have been observed to not significantly change (Frothingham and Rhoads, 2003). Therefore, the measurements we collected across different cross-sections in our study case bends have been repeated twice on average, with a maximum of four repetitions at each transect. For each bend, data have been collected during both ebb and flood phases near the maximum velocity stages and analyzed by means of the USGS Velocity Mapping Toolbox (VMT) (Parsons et al., 2013). Data from repeated transects were firstly projected to a mean, linear cross-section and interpolated to uniform grid. Particularly, the velocity field was divided into three different components, namely the streamwise velocity u (perpendicular to the mean cross-section), the transverse velocity v (parallel to the mean cross-section) and the vertical velocity w (Lane et al., 2000). Velocity magnitude and direction were recomputed at each grid node from their averaged component, in order to reduce the data noise and minimize turbulent fluctuations (Dinehart and Burau, 2005a). Data plan-views were then plotted in the form of depth-averaged velocities, providing valuable information about flow structures, flow separation zones and their interactions with channel banks. Furthermore, VMT allows for exploring patterns of secondary velocities, that is velocities perpendicular to the streamwise ('primary') flow. As for the definition of secondary flows, we adopted the "zero-net secondary discharge" (ZSD) convention, which is generally best suited for meander bends (Lane et al., 2000; Parsons et al., 2013). According to the ZSD definition, a new linear cross-section is computed so that no net secondary discharge flows through the entire cross-section. The component of velocity perpendicular (i.e. primary velocity, V_p) and parallel (i.e. secondary velocity, V_s) to the new rotated cross-section were finally computed and visualized in the cross-sectional plane.
A total number of 5 and 4 transects were surveyed for the "E" and "T" bend, respectivley, whereas 6 cross-sectional measurements were performed in the "C" bend. The pahts of all the surveyed sections are reported in Figure 3.3, 3.4 and 3.5.

3.1.5 Results

For the sake of clarity, we hereinafter consider a river-like reference system, where velocities are assumed to be positive when flowing seaward. Therefore, the channel is accordingly divided into a landward and seaward side. Cross-sectional views will always assume a seaward-directed observation point. Such a view determines the orientation of secondary circulations hereinafter. The term inner (outer) bank is instead used to indicate the convex (concave) bank of a mean-

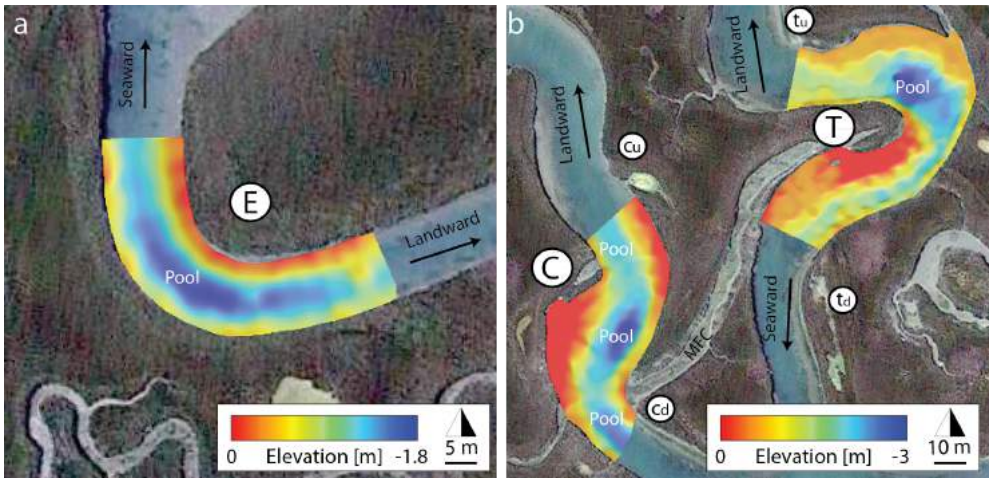

Figure 3.2: Multibeam bathymetric data of study case bends obtained from ADCP surveys. Blank circles are placed along the inner bank of individual bends, representing their own names.

der bend, regardless of the flow direction or view-point orientation. Finally, both water levels and bottom elevations are measured with respect to the mean sea level. Water depth is measured with respect to the instantaneous water level.

Bathymetric data

The bathymetry of the expansional meander (bend "E", see Figure 3.2-a) essentially resembles the classic bottom topography of river meanders, with a point bar located along the inner (convex) bank. The point bar, that displays an elongated shape, is sloped toward the channel axis, where a well developed pool is present in correspondence of the bend apex. The pool is about 1.8 m deep and occupies an approximately symmetrical position with respect to the channel flanks (i.e. it is located along the channel thalweg). Along the outer bank a series of irregularly-spaced shallow areas are observed. It is finally worth noting that another secluded shallow area protrudes from the landward side of the inner bank up to the channel axis.
On the contrary, an asymmetric bottom configuration is exhibited by the translating meander (bend "T", see Figure 3.2-b). A 3 m deep pool is present slightly landward of the bend apex, displaying width and depth noticeably larger than those characterizing the remaining portions of channel thalweg. Low-depth regions, possibly stemming for depositional zones, are located along both the seaward side of the inner bank and the landward portion of the outer bank.
Shallow areas located along concave banks seem to be the dominant feature of the cusp-shaped meander (bend "C", see Figure 3.2-b), where the deepest regions are constrained in the mid-channel area. Bathymetric data seem to suggest a periodicity in the thalweg topography,

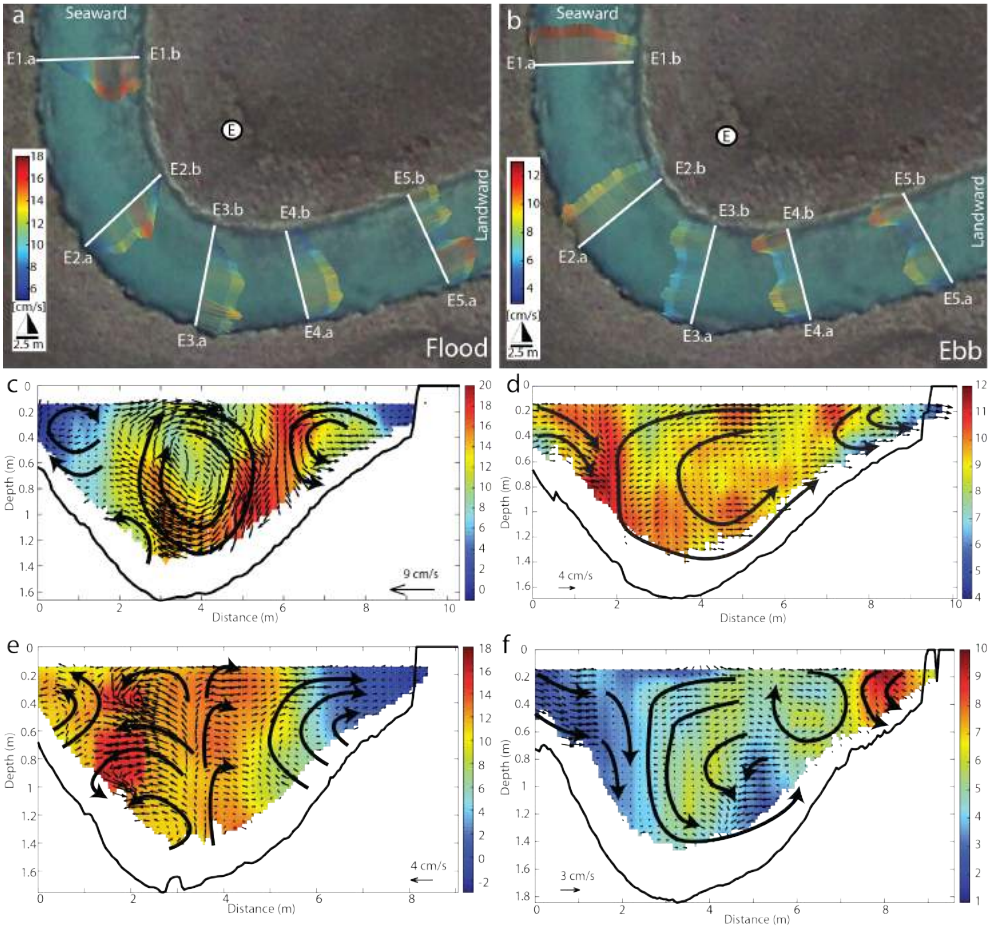

Figure 3.3: "E" bend study case. (a) and (b): Depth-averaged velocity (zero-net secondary discharge definition) during the flood and ebb phases, respectively. Cross-section names are also reported, where the ".a" label denotes starting points of the ADCP surveys. (c) to (f): Secondary flow overimposed to primary velocity magnitude (zero-net secondary discharge definition is applied) for section E2 (c,d) and E3 (e,f). Vertical exaggeration is x3. Data were collected on September 16th, 2016.

with pool zones located both upstream and downstream of every bend apex.

Velocity distributions

Velocity profiles collected using the SonTek River Surveyor M9 ADCP at different cross-sections enabled us to identify the main characteristics of the hydrodynamic flow field along the study case bends. Data were collected during both the flood phase and the subsequent ebb phase, and analyzed in terms of both primary and secondary velocity fields, as well as by depth-averaging the cross-sectional flow fields (Lane et al., 2000). The latter procedure allowed us to detect undeniable shifts in the position of the maximum velocity filament (MVF) between the ebb and flood phases for all the considered bends.

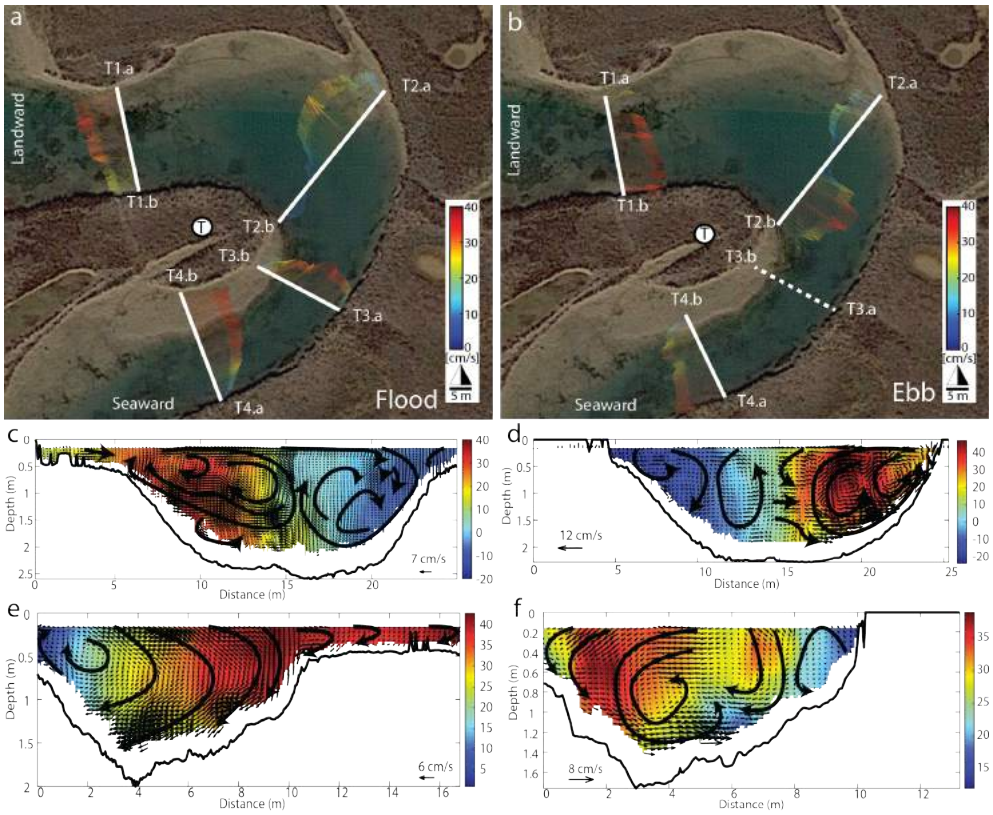

Figure 3.4: "T" bend study case. (a) and (b): Depth-averaged velocity (zero-net secondary discharge definition) during the flood and ebb phases, respectively. Cross-section names are also reported, where the ".a" label denotes starting points of the ADCP surveys. (c) to (f): Secondary flow overimposed to primary velocity magnitude (zero-net secondary discharge definition is applied) for section T2 (c,d) and T4 (e,f). Vertical exaggeration is x3. Data were collected on June 20th, 2016.

EXPANSIONAL MEANDER (BEND "E"): During the flood, the MVF in the expansional meander "E" is located along the seaward side of the inner bank (section E1 in Figure 3.3-a). Moving landward, the flow detaches from the inner banks, crosses the channel reducing its magnitude (s.E2 and E3), impinges the outer bank (s.E4) and regains strength while keeping flowing along it (s.E5). An area of small depth-averaged velocity (DAV) is observed along the landward-side of the inner bank (s.E2, E3 and E4) where a weak flow separation takes also place (s.E3). Section E5 exhibits two MFVs, separated by an area where velocities remain small. The behaviour observed during the flood phase is substantially overturned during the ebb phase, with the MVF flowing along the inner bank (s.E5 and E4) before moving along the outer bank (s.E1) after having clashed with it (s.E2, Figure 3.3-b). The double MFV in section E5 is still present, and in this case propagates landward in sections E4 and E3, eventually disappearing in section E2. During the flood phase, velocities are generally greater in

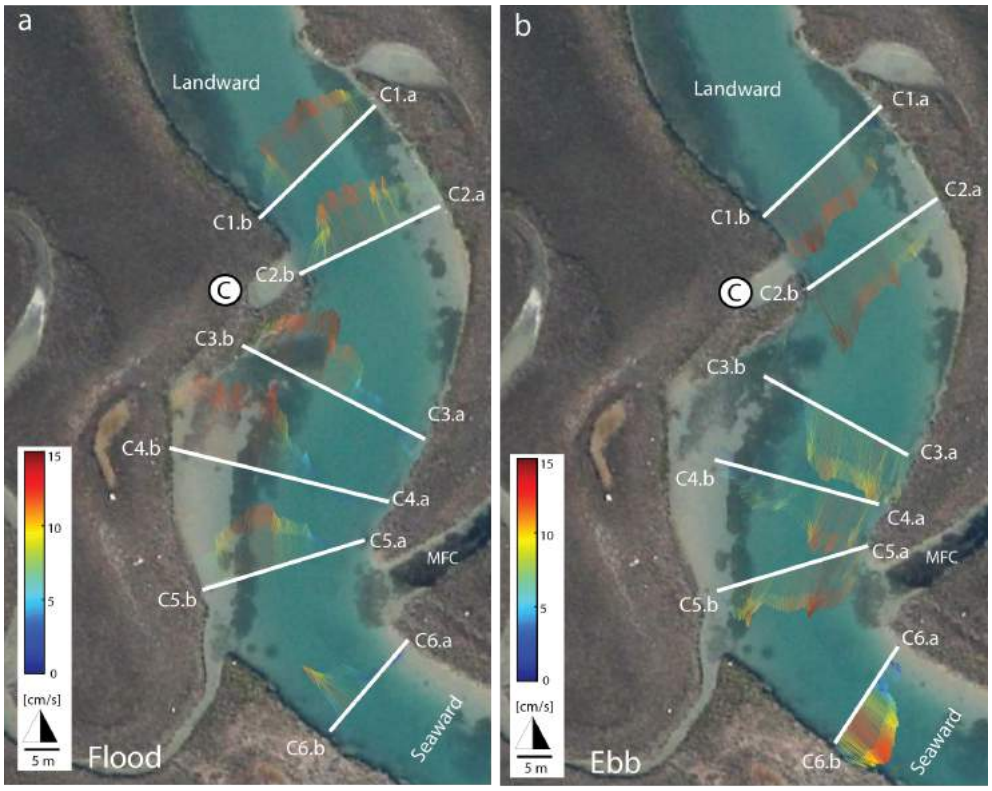

Figure 3.5: "C" bend study case. Depth-averaged velocity (zero-net secondary discharge definition) during the flood (a) and ebb (b) phases. Cross-section names are also reported, where the ".a" label denotes starting points of the ADCP surveys. Data were collected on July 19th, 2016.

terms of both DAV, primary and secondary velocity, the latter being showed in Figure 3.3-c,d,e,f. A well-established counter clockwise secondary current clearly characterizes the mid-channel area during the ebb phase (Figure 3.3-d,f) with water flowing toward the outer bank in the upper part of the cross-section and toward the inner bank in its lower part. A similar, yet smaller, secondary velocity cell is observed close to the inner bank, whereas at the outer bank no strong circulations take place and the flow is mainly directed toward the channel axis. On the contrary, flood flow in section E2 is characterized by clockwise secondary circulations at both mid-channel and inner-bank area, while at the inner bank, where the primary velocity is higher, the flow tends to climb the point bar moving counterclockwise (Figure 3.3-c). In section E3 the channel axis separates two subregions, with two velocity cells each. The outermost subregion displays counter clockwise secondary flow, that rotates in the opposite way toward the inner bank (Figure 3.3-e).

TRANSLATING MEANDER (BEND "T"): The complex morphology of the translating meander ("T") gives rise to elaborated patterns of DAVs (Figure 3.4-a,b). During the flood phase MVF (ca. 40 cm/s) is located

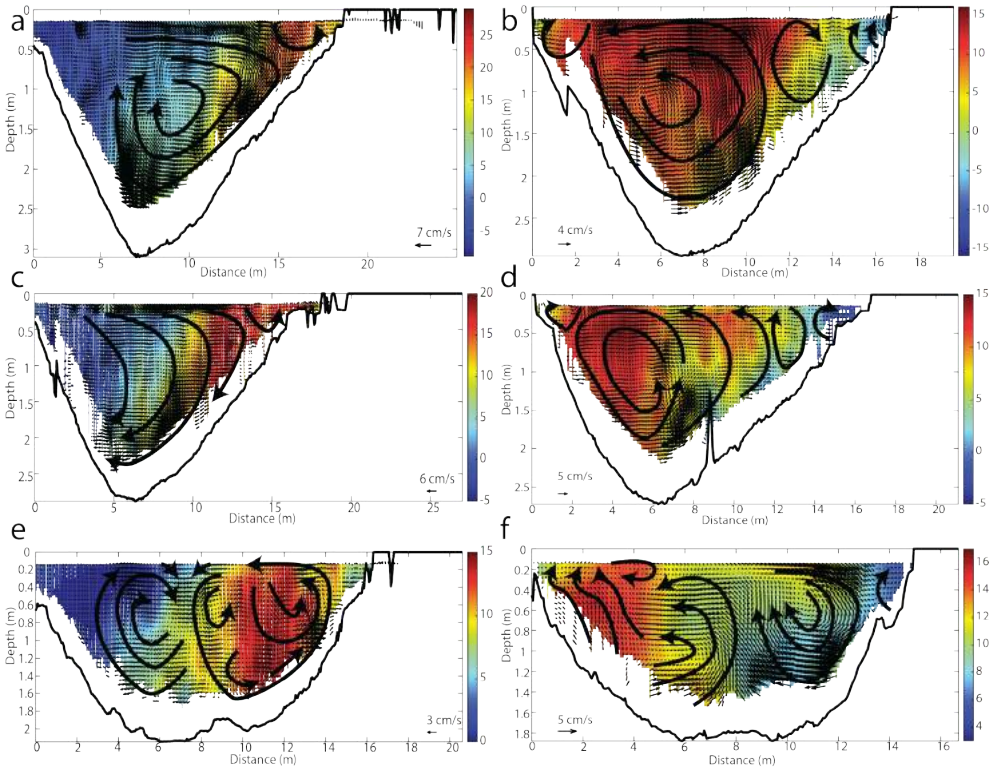

Figure 3.6: "C" bend study case. Secondary flow overimposed to primary velocity magnitude (zero-net secondary discharge definition is applied) for section C3 (a,b), C4 (c,d) and C5 (e,f). Flood is on the left side of the figure. Vertical exaggeration is x4. Data were collected on July 19th, 2016.

along the seaward side of the point bar (s.T4). Moving landward the flux tends to concentrate along the outer bank (s.T3 and T2). A quite large eddy forms close to the point bar apex (s.T2). During the ebb phase, on the contrary, the flux is almost uniform before flowing through the bend (s.T1, Figure 3.4-b) and, moving seaward, tends to concentrate along the inner bank (s.T2) before shifting toward the outer bank after the bend apex (s.T4). In the landward portion of the bend, a large outer-bank eddy takes place (s.T2).

During the flood phase, section T4 is characterized by the presence of a well-established, clockwise secondary current (Figure 3.4-e) with water flowing toward the inner bank in the upper part of the cross-section and toward the outer bank in its lower part. On the contrary, during the ebb phase (Figure 3.4-f) a counter clockwise secondary currents is present with water flowing toward the outer bank in the upper part of the water column and toward the inner bank in the lower part of the cross-section.

Secondary circulations with similar orientation are found in the apex ("T2") section (Figure 3.4-c,d), although their extension is limited to the channel portions where primary velocity are more sustained.

CUSPATE MEANDER (BEND "C"): MVFs are sistematically shifted along opposite sides of the channel by the tidal current turnover, with large recirculating eddies occurring on the sides opposite to the MVF locations (Figure 3.5). The same shift causes the cuspate-inner bank to be impinged during both ebb and flood phases along the landward and seaward side of the bank, respectively. From a cross-sectional point of view, the ebb phase in the seaward portion of the channels (s.C3) is characterized by a counter clockwise circulation in the central-left part of the channel, where primary velocities are more sustained (Figure 3.6-b). Two clockwisely oriented cells occur instead along the inner bank (Figure 3.6-b). Aside from a bulb of maximum velocity more shifted toward the outer bank, the same secondary circulation patterns are mantained moving landward, with the outer-bank clockwise circulation widening progressively (s.C4 and C.5, Figure 3.6-d,f). The situation observed during the ebb phase is essentially capsized during the flood phase, when sections C3 (Figure 3.6-a) and C4 (Figure 3.6-b) are mainly occupied by transverse flows oriented toward the left bank along the channel bottom, and toward the right bank in the uppermost part of the water column. Half of the cross-sectional area in section C5 displays a similar, yet smaller, secondary flow pattern (Figure 3.6-c), that is however counterbalanced by a proximal counter clockwise circulation. The latter seems to be flowing around the maximum primary velocity kernel situated in the right portion of the cross-section. Moving landward, such kernel is invariably placed along the right side of the bend, while its size decreases progressively. It is finally worth noting how the maximum magnitude of the primary velocity during the ebb is generally lower than that in the flood, albeit the latter occupies a much smaller portion of the section than the first.

3.1.6 Discussion

EXPANSIONAL MEANDER (BEND "E"): With a symmetric, well developed point-bar and a pool zone located in corrispondence of the apex, the "E" bend represents an expansional meander in the classic fluvial fashion. The occurence of mutually-evasive paths taken by tidal currents leads to the development of a neither asymmetrical nor cusp-shaped bar. This is in contrast with classical models which link the occurence of shifting currents to the growth of cuspate morphologies (Ahnert, 1960; Hughes, 2012). Furthermore, channel width does not show any substantial variation along the bend, and no significant flow recirculation is observed from the depth-averaged velocity (DAV) in spite of the relative sharpness of the bend (Ferguson et al., 2003). Accordingly to the classic meander evolution models, such a planform is related to point bar growing uniformely along both its landward and sea-

ward side, although Figure 3.1-a depicts a slightly more pronounced growth on the landward side of inner bank. This might suggest a flood dominance, an hypothesis that is further supported by the greatest velocity magnitudes that the bend exhibits during the flood phase (Figure 3.3), even though speculating on velocity magnitudes could be misleading without having monitored several complete tidal cycles. We furthermore underline that the Venice Lagoon is known for being an ebb-dominated system (Gatto and Carbognin, 1981) and that, in landward parts of salt marshes, the ebb tides should increasingly control creek morphology (Bayliss-Smith et al., 1979; Ranwell, 1972). Nonetheless, it is worth noting how the maximum velocity filament (MVF) is sharper during the flood phase, in particular when it hits the outer bank in section E3 (Figure 3.3-a). On the contrary, during the ebb phase the flow ties the left bank in section E2 where the DAVs are nearly uniform (Figure 3.3-b). A strong asymmetry between tidal phases takes also place in cross-sections: during the flood phase, the separation between high and low primary velocity cores is sharper, and secondary circulations are more well defined (Figure 3.3-c,d,e,f). A possible explanation for the apparent dominance of flood flows could be represented by the shoal occurring in the central part of the channel along the landward side of the bend (Figure 3.2-a). In this area, during both the ebb and flood stages a double peak in DAV are documented (s.E5 in Figure 3.5-a,b). Field observations revealed that this shoal consists of a patch of bottom-channel vegetation, namely *Posidonia oceanica*. *Posidonia oceanica* is known to be able to affect flow field in small channels (relatively to the dimension of vegetation patch), especially by increasing turbulence (Folkard, 2005), and the collected data exhibit a kernel of low primary velocity (Figure 3.7-b) around the vegetation-bulge protruding from channel bottom, further supporting our hypothesis. Moreover, the alternating unregular patterns of streamwise vorticity (i.e. vortexes whose axes are parallel to the streamwise primary velocity) seem to resemble those obtained by Stoesser et al. (2015) for non uniformly roughed channel bed.

Even though the flow-vegetation interaction is not the focus of the present contribution, it is worth recalling how this topic has been extensively studied in the literature on river meanders (e.g., Gurnell, 2014). However, most of the contributions focused on the influence of riparian, rather than acquatic ("in-stream"), vegetation in stabilizing banks, preventing erosion and maintaining single-thread channels (e.g., Murray and Paola, 2003; Tal and Paola, 2007). This hypotheses are largely supported by both modelling (e.g., Millar, 2000; Murray and Paola, 2003; Parker et al., 2010; Crosato and Saleh, 2011) and experimental studies (e.g., Gran and Paola, 2001; Tal et al., 2004; Tal and Paola, 2007; Tal and Paola, 2010), as well as by evidences from the field (e.g., Hickin and Nanson, 1984; Bertoldi et al., 2011) and fossil

record (e.g., Davies and Gibling, 2010a; Davies and Gibling, 2010b; Gibling and Davies, 2012; Ielpi et al., 2015). As elegantly summarized by Perucca et al. (2007): "*River planform evolution forces the riparian vegetation dynamics, which, in turn, affect the mechanical characteristics of the river banks and influence the meandering dynamics of the river itself*".
Well known is also the role of submerged, acquatic vegetation in modifying flow and transport within open channels (e.g., Nepf and Ghisalberti, 2008; Nepf et al., 2013), whereas very few studies have investigated the flow-vegetation interaction along meander bends. Nevertheless, a recent contribution by Termini (Termini, 2013; Termini, 2016) highlighted how the presence of submerged flexible vegetation along channel bends i) causes the curvature-induced secondary flows to be suppressed, ii) alters the directionality of turbulent structures thus possibily reducing sediment transport at the banks, and iii) maintains the core of highest bed-shear stress far from the outer bank. These results are also in accordance with those obtained by Schnauder and Sukhodolov (2012) for the meandering Tollense River (GER). The transport capacity of secondary circulations is therefore drastically reduced by the presence of acquatic vegetation, with direct consequences on migration rates and, ultimately, on meander dynamics. Such a result seems to supprot our hypothesis: along our study case bend, a vegetation patch weakens secondary flows during the ebb phase, thus reducing the outer bank erosion along the bend, as well as preventing deposition on the seaward side of the inner bank thanks to both a greater retention of suspended particles (Stoesser et al., 2015) and a reduced sediment transport nearby channel bank (Nepf et al., 2013; Termini, 2016), thus leading to the observed preferential point-bar growth along the inner bank landward side. This hypothesis is further supported by two recent scientific contributions from Gurnell (2014) and Tambroni et al. (2016), which emphasized the role of vegetation in modifying flow field and sediment transport.

TRANSLATING MEANDER (BEND "T"): The "T" meander bend exhibits a marked translational behavior (Figure 3.1-b), with a progressive shift of the point-bar apex along a trajectory that is almost transverse to the bend axis. Such an evolution challenges the classical "expansional" (sensu Jackson, 1976) planform behavior of tidal meander bends (Hughes, 2012). Similar processes are documented in other sites of the Venice Lagoon and in other tidal environments worldwide (see also Appendix B), pointing to a common incidence of these processes in tidal networks. The strong channel-axis curvature leads to a well developed DAVs recirculation in outer bank areas (Figure 3.4). The latter invariantly displays a limited depth, exhibiting a noteworthy similarity with fluvial counter-pointbar deposits (Smith et

(a) Presence of vegetation in section E5 highlighted from aerial photo. Vegetation patches are circled in red (©2016 Google, TerraMetrics).

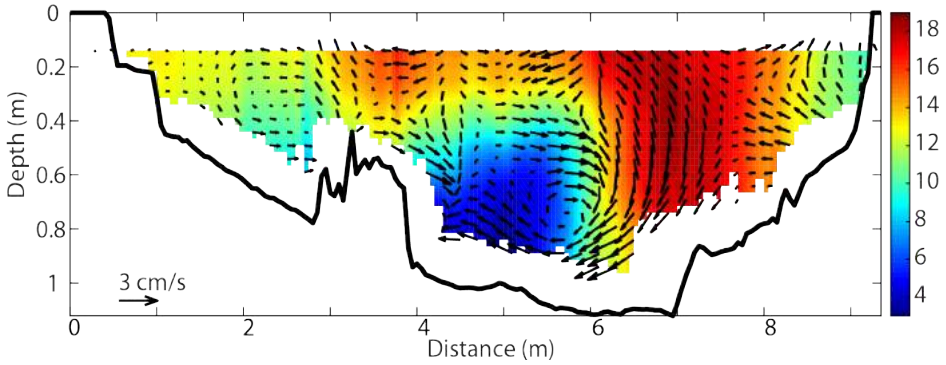

(b) Section E5 - Ebb secondary flow overimposed to primary velocity (zero-net secondary discharge deinition applied). Vertical exaggeration is x3

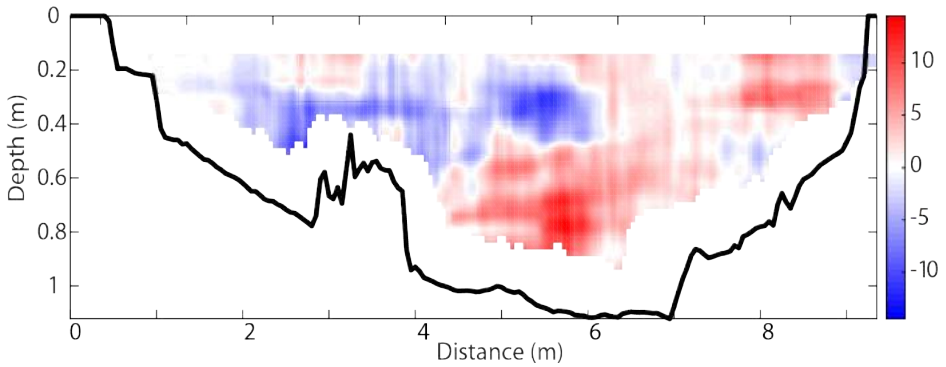

(c) Section E5 - Ebb phase streamwise vortcity (positive vorticities stand for clockwisely circulating areas). Vertical exaggeration is x3.

Figure 3.7: Possible evidences of channel-bottom vegetation in section E5.

al., 2009). The landward side of the inner bank appears to be progressively eroded and migrates downstream, whereas the observed low

depths suggest deposition and preservation along the seaward side. Such a behavior is consistent with the general ebb-dominated character of minor tidal creeks (Bayliss-Smith et al., 1979; Ranwell, 1972), and of the Venice Lagoon in particular (Gatto and Carbognin, 1981). This instance is further supported by the secondary velocity paths in section T4 (Figure 3.4-e,f): the differential paths of the high-velocity streamlines allows the outer side of the bank to cyclically experience both high (flood flow) and low (ebb flow) velocity stage. While the first should promote bank erosion and sediment transport toward the channel axis (clockwise secondary flow rotation), the latter should carry fine sediment over the bar (counter clockwise rotation). Given that the point-bar grows along its seaward side, the ebb-depositional mechanism is believed to prevail.
Along the apical cross-section (T2), significant secondary-velocity flows occur exclusively around the bulb of maximum primary velocity, that in its turn affects about half of the cross-sectional area during both the tidal phases (Dietrich and Smith, 1983). More interestingly, secondary velocities are unconditionally directed inward (i.e., toward the channel axis) along the surface, and outward (i.e., toward the channel bank) at the bottom, whereas an opposite rotation would be expected (Dietrich and Smith, 1983; Frothingham and Rhoads, 2003). This odd behaviour is likely due to nonlinear interactions between the flow, the bed topography and the channel planform (Seminara et al., 2001) and, together with different erodibility of channel banks, might contribute to explain why such a sharp bend translates instead of expanding. We finally point out how the seaward translation process offers to the outer-bank deposit the possibility of being progressively cover by the landward-located adjacent bar that migrates seaward, thus leading to the formation of depositional body with high preservation potential.

CUSPATE MEANDER (BEND "C"): In the cuspate meandering channel, an unexpected meander evolution is observed, that reduces channel sinuosity rather than increasing it (Figure 3.1-b). This study case represents a bright example of the mutual evasion of tidal currents, with well developed recirculating DAV cells taking place on opposite banks during different tidal phases (Figure 3.5). Deposition along concave banks recalls fluvial couter-pointbar deposits, which however take place on sharp bend whereas the study case tidal channel is weakly sinuous. The weary sinuosity allows a comparison with the tidal-meander model proposed by Solari et al. (2002), which highlighted symmetric oscillations of the pointbar-pool pattern around the locations of maximum curvature, as well as the absence of net bar migration in a tidal cycle. Accordingly, the first conditions is quite well resembled by the channel bathymetry (Figure 3.2-b) where pools are observed on both sides of the cuspate apex. On the contrary, with

respect to the migration of bars, we note a progressive dismantling of pointbars in time (Figure 3.1-b), with erosion occurring at both the landward and seaward sides of the bar. This is likely related to the MVF that alternately impinges opposite flanks of the bar, thus shaping the peculiar cuspate morphology and causing accretion of the outer-bank deposits (Ahnert, 1960; Dalrymple et al., 2010; Hughes, 2012). Besides leading to a progressive meander straightening, the depositional areas along the concave banks appear to be the most preservable part of the channel. Furthermore, following the trajectories of cusp-apexes through time a clear downstream migration is detectable, stemming from a likely ebb dominance.
The analysis of secondary velocities confirms the latter instance: during the ebb phase, the balance between centrifugal force and pressure gradient induced by the MFV shifting toward the outer bank, produces secondary velocities that flow outward on the water surface and inward at the channel bottom (Figure 3.6-b,d,f). The same mechanism acts in the opposite manner during the flood stages (Figure 3.6-a,c,e); notwithstanding, the bar deepens inward from the right bank, thus highlighting the dominant role of the ebb flow.
During both the tidal phases, we finally record the possible subsistence of small secondary cells, counter rotating with respect to the main cell (see section C3 and C4 in Figure 3.6-a,c and b,d respectively). These cells, named outer-bank cells, are well known to exist (e.g., Einstein and Harder, 1954; Rozovskii, 1957; Dietrich and Smith, 1983) and to play a crucial role in limiting the growth of the center-region cell, preventing bank erosion by keeping the core of maximum velocity far from it. In our study-case bend, the simultaneous presence of this type of cells and flow-separations in DAV may suffice to explain the odd morphological evolution observed in the channel.

3.1.7 Conclusions

Three different types of tidal meander bends located in the northern part of the Venice Lagoon have been studied through integration between analyses of historical aerial photos and measurements of flow velocity patterns. Results stemmed out from this work provided new insights to understand the link between the morphodynamic evolution of tidal point bars and related hydrodynamic processes.
These results can be summarized as follows:

- the maximum velocity filament is constantly observed to shift its position along meander bends over different tidal phases. These mutually-evasive paths of the ebb and flood high-velocity streams during a tidal cycle appear to be a common feature of tidal meanders, regardless of the considered meander typology;

- flow separations during the dominant tidal regime are often associated with the growth of depositional features, namely point-bar and counter-pointbar. The latter phenomenon is observed to take place also along weakly sinuos meander;
- as for fluvial meander bends, secondary velocity circulations arise from the unbalancing between centrifugal force and the lateral pressure gradient driven by free-surface lateral slope. However, in tidal meanders the direction of such circulations is occasionally inverted if compared to that occurring in fluvial bends, with water flowing toward the inner (convex) bank on the surface and toward the outer (concave) bank at the channel bottom. Similarly to fluvial meander instead, outer-bank secondary cells are also present, whose main effect is to keep the main secondary cell far from channel banks, thus inhibiting bank erosion;
- counter-pointbar deposits in tidal meander are rather common, and are usually endowed with an high preservation potential;
- in shallow channels, channel-bottom vegetation may significantly alter the hydrodynamic field, influencing the morphodynamic evolution of meander bends.

3.2 OVERTIDES, BIDIRECTIONAL FLOWS AND LATERAL TRIBUTARIES: DISENTANGLING THE ROLE OF TIDAL ASYMMETRIES ON MEANDER EVOLUTION.

This chapter is a manuscript in preparation, whose primary goal is to investigate the role of bidirectional flow, tidal asymmetries and lateral tributaries in shaping tidal meanders. By integrating two different physically-based numerical models, a series of simulations were carried out to reproduce the evolution of a meander bend located in the Venice Lagoon. In order to provide a comprehensive framework, the results were compared to both available historical data and the evidences obtained from a parallel geophysical study on the same study-case bend. This work highlights that i) the presence of some, yet small, tidal asymmetries influences the morphodynamic evolution of tidal meanders in a significant manner; ii) fundamental differences subsist between fluvial (i.e. unidirectional flow) and tidal (i.e. bidirectional flows) conditions; iii) under certain conditions, lateral tributaries may crucially influence the evolution of the main channel.

As mentioned before, part of the results shown in this chapter were obtained from a parallel study carried out on the same bend. The results of this study are described in a manuscriptready to be submitted to the journal "Geology" (see Appendix C). The collection and analysis of geophysical data, as well as the "Geomorphological settings" section reported in the present chapther have been fully contributed by Lara Brivio, Massimiliano Ghinassi and Andrea D'Alpaos, which are deeply acknowledged together with the other authors.

PAPER

Finotello, Alvise[1], Alberto Canestrelli[2], Andrea D'Alpaos[1], Luca Carniello[3], Lara Brivio[1] and Massimiliano Ghinassi[1]

[1]Dept. of Geosciences, University of Padova, via G.Gradenigo 6, Padova, PD I-35131, Italy

[2]Istituzione Centro Previsioni Segnalazione Maree, San Marco 4136, Venezia, VE I-30124, Italy

[3]Dept. ICEA, University of Padova, via Loredan 20, Padova, PD I-35131, Italy

3.2.1 Abstract

Meandering channel networks exert a fundamental control on hydrodynamic and morphodynamic processes within tidal landscapes. However, most studies have interpreted the evolution of tidal mean-

ders based on observations and models developed for their fluvial counterparts. The present study investigates the influence of bidirectional flow, tidal asymmetries and lateral tributaries on tidal meanders morphodynamics. An approach based on the integration of 2D and 3D numerical modelling is employed to model the morphdynamic evolution of a meander bend in Venice Lagoon (Italy). The results of numerical simulations are benchmarked with both historical and modern field data. Firstly, we found that the main component of astronomical tide suffices to reproduce the observed meander evolution, although the presence of some, yet small, asymmetries in tidal forcings influences the morphodynamic evolution of tidal meander in a significant manner. Secondly, the results of simulations carried out under fluvial conditions (i.e. unidirectional flow), highlighted the fundamental peculiarities of tidal meanders. Particularly, we showed that the position of depositional bodies along the bend represents an appropriate proxy to detect the dominance of either ebb or flood flow. Finally, the influence of lateral tributaries was investigated, that under certain conditions may crucially influence sedimentation patterns in the main channel. By highlighting the relative importance among the complex set of morphodynamic forcings, our findings might be relevant for extending to the tidal case the 1-D or depth-averaged 2-D models which are commonly used in long-term investigations on river-meander evolution.

3.2.2 Introduction

Branching and meandering tidal channels form the pathways for tidal currents to propagate and distribute clastic sediments and nutrients (e.g., D'Alpaos et al., 2005; Hughes, 2012; Coco et al., 2013), thus providing a primary control on tidal landscapes ecomorphodynamics (Fagherazzi et al., 2012). Most tidal channels in both estuarine and lagoonal landscapes have a tendency to meander (Solari et al., 2002), but nevertheless very few studies have analyzed their morphometric characteristics and morphodynamic evolution (Gabet, 1998; Marani et al., 2002; Solari et al., 2002; Fagherazzi et al., 2004). As for the fluvial case, the meandering process in tidal channels is likely to be controlled by several components such as flow conditions, abundance and type of sediments, vegetation, and sedimentological characteristics of the channel boundaries (Abad and García, 2005). Channel evolution, both in time and space, results from complex interactions among the aforementioned components. However, in spite of the recent breakthroughs in numerical, experimental and field techniques, a truly investigation on the full-spectrum variability of all the chief landforming processes is yet not feasible, and process interactions remain mostly unknown. Hence, researchers and scientists have usu-

ally adopted simplified approaches according on the objectives of the study. Simplifications include the employment of straight and/or idealized planforms (Seminara et al., 2001; Lanzoni and Seminara, 2002; Solari et al., 2002; Tambroni et al., 2005; Garotta et al., 2006; Garotta et al., 2007; Seminara et al., 2010; Toffolon and Lanzoni, 2010; Canestrelli et al., 2014; Bolla Pittaluga et al., 2015; Lanzoni and D'Alpaos, 2015), constant width (Seminara et al., 2001; Solari et al., 2002; Tambroni et al., 2005; Garotta et al., 2007; Seminara et al., 2010), non-erodible banks (Seminara et al., 2001; Lanzoni and Seminara, 2002; Garotta et al., 2007; Seminara et al., 2010), non-cohesive sediments (Seminara et al., 2001; Solari et al., 2002; Lanzoni and Seminara, 2002; Tambroni et al., 2005; Garotta et al., 2007), simplified hydrodynamics or tidal forcings (Seminara et al., 2001; Lanzoni and Seminara, 2002; Solari et al., 2002; Tambroni et al., 2005; Garotta et al., 2007; Seminara et al., 2010; Lanzoni and D'Alpaos, 2015), as well as neglecting the presence of tidal flats and marshes adjacent to the main channel (Seminara et al., 2001; Lanzoni and Seminara, 2002; Solari et al., 2002; Tambroni et al., 2005; Garotta et al., 2007; Seminara et al., 2010). Furthermore, very few studies account for meandering in tidal streams, namely the laboratory-based study from Garotta et al. (2007) and the mathematical model of Solari et al. (2002), both including simplifying assumptions.

In the experiments of Garotta et al. (2007), channel banks were fixed, whereas channel bottom was made up of low density, non-cohesive sediments that were entrained and redeposited by tidal fluxes. The latter consisted of a sinusoidal tide generated in the sea basin by a mechanical system. In the seaward half of the channel, empirical evidences highlighted odd depositional pattern, characterized by inner bank scour and deposition along the outer bank similar to that we observed in the field (see bend "C" in section 3.1). The author claimed these patterns would have been *"planimetrically unstable if the channel walls were erodible"*, recalling the common quasi-straight paths displayed by tidal channels nearby inlets as evidence.

In the beautiful work of Solari et al. (2002), likely representing the best mathematical model for tidal meanders thus far, the linearization of the three-dimensional mathematical formulation proposed by Seminara et al. (2001) read to a linear solution for the flow and bed topography fields in a long, weakly meandering tidal channel with erodible bed and non-erodible banks. The channel was forced by a periodic sinusoidal tide with zero mean, whose amplitude and wavelength were assumed to be small enough compared to channel depth and meander wavelength, respectively. A fluvial-like behaviour was observed, with high velocity thread and channel thalweg shifted toward meander outer banks. The bar–pool pattern however oscillatd in time around the bend apexes, withouth displaying any net bar mi-

gration in a tidal cycle. The authors also proposed, for tidal meanders, a linear "bend" instability theory (sensu Ikeda et al., 1981; Blondeaux and Seminara, 1985) with erodible banks, assuming a close similarity with fluvial-meander behaviour based on their analogous planimetric shapes. We have however proved this conjecture to fail (see section 2.2), further observing that, contrary to fluvial meanders, outer bank in tidal channel is quite often subjected to depositional rather than erosional mechanisms (see section 3.1).

On the one hand, the adoption of simplified conditions allows for a better understanding of specific processes underlying morphodynamics. On the other hand, however, oversimplifications might sometimes lead to misleading results. As a matter of example, Garotta et al. (2006) demonstrated that alternate free bars in straight tidal channels display net migration in a tidal cycle if the role of overtides (i.e. secondary tide of higher frequency than the principal tide) is taken into account. The overtide-induced tidal asymmetry contributes to net sediment transport (Dronkers, 1986; Boon, 1975; Toffolon and Lanzoni, 2010), and overlaps other differently generated asymmetries such as those typically observed in salt-marsh creeks (e.g., Boon, 1975; Bayliss-Smith et al., 1979; Pethick, 1980). Even the wind action, causing tidal surges and inducing resuspension of fine sediments, may somehow represent a tidal asymmetry (Dronkers, 1986; Carniello et al., 2005; Mancero-Mosquera et al., 2010; Carniello et al., 2011). Furthermore, most tidal meanders present asymmetric planform configurations, characterized by the presence of many minor lateral tributaries (Fagherazzi et al., 1999). However, the role of such asymmetries and peculiarities have often escaped close scrutinies, mostly because of the lack of benchmarking field-data. Such framework is further complicate by interplay of factors acting at different scales. For instance, the channel evolution at the meander length-scale is related to phenomena occurring at wider spatial scales, such as tide propagation and wind-wave sediment entrainment, which in their turns depend on channel morphologies.
It is therefore the aim of the present work to perform, by means of suitable numerical models, qualitative and quantitative analyses on the morphodynamic evolution of a tidal meander bend located in the Venice lagoon. Thanks to the availability of several field data, deriving from both historical and recent aerial photos, tide gauge measurements, bathymetric field surveys, geophysical investigations and numerical modelling itself, the selected channel represent an appropriate target for investigating the role of the above-mentioned peculiarities and asymmetries in the morphodynamic evolution of tidal meandering channels.

The plan of the paper is as follows. The next section is devoted to a brief description of the geomorphological setting. Sections 3.2.4

describes the materials and the models employed in the study. Section 3.2.5 reports the experimental results, which are discussed in section 3.2.6. Section 3.2.7 concludes the paper with some final remarks.

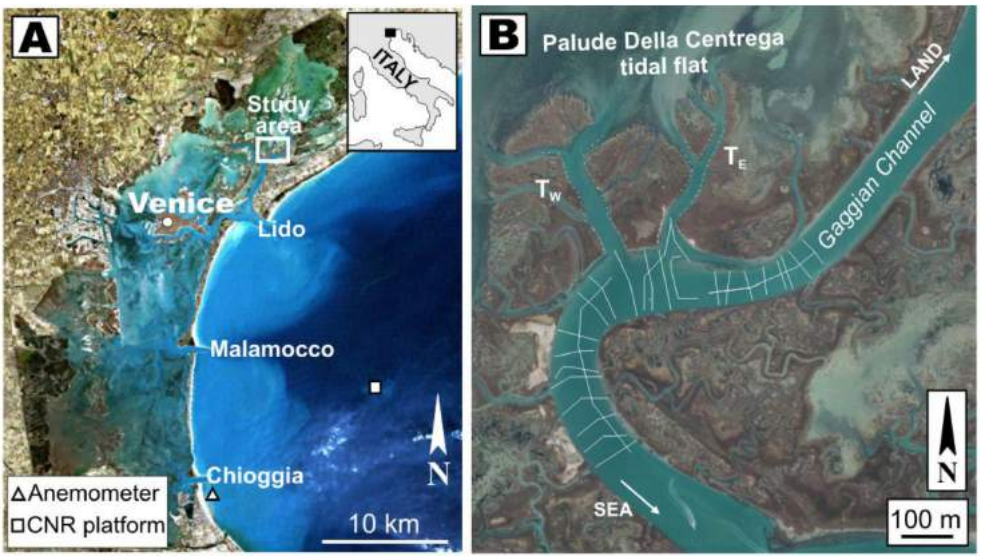

Figure 3.8: The study site. (A) Geographic location of the study area, in northeastern portion of the Venice Lagoon, Italy. Locations of wind anemometer and CNR platform tide gauge are also highlighted. (B) Satellite image (2012) of the Gaggian channel showing the acquisition scheme of sub bottom profiles (white lines).

3.2.3 Geomorphological Setting

We analyzed a meander bend of the Gaggian Channel, located in the Northern, and best naturally preserved, part of the Venice Lagoon (Figure 3.8-A). The Venice Lagoon, which formed over the last 7500 years covering alluvial Late Pleistocene deposits locally known as Caranto (Zecchin et al., 2008), is the largest Mediterranean brackish water body, with an area of about 550 km^2. It is connected to the Adriatic Sea through three inlets (Lido, Malamocco and Chioggia) and is subjected to a semidiurnal tidal regime, with an average tidal range of about 1.0 m and peak tidal amplitudes of about 0.75 m around Mean Sea Level (MSL) which can suddenly be increased by meteorological forcing (Carniello et al., 2011; Mel et al., 2014). The lagoon experienced a constant relative sea level rise until the beginning of Fifties, when subsidence increased in response to the groundwater extraction for industrial exploitation that proceeded until the 1970s when the withdrawal ended (Gatto and Carbognin, 1981; Carniello et al., 2009; Ferrarin et al., 2015). The morphodynamic of the lagoon is affected by seasonal storm events, among which the most "morphologically meaningful" are storms characterized by Bora wind, that is the most

intense wind in the Gulf of Venice, blowing from NE with a speed that can easily exceed 20 m/s (Carniello et al., 2009; Carniello et al., 2016).

The study site is a 900 m long meander bend, which develops around a point bar with a mean radius of curvature of about 200 m (Figure 3.8-B). The channel is about 100 m wide, up to 8 m deep and receives tributaries on both its inner and the outer bank. Two main tributaries along the outer bank, named hereafter as TW (Western Tributary) and TE (Eastern Tributary), enter the Gaggian channel near the bend apex and connect it with the "Palude della Centrega" tidal flat to the North (Figure 3.8-B). Medium to coarse-grained sand is common in the deepest part of the Gaggian channel, whereas fine-grained silty sand occurs in shallower areas and along the thalweg of the TW and TE tributaries. The TW and TE tributaries, which are about 40 and 30 m wide and 3.6 and 3.0 m deep, respectively, branch northward into a number of minor channels which cut through the 0.55 m deep Palude della Centrega tidal flat. High-resolution geophysical data were acquired in 2011, through the use of a sub-bottom profiler, along the Gaggian channel (see Figure 3.8-B) and interpreted through a specific 3D modeling software. Geophysical data highlight the presence of two laterally extensive key surfaces, which divide the channel deposits into three sedimentary units, that were associated with three main depositional stages of meander bend evolution (Figure 3.9). All these stages, especially in the first and in the second ones, emphasize the occurrence of an ebb-dominated transport. The first stage is associated with development of point-bar deposits and is characterized by lateral accreting beds dipping toward the channel thalweg at about 10-20^{0}. The second stage is associated with deposition in the landward side of the meander bend, where both aggradation and lateral accretion are documented. The third stage is characterized by accumulation of deposits at the outlet of two minor tributaries entering along the outer bank of the channel.

3.2.4 Material and Methods

Remote Sensing Data

A long historical record of high-resolution aerial photographs and satellite images of the Gaggian Channel and its surrounding area is available (Figure 3.10), ranging from 1938 to nowadays. Bathymetric data were obtained from the 1930 and 2012 bathymetries (Figure 3.10)L,N and see also Carniello et al., 2009 for further details), and employed to determine morphological changes of the Gaggian channel and its lateral tributaries.

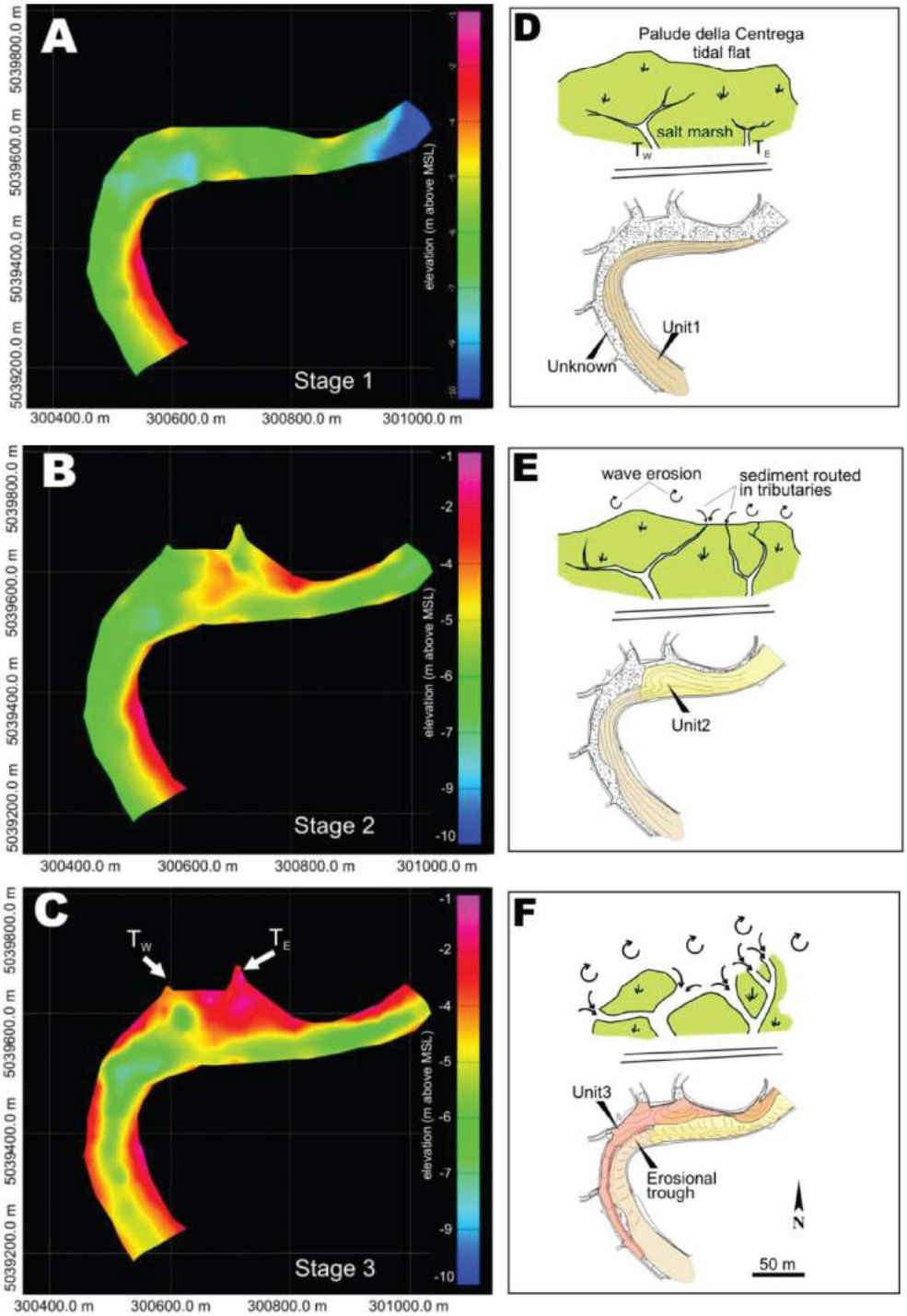

Figure 3.9: Morphological evolution of the Gaggian channel as derived from the geophysical data. (A - C) Top morphologies of Unit 1 to 3 as they emerge from the spatial interpolation of seismic profiles obtained through a kriging procedure. Panels A – C highlight the development of lobes at the tributary outlets and the related deposition patterns along the outer bank. (D – F) Conceptual model portraying the three stages of the Gaggian channel evolution. (D) TW and TE tributaries do not receive sediment from the Palude della Centrega tidal flat and the Gaggian channel bend is dominated by inner bank deposition. (E) Ongoing inner bank sedimentation. (F) Sediments resuspend by wind waves in the Palude della Centrega are routed into the Gaggian channel through the TW and TE tributaries causing accumulation along the outer bank.

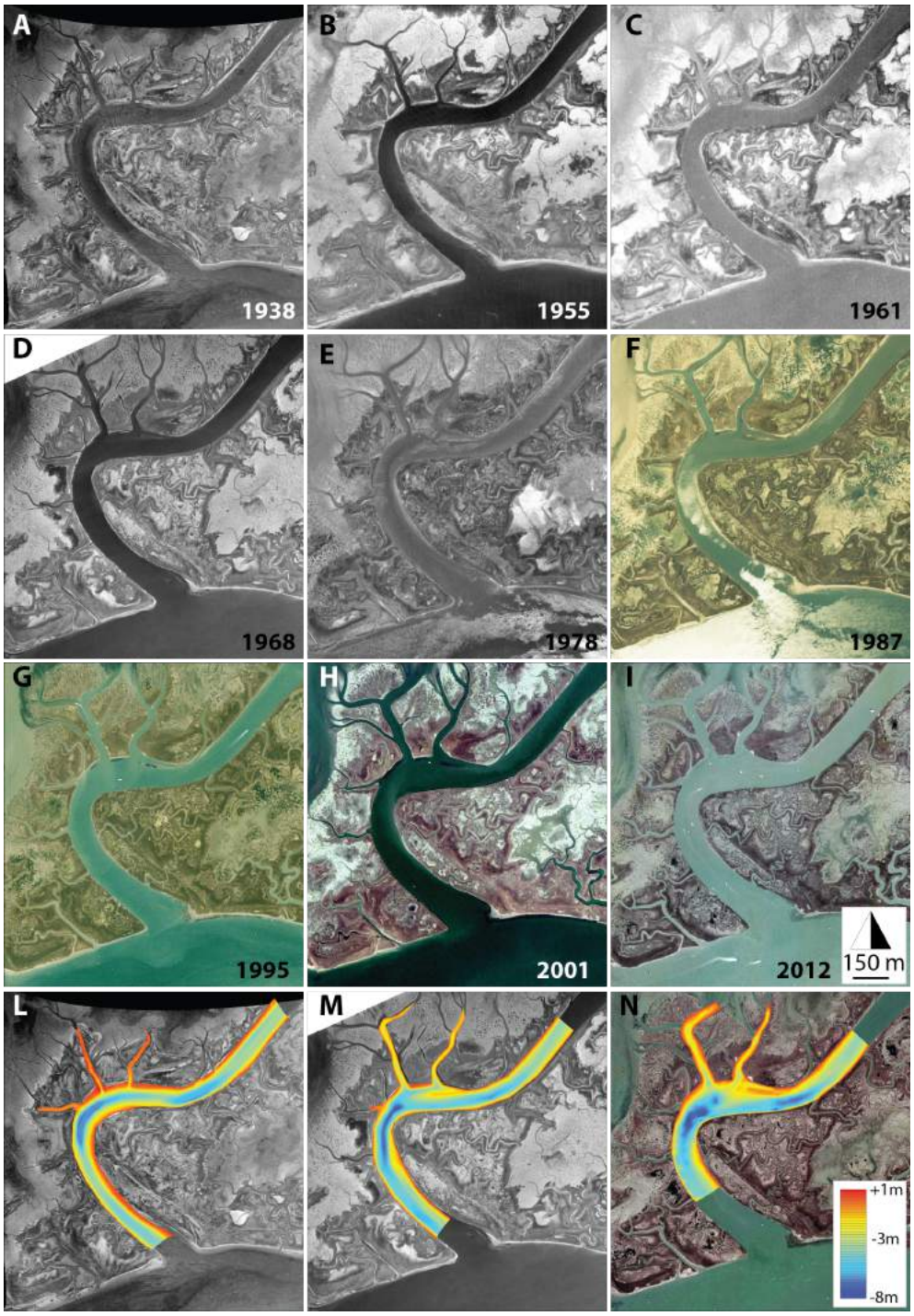

Figure 3.10: Digitalized orthophotos of the Gaggian channel in: 1938 (A), spatial resolution of 600 dpi (1pixel = 0.897 m); 1955 (B), spatial resolution of 600 dpi (1pixel = 1.124 m); 19611(C) spatial resolution of 600 dpi (1pixel = 1.269 m); 1968 (D), spatial resolution of 600 dpi (1pixel = 0.599 m); 1978 (E), spatial resolution of 600 dpi (1pixel = 0.921 m); 1987 (F), spatial resolution of 600 dpi (1pixel = 0.888 m); 1995 (G), spatial resolution of 600 dpi (1pixel = 1 m); 2001 (H), spatial resolution of 600 dpi (1pixel = 1.1 m); 2012 (I), spatial resolution of 600 dpi (1pixel = 0.73 m); bathymetric data of the Gaggian channel in 1932 (L), 1970 (M) and 2012 (N).

Numerical Modelling

The Coupling of both 2D and 3D models is necessary since that the evolution of tidal meanders depends on factors acting at different spatial scales. Hence the bidimensional (depth averaged) hydrodynamic wind-wave model WWTM (Carniello et al., 2005; Carniello et al., 2011), capable of accounting for the wetting- drying processes within intertidal areas and describing sediment transport processes (Carniello et al., 2012), is useful for simulating processes acting at the basin length-scale (tide propagation, wind waves effects) optimizing computation time. The results obtained from the 2D-model can be used as boundary conditions for running detailed 3D simulations at the meander length-scale, where reproducing the complete flow field, including secondary-3D helical flows which occur in correspondence to a meander bend, is of primary importance. A fully fledged 3D model, namely Delft3D, was therefore employed. This integrated approach allows to account for the effect of different types of tidal asymmetries, such as ebb (or flood) dominance, in the study of the Gaggian channel evolution. Both the models are briefly presented in the following sub-sections.

BI-DIMENSIONAL MODEL consists of three modules: the hydrodynamic module coupled with the wind-wave module (WWTM - Carniello et al. (2005) and Carniello et al. (2011)) and the sediment transport and bed evolution module (STABEM - Carniello et al. (2012)), which describes the relevant morphodynamic processes.
The *hydrodynamic module* solves the 2D shallow water equations suitably modified in order to reproduce wetting and drying processes in very shallow and irregular domains. The governing equations are solved using a semi-implicit staggered finite element method based on Galerkin's approach (see Defina (2000), Martini et al. (2004), and D'Alpaos and Defina (2007) for a detailed description of the equations and of the numerical scheme). Considering the case of a turbulent flow over a rough wall, the bottom shear stress induced by tidal currents, τ_{tc}, is evaluated using the Strickler formula. The hydrodynamic module provides the wind-wave module with the flow field characteristics necessary to describe the processes affecting wind wave generation and propagation.
The *wind-wave module* (Carniello et al., 2011) is based on the solution of the wave action conservation equation parameterized using the zero-order moment of the wave action spectrum in the frequency domain. The spatial and temporal distribution of the wave period is determined through an empirical correlation function relating the peak wave period to the local wind speed and water depth (Young and Verhagen, 1996; Breugem and Holthuijsen, 2006; Carniello et al., 2011)]. The bottom shear stress induced by wind waves, τ_{ww}, is computed

in the wind-wave module as a function of the maximum horizontal orbital velocity at the bottom, which is related to the significant wave height through the linear theory. Because of the nonlinear interaction between the wave and current boundary layers, the maximum bottom shear stress, τ_{wc}, resulting from the combined effect of tidal currents and wind waves is enhanced beyond the sum of the two contributions, as accounted for in the WWTM on the basis of the empirical formulation suggested by Soulsby (1997). It is worthwhile pointing out that the WWTM has been widely tested by comparing model results to hydrodynamic and wind-wave data collected not only in the Venice lagoon (Carniello et al., 2005; D'Alpaos and Defina, 2007; Carniello et al., 2011) but also in the lagoons of the Virginia Coast Reserve, USA (Mariotti et al., 2010).

The *sediment transport and bed evolution module* (STABEM) solves the advection diffusion equation and the Exner's equation considering the same computational gird of WWTM . In order to consider the simultaneous presence of cohesive and non-cohesive sediment typically characterizing tidal lagoons, STABEM uses two size classes of sediments to describe the bed composition: non-cohesive sand and cohesive mud (sum of clay and silt) Van Ledden et al., 2004. The transition between non-cohesive and cohesive behavior of the mixture and the critical value for the bottom shear stress are determined as a function of the updated local mud content (which varies both in space and time) on the basis of the critical value assumed for pure sand and pure mud. The use of a sediment mixture requires a reliable reconstruction of the initial configuration of the bed composition, which is a difficult and site-specific task. Available field data are, in most cases, limited as compared to the spatial variability of bed composition, thus preventing the use of purely statistical approaches. To overcome this problem, available field data form the Venice lagoon were considered, that allowed the identification of an empirical relationship between the local bed composition and both the local bottom elevation and the distance from the nearest inlet. This relationship was used to reconstruct a reliable initial bed composition (see Carniello et al., 2016 for further details).

Another peculiar feature of the sediment transport module is the stochastic approach (similar to that suggested by Grass, 1970) adopted to reproduce the near-threshold conditions for sediment entrainment, which usually characterize shallow tidal basins where resuspension events occur periodically driven by bottom shear stresses that slightly exceed the erosion threshold. Both the total bottom shear stress (induced by the combined effect of waves and currents) and the critical shear stress for erosion are treated as random variables (τ'_{wc} and τ'_{c}, respectively) with log-normal probability distributions. The space- and time-varying values of the total bottom shear stress, τ_{wc}, and of the

critical shear stress, τ_c, computed by STABEM represent the expected values of the two distributions. Following the stochastic approach, the erosion rate is assumed to depend on the probability that τ'_{cw} exceeds τ'_c which is calculated accounting for the randomness of τ_{wc} and τ_c. For a complete description of STABEM and further comparisons with field data from the Venice Lagoon the reader is referred to Carniello et al., 2012; Carniello et al., 2014.
For the sake of simplicity, the bidimensional model (WWTM+STABEM) will be shortly name WWTM hereinafter.

THREE-DIMENSIONAL MODEL The three dimensional model employed in this work is the Delft3D model (Deltares, 2016). In a rectilinear Cartesian coordinate system (x, y, z), assuming hydrostatic equilibrium in the vertical direction (with z-axis vertically upward), the system of governing three-dimensional shallow-water equations for fluid flow reads:

$$\left(\frac{\partial u}{\partial t} + u\frac{\partial u}{\partial x} + v\frac{\partial u}{\partial y} + w\frac{\partial u}{\partial z}\right) = -\frac{1}{\rho}\frac{\partial p}{\partial x} + F_x + \frac{\partial}{\partial z}\left(\nu_V\frac{\partial u}{\partial z}\right) \tag{3.1}$$

$$\left(\frac{\partial v}{\partial t} + u\frac{\partial v}{\partial x} + v\frac{\partial v}{\partial y} + w\frac{\partial v}{\partial z}\right) = -\frac{1}{\rho}\frac{\partial p}{\partial y} + F_y + \frac{\partial}{\partial z}\left(\nu_V\frac{\partial v}{\partial z}\right) \tag{3.2}$$

$$\rho g = -\frac{\partial p}{\partial z} \tag{3.3}$$

$$\left(\frac{\partial u}{\partial x} + \frac{\partial v}{\partial y} + \frac{\partial w}{\partial z}\right) = 0 \tag{3.4}$$

In the above equations u, v, and w are the flow velocities in the x, y, and z directions, respectively. p is the water pressure, ρ is the water density, g is the gravitational acceleration, F_x and F_y are the horizontal diffusion terms, and ν_V is the vertical eddy viscosity. The Reynolds stresses are modeled by using the eddy viscosity concept, therefore F_x and F_y read:

$$F_x = \frac{\partial}{\partial x}\left(2\nu_H\frac{\partial u}{\partial x}\right) + \frac{\partial}{\partial y}\nu_H\left(\frac{\partial v}{\partial x} + \frac{\partial u}{\partial y}\right) \tag{3.5}$$

$$F_y = \frac{\partial}{\partial x}\nu_H\left(\frac{\partial v}{\partial x} + \frac{\partial u}{\partial y}\right) + \frac{\partial}{\partial y}\left(2\nu_H\frac{\partial v}{\partial y}\right) \tag{3.6}$$

where ν_H is the horizontal eddy viscosities. The vertical and horizontal viscosity coefficients are computed by:

$$\nu_V = \nu_{mol} + \nu_{3D} \tag{3.7}$$

$$\nu_H = \nu_{mol} + \nu_{3D} + \nu_{2D} \tag{3.8}$$

in which ν_{mol} is the molecular viscosity, ν_{3D} is the viscosity coefficient modeling three-dimensional turbulence and ν_{2D} is simply approximated as a constant in this work. The coefficient ν_{3D} is given by (Rodi, 1993):

$$\nu_{3D} = c'_\mu L\sqrt{K} \tag{3.9}$$

where $c'_\mu = c_\mu^{1/4}$, with $c_\mu = 0.09$, L is the mixing length and K is the turbulent kinetic energy. The turbulence closure model used is the $k-\varepsilon$ model (Rodi, 1993). The hydrodynamic module is coupled with a morphodynamic module which solves the two-dimensinal Exner equations for bedload and with the three dimensional advection - diffusion equation for the suspended load. For further details on the model we refer the reader to Deltares (2016)

Numerical simulations

We followed a cascade-approach, running 2D WWTM simulations which provided us the boundary conditions for carrying out detailed 3D simulations.

BI-DIMENSIONAL SIMULATIONS are based on two previously tested and calibrated computational grids of WWTM. The grids represent the whole Venice lagoon (Carniello et al., 2009; D'Alpaos, 2010) in its 1932 and current (2012) configurations. Both the grid have been refined in the Gaggian channel area, in order to provide more detailed results, especially along the two lateral tributaries TE and TW. In order to provide a preliminary overview on the modifications in the hydrodynamics characterizing the Gaggian channel area during the last century, both the models were firstly forced by using 30 days (from 11/16/2005 to 12/16/2005) of hourly tidal levels measured at the CNR Oceanographic Platform, located in the Adriatic Sea in front of the Venice Lagoon, and wind velocities and directions observed at the Chioggia anemometric station (Figure 3.8B). The year 2005 was selected as "representative" of the typical behavior of wind fields in the Venice lagoon (D'Alpaos et al., 2013) because it embodies a probability distribution of wind velocities that is the most similar to the average distribution observed between 2000 and 2008. These runs are referred to as R_{1930} and R_{2012} hereafter.
Secondly, we studied the propagation of a semidiurnal (M2) sinuosidal tidal, characterized by an amplitude of 0.5 m, within the Venice lagoon in its 1930 configuration. No wind effects were considered in this simulation, named $M2_{1930}$.

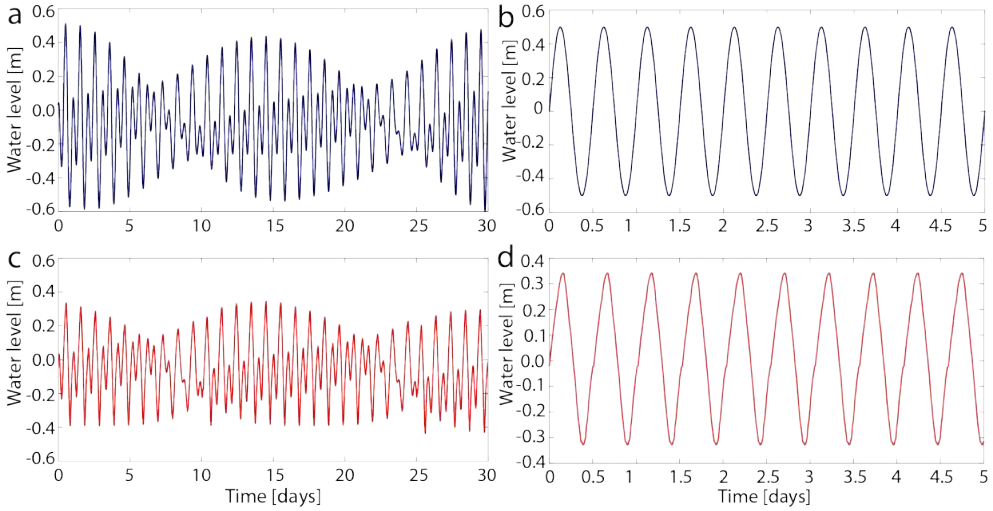

Figure 3.11: Different tides used as forcings for the numerical simulations. a) Multi-harmonic tide reconstructed using the first 8 harmonics of the 1940 data; b) semidiurnal sinusoidal tide, with an amplitude of 0.5 m; c) and d) represent the propagation of tides in a) and b), respectively, as measured along the Gaggian channel (data derived from WWTM simulations).

Finally, the 1930 computational grid was forced with a multi-harmonic tide. The latter was built using amplitudes, periods and phase-lags of the first 8-tide components as derived from the 1940 tide-level record, which is the first available complete dataset (data were provided by the ICPSM, that is fully acknowledged). This simulation is named $8H_{1930}$.

The results of the simulations carried out with WWTM provided the boundary conditions for running 3D simulations in Delft3D. Specifically, we extracted sediment and water discharges, as well as water level data, along two different cross-sections of the Gaggian channel, located landward and seaward the outflow of the TE and TW tributaries, for which data where were collected as well.

THREE-DIMENSIONAL SIMULATIONS have been carried out on a Delft3D computational grid consisting of 5746 nodes, with a minum resolution of 5 and 10 meters in the cross-sectional and streamwise directions, respectively. We employed 10 vertical layers, since tests with more layers showed negligible effect on the modeled channel morphology. Channel sediments are assumed to be uniform, non-cohesive medium-fine sand ($D_{50} = 150\mu m, \rho = 2650 kg/m^3$), wich represents a good approximation of the grainsizes observed in the field through specific sedimentological surveys. At the boundaries a Neumann boundary condition is prescribed for the suspended sediment both in case of entering and exiting flow. As a consequence, both the entering and exiting flows carry a concentration which is in equilibrium with the

local hydrodynamics. As for the channel roughness, we set a Strickler coeffient of $K_S = 35 m^{1/3}/s$ (corresponding to a Manning coeff. of $n = 2.68 \cdot 10^{-2} s/m^{1/3}$), that is equal to that employed in WWTM. The phase-lag between the landward and seaward boundary sections was obviously taken into account, and represent the main forcing for determining flow directions and intensities. The free-slip boundary conditions was applied at all channel boundaries. The boundary conditions typically consist of WWTM-extracted water levels imposed at the landward and seaward boundary cross-section, although in some cases water discharges have been employed. We run the model with 24 hours of hydrodynamic spin-up time, and then performed a fully coupled hydro and morphodynamic simulations of 30 days. A scaling morphological factor of 24 was used to multiply bed erosion and deposition. Therefore, the model approximately reproduces 2 years of morphological changes. Channel banks are assumed to be fixed, an approximation that is justifiable given the small rates of migration shown by the channel (Figure 3.10).
Our goal is to investigate the channel evolution starting from the 1930 configuration. Therefore, unless otherwise specified, the initial topography is assumed to be uniform, with a depth of 4 m that represents the averaged value of 1930 bathymetry. After preliminary tests, during which a sensibility analysis was performed, three different series of simulations were carried out, which are named as follows:

- Series O consists of three different runs, and investigates the role of overtides and flood dominance. In the O1 run the channel is subjected to a sinusoidal M2 tide, 0.3 m of amplitude, that represents the best fitting function for the Gaggian channel water levels derived from the $M2_{1930}$ WWTM run (Figure 3.11-d). The latter tide actually exhibits a slight ebb dominance, a condition that is modelled in the O2 run. Finally, the effects of multiharmonic tide is investigated in the O3 simulation, that is based on the $8H_{1930}$ outputs (Figure 3.11-c).

- Series F investigates the role of bidirectional flows by forcing the channel with a steady water discharge of 130 m^3/s flowing alternatively seaward (F1) or landward (F2). Such a discharge value corresponds to the highest value observed from the $M2_{1930}$ simulation. Since the periodic flow reversal makes the concept of stage-discharge function meaningless, the same water stage corresponding to different value of incoming and outcoming discharges, the water level at the outflow boundary section has been kept fixed at 0.0 m a.m.s.l.. The latter is observed to be the level at which water discharges are maximum, according to WWTM simulations.

- Series T aims at providing supporting informations to the geophysical data, pointing out the role of lateral tributaries in the morphodynamic evolution of the Gaggian channel. We therefore included within the computational grid the TE and TW channels, whose role is intentionally emphasized by dictating a constant discharge of $10 m^3/s$ flowing seaward, a value that roughly corresponds to the mean ebb discharge observed from the R_{2012} run. Such an assumption is also helpful for preventing numerical instabilities, which could arise if water levels were imposed at each boundary sections. Furthermore, at the inflow of both TE and TW, a constant suspended sediment concentration (SSC) of 100 mg/l is assumed. This value is overstated if compared to those obtained from R_{1930} simulations, but notwithstanding reasonable since SSC in the Venice lagoon can easily exceed 100 mg/l (Carniello et al., 2016). Two different runs are included in the T-series, both of them assuming the tide of $M2_{1930}$ as forcing. T1 experiment starts from a uniform 4 m deep bathymetry, whereas T2 takes advantage of the bathymetry generated from the O2 run. The depth of the TE and TW tributaries is set at 2.5 meter at the boundary, and linearly interpolated with the Gaggian channel depth at the tributary outflows.

The parameters for all the 2D and 3D runs are resumed in table 3.1 and 3.2, respectively.

Table 3.1: Parameters used in the bidimensional simulations with WWTM. Data from CNR tida gauge and Chioggia anemometer range from 11/16/22005 to 12/16/2015.

Run name	Lagoon	Tide	Wind
R_{1930}	1930	CNR gauge	Chioggia anemometer
R_{2012}	2012	CNR gauge	Chioggia anemometer
$M2_{1930}$	1930	Sinuosidal (T = 12 hrs, A = 0.5m)	Not considered
$8H_{1930}$	1930	Multi-harmonic 1940 (ICPSM data)	Not considered

Table 3.2: Parameters used in the three-dimensiona simulations with Delft3D

Series	Run	Boundary conditions	Initial depth [m]	Lateral tributaries
O	O1	T=12 hrs, A = 0.3 m tide	4 (uniform)	Not considered
	O2	$M2_{1930}$ (WWTM)	4 (uniform)	Not considered
	O3	$8H_{1930}$ (WWTM)	4 (uniform)	Not considered
F	F1	$Q = 130 m^3/s$ seaward	4 (uniform)	Not considered
	F2	$Q = 130 m^3/s$ landward	4 (uniform)	Not considered
T	T1	Derived from $M2_{1930}$	4 (uniform)	Included
	T2	Derived from $M2_{1930}$	Generated from O2	Included

3.2.5 Results

Remote sensing data

Historical aerial photos (Figure 3.10-A,B,C,D,E,F,G,H) show that the TW and TE tributaries were narrower than they are today and used to drain a salt marsh platform, thus likely conveying smaller water and sediment fluxes into the Gaggian channel compared to modern conditions (Brivio et al., 2015, see Appendix C). On the contrary, the Gaggian channel is observed to slightly increase its width, especially in correspondence to the tributary outflows, while not significantly changing its planform configuration.
Bathymetric data show a progressive deepening of the Gaggian channel from 1930 to nowadays. Pool zone in the apex area are constantly observed, whereas the progressive growth of a depositional spit occurs from 1930 to 1970 along the landward side of the outer bank, where the TE and TW flow into the Gaggian channel. From 1970 to 2012 the spit became wider and shallower, and the tributaries are shown to deepen progressively.

Numerical Simulations

BI-DIMENSIONAL SIMUALTIONS The comparison between the R_{1930} and R_{2012} runs (Figure 3.12) shows an increase of maximum velocities, especially during the ebb phase. Overall, a balanced situation between the ebb and the flood is observed for the 1930 configuration (Figure 3.12-a and c), whereas in 2012 the channel seems to be decisively ebb dominated. Across the "Palude della Centrega" tidal flat, the maximum bottom shear stresses induced by the action of wind-generated waves strong increased in both their spatial extension and magnitude. As for the TE and TW tributaries, results are reported in Figure 3.13, where the first 250 hours (11/16/2005 - 11/26/2005) of simulation are shown. A pronounced increase of water and solid discharges occurred in both the tributaries from 1930 to nowadays (Figure 3.13- B,C,D,E,F,G). Particularly, the presence of suspended muddy sediment in 2012 appears to be strongly correlated with Bora wind events (Figure 3.13-E), whereas sandy sediment flow are observed also in correspondence to the more sustained tidal stages (Figure 3.13-G).

THREE DIMENSIONAL SIMULATIONS invariably show periodic shift of both the maximum depth-averaged velocity stream and the cross-stream maximum velocity kernel. An example is reported in Figure 3.14. Independently on the tidal phases, secondary circulations are observe to flow in the same direction, that is toward the outer bank near the surface, and towad the inner bank at the channel bottom. Close to the ebb slack-water, a slight flow separation is observed

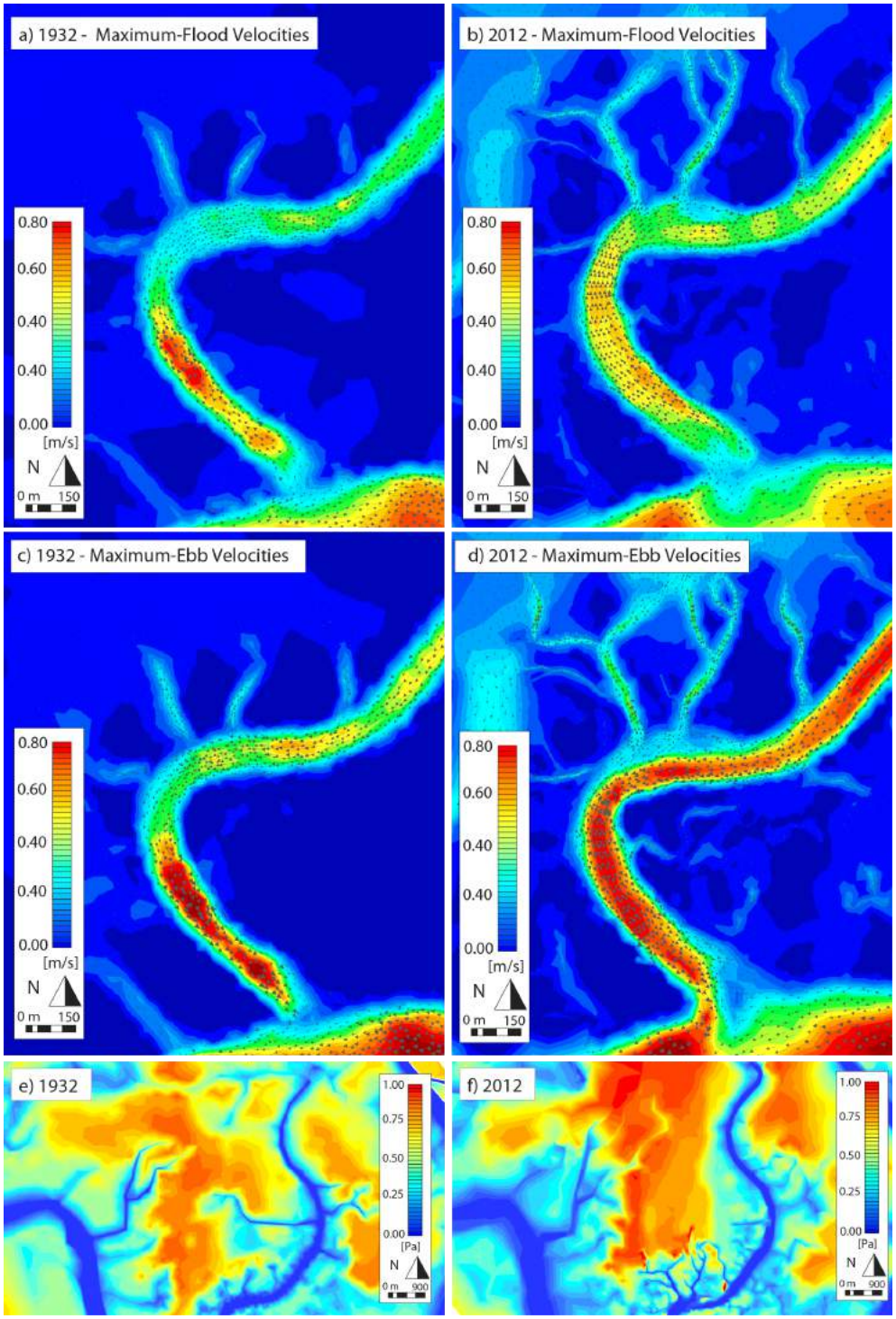

Figure 3.12: Results of the R_{1930} (left) and R_{2012} (right) WWTM runs. a) and b): maximum velocities during the flood phase; c) and d): maximum velocity during the ebb phase; e) and f) maximum bottom shear stresses induced by wind-generated waves in the "Palude della Centrega" tidal flat (no hydrodynamic-induced bottom shear stress is considered).

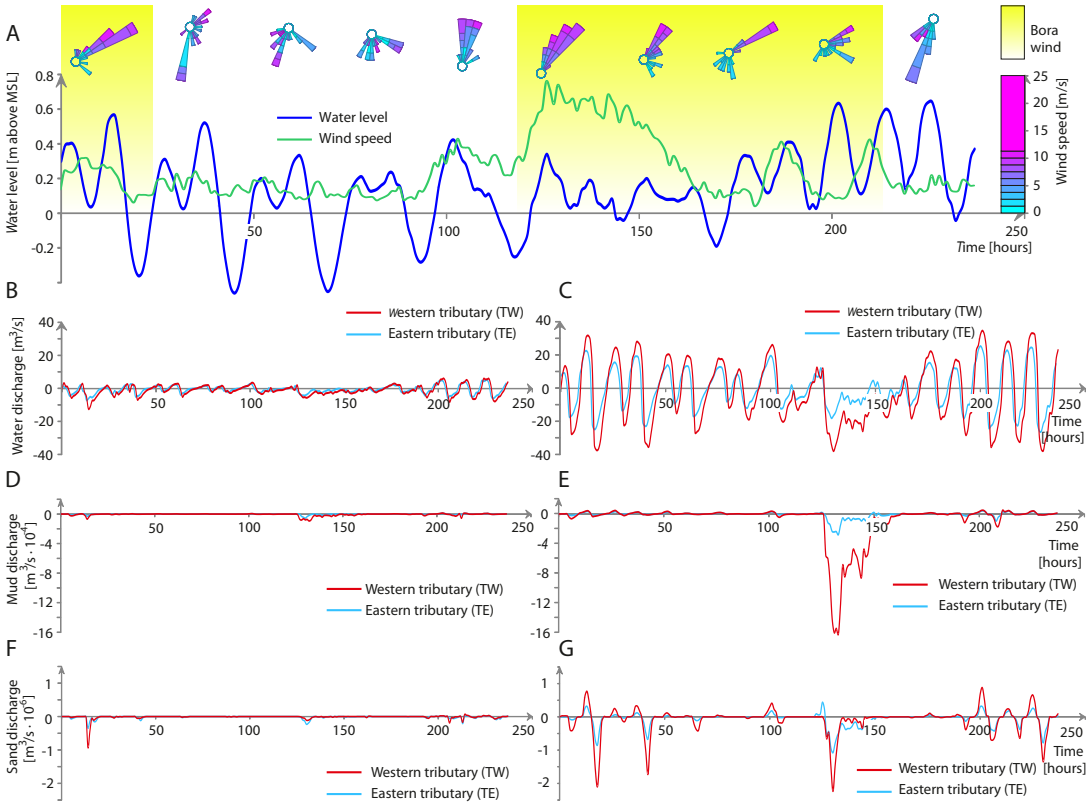

Figure 3.13: Results of the R_{1930} (left) and R_{2012} (right) WWTM runs along the lateral tributaries TW and TW. A) The data used as boundary conditions. Rose-diagrams indicate wind directions. Bora-wind period are also highlighted in yellow; B) and C): observed water discharges along TW (red) and TE (blue) in 1930 (left) and 2012 (right); D) and E): observed solid discharges of muddy sediments along TW (red) and TE (blue) in 1930 (left) and 2012 (right); F) and G): observed solid discharges of sandy sediments along TW (red) and TE (blue) in 1930 (left) and 2012 (right).

along the outer bank.

The O1 experiments (Figure 3.15-a) produced a double pool-zone and a well developed mid-channel bar. Erosion are located along the concave side of the banks, whereas at the inner bank deposition occurs at the landward side in one case, and on the seaward side in another. The O2 run, forced with a tide that is very similar to that of the O1 although containing small asymmetries, generated a completely different erosional and depositional patterns. Pool are located in the zone of maximum curvature, and the double pool zone is not present anymore. Deposition now occurs only along the seaward side of the inner bank, and the mid-channel bar is substituted by a inner-bank spit that develops seaward. A similar behaviour is observed considering the O3 run, for which the magnitude of erosion and deposition phenomena are slightly higher, likely because an higher tidal range is considered that increases the tidal prism.

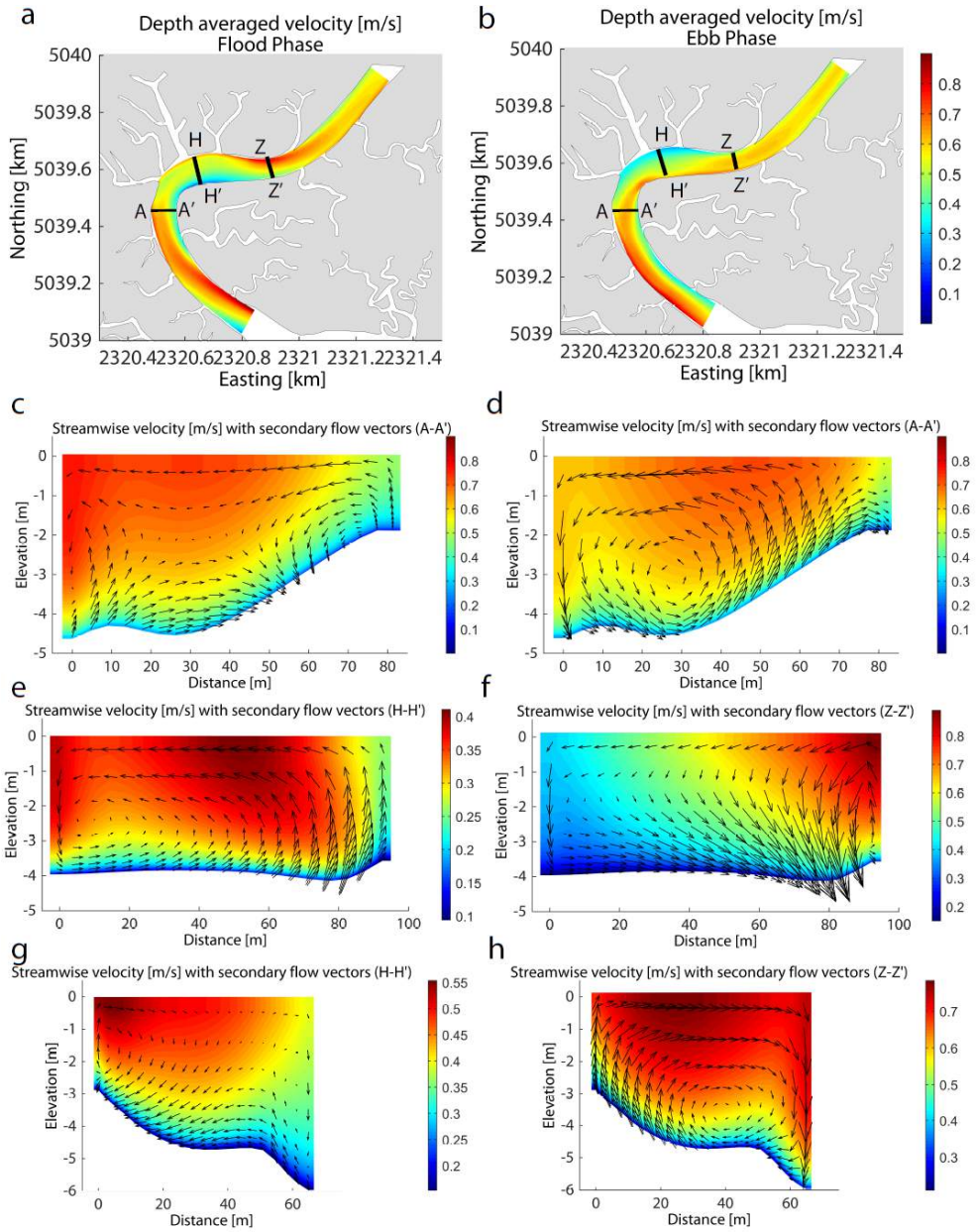

Figure 3.14: Depth-averaged and cross-stream velocity for the O2 run during both the flood (right)and ebb (left) phase. All the pictures are referred to the last modelled tidal cycle.

The F1 runs, where the flow was invariably directed seaward, generated erosional and depositional pattern very similar to those obtained in the O2 run (Figure 3.16-a). Particularly, it is worth noting that deposition occurs exclusively on the seaward side of the inner banks, with a well developed depositional spit resembling that of the O2 run. On the contrary, when the flow is directed landward (F2 run, Figure 3.16-b), point-bars form along the landward side of the inner banks. The secondary-velocity patterns (Figure 3.16-c,d) show that secondary circulations of both F1 and F2 experiments flow counter

clockwisely, whereas the kernel of maximum velocity is shifted along opposite banks.

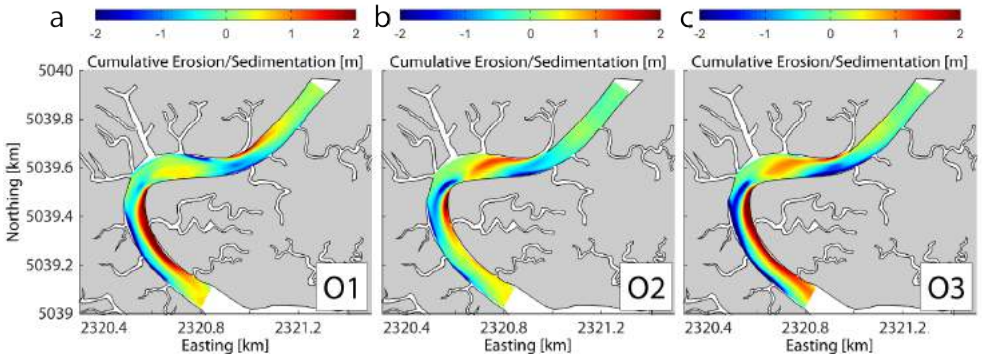

Figure 3.15: Cumulative erosion and sedimentation patterns for the O-series experiments.

The effect of the lateral tributaries in the T series seems to produce localize scour at the tributary outflows, particularly in the TW tributary (Figure 3.17-a,b). In the T2 run, the already-shaped depositional spit is slightly eroded and shifted toward the opposite bank (Figure 3.17-d). The growth of some, yet small, depositional features seems to occur in the outflow area, as highlighted by the cross-sectional profile (Figure 3.17-c,d).

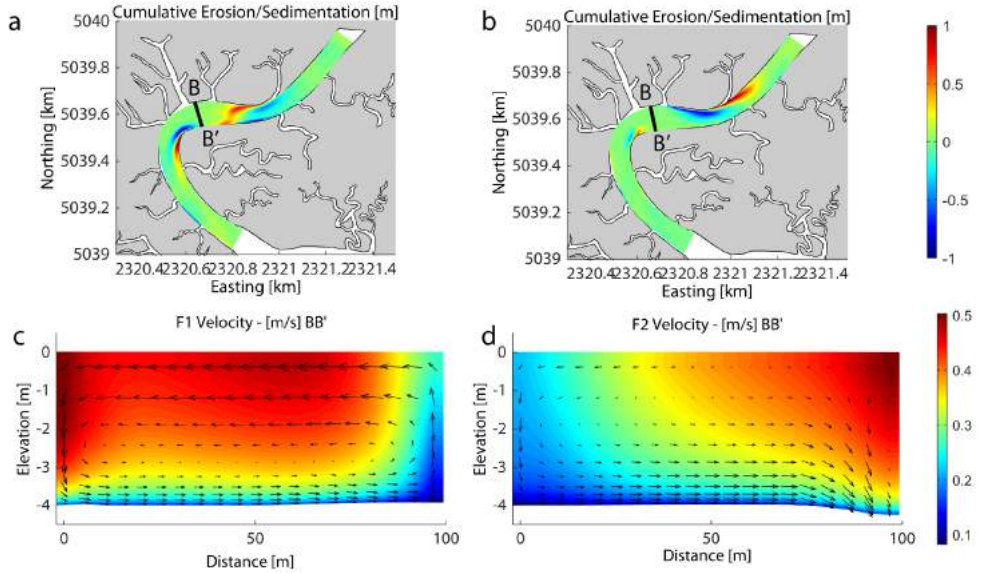

Figure 3.16: F-Series experiments. a) and b): cumulative erosion/sedimentation patterns; c) and d): cross-sectional view of the streamwise velocity with overimposed cross-sectional velocity vectors.

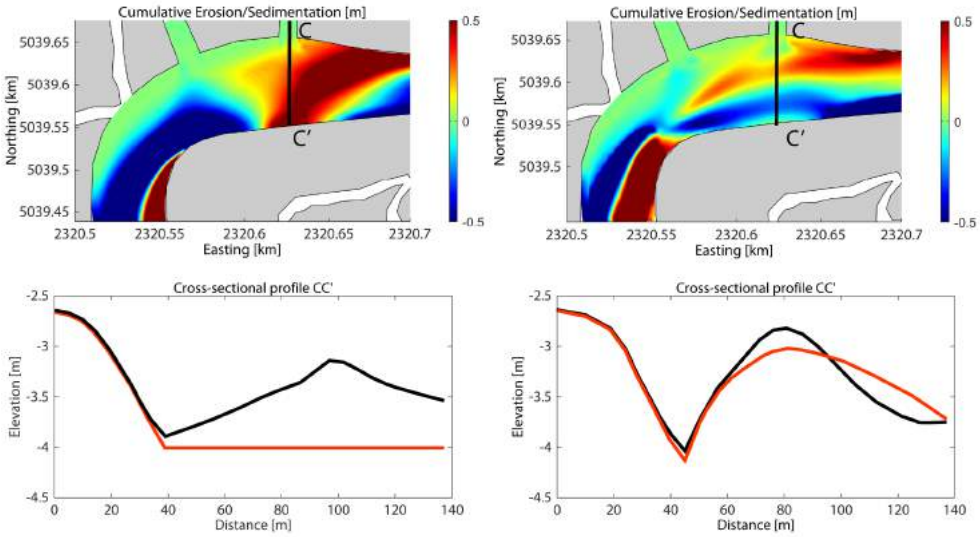

Figure 3.17: T-series experiment. a) and b): zoomed view of the TE and TW outflow area, showing cumulative erosional and depositional patterns; c) and d) cross-sectional profile along the TE tributary. Red lines stand for the profile at the beginning of the simulation, whereas black lines represent the final profile. The position of channel outflow is also highlighted.

3.2.6 Discussion

BI-DIMENSIONAL SIMULATIONS The framework depicted by the preliminary bi-dimensional simulations (R_{1930} and R_{2012}) highlight that strong variations in the hydrodynamic of the Gaggian channel occurred during the last century, the channel exhibiting a more pronounced ebb-dominated character nowadays. Furthermore, the hydrodynamic regime of the lateral tributaries became more intense, with higher water discharges during both the ebb and the flood phase. The increase in the wind-induced bottom shear stresses in the adjoining "Palude della Centrega" tidal flat is likely to produce more intense resuspension events, thus carrying much more sediments within the TE and TW tributaries, as confirmed by the raised values of solid discharges in Figure 3.13. The more intense water and solid discharges are likely to have caused the widening and deepening of both the tributaries that we observed from the historical data.

THREE-DIMENSIONAL SIMULATIONS The shift in velocity maxima displayed by our 3D simulations (see Figure 3.14) is in good accordance with the existing literature (e.g., Ahnert, 1960; Fagherazzi et al., 2004; Hughes, 2012; Dalrymple et al., 2010), as well as with the few numerical models existing for tidal meanders (e.g., Solari et al., 2002). We however notice that, although the kernel of maximum velocity is shifted over the different tidal phases, the secondary circulations

invariably flow in the same direction, that is toward the outer (concave) bank near the water surface, and toward the inner (convex) bank close to the channel bottom. This instance might have important implications for the morphodynamic evolution of the channel, since depositional and erosional phenomena likely depend on the position of the maximum-velocity kernel relatively to the axis of the cross-stream secondary circulations, and therefore deserves a closer investigation in the near future. It might be also interesting to investigate whether, and in which part of the bend, outer-bank cells (sensu Blanckaert, 2009) are present. However, the grid refinement in our experiments was likely not sufficient to provide such results, although a small outer bank cell is identifiable in Figure 3.14-g. It is finally worth noting that the ebb flow is usually stronger than the flood, the scale between the two being different in Figure 3.14.

O-series experiment show that, although the first tidal component may suffice to qualitatively reproduce the morphodynamic evolution of the channel, the presence of some, yet small, asymmetry in the first tide-harmonic component influences the evolution in a significant manner. In fact, the morphologies obtained form the O1 and O2 runs are decisively different, the latter being much more similar to that observed in 1970 (Figure 3.10-M). The inclusion of higher order tidal components (O3 run) further refines the latter result.

Our results are in accordance with the analysis of Garotta et al. (2006), that demonstrated the role of tidal asymmetries in promoting migration of free bars, and therefore challenge the common assumption of symmetric tides as forcing for morphodynamic models (e.g., Seminara et al., 2001; Lanzoni and Seminara, 2002; Solari et al., 2002; Lanzoni and D'Alpaos, 2015). A better approach would indeed either account for the distorsions due to the tide propagation, or employ models that reproduce the tide propagation itself (e.g., Tambroni et al., 2005; Stefanon et al., 2010).

The simulations carried out with unidirectional steady flows (F1 and F2) seem to suggest an ebb dominance within the Gaggian channel, since the erosional and depositional patterns of the F1 experiment resemble those obtained from the O2 and O3 experiments. The ebb-dominance hypothesis is further justified by the the result obtained from the 2D simulations, and challenges the assumption that the relative dominance of tidal flows might be evaluated from the channel planform (Fagherazzi et al., 2004). In fact, the Gaggian channel exhibit a quite symmetric planform morphology, although our evidences strongly support a dominance of the ebb flow. We therefore suggest that the position of point-bars and depositional features is a more appropriate proxy for detecting which phase of the flow is dominant.

Finally, the analysis of the lateral tributary influence on the morpho-

dynamic evolution of the Gaggian channel, seem to support the evolution model derived from the geophysical data (Figure 3.9 and see Appendix C for details). We however highlight that the growth of a depositional spit along the Gaggian channel is not related to the TW and TE contribution. On the contrary, the changes in the morphodynamic regime of the "Palude della Centrega" cause the lateral tributaries to carry more water and sediments within the main channel. This modifies the bottom configuration of the yet-formed depositional spit and shape two small outflow deltas, which are likely to grow through time thus producing depositional structures detected from the geophysical inspection.

3.2.7 Conclusions

The numerical modelling of the Gaggian channel showed that the presence of some, yet small, asymmetry in the first tide-harmonic component influences the morphodynamic evolution in a significant manner. Using simplified conditions, we were able to reproduce a channel time-evolution very similar to that observed from historical data. Secondly, running simulations under fluvial conditions (i.e. unidirectional water discharges), we were able to highlight the fundamental differences with the tidal case. Particularly, we showed that point-bar position is the appropriate proxy to detect ebb or flood dominance, whereas the asymmetry index is probably not. Finally, the influence of lateral tributaries has been studied and the results compared with a parallel study that integrates high-resolution geophysical investigation, bathymetric field surveys and historical aerial photos. Our investigation seem to confirm that modifications in boundary conditions may cause the lateral tributaries to influence the sedimentation pattern in the main channel in a crucial way.

4 EXPERIMENTAL TIDAL NETWORKS

4.1 ON THE ROLE OF TIDAL RANGE, INITIAL BATHYMETRY AND SHORELINE CONFIGURATION

This chapter is a manuscript in preparation, whose primary goal is to address the role exerted by different tidal ranges, initial bathymetries and shoreline configurations on the evolution of tidal-channel networks, particularly with respect to the meandering character of the channels. Three different series of physical experiments were carried out in a experimental facility at the Saint Anthony Falls Laboratory (University of Minnesota - Twin Cities) during an abroad-research period of 6 months. The results stemming out from this work show that different tidal ranges and inital bathymetries lead to networks with different morphological features, whereas the evolution of channel patterns does not seem to be much influenced by the initial shoreline configuration, that we investigated in term of number of shoreline breaches, thus highlighting a possible autogenic behaviour of the system.

Another series of experiments was carried out to investigate the adaptation of tidal channel networks to different climate-changing scenarios. The results emerging from these experiments are still under processing and will not be presented herein. In particular, additional effort is needed to perform detailed network extraction, in order to obtain precise measurements of channel widths and depths. Such achievement will also improve the results exposed in the present work, allowing a comparison with both field-data and existing physical experiments.

PAPER

Finotello, Alvise[1], Chris Paola[2], Andrea D'Alpaos[1], Massimiliano Ghinassi[1], Nathan Lentsch[2] and Alessandro Cantelli[3]

[1]Dept. of Geosciences, University of Padova, via G.Gradenigo 6, Padova, PD I-35131, Italy
[2]Dept. of Earth Sciences, St. Anthony Falls Laboratory, University of Minnesota, Minneapolis, MN 55414, USA.
[3]Shell Technology Center Houston, 3333 Highway 6 South Houston, TX 77082-3101, USA

4.1.1 Abstract

Landscapes of tidal embayments are characterized by the extensive presence of branching and meandering tidal channel networks. The morphological evolution of these features depends on the initial geological setting, as well as on a number of hydrodynamic and ecological drivers, whose role and interaction have been only partially explored. In this paper we present the results of three series of laboratory experiments, carried out in a large experimental facility, aimed at assessing the influence of basin geometry, number of shoreline breaches and tidal amplitude on the inception and morphodynamic evolution of tidal channel patterns. All the simulated networks exhibited an initial, relatively rapid, growing stage followed by a period of slow morphodynamic adaptation toward the final equilibrium stage. The continuous monitoring of the basin hypsometry indicated that the evolution of tidal channel networks occurred more rapidly in the presence of sloped basin and for higher tidal range. Flat shorelines and sustained tidal excursions favour the development of more branching networks, while channel sinuosity is enhanced when wide shoreline breaches favor the flooding of shoreline areas. On the contrary, the evolution of the network and its final branching character appear to be quite insensitive to the initial number of breaches along the shoreline, thus suggesting an autogenic behavior that depends primarily on the characteristics of tidal forcings.

4.1.2 Introduction

Tidal embayments are characterized by the widespread presence of branching channel networks, that sinuously wander through the intertidal regions (Fagherazzi et al., 1999; D'Alpaos et al., 2005; Stefanon et al., 2010; Van Maanen et al., 2013). These networks represent one of the most fascinating morphologies in nature, and the control they exerted on the hydrodynamics of coastal areas, as well as on the ecology and sediment dynamics, is of primary importance for both the short and long term morphodynamic evolution of these environments (Dronkers, 2005; Van Maanen et al., 2013). The worldwide-increasing anthropogenic pressures in coastal wetlands, combined with changes in the relative sea level, further emphasizes the critical importance of tidal channel networks, thus calling for new insights on the processes which govern their evolution. In the last decades, a number of studies were in fact performed to investigate the initiation and growth of tidal channel systems, as well as their morphological characteristics (de Swart and Zimmerman, 2009). If on the one hand remote sensing techniques and field investigations (e.g., Pestrong, 1965; French and Stoddart, 1992) are suitable for the analysis of channel-morphometric

features, having for instance allowed Rinaldo et al. (1999b) to demonstrate that, contrary to their fluvial homologous, tidal channel networks usually lack scale-invariant features, on the other hand numerical models and laboratory experiments have been developed in order to pursue a complete characterization of the long term evolution of tidal channel networks (Stefanon et al., 2010; Vlaswinkel and Cantelli, 2011; Coco et al., 2013). The latter approach is also necessary in the light of the wide variety of environmental-forcing conditions which can occur in tidal landscapes (Van Maanen et al., 2013).

Many mathematical models have therefore been proposed to analyze the evolution of tidal networks, describing their planimetric development together with the vertical accretion of the adjacent salt marshes and tidal flats as a consequence of tidal forcings, varying sediment inputs and relative sea level changes (e.g., D'Alpaos et al., 2005; Marciano et al., 2005; Temmerman et al., 2005; Kirwan and Murray, 2007; Di Silvio et al., 2010; Van Maanen et al., 2013; Zhou et al., 2014). With respect to laboratory experiments, the first physical model for investigating the initiation and evolution of tidal channel networks was set up by Stefanon et al. (2010). The authors employed a schematic back-barrier lagoonal system consisting of a flat platform of non-cohesive plastic grains, whose density was chosen in order to fulfill the most accurate, yet partial, scaling of the experiments. The system was forced with a sinusoidal tide (period 8-12 min, amplitude 0.5-2 cm) propagating from the offshore boundary into the lagoon. The experiments emphasized the possibility of experimentally reproducing the formation of a tidal network even in the presence of cohesionless sediments. The networks were observed to growth via headward erosion, a positive feed-back mechanism according to which small morphological depressions initially cause the flow to concentrate, thus increasing the bed shear stress that enhances erosion, further deepening the initial depressions (Montgomery and Dietrich, 1989; Whitehouse et al., 2000; Symonds and Collins, 2007). The authors investigated different tidal forcings concluding that, for tidal range able to induce headward erosion, both the tidal amplitude and period exert a weak influence on the lagoonal bottom evolution.
Almost simultaneously, Vlaswinkel and Cantelli (2011) studied the network growth in a open basin (width = 3 m, length = 2.5 m) without any sort of barrier islands. By using fine quartz silt, the experiment was able to reproduce a network of channels with morphometric features, such as width-depth ratios and channel funnelling, resembling those observed in nature.
The same setting of Stefanon et al. (2010) was employed by Stefanon et al. (2012) to investigate the network responses to variations in the mean sea level. Iwasaki et al. (2013) used an approach similar to Stefanon et al. (2010), particularly for the considered scaling rules of

flow and sediment transport, although the experimental setting was smaller (0.9 m wide and 0.8 m long) and the tidal forcings weaker (2 min period and 75 mm of amplitude). Nonetheless, the experiments succeeded in shaping real-like network growth and development, and the employment of small basin and short tidal periods allowed for a more rapid equilibrium achievement. The latter in fact, according to Cowell et al. (2003), is strictly dependent on the size of the tidal basin. More recently, the evolution of a back-barrier tidal basin has been investigated by Kleinhans et al. (2015) in a novel tilting basin, designed in the wake of Kleinhans et al. (2012)'s work. Despite providing a useful mean for reproducing sediment transport during both the ebb and flood phase, thus overcoming the purely erosional character of the previous experiments, the channelized portion of the basin was constrained to the inlet region where both an ebb and flood delta developed.

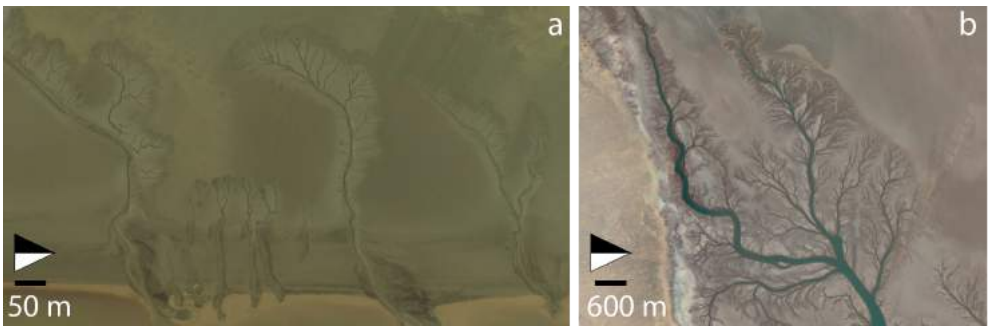

Figure 4.1: Tidal channels evolving via headward growth. a) Hangzhou Bay, Zhejiang, China; b) Colorado River Delta, Baja California, Mexico (©Google 2016, DigitalGlobe)

In spite of the wide variety of settings used, the aforementioned experiments proved that real-like tidal channel patterns can successfully be reproduced in small-scale experimental settings (Coco et al., 2013). Furthermore, it emerged that morphodynamic equilibrium is achievable, within timescales and with network-final characteristics depending on both the geometry and tidal forcings adopted for the experiment. Nonetheless, the role played by other factors in the final configuration displayed by the modelled networks have still to be addressed. Particularly, the effects of the initial basin configuration (plane in the existing exeriments) have not been analyzed thus far (Coco et al., 2013). Furthermore, while back-barrier lagoonal systems have been widely investigated (e.g., Stefanon et al., 2010; Di Silvio et al., 2010; Stefanon et al., 2012; Van Maanen et al., 2013), the study of the influence exerted by different configurations of the initial shoreline, in terms of number of existing breaches deserves further attention. The importance of studying the role of initial conditions has been already emphasized in the tidal environment literature

(Davidson-Arnott et al., 2002), as well as by the contribution by (Taylor Perron and Fagherazzi, 2012) who demonstrated how different characteristics of the initial topographic surface may result in landforms with different morphological features.

With the purpose of providing new insights into the role played by different morphodynamic factors, we have therefore run a series of physical experiments for simulating the long-term morphological evolution of tidal channel networks. The model was used to explore the effects of different tidal ranges, basin slopes and number of breaches in the initial shoreline. We examined the results in terms of network complexity and extension, as well as channel sinuosity and time required to reach the morphodynamic equilibrium. The network evolution analysed herein is representative of the processes that occur when the action of tides expand over previously partially- or non-channelized areas, leading to the formation of new channel systems. This condition occurs when either the relative sea level increases, flooding new coastal areas, or when depositional processes, driven for instance by river or longshore currents, expose the bed surface to the action of tidal flows (Figure 4.1).
Because it is generally agreed that both the first network imprinting and the later establishment are processes occurring over time scales much shorter than those characterizing the evolution of the whole tidal environment (Allen, 2000; D'Alpaos et al., 2005; D'Alpaos et al., 2007; Stefanon et al., 2010), some morphodynamic factors acting over longer time-scales, such as vegetation and sediment supply, are purposefully neglected in the present work. Moreover, the lack of sediment supply is a condition currently being experienced by many coastal areas worldwide as a consequence of river anthropization. Famous examples are represented by the Venice lagoon and the delta of both the Colorado and Mississippi rivers. Finally, neglecting a certain number of factors allows us to isolate and better understand the effects of the included variables, thanks to a top-down approach (Murray, 2013; Coco et al., 2013).

The rest of the chapter is organized as follows. The experimental apparatus is described in section 4.1.3, together with the boundary conditions of every experiment. A brief discussion on the methods employed for the analysis and on the experiment-scaling issue is reported as well. Section 4.1.4 lists, one at a time, the results of the three experimental series, which are discussed in section 4.1.5. Finally, section 4.1.6 sets the conclusions and traces possible future developments for the present research.

4.1.3 Material and methods

Experimental settings

The experiments were carried out in the "DeltaBasin2" experimental facility at St. Anthony Falls Laboratory (University of Minnesota). DeltaBasin2 (Martin et al., 2009; Baumgardner, 2015) consists of a 5 m by 5 m basin, 0.62 m deep, equipped with a computer-controlled weir and attached siphon through which the water level within the basin is regulated. A sonar probe continuously monitors the water elevation, and consequently adjusts the weir position thanks to a feed-back algorithm specifically developed. A small auxiliary basin (2 m by 2m by 0.62 m) is connected to the main basin through a system of pumps, that allows one to reproduce periodic tides (Figure 4.2). During the experiments, water is dyed blue for allowing channel identification from time-lapse photos taken by an overhead camera. A cart-mounted scanner records topography using a 3D SICK^{TM} camera, that records five linescans with millimetrical horizontal and vertical resolution. The five passes are finally stitched together.

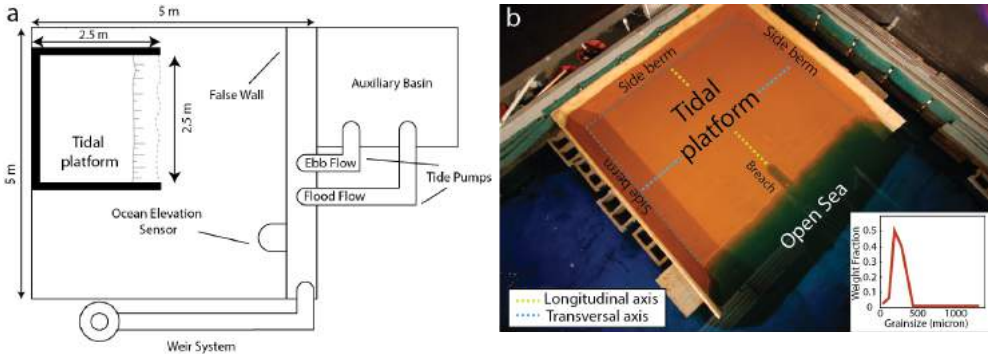

Figure 4.2: Experimental setting. a) Sketch of DeltaBasin2 experimental facility at the St. Anthony Falls Laboratory (adapted from Baumgardner, 2015); b)Photos of the basin immediately before the beginning of the "REF" experiment. The grainsize distribution of the crashed walnut employed in the experiments is reported in the low-right inset.

The experiments were run using a 2.5 by 2.5 m wall-sided wood platform, placed within the main basin (Figure 4.2) and filled with well sorted crushed walnut shells ($D_{50} = 250\mu m$, Figure 4.2-b). This material was selected for its low bulk density ($\rho = 1.35 g/cm^3$) that allows it to be easily eroded, transported and re-deposited by tidal fluxes. At the beginning of every experiment, sediments were mixed with water up to the saturation point. Capillary forces provided the wet sediments a slight cohesion, sufficient to maintain channel-bank morphology during the experiment. Sediments were then poured into the basin, forming a 20 cm thick layer, and flattened using a board sliding on the wood-platform sides. A significant effort was required

to ensure either the surface flatness or the desired slope, such that the elevation of the platform perfectly tied the mean sea level (Figure 4.2-b). Along the shoreline the bottom elevation decreased toward the open sea accordingly to the walnut angle of repose (30^0). In order to avoid flow concentration along the platform walls, which would have led to localize scour thus producing distorted results, a 10 cm wide berm was built along each side of the platform (Figure 4.2-b). It is important to underline that the system is purely erosional, because no sediment supply is provided.

Experiment series and parameters

All the experiments employed a sinusoidal tide with fixed tidal period of 1.5 minutes, that produced reversing quasi-steady flow. The total length of a run was of 10 hours (400 tidal cycles). Three different series of experiments, each consisting of 2 different experiments, were carried out and compared with a reference experiment. A total number of 7 experiments was therefore performed, according to the following descriptions.

The reference experiment ("REF") consists of a flat, horizontal platform, where the initial shoreline is characterized by the presence of a 5 cm wide and 15 cm long breach (depth = 2 cm) along the longitudinal axis (Figure 4.2-b). The system is subjected to a tide with an amplitude of 1 cm.

The experiments on tidal range influence ("TR") are carried out by forcing the system with tides of different amplitude, namely 1.5 cm (TR1) and 0.75 cm (TR2). The platform geometry is identical to the "RF" run.

The experiments on basin slope influence ("BS") were carried out to compare the flat configuration of the "REF" run with a sloped platform. In the BS1 run the basin has 0.8% transversal slope (i.e. convergent toward the longitudinal axis), wheres in the BS2 experiment the slope is of about $\cong$ 0.5% in the longitudinal direction (i.e. toward the open sea sea).

The experiments on the initial shoreline configuration ("IS") are referred to a perfectly flat shoreline configuration (IS1), where no breaches were purposefully dredged, and to a shoreline whit 15 small breaches were traced. In the latter case, the breach spacing was obtained by picking a set of 15 random values drawn from a normal distribution with a mean of 15 cm and a standard deviation of 5 cm (Figure 4.3).

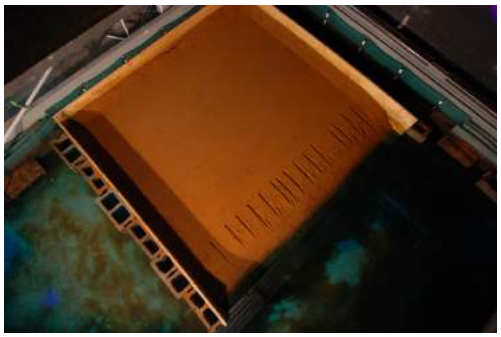

Figure 4.3: Initial setting for the IS2 experiment.

During the experiments time-lapse photos were taken every 15 seconds by the overhead camera, and postprocessed and rectified at the end of the run. The bathymetric survey of the bottom elevation, taken at varying time intervals (from 15 minutes at the beginning of a run to 1 hour over the last 3 hours of experiment), was performed by completely drying the platform surface. The basin was slowly dried and refilled (15 mins), in order to avoid undesired perturbations of platform topography. Sediments within the platform were changed at the beginning of every run, in order to prevent walnuts from decomposing.

Scaling argument

Although the large differences between experimental and real length- and time-scales do not usually permit to reach a complete dynamic scaling (Vlaswinkel and Cantelli, 2011), simplified experimental stratigraphy performed in very small facilities has proved to be a suitable mean for reproducing spatial structure and kinematics that resemble those of the investigated natural systems (Paola et al., 2001; Paola et al., 2009; Lajeunesse et al., 2010). Contrary to the approach adopten by Stefanon et al. (2010) and Iwasaki et al. (2013), no attempt was made in the present work to pursue a dynamic scaling. The so called "natural similarity" (see Vlaswinkel and Cantelli, 2011) was therefore applied, whose main goal is to reproduce real-like patterns from which one can derive useful insights into the key processes acting on larger scales. Furthermore, rather than obtaining perfectly scaled version of real tidal channel networks, our main purpose is to attain a qualitative comparison between the effects that different environmental conditions exert on the morphology of the networks themselves.

Metrics for network analysis

Channel centerlines are important for the identification of network features. The implementation of automated approaches allows one to perform faster and more objective analyses, particularly when dealing

with a wide number of channels. Given the purely erosive character of the modeled network, we have to a first approximation applied the D_∞ network-extraction algorythm proposed by Tarboton (1997) (see also Tarboton et al., 1991) to obtain channel centerlines. Despite bearing some limitations (which are further discussed in the discussion, where alternative methodologies are also proposed), such procedure proved to be able to identify the morphologies generated during the experiments. Furthermore, the employment of constant parameters during the extraction procedure allowed for a direct comparison between different runs. Particularly, we wonder whether the modeled networks differ one from the other in terms of channel branching and sinuosity. Therefore, the D_∞-generated networks have been analyzed in terms of both Strahler's order (Horton, 1945; Strahler, 1957) and sinuosity of each individual network member. For the first parameter, the total length of channels belonging to the i^{th} order (l_i) has been normalized with the overall channelized length of the network (L_N), finally computing the relative frequency of l_i/L_N. The probability density frequency of channel sinuosity has instead been calculated to account for the meandering character of the networks.

Finally, the evolution of the whole tidal basin has been studied by analyzing the evolution of its mean bottom elevation (z_b), normalized with the initial averaged platform elevation z_0.

4.1.4 Results

Some common results characterized all of the experiments, which gave rise to multiple tree-like networks within the platform. Particularly, network formation was observed to occur very rapidly, with channels progressively elongating landward via headward growth (Figure 4.4). The latter phenomenon occurred chiefly during the ebb phase, with a strong sediment transport directed seaward which occurred during the first (1 hour) tidal cycles. At the beginning of every exeperiment, a strong dynamism was observed in the system inlets and in channels located along the shoreline, where channel pairings and connections occurred frequently. As time passed, the overall amount of sediment transport appeared to decrease and concentrated exclusively along the already formed channels. During the final stages, morphological changes occurred at extremely slow rates. The occurrence of residual ebb-sediment transport was observed in the basin portions located farther from both the major channels and the inlets. The lighter fraction of the crashed walnut shell, characterized by a dark color, tended to be piled in the most landward portion of the basin by the action of the flood flow (Figure 4.4) and contributed to increase surface irregularity, thus favoring flow concentration and further promoting headward erosion.

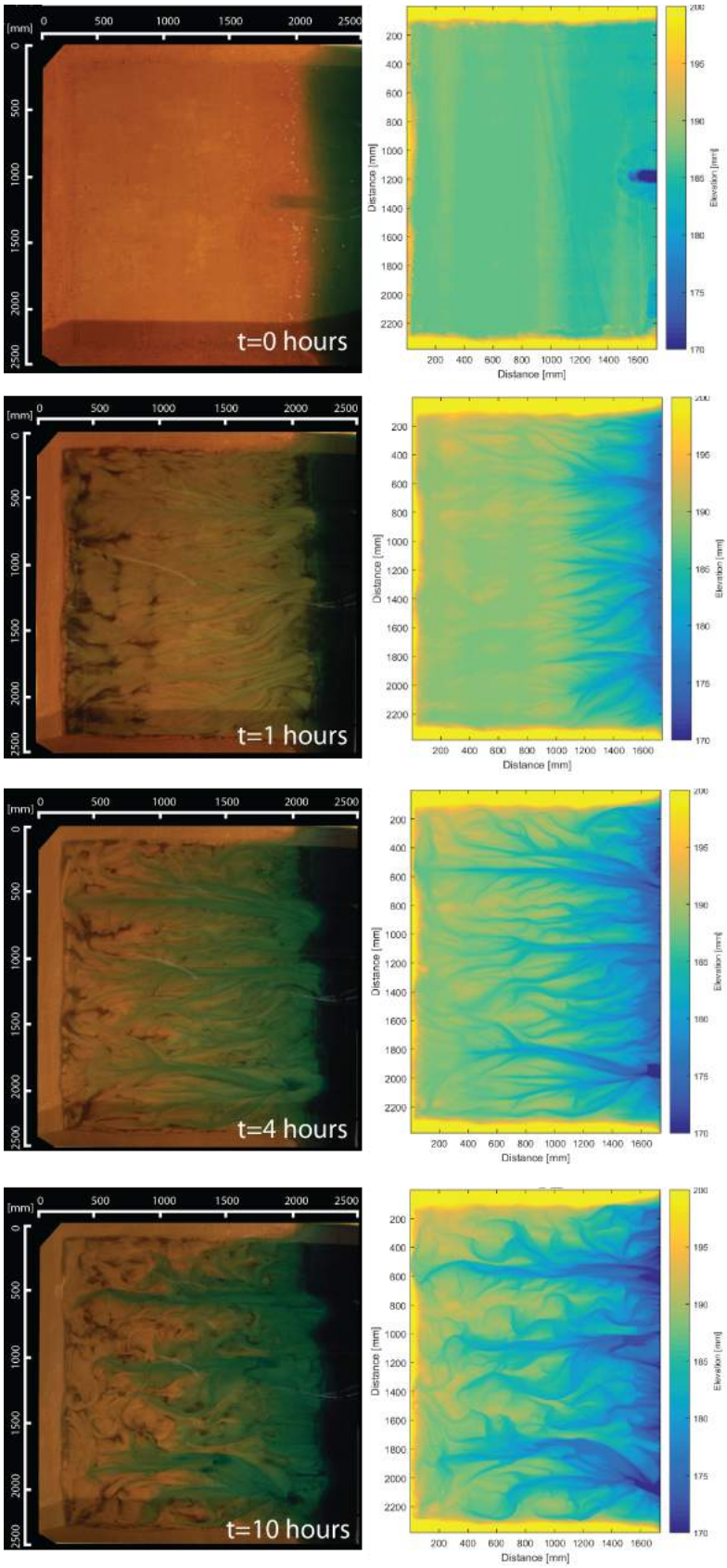

Figure 4.4: Network evolution during the "REF" experiment. Left side: Rectified overhead photos: Right side: scanned bottom elevation.

Moreover, some peculiar tidal-channel morphologies were obtained, among which worth mentioning are the funnelling character of the creeks and the widespread presence of channel bifurcations, as well as the occurrence of sinuous bends resembling the typical box- and cuspate-shapes of tidal meanders (Figure 4.5).

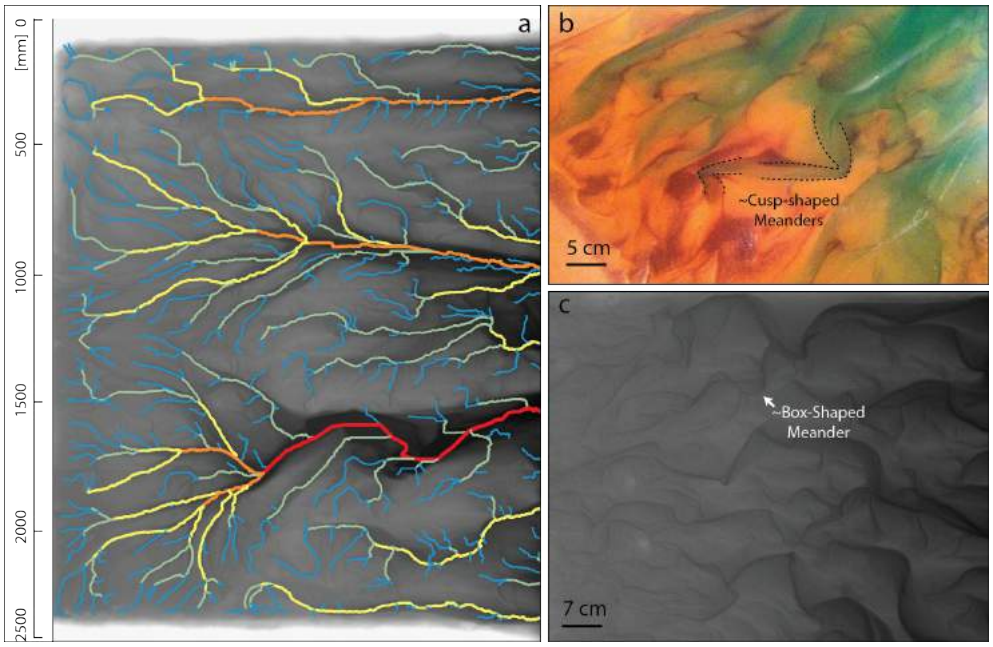

Figure 4.5: Morphologies generated from different experiments. a) Strahler ordering for the final configuration of the IS2 run; b) Picture showing the presence of cusp-shaped meanders during an intermediate stage of the REF run; c) Hill-shade view of a portion of the basin (BS2 run) highlighting the presence of multiple bifurcations, sharp bends and a box-shaped meander.

The reference experiment ("REF") (Figure 4.4) generated a network where 3 major systems, interspersed with small networks of smaller order, elongated up to the platform rear wall before channel sinuosity started incresing. The latter occurrence was also associated with channel widening, especially in the shoreline area, thus enhancing creek funnelling.

In the TR1 and TR2 experiments the platform mean elevation decreased faster and slower than in the REF experiment, respectively (Figure 4.6-d). The final mean elevation of TR1 was lower than that of REF, whereas the opposite was true for TR2 (Figure 4.6-a,b,c,d). TR1 exhibited the greatest relative frequency of 1^{st} order channels (60%), while the highest network order was observed for the REF experiment (Figure 4.6-e). The mode of channel sinuosity in run TR2 (Figure 4.6-f) was observed to be smaller than those of TR1 and REF,

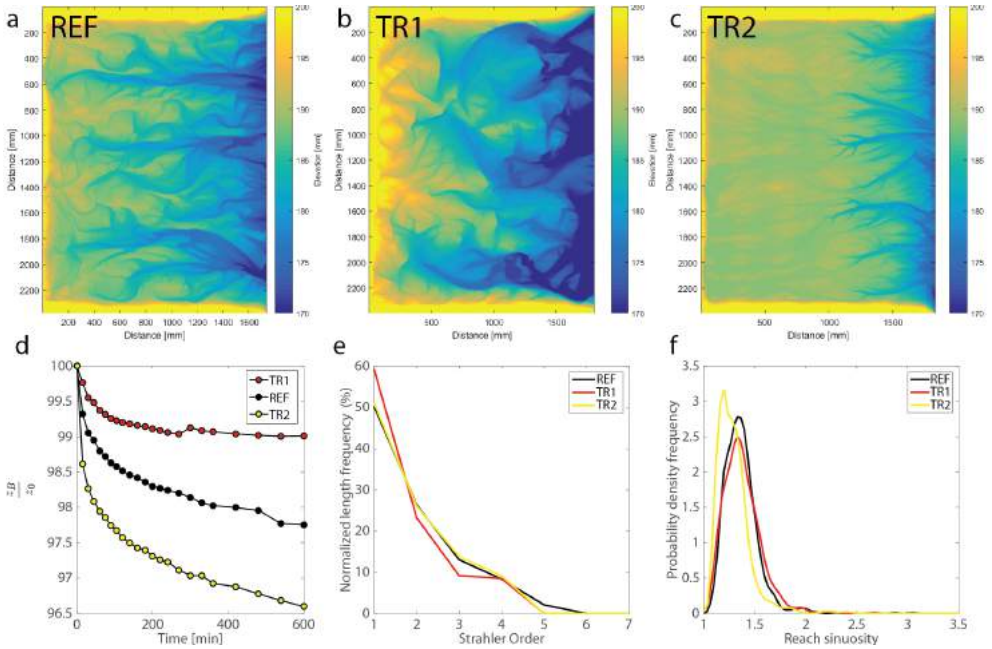

Figure 4.6: Results from the TR experiment series. Final bottom elevations for a) REF experiment, b) TR1 experiment and c) TR2 experiment. d) Evolution of the mean bottom elevation in time; e) Normalized frequency of channel lenght based on Strahler-channel order; f) Probability density frequency of channel sinuosity.

which appeared to be slighlty different one from the other. Nonetheless, the frequency distribution of sinuosity for TR1 resulted slightly more sparse with a heavier right tail.

BS1 and Bs2 experiments were characterized by the development of platforms with mean bottom elevations that decreased more slowly than in run REF. The latter experiment produced the smaller final elevation of the platform (Figure 4.7-a,b,c,d). Execept for a slight prevalence of the 4^{th}-order channels in the BS2 run, the normalized frequency of channel length did not display any significant differences among the experiments (Figure 4.7-e). Sinuos channels resulted to be more frequent in the REF and BS2 experiments, while BS1 channel were straighter (Figure 4.7-f).

The experiment-series on the effect of initial shoreline ("IS") did not produce significat differences in the evolution of the mean-bottom elevation (Figure 4.8-d). Although slightly different configurations of final networks are revealed by the surveyed bathymetries (Figure 4.8-a,b,c), the IS2 run apparently did not display as many shoreline channels as REF and IS1. The analysis of channel-order length showed approximately the same patterns for all the three considered experiments (Figure 4.8-d). Moreover, all the experiments produced four major in-

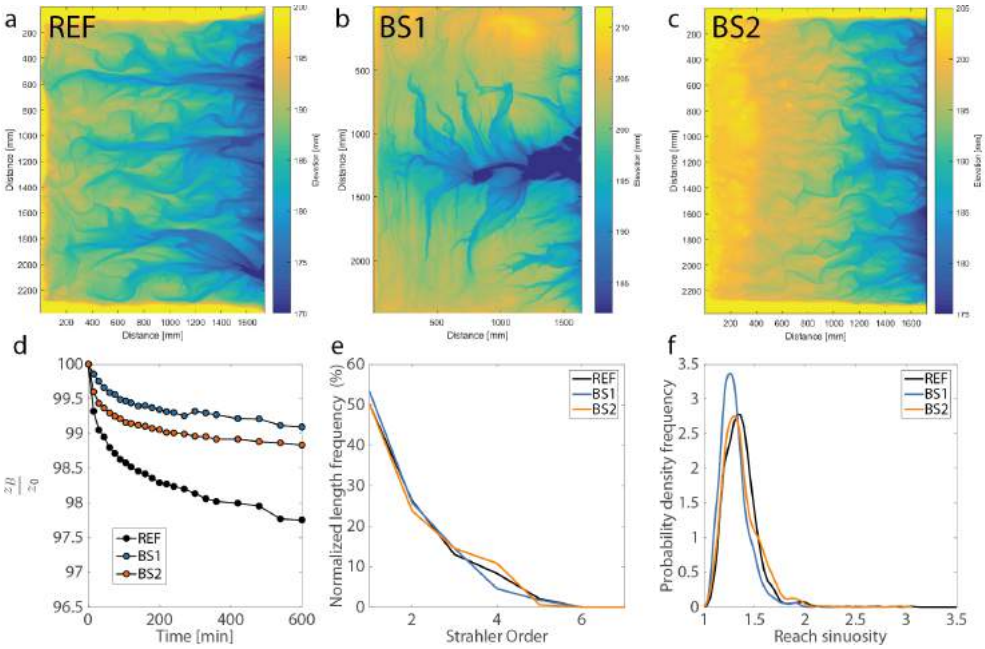

Figure 4.7: Results from the BS experiment series. Final bottom elevations for a) REF experiment, b) BR1 experiment and c) BR2 experiment. d) Evolution of the mean bottom elevation in time; e) Normalized frequency of channel lenght based on Strahler-channel order; f) Probability density frequency of channel sinuosity.

lets along the platform shoreline (Figure 4.8-a,b,c). Even though less sinuous channel appeared to be more frequent in the IS1 experiment, the probability density frequencies of all the three experiments displayed almost identical patterns.

Finally, given that the platform dimension was kept fixed, a direct comparison of the total channelized length produced by each experiment was carried out. The REF experiment exhibited the longest channelized length (9 m), whereas the shortest length was attained for seaward-sloped platform of BS2 run (Figure 4.9).

4.1.5 Discussion

Our results suggest that higher tidal ranges (TR1) lead to a stronger erosional character of the platform (Figure 4.6-d), shaping deeper channels (Figure 4.6-b) and favoring network branching (Figure 4.6-e). On the contrary, less sinuos networks are produced by a smaller tidal range (Figure 4.6-f), that also reduces the time required to achieve a morphodynamic equilibrium (Figure 4.6-d).
The morphological characteristics of the modeled networks are greatly influenced by the initial bed slope. A slope convergent to the basin axis (BS1) favors flow concentration, thus preventing generalized ero-

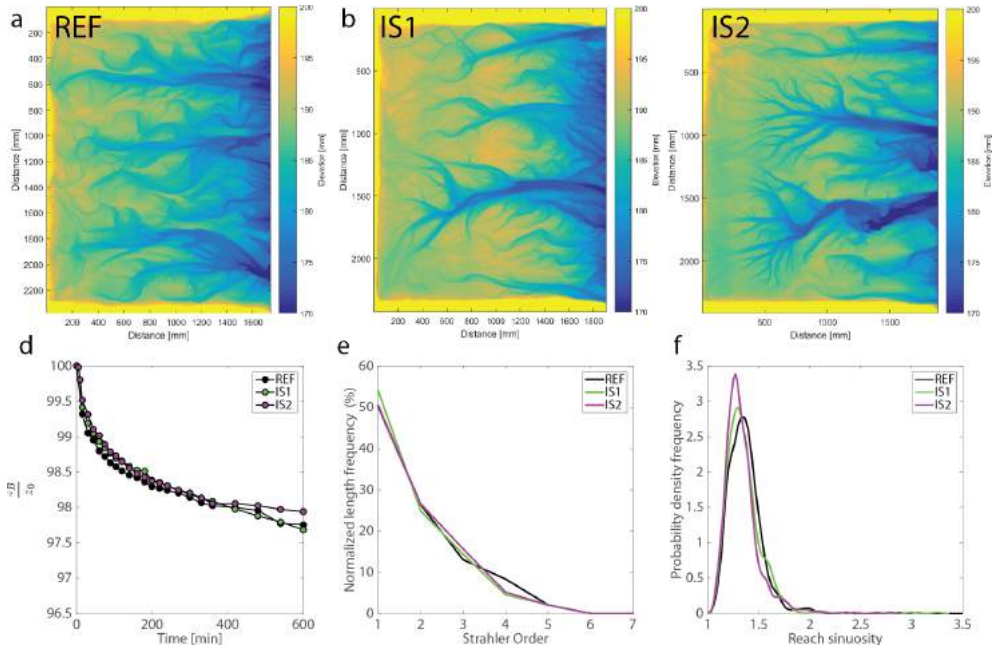

Figure 4.8: Results from the IS experiment series. Final bottom elevation for a) REF experiment, b) BR1 experiment and c) BR2 experiment. d) Evolution of the mean bottom elevation; e) Normalized frequency of channel lenght based on Strahler-channel order; f) Probability density frequency of channel sinuosity.

sion of the platform . The final configuration displays a single major network located in the middle of the basin, with moderate branching and low-sinuosity channels (Figure 4.7-b). On the other hand, a seaward sloped platform (BS2) exhibits high erosional behavior, and requires longer time to reach a quasi-steady situation (Figure 4.7-d). This configuration seems also to promote the pairing of neighbouring channels, thus shaping a network rich in bifurcations (Figure 4.7-c) as testified by the relatively high frequency of 4^{th} order channels (Figure 4.7-e). When compared to those developed over a flat platform, however, channels do not strongly elongate landward, thus causing the most distal part of the platform to remain partially unchannelized. This might explain why the BS2 run generated the shortest channelized length among all the experiments (Figure 4.9).
Finally, the three different examined configurations of the initial shoreline proved to be essentially identical in terms of erosional character, equilibrium-achieving time and final number of main networks generated (Figure 4.8). Such a result might suggest an autogenic behavior of the system, whose dynamic response, rather than being excited by irregularities in the shoreline template, is dictated by the characteristics of the basin relatively to those of the tidal forcing. A similar theory was recently proposed by Lazarus and Armstrong (2015), who demonstrated how the quasi-periodic pattern of storm-driven overwashes

are not related to perturbations or irregularities in the initial shoreline topography. Nonetheless, Figure 4.6-a,b,c apparently suggests that qualitative differences exist between the IS-series experiments. Particularly, the system with 1 initial wide breach (REF) gave in general birth to deeper and larger channels, whereas the platform with many breaches and that without breaches determined more branching networks. This result calls for an audit of the metrics that have been used for analyzing the modeled networks.

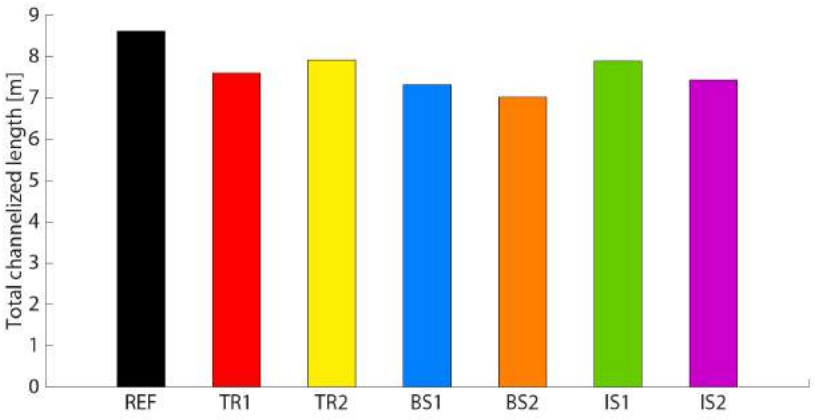

Figure 4.9: Comparison of the total channelized length produced by the all the experiments.

Feola et al. (2005) pointed out how, for the characterization of netwrok morphologies, the employment of tools that might not be unequivocal could lead to misleading results (Coco et al., 2013). Particularly, several authors have addressed the unsuitableness of Strahler's order as a metric for comparing network strucutres (Kirchner, 1993; Rinaldo et al., 1998; D'Alpaos et al., 2005). Besides using different metrics, the morphological comparison of different networks might be improved by including the channel width as a normalizing factor. This would also enable the calculation of other significant morphometric variables, such as the probability distributions of unchanneled lengths (Marani et al., 2003; D'Alpaos et al., 2005; Stefanon et al., 2010) that could also provide an assessment of network drainge efficiency. Furthermore, the complete delineation of channelized areas would also allow one to both determine the real channel axis, thus estimating channel sinuosity more precisely, and analyze the morphology of individual meander bends.
An attempt was made in order to apply the procedure proposed by Fagherazzi et al. (1999), based on a double elevation and surface-curvature threshold, for extracting channel networks in low relief areas. However, the platform drying implemented before carrying out topographic scans caused the exposure of convex channel-bottom morphologies, similar to free-bars, thus complicating the delineation

of channel boundaries. An approach based on noise removal would therefore be necessary, similar to that adopted by Passalacqua et al. (2010) who preprocessed the data by performing nonlinear diffusion in order to enhance critical features for the network extraction. Furthermore, a detailed description of network evolution should take advantage from an accurate identification of channel heads, which are progressively eroded thus leading to channel elongation and development. In order to perform an objective extraction of channel heads, a suitable approach might provided by the methodology proposed by Clubb et al. (2014), that capture channel-hillslope transition using a transformed channel-longitudinal coordinate system (Mudd et al., 2014). However, we believe that a physically-based procedure for network extraction, that indentifies channels based on the physical attributes of their chief-landforming processes, would be even more suitable. Such a procedure might be based on the definition of threshold for the bottom shear-stress, the latter having been previously computed by means of a numerical hydrodynamic model reproducing the experimental conditions. We are currently investigating the feasibility of this latter idea.

It is finally appropriate to point out that, in spite of all the aforementioned limitations, we have been able to reproduce tidal channel morphologies which resemble qualitatively well those observed in nature. In addition to the previously mentioned cusp- and box-shaped bend morphologies, we were able to obtain quite sinuous channels, some of them displaying sharp bends (Figure 4.5-c) very similar to those observed by Kleinhans et al. (2009) in a higly cohesive tidal-flat. Similar sharp morphologies have also been obtained in a small fluvial experimental setting by Smith (1998), who employed higly cohesive materials such as kaolinite clay. On the contrary, our results have been attained by using sifted, yet non-cohesive, sediments.

Although the results need to be further improved, we confidently believe that these experiments could provide valuable insights to improve the current understanding on tidal-network morphodynamics.

5 CONCLUSIONS

Using a multidisciplinary approach, that couples field investigations, numerical modelling and laboratory experiments, the present study focused on three main topics: i) the analysis of tidal meander planform features and dynamics, and a quantitative comparison with their fluvial counterparts, also based on field investigations of tidal meander hydrodynamics; ii) the influence of tidal asymmetries, as well as lateral tributaries, on the morphodynamic evolution of tidal channel bends; iii) the assessment of the role of basin slope, shoreline morphology and tidal amplitude on the inception and growth of tidal-channel networks.

The main results stemmed from this research can be summarized as follows:

i. tidal meanders display modes of migration and migration rates per unit width quite similar to those characterizing their fluvial counterparts, thus challenging the current paradigm of tidal meanders as stable landscape features;

ii. at the meander-length scale, tidal meanders exhibit less complex morphologies than their fluvial counterparts. On the contrary, at the reach length-scale (i.e., considering a series of adjacent multiple meanders), fluvial patterns appear to be more regular. We interpreted this occurrence as a consequence of the higher regularity of the chief-landforming processes which shape tidal environments. Moreover, we demonstrated that planform differences between tidal and fluvial meanders can be successfully detected and quantified;

iii. strong asymmetries in velocity distributions between flood and ebb phases invariably occur in tidal meanders. However, the effects of such asymmetries on channel morphodynamics are strictly dependent on the geometry of the study bend. The periodic shift of velocity maxima is also responsible for the varying position, intensity and type of secondary circulations and flow-separation zones that occur within a given bend. In some cases, subaqueous vegetation is shown to strongly affect the flow field within the channel;

iv. the presence of some, yet small, tidal asymmetries may influence the morphodynamic evolution of tidal meanders in a significant manner.

v. The position of bar deposits represent an appropriate proxy to detect ebb or flood dominance within a given bend, even though under certain conditions lateral tributaries may crucially influence sedimentation pattern in the main channel;

vi. physical experiments on reduced length-scale proved to be a useful mean for reproducing tidal channel morphologies which resemble qualitatively well those observed in nature. Different initial conditions, particularly the slope of tidal basin and the amplitude of tide oscillations, significantly influence the final morphology of the modeled networks. On the contrary, the number of irregularities of initial shorelines does not seem to strongly affect the network evolution, although an improvement in the metrics employed to analyze our experiment is necessary to support this observation.

BIBLIOGRAPHY

Abad, Jorge D. and Marcelo H. García (2005). "Hydrodynamics in kinoshita-generated meandering bends: importance for river-planform evolution". In: *The 4th IAHR Symposium on River, Coastal and Estuarine Morphodynamics RCEM. Taylor and Francis Group* 1974, pp. 761–771.

Ahnert, Frank (1960). "Estuarine Meanders in the Chesapeake Bay Area". In: *Geographical Review* 50.3, pp. 390–401.

Allen, John R.L. (1965). "A review of the origin and characteristics of recent alluvial sediments". In: *Sedimentology* 5.2, pp. 89–191. DOI: 10.1111/j.1365-3091.1965.tb01561.x.

Allen, John R.L. (1982). "Sedimentary structures". In: *Developments in Sedimentology vol. 2.y*. Ed. by John R.L. Allen. Elsevier. Amsterdam, pp. 53–100.

Allen, John R.L. (2000). "Morphodynamics of Holocene salt marshes: A review sketch from the Atlantic and Southern North Sea coasts of Europe". In: *Quaternary Science Reviews* 19.12, pp. 1155–1231. DOI: 10.1016/S0277-3791(99)00034-7.

Bain, Rachel Louise (2014). "A Comparison of the Planforms of Meandering Tidal and Fluvial Channels on the Ganges-Brahmaputra-Jamuna Delta, Bangladesh". Master Thesis. University of Minnesota.

Barton, Donald C. (1928). "Meandering in Tidal Streams". In: *The Journal of Geology* 36.7, pp. 615–629. DOI: 10.1086/623561.

Barwis, John H. (1978). "Sedimentology of Some South Carolina Tidal-Creek Point Bars, and a Comparison With Their Fluvial Counterparts". In: *Fluvial Sedimentology*. Ed. by A.D. Miall. Canadian Society of Petroleum Geologist Memoir 5, pp. 129–160.

Baumgardner, Sarah (2015). "Quantifying Galloway: Fluvial, Tidal and Wave Influence on Experimental and Field Deltas". Ph.D. Thesis. University of Minnesota, p. 122.

Bayliss-Smith, T. P., R. Healey, R. Lailey, T. Spencer, and D. R. Stoddart (1979). "Tidal flows in salt marsh creeks". In: *Estuarine and Coastal Marine Science* 9.3, pp. 235–255. DOI: 10.1016/0302-3524(79)90038-0.

Belluco, Enrica, Monica Camuffo, Sergio Ferrari, Lorenza Modenese, Sonia Silvestri, Alessandro Marani, and Marco Marani (2006). "Mapping salt-marsh vegetation by multispectral and hyperspectral remote sensing". In: *Remote Sensing of Environment* 105.1, pp. 54–67. DOI: 10.1016/j.rse.2006.06.006.

Bertoldi, W., A. M. Gurnell, and N. A. Drake (2011). "The topographic signature of vegetation development along a braided river: Results of a combined analysis of airborne lidar, color air photographs, and ground measurements". In: *Water Resources Research* 47.6. W06525. DOI: 10.1029/2010WR010319.

Biedenharn, D.S., P.G. Combs, G.J. Hill, C.F.J. Pinkard, and C.B. Pinkston (1989). "Relationship between channel migration and radius of curvature on the Red River". In: *Sediment Transport Modeling*. Ed. by S. S. Y. Wang. New York: Am. Soc. Civ. Eng., pp. 536–541.

Blanckaert, K. (2009). "Saturation of curvature-induced secondary flow, energy losses, and turbulence in sharp open-channel bends: Laboratory experiments, analysis, and modeling". In: *Journal of Geophysical Research: Solid Earth* 114.3, pp. 1–23. DOI: 10.1029/2008JF001137.

Blanckaert, Koen (2011). "Hydrodynamic processes in sharp meander bends and their morphological implications". In: *Journal of Geophysical Research: Earth Surface* 116.1, pp. 1–22. DOI: 10.1029/2010JF001806.

Blanckaert, Koen and Huib J. de Vriend (2003). "Nonlinear modeling of mean flow redistribution in curved open channels". In: *Water Resources Research* 39.12, pp. 1–14. DOI: 10.1029/2003WR002068.

Blanckaert, Koen and Huib J. de Vriend (2004). "Secondary flow in sharp open-channel bends". In: *Journal of Fluid Mechanics* 498, pp. 353–380. DOI: 10.1017/S0022112003006979.

Blondeaux, Paolo and Giovanni Seminara (1985). "A unified bar–bend theory of river meanders". In: *Journal of Fluid Mechanics* 157.-1, p. 449. DOI: 10.1017/S0022112085002440.

Boldt, Justin A. and Kevin A. Oberg (2015). "Validation of streamflow measurements made with M9 and RiverRay acoustic Doppler current profilers". In: *Journal of Hydraulic Engineering*. DOI: 10.1061/(ASCE)HY.1943-7900.0001087.

Bolla Pittaluga, Michele, Nicoletta Tambroni, Alberto Canestrelli, Rudy Slingerland, Stefano Lanzoni, and Giovanni Seminara (2015). "Where river and tide meet: The morphodynamic equilibrium of alluvial estuaries". In: *Journal of Geophysical Research F: Earth Surface* 120.1, pp. 75–94. DOI: 10.1002/2014JF003233.

Boon, John D. (1975). "Tidal discharge asymmetry in a salt marsh drainage system". In: *Limnology and Oceanography* 20.1, pp. 71–80. DOI: 10.4319/lo.1975.20.1.0071.

Breugem, W.A. and L.H. Holthuijsen (2006). "Generalized Shallow Water Wave Growth from Lake George". In: *Journal of Waterway, Port, Coastal, and Ocean Engineering* 133.3. DOI: 10.1061/(ASCE)0733-950X(2007)133:3(173).

Brice, James C. (1974). "Evolution of meander loops". In: *Bulletin of the Geological Society of America* 85.4, pp. 581–586. DOI: 10.1130/0016-7606(1974)85<581:EOML>2.0.CO;2.

Bridge, J.S. and J. Jarvis (1982). "The dynamics of a river bend: a study in flow and sedimentary processes". In: *Sedimentology* 29.4, pp. 499–541. DOI: 10.1111/j.1365-3091.1982.tb01732.x.

Bridge, J.S., N.D. Smith, F. Trent, S.L. Gabel, and P. Bernstein (1986). "Sedimentology and morphology of a low-sinuosity river: Calamus River, Nebraska Sand Hills". In: *Sedimentology* 33.6, pp. 851–870. DOI: 10.1111/j.1365-3091.1986.tb00987.x.

Bridges, Paul H. and Michael R. Leeder (1976). "Sedimentary model for intertidal mudflat channels, with examples from the Solway Firth, Scotland". In: *Sedimentology* 23.4, pp. 533–552. DOI: 10.1111/j.1365-3091.1976.tb00066.x.

Brierley, Gary J. (1991). "Bar Sedimentology of the Squamish River, British Columbia: Deinition and Application of Morphostratigraphic Units". In: *Journal of Sedimentary Petrology* 61.2, pp. 211–225.

Brivio, Lara, Massimiliano Ghinassi, Andrea D'Alpaos, Alvise Finotello, Alessandro Fontana, Alvise Finotello, Marcella Roner, and Nick Howes (2015). "3D internal architecture and morphodynamic evolution of tidal point bars : inferences from the Venice Lagoon (Italy)Paper, Conference". In: *IAS 31st Meeting of Sedimentology*. Krakow.

Brivio, Lara, Massimiliano Ghinassi, Andrea D'Alpaos, Alvise Finotello, Alessandro Fontana, Marcella Roner, and Nick Howes (2016). "Aggradation and lateral migration shaping geometry of a tidal point bar: An example from salt marshes of the Northern Venice Lagoon (Italy)". In: *Sedimentary Geology* 343, pp. 141–155. DOI: 10.1016/j.sedgeo.2016.08.005.

Burningham, Helene (2008). "Contrasting geomorphic response to structural control: The Loughros estuaries, northwest Ireland". In: *Geomorphology* 97.3–4, pp. 300–320.

Campbell, Marius R. (1927). "Meaning of Meanders in Tidal Streams". In: *Bulletin of the Geological Society of America* 38, pp. 537–556.

Canestrelli, A., A. Defina, S. Lanzoni, and L. D'Alpaos (2007). "Long-term evolution of tidal channels flanked by tidal flats". In: *River, Coastal and Estuarine Morphodynamics: RCEM 2007 - Proceedings of the 5th IAHR Symposium on River, Coastal and Estuarine Morphodynamics* 1, pp. 145–153. DOI: doi:10.1201/NOE0415453639-c19.

Canestrelli, Alberto, Stefano Lanzoni, and Sergio Fagherazzi (2014). "One-dimensional numerical modeling of the long-term morphodynamic evolution of a tidally-dominated estuary: The Lower Fly River (Papua New Guinea)". In: *Sedimentary Geology* 301, pp. 107–119. DOI: 10.1016/j.sedgeo.2013.06.009.

Carniello, L., S. Silvestri, M. Marani, A. D'Alpaos, V. Volpe, and A. Defina (2014). "Sediment dynamics in shallow tidal basins: In situ observations, satellite retrievals, and numerical modeling in the Venice Lagoon". In: *Journal of Geophysical Research: Earth Surface* 119.4, pp. 802–815. DOI: 10.1002/2013JF003015.

Carniello, Luca, Andrea D'Alpaos, Gianluca Botter, and Andrea Rinaldo (2016). "Statistical characterization of spatio-temporal sediment dynamics in the Venice lagoon". In: *Journal of Geophysical Research: Earth Surface* January. DOI: 10.1002/2015JF003793.

Carniello, Luca, Andrea D'Alpaos, and Andrea Defina (2011). "Modeling wind waves and tidal flows in shallow micro-tidal basins". In: *Estuarine, Coastal and Shelf Science* 92.2, pp. 263–276. DOI: 10.1016/j.ecss.2011.01.001.

Carniello, Luca, Andrea Defina, and Luigi D'Alpaos (2009). "Morphological evolution of the Venice lagoon: Evidence from the past and trend for the future". In: *Journal of Geophysical Research: Earth Surface* 114.4, pp. 1–10. DOI: 10.1029/2008JF001157.

Carniello, Luca, Andrea Defina, and Luigi D'Alpaos (2012). "Modeling sand-mud transport induced by tidal currents and wind waves in shallow microtidal basins: Application to the Venice Lagoon (Italy)". In: *Estuarine, Coastal and Shelf Science* 102-103, pp. 105–115. DOI: 10.1016/j.ecss.2012.03.016.

Carniello, Luca, Andrea Defina, Sergio Fagherazzi, and Luigi D'Alpaos (2005). "A combined wind wave-tidal model for the Venice lagoon, Italy". In: *Journal of Geophysical Research: Earth Surface* 110.4, pp. 1–15. DOI: 10.1029/2004JF000232.

Choi, Kyungsik S. (2011). "External controls on the architecture of inclined heterolithic stratification (IHS) of macrotidal Sukmo Channel: Wave versus rainfall". In: *Marine Geology* 285.1-4, pp. 17–28. DOI: 10.1016/j.margeo.2011.05.002.

Choi, Kyungsik S., Robert W. Dalrymple, S. S. Chun, and S-P Kim (2004). "Sedimentology of modern, Inclined Heterolithic Stratification (IHS) in the macrotidal Han River Delta, Korea". In: *Journal of Sedimentary Research* 74.5, pp. 677–689. DOI: 10.1306/030804740677.

Choi, Kyungsik S., Chang Min Hong, Mi Hee Kim, Chung Rok Oh, and Jae Hoon Jung (2013). "Morphologic evolution of macrotidal estuarine channels in Gomso Bay, west coast of Korea: Implications for the architectural development of inclined heterolithic stratification". In: *Marine Geology* 346.September, pp. 343–354. DOI: 10.1016/j.margeo.2013.10.005.

Choi, Kyungsik S. and Joo Hee Jo (2015). "Morphodynamics of Tidal Channels in the Open Coast Macrotidal Flat, Southern Ganghwa Island in Gyeonggi Bay, West Coast of Korea". In: *Journal of Sedimentary Research* 85.6, pp. 582–595. DOI: 10.2110/jsr.2015.44.

Clubb, Fiona J., Simon M. Mudd, David T. Milodowski, Martin D. Hurst, and Louise J. Slater (2014). "Objective extraction of channel heads from high-resolution topographic data". In: *Water Resources Research* 50.5, pp. 4283–4304. DOI: 10.1002/2013WR015167.

Coco, Giovanni, Zeng Zhou, B. van Maanen, Maitane Olabarrieta, R. Tinoco, and Ian H. Townend (2013). "Morphodynamics of tidal networks: Advances and challenges". In: *Marine Geology* 346, pp. 1–16. DOI: 10.1016/j.margeo.2013.08.005.

Constantine, José Antonio and Thomas Dunne (2008). "Meander Cutoff and the Controls onthe Production and Evolution of Oxbow Lakes." In: *Geology* 36.1, pp. 23–26. DOI: 10.1130/GxxxxA.1.

Cowell, Peter J., Marcel J. F. Stive, Alan W. Niedoroda, Don J. P. Swift, Huib J. de Vriend, Maarten C. Buijsman, Robert J. Nicholls, Peter S. Roy, George M. Kaminsky, Jelmer Cleveringa, Chris W. Reed, and Poppe L. de Boer (2003). "The Coastal-Tract (Part 2): Applications of Aggregated Modeling of Lower-Order Coastal Change". In: *Journal of Coastal Research* 19.4, pp. 828–848.

Crosato, Alessandra and May Samir Saleh (2011). "Numerical study on the effects of floodplain vegetation on river planform style". In: *Earth Surface Processes and Landforms* 36.6, pp. 711–720. DOI: 10.1002/esp.2088.

Czuba, Jonathan A., James L. Best, Kevin A. Oberg, Daniel R. Parsons, P. Ryan Jackson, Marcelo H. Garcia, and Peter Ashmore (2011). "Bed morphology, flow structure, and sediment transport at the outlet of Lake Huron and in the upper St. Clair River". In: *Journal of Great Lakes Research* 37.3, pp. 480–493. DOI: 10.1016/j.jglr.2011.05.011.

D'Alpaos, Andrea, Luca Carniello, and Andrea Rinaldo (2013). "Statistical mechanics of wind wave-induced erosion in shallow tidal basins: Inferences from the Venice Lagoon". In: *Geophysical Research Letters* 40.13, pp. 3402–3407. DOI: 10.1002/grl.50666.

D'Alpaos, Andrea, Stefano Lanzoni, Marco Marani, Sergio Fagherazzi, and Andrea Rinaldo (2005). "Tidal network ontogeny: Channel initiation and early development". In: *Journal of Geophysical Research: Earth Surface* 110.2, pp. 1–14. DOI: 10.1029/2004JF000182.

D'Alpaos, Andrea, Stefano Lanzoni, Marco Marani, and Andrea Rinaldo (2007). "Landscape evolution in tidal embayments: Modeling the interplay of erosion, sedimentation, and vegetation dynamics". In: *Journal of Geophysical Research: Earth Surface* 112.1, pp. 1–17. DOI: 10.1029/2006JF000537.

D'Alpaos, Andrea, Simon M. Mudd, and Luca Carniello (2011). "Dynamic response of marshes to perturbations in suspended sediment concentrations and rates of relative sea level rise". In: *Journal of Geophysical Research: Earth Surface* 116.4, pp. 1–13. DOI: 10.1029/2011JF002093.

D'Alpaos, L. and A. Defina (2007). "Mathematical modeling of tidal hydrodynamics in shallow lagoons: A review of open issues and applications to the Venice lagoon". In: *Computers and Geosciences* 33.4, pp. 476–496. DOI: 10.1016/j.cageo.2006.07.009.

D'Alpaos, Luigi (2010). *Fatti e misfatti di idraulica lagunare. La laguna di Venezia dalla diversione dei fiumi alle nuove opere delle bocche di porto*, p. 329.

Dalrymple, Robert W., Duncan A. Mackay, Aitor A. Ichaso, and Kyungsik S. Choi (2010). "Processes, morphodynamics, and facies of tide-dominated estuaries". In: *Principles of Tidal Sedimentology*. Ed. by Richard A. Jr. Davis and Robert W. Dalrymple. Elsevier, pp. 79–107. DOI: 10.1007/978-94-007-0123-6_18.

Dalrymple, Robert W., Duncan A. Mackay, Aitor A. Ichaso, and Kyungsik S. Choi (2012). "Processes, Morphodynamics, and Facies of Tide-Dominated Estuaries". In: *Principles of Tidal Sedimentology*. Ed. by Richard A. Davis Jr. and Robert W. Dalrymple. Dordrecht: Springer Netherlands, pp. 79–107. DOI: 10.1007/978-94-007-0123-6_5.

Daniel, James F. (1971). "Channel movement of meandering Indiana streams". In: *U.S. Geological Survey Professional Paper* 732-A.

Davidson-Arnott, Robin G D, Danika Van Proosdij, Jeff Ollerhead, and Laura Schostak (2002). "Hydrodynamics and sedimentation in salt marshes: Examples from a macrotidal marsh, Bay of Fundy". In: *Geomorphology* 48.1-3, pp. 209–231. DOI: 10.1016/S0169-555X(02)00182-4.

Davies, Neil S. and Martin R. Gibling (2010a). "Cambrian to Devonian evolution of alluvial systems: The sedimentological impact of the earliest land plants". In: *Earth-Science Reviews* 98.3-4, pp. 171–200. DOI: 10.1016/j.earscirev.2009.11.002.

Davies, Neil S. and Martin R. Gibling (2010b). "Paleozoic vegetation and the Siluro-Devonian rise of fl uvial lateral accretion sets". In: *Geology* 38.1, pp. 51–54. DOI: 10.1130/G30443.1.

de Mowbray, Tessa (1983). "The genesis of lateral accretion deposits in recent intertidal mudflat channels, Solway Firth, Scotland". In: *Sedimentology* 30.3, pp. 425–435. DOI: 10.1111/j.1365-3091.1983.tb00681.x.

de Swart, H.E. and J.T.F. Zimmerman (2009). "Morphodynamics of Tidal Inlet Systems". In: *Annual Review of Fluid Mechanics* 41.1, pp. 203–229. DOI: 10.1146/annurev.fluid.010908.165159.

Defendi, V., V. Kovačević, F. Arena, and Luca Zaggia (2010). "Estimating sediment transport from acoustic measurements in the Venice Lagoon inlets". In: *Continental Shelf Research* 30.8, pp. 883–893. DOI: 10.1016/j.csr.2009.12.004.

Defina, Andrea (2000). "Two-dimensional shallow flow equations for partially dry areas". In: *Water Resources Research* 36.11, p. 3251. DOI: 10.1029/2000WR900167.

Deltares (2016). *Delft3D-FLOW: Simulation of Multi-Dimensional Hydrodynamic Flows and Transport Phenomena, Including Sediments-User Manual*. Delft, Netherlands: Deltares.

Di Silvio, Giampaolo, Chiara Dall'Angelo, Davide Bonaldo, and Giacomo Fasolato (2010). "Long term model of planimetric and bathymetric evolution of a tidal lagoon". In: *Continental Shelf Research* 30.8, pp. 894–903. DOI: 10.1016/j.csr.2009.09.010.

Dietrich, William E. and J. Dungan Smith (1983). "Influence of the point bar on flow through curved channels". In: *Water Resources Research* 19.5, pp. 1173–1192. DOI: 10.1029/WR019i005p01173.

Dietrich, William E., J. Dungan Smith, and Thomas Dunne (1979). "Flow and Sediment Transport in a Sand Bedded Meander". In: *The Journal of Geology* 87.3, pp. 305–315. DOI: 10.1086/628419.

Díez-Canseco, D., J.A. Arz, J.I. Benito, M. Díaz-Molina, and I. Arenillas (2014). "Tidal influence in redbeds: A palaeoenvironmental and biochronostratigraphic reconstruction of the Lower Tremp Formation (South-Central Pyrenees, Spain) around the Cretaceous/Paleogene boundary". In: *Sedimentary Geology* 312, pp. 31–49. DOI: http://dx.doi.org/10.1016/j.sedgeo.2014.06.008.

Dinehart, R. L. and J. R. Burau (2005a). "Averaged indicators of secondary flow in repeated acoustic Doppler current profiler crossings of bends". In: *Water Resources Research* 41.9, pp. 1–18. DOI: 10.1029/2005WR004050.

Dinehart, R. L. and J. R. Burau (2005b). "Repeated surveys by acoustic Doppler current profiler for flow and sediment dynamics in a tidal river". In: *Journal of Hydrology* 314.1-4, pp. 1–21. DOI: 10.1016/j.jhydrol.2005.03.019.

Dronkers, J. (1986). "Tidal asymmetry and estuarine morphology". In: *Netherlands Journal of Sea Research* 20.2-3, pp. 117–131. DOI: 10.1016/0077-7579(86)90036-0.

Dronkers, J. (2005). *Dynamics of Coastal Systems*. Singapore: World Scientific.

Dury, G.H. (1971). "Channel Characteristics in a Meandering Tidal Channel : Crooked River , Florida". In: *Geografiska Annaler, Seriea A, Physical Geography* 53.3, pp. 188–197.

Dzwonkowski, Brian, Kuo-Chuin Wong, and William J Ullman (2014). "Water Level and Velocity Characteristics of a Salt Marsh Channel in the Murderkill Estuary, Delaware". In: *Journal of Coastal Research* 30.1, pp. 63–74. DOI: 10.2112/JCOASTRES-D-12-00161.1.

Einstein, H. A. and J. A. Harder (1954). "Velocity distribution and the boundary layer at channel bends". In: *Eos, Transactions American Geophysical Union* 35.1, pp. 114–120. DOI: 10.1029/TR035i001p00114.

Eke, Esther C., M. Czapiga, E. Viparelli, Yasuyuki Shimizu, J. Imaran, T. Sun, and Gary Parker (2014). "Coevolution of width and sinuosity in Meandering rivers". In: *Journal of Fluid Mechanics* 760, pp. 127–174. DOI: 10.1017/jfm.2014.556.

Engel, Frank L. and Bruce L. Rhoads (2016). "Three-dimensional flow structure and patterns of bed shear stress in an evolving compound meander bend". In: *Earth Surface Processes and Landforms* 41.9, pp. 1211–1226. DOI: 10.1002/esp.3895.

Engelund, F. (1974). "Flow and bed topography in channel bends". In: *Journal of the Hydraulics Division, American Society of Civil Engineers* 100.HY11, pp. 1631–48.

Fagherazzi, Sergio (2008). "Self-organization of tidal deltas." In: *Proceedings of the National Academy of Sciences of the United States of America* 105, pp. 18692–18695. DOI: 10.1073/pnas.0806668105.

Fagherazzi, Sergio, Annalisa Bortoluzzi, William E. Dietrich, Attilio Adami, Stefano Lanzoni, Marco Marani, and Andrea Rinaldo (1999). "Tidal networks 1. Automatic network extraction and preliminary scaling features from digital terrain maps". In: *Water Resources Research* 35.12, pp. 3891–3904. DOI: 10.1029/1999WR900236.

Fagherazzi, Sergio and David Jon Furbish (2001). "On the shape and widening of salt marsh creeks". In: *Journal of Geophysical Research* 106.C1, p. 991. DOI: 10.1029/1999JC000115.

Fagherazzi, Sergio, Emmanuel J. Gabet, and David Jon Furbish (2004). "The effect of bidirectional flow on tidal channel planforms". In: *Earth Surface Processes and Landforms* 29.3, pp. 295–309. DOI: 10.1002/esp.1016.

Fagherazzi, Sergio, Matthew L. Kirwan, Simon M. Mudd, Glenn R. Guntenspergen, Stijn Temmerman, Andrea D'Alpaos, Johan van de Koppel, John M. Rybczyk, Enrique Reyes, Chris Craft, and Jonathan Clough (2011). "Numerical Models of Salt Marsh 2 Evolution : Ecological , Geomorphic , 3 and Climatic Factors". In: *Review of Geophysics* 49, pp. 1–28. DOI: 10.1029/2011RG000359.36.

Fagherazzi, Sergio, Matthew L. Kirwan, Simon M. Mudd, Glenn R. Guntenspergen, Stijn Temmerman, Andrea D'Alpaos, Johan van de Koppel, John M. Rybczyk, Enrique Reyes, Chris Craft, and Jonathan Clough (2012). "Numerical models of salt marsh evolution: Ecological, geomorphic, and climatic factors". In: *Reviews of Geophysics* 50.1.

Fagherazzi, Sergio, Patricia L. Wiberg, and Alan D. Howard (2003). "Tidal flow field in a small basin". In: *Journal of Geophysical Research: Oceans* 108.C3. DOI: 10.1029/2002JC001340.

Feola, Alessandra, Enrica Belluco, Andrea D'Alpaos, Stefano Lanzoni, Marco Marani, and Andrea Rinaldo (2005). "A geomorphic study of lagoonal landforms". In: *Water Resources Research* 41.6, pp. 1–11. DOI: 10.1029/2004WR003811.

Ferguson, Robert I. and Dan R. Parsons (2004). "Flow structures in natural meander bends with recirculation". In: *River Flow*, pp. 325–331.

Ferguson, Robert I., Dan R. Parsons, Stuart N. Lane, and Richard J. Hardy (2003). "Flow in meander bends with recirculation at the inner bank". In: *Water Resources Research* 39.11, n/a–n/a. DOI: 10.1029/2003WR001965.

Ferrarin, Christian, Andrea Cucco, Georg Umgiesser, Debora Bellafiore, and Carl L. Amos (2010). "Modelling fluxes of water and sediment between Venice Lagoon and the sea". In: *Continental Shelf Research* 30.8, pp. 904–914. DOI: 10.1016/j.csr.2009.08.014.

Ferrarin, Christian, Alberto Tomasin, Marco Bajo, Antonio Petrizzo, and Georg Umgiesser (2015). "Tidal changes in a heavily modified coastal wetland". In: *Continental Shelf Research* 101, pp. 22–33. DOI: 10.1016/j.csr.2015.04.002.

Flener, Claude, Yunsheng Wang, Leena Laamanen, Elina Kasvi, Jenni Mari Vesakoski, and Petteri Alho (2015). "Empirical modeling of spatial 3D flow characteristics using a remote-controlled ADCP system: Monitoring a spring flood". In: *Water (Switzerland)* 7.1, pp. 217–247. DOI: 10.3390/w7010217.

Folkard, Andrew M. (2005). "Hydrodynamics of model Posidonia oceanica patches in shallow water." In: *Limnology and Oceanography* 50.5, pp. 1592–1600. DOI: 10.4319/lo.2005.50.5.1592.

Frascati, Alessandro and Stefano Lanzoni (2009). "Morphodynamic regime and long-term evolution of meandering rivers". In: *Journal of Geophysical Research: Earth Surface* 114.2, pp. 1–12. DOI: 10.1029/2008JF001101.

Frascati, Alessandro and Stefano Lanzoni (2010). "Long-term river meandering as a part of chaotic dynamics? A contribution from mathematical modelling". In: *Earth Surface Processes and Landforms* 35.7, pp. 791–802. DOI: 10.1002/esp.1974.

Frascati, Alessandro and Stefano Lanzoni (2013). "A mathematical model for meandering rivers with varying width". In: *Journal of Geophysical Research: Earth Surface* 118.3, pp. 1641–1657. DOI: 10.1002/jgrf.20084.

Fredsoe, Jorgen (1978). "Meandering and Braiding of Rivers". In: *Journal of Fluid Mechanics* 84.November, pp. 609–624. DOI: 10.1017/S0022112078000373.

French, Jonathan R. and Tom Spencer (1993). "Dynamics of sedimentation in a tide-dominated backbarrier salt marsh, Norfolk, UK". In: *Marine Geology* 110.3-4, pp. 315–331. DOI: 10.1016/0025-3227(93)90091-9.

French, J.R. and D.R. Stoddart (1992). "Hydrodynamics of salt marsh creek systems: Implications for marsh morphological development and material

exchange". In: *Earth Surface Processes and Landforms* 17.3, pp. 235–252. DOI: 10.1002/esp.3290170304.

Friedkin, J.F. (1945). *A laboratory study of the meandering of alluvial rivers*. Tech. rep. War Department - Corps of Engineers, U.S. Army.

Friedrichs, Carl T. (2012). *Tidal Flat Morphodynamics: A Synthesis*. Vol. 3. Elsevier Inc., pp. 137–170. DOI: 10.1016/B978-0-12-374711-2.00307-7.

Friedrichs, Carl T. and James E. Perry (2001). "Tidal Salt Marsh Morphodynamics: A Synthesis". In: *Journal of Coastal Research* SI.27, pp. 7–37. DOI: 10.2307/25736162.

Frothingham, Kelly M. and Bruce L. Rhoads (2003). "Three-dimensional flow structure and channel change in an asymmetrical compound meander loop, Embarras River, Illinois". In: *Earth Surface Processes and Landforms* 28.6, pp. 625–644. DOI: 10.1002/esp.471.

Furbish, David Jon (1988). "River-bend curvature and migration: how are they related?" In: *Geology* 16.8, pp. 752–755. DOI: 10.1130/0091-7613(1988)016<0752:RBCAMH>2.3.CO.

Gabet, Emmanuel J. (1998). "Lateral Migratiion and Bank Erosion in a Saltmarsh Tidal Channel in San Francisco Bay, California". In: *Estuaries* 21.4B, pp. 745–753. DOI: 10.2307/1353278.

García, Carlos M., Kevin Oberg, and Marcelo H. García (2007). "ADCP Measurements of Gravity Currents in the Chicago River, Illinois". In: *Journal of Hydraulic Engineering* 133.12, pp. 1356–1366. DOI: 10.1061/(ASCE)0733-9429(2007)133:12(1356).

Garofalo, Donald (1980). "The Influence of Wetland Vegetation on Tidal Stream Channel Migration and Morphology". In: *Estuaries* 3.4, pp. 258–270. DOI: 10.2307/1352081.

Garotta, Valeria, Michele Bolla Pittaluga, and Giovanni Seminara (2006). "On the migration of tidal free bars". In: *Physics of Fluids* 18.9, p. 096601. DOI: 10.1063/1.2221346.

Garotta, Valeria, Andreas Christof Rummel, and Giovanni Seminara (2007). "Long-term morphodynamics and hydrodynamics of tidal meandering channels". In: *5th IAHR Symposium on River, Coastal and Estuarine Morphodynamics*. 105, pp. 163–168.

Gatto, P. and L. Carbognin (1981). "The Lagoon of Venice: natural environmental trend and man-induced modification / La Lagune de Venise:

l'évolution naturelle et les modifications humaines". In: *Hydrological Sciences Bulletin* 26.4, pp. 379–391. DOI: 10.1080/02626668109490902.

Geyer, W. Rockwell and Richard Signell (1990). "Measurements of tidal flow around a headland with a shipboard acoustic Doppler current profiler". In: *Journal of Geophysical Research* 95.C3, p. 3189. DOI: 10.1029/JC095iC03p03189.

Ghil, M., M. R. Allen, M. D. Dettinger, K. Ide, D. Kondrashov, M. E. Mann, A. W. Robertson, A. Saunders, Y. Tian, F. Varadi, and P. Yiou (2002). "Advanced spectral methods for climate time series". In: *Reviews of Geophysics* 40.1, pp. 1–41. DOI: 10.1029/2001RG000092.

Ghinassi, Massimiliano, Andrea D'Alpaos, Andrea Gasparotto, Luca Carniello, Lara Brivio, Alvise Finotello, Marcella Roner, Erica Franceschinis, Nicola Realdon, and Nick Howes (in rev.). "Morphodynamics Evolution And Stratal Architecture Of Translating Tidal Point Bars: Inferences From The Northern Venice Lagoon (Italy)." In: *Sedimentology*.

Gibling, Martin R. and Neil S. Davies (2012). "Palaeozoic landscapes shaped by plant evolution". In: *Nature Geoscience* 5.2, pp. 99–105. DOI: 10.1038/ngeo1376.

Gran, Karen and Chris Paola (2001). "Riparian vegetation controls on braided stream dynamics". In: *Water Resources Research* 37.12, pp. 3275–3283. DOI: 10.1029/2000WR000203.

Grass, A.J. (1970). "TInitial instability of fine bed sand". In: *Journal of Hydraulic Division* 96, pp. 619–632.

Guneralp, Inci and Bruce L. Rhoads (2011). "Influence of floodplain erosional heterogeneity on planform complexity of meandering rivers". In: *Geophysical Research Letters* 38.14. DOI: 10.1029/2011GL048134.

Gurnell, Angela (2014). "Plants as river system engineers". In: *Earth Surface Processes and Landforms* 40.1, pp. 135–137. DOI: 10.1002/esp.3671.

Hack, J.T. (1957). "Studies of longitudinal stream profiles in Virginia and Maryland". In: *USGS Professional Paper 249*, p. 97.

Hackney, Christopher, Jim Best, Julian Leyland, Stephen E. Darby, Daniel Parsons, Rolf Aalto, and Andrew Nicholas (2015). "Modulation of outer bank erosion by slump blocks: Disentangling the protective and destructive role of failed material on the three-dimensional flow structure". In: *Geophysical Research Letters* 42.24, pp. 10, 663–10, 670. DOI: 10.1002/2015GL066481.

Hamming, R. W. (1989). *Digital Filters (3rd Ed.)* Hertfordshire, UK: Prentice Hall International (UK) Ltd.

Hathout, Dean (2015). "Sine-Generated Curves : Theoretical and Empirical Notes". In: *Advances in Pure Mathematics* 5.September, pp. 689–702. DOI: 10.4236/apm.2015.511063.

Hayes, Monson H. (1996). *Statistical Digital Signal Processing and Modeling*. John Wiley and Sons, p. 335. DOI: 10.2307/1271141.

Healey, R.G, K. Pye, D.R. Stoddart, and T.P. Bayliss-Smith (1981). "Velocity variations in salt marsh creeks, Norfolk, England". In: *Estuarine, Coastal and Shelf Science* 13.5, pp. 535–545. DOI: 10.1016/S0302-3524(81)80056-4.

Heo, Joon, Trinh Anh Duc, Hyung Sik Cho, and Sung Uk Choi (2009). "Characterization and prediction of meandering channel migration in the GIS environment: A case study of the Sabine River in the USA". In: *Environmental Monitoring and Assessment* 152.1-4, pp. 155–165. DOI: 10.1007/s10661-008-0304-8.

Hickin, Edward J. (1974). "The development of meanders in natural river-channels". In: *American Journal of Science* 274.4, pp. 414–442. DOI: 10.2475/ajs.274.4.414.

Hickin, Edward J. and Gerald C. Nanson (1975). "The character of channel migration on the Beatton River, Northeast British Columbia, Canada". In: *Bulletin of the Geological Society of America* 86.4, pp. 487–494. DOI: 10.1130/0016-7606(1975)86<487:TCOCMO>2.0.CO;2.

Hickin, Edward J. and Gerald C. Nanson (1984). "Lateral Migration Rates of River Bends". In: *Journal of Hydraulic Engineering* 110, pp. 1557–1567. DOI: 10.1061/(ASCE)0733-9429(1984)110:11(1557).

Hoitink, A. J F and P. Hoekstra (2005). "Observations of suspended sediment from ADCP and OBS measurements in a mud-dominated environment". In: *Coastal Engineering* 52.2, pp. 103–118. DOI: 10.1016/j.coastaleng.2004.09.005.

Hood, W. Gregory (2010). "Tidal channel meander formation by depositional rather than erosional processes: Examples from the prograding Skagit River Delta (Washington, USA)". In: *Earth Surface Processes and Landforms* 35.3, pp. 319–330. DOI: 10.1002/esp.1920.

Hooke, Janet M. (1979). "An analysis of the processes of river bank erosion". In: *Journal of Hydrology* 42.1–2, pp. 39–62. DOI: 10.1016/0022-1694(79)90005-2.

Hooke, Janet M. (1980). "Magnitude and distribution of rates of river bank erosion". In: *Earth Surface Processes* 5.2, pp. 143–157. DOI: 10.1002/esp.3760050205.

Hooke, Janet M. (1984). "Changes in river meanders : a review of techniques and results of analyses". In: *Progress in Physical Geography* 8.4, pp. 473–508. DOI: 10.1177/030913338400800401.

Hooke, Janet M. (1987). "Changes in Meander Morphology". In: *International Geomorphology, 1986: Proceedings of the First International Conference on Geomorphology*. Ed. by V. Gardiner. Chichester, UK: John Wiley and Sons, pp. 591–609.

Hooke, Janet M. (2007). "Complexity, self-organisation and variation in behaviour in meandering rivers". In: *Geomorphology* 91.3-4, pp. 236–258. DOI: 10.1016/j.geomorph.2007.04.021.

Hooke, Janet M. (2013). "River Meandering". In: *Treatise on Geomorphology*. Vol. 9. Elsevier Ltd., pp. 260–288. DOI: 10.1016/B978-0-12-374739-6.00241-4.

Horton, Robert E (1945). "Geological Society of America Bulletin". In: *Geological Society Of America Bulletin* 56.1, pp. 151–180. DOI: 10.1130/0016-7606(1945)56.

Howard, Alan D. (1996). "Modelling Channel Evolution and Floodplain Morphology". In: *Floodplain Processes*. Ed. by Malcom G. Anderson, Des E. Walling, and Paul D. Bates. 1996 John. John Wiley & Sons, pp. 15–62.

Howard, Alan D. and Allen T. Hemberger (1991). *Multivariate characterization of meandering*. DOI: 10.1016/0169-555X(91)90002-R.

Howard, Alan D. and Thomas R. Knutson (1984). *Sufficient conditions for river meandering: A simulation approach*. DOI: 10.1029/WR020i011p01659.

Howes, Nick, Duncan M. FitzGerald, Zoe J. Hughes, Ioannis Y. Georgiou, Mark Kulp, Michael D. Miner, Jane M. Smith, and John Barras (2010). "Hurricane-induced failure of low salinity wetlands." In: *Proceedings of the National Academy of Sciences of the United States of America* 107.32, pp. 14014–14019. DOI: 10.1073/pnas.0914582107.

Hudson, P. F. and R. H. Kessel (2000). "Channel migration and meander-bend curvature in the lower Mississippi River prior to major human modification". In: *Geology* 28.6, pp. 531–534. DOI: 10.1130/0091-7613(2000)28<531:CMAMCI>2.0.CO;2.

Hughes, Zoe J. (2012). "Tidal CHannles on Tidal Flats and Marshes". In: *Principles of Tidal Sedimentology*. Ed. by Richard A. Davis and Robert W. Dalrymple. Chap. 11, pp. 269–300. DOI: 10.1007/978-94-007-0123-6_11.

Ielpi, Alessandro, Martin R. Gibling, Arden R. Bashforth, and Chinemerem I. Dennar (2015). "Impact of Vegetation on Early Pennsylvanian Fluvial Channels: Insight From the Joggins Formation of Atlantic Canada". In: *Journal of Sedimentary Research* 85.8, pp. 999–1018. DOI: 10.2110/jsr.2015.50.

Ikeda, Syunsuke and Gary Parker (1989). *River meandering*. Water Resources Monograph 12. American Geophysical Union.

Ikeda, Syunsuke, Gary Parker, and Kenji Sawai (1981). "Bend theory of river meanders. Part 1. Linear development". In: *Journal of Fluid Mechanics* 112, pp. 363–377. DOI: 10.1017/S0022112081000451.

Iwasaki, Toshiki, Yasuyuki Shimizu, and Ichiro Kimura (2013). "Modelling of the initiation and development of tidal creek networks". In: *Proceedings of the Institution of Civil Engineers - Maritime Engineering* 166.2, pp. 76–88. DOI: 10.1680/maen.2012.12.

Jackson, Roscoe G. II (1976). "Depositional Model of Point Bars in the Lower Wabash River". In: *Journal of Sedimentary Petrology* 46.3, pp. 579–594.

Jamieson, E. C., C. D. Rennie, R. B. Jacobson, and R. D. Townsend (2011). "3-D flow and scour near a submerged wing dike: ADCP measurements on the Missouri River". In: *Water Resources Research* 47.7. DOI: 10.1029/2010WR010043.

Johannesson, Helgi and Gary Parker (1985). *Computer simulated migration of meandering rivers in Minnesota*. Tech. rep. 242. Minneapolis: Saint Anthony Falls Laboratory, pp. 1–98.

Johannesson, Helgi and Gary Parker (1989). "Secondary flow in mildy sinuous channel". In: *Journal of Hydraulic Research* 115.3, pp. 289–308.

Johnson, Douglas (1929). "Meanders in Tidal Streams : A Review and Discussion". In: *Geographical Review* 19.1, pp. 135–139.

Jugaru Tiron, Laura, Jérôme Le Coz, Mireille Provansal, Nicolae Panin, Guillaume Raccasi, Guillaume Dramais, and Philippe Dussouillez (2009). "Flow and sediment processes in a cutoff meander of the Danube Delta during episodic flooding". In: *Geomorphology* 106.3-4, pp. 186–197. DOI: 10.1016/j.geomorph.2008.10.016.

Kawai, S. and P.Y. Julien (1996). "Point bar deposits in narrow sharp bends". In: *Journal of Hydraulic Research* 34.2, pp. 205–218. DOI: 10.1080/00221689609498497.

Kinoshita, R. (1961). *An investigation of channel deformation of the Ishikari River,* tech. rep. Tokyo: Nat. Resour. Div., Minist. of Sci. and Technol. of Japan, p. 139.

Kirchner, James W. (1993). "Statistical inevitability of Horton's laws and the apparent randomness of stream channel networks". In: *Geology* 21.7, pp. 591–594. DOI: 10.1130/0091-7613(1993)021<0591:SIOHSL>2.3.CO;2.

Kirwan, Matthew L. and A. Brad Murray (2007). "A coupled geomorphic and ecological model of tidal marsh evolution." In: *Proceedings of the National Academy of Sciences of the United States of America* 104.15, pp. 6118–22. DOI: 10.1073/pnas.0700958104.

Kitanidis, Peter K. and John F. Kennedy (1984). "Secondary current and river-meander formation". In: *Journal of Fluid Mechanics* 144.-1, p. 217. DOI: 10.1017/S0022112084001580.

Kleinhans, Maarten G., Renske Terwisscha Van Scheltinga, Maarten Van Der Vegt, and Henk Markies (2015). "Turning the tide : Growth and dynamics of a tidal basin". In: *Journal of Geophysical Research : Earth Surface* 120, pp. 95–119. DOI: 10.1002/2014JF003127.Abstract.

Kleinhans, Maarten G., Filip Schuurman, Wiecher Bakx, and Henk Markies (2009). "Meandering channel dynamics in highly cohesive sediment on an intertidal mud flat in the Westerschelde estuary, the Netherlands". In: *Geomorphology* 105.3-4, pp. 261–276. DOI: 10.1016/j.geomorph.2008.10.005.

Kleinhans, Maarten G., M. Van Der Vegt, R. Terwisscha Van Scheltinga, A. W. Baar, and H. Markies (2012). "Turning the tide: Experimental creation of tidal channel networks and ebb deltas". In: *Geologie en Mijnbouw/Netherlands Journal of Geosciences* 91.3, pp. 311–323. DOI: 10.1017/S0016774600000469.

Kostaschuk, Ray, Jim Best, Paul Villard, Jeff Peakall, and Mark Franklin (2005). "Measuring flow velocity and sediment transport with an acoustic Doppler current profiler". In: *Geomorphology* 68.1-2, pp. 25–37. DOI: 10.1016/j.geomorph.2004.07.012.

Kostaschuk, Ray, Paul Villard, and Jim Best (2004). "Measuring Velocity and Shear Stress over Dunes with Acoustic Doppler Profiler". In: *Journal of Hydraulic Engineering-ASCE* 130.9, pp. 932–936. DOI: 10.1061/(ASCE)0733-9429(2004)130:9(932).

Lagasse, P. F., L.W. Zevenbergen, W.J. Spitz, and Colin R. Thorne (2001). *A Methodology for Predicting Channel Migration NCHRP Project No. 24-16.* Vol. 67. Ayres Associates, Inc. - Fort Collins, Colorado. DOI: 10.1061/40581(2001)106.

Lagasse, P.F., W.J. Spitz, and L.W. Zevenbergen (2004). *Handbook for predicting stream meander migration*, p. 107.

Lajeunesse, Eric, Luce Malverti, Pierre Lancien, Lawrence Armstrong, Francois Métivier, Stephen Coleman, Charles E. Smith, Timothy Davies, Alessandro Cantelli, and Gary Parker (2010). "Fluvial and submarine morphodynamics of laminar and near-laminar flows: A synthesis". In: *Sedimentology* 57.1, pp. 1–26. DOI: 10.1111/j.1365-3091.2009.01109.x.

Lane, S. N., D. R. Parsons, J. L. Best, O. Orfeo, R. A. Kostaschuk, and R. J. Hardy (2008). "Causes of rapid mixing at a junction of two large rivers: Río Paraná and Río Paraguay, Argentina". In: *Journal of Geophysical Research: Earth Surface* 113.F2. F02024. DOI: 10.1029/2006JF000745.

Lane, Stuart N., K.F. Bradbrook, K.S. Richards, P.M. Biron, and A.G. Roy (2000). "Secondary circulation cells in river channel confluences : measurement artefacts or coherent flow structures ?" In: *Hydrological Processes* 14.June 1998, pp. 2047–2071. DOI: 10.1002/1099-1085(20000815/30)14:11/12<2047::aid-hyp54>3.0.co;2-4.

Langbein, W.B. and Luna B. Leopold (1966). "River meanders - Theory of minimum variance. Physiographic and hydraulic studies of rivers". In: *U.S. Geological Survey Professional Paper 422-H*, pp. 1–15.

Lanzoni, Stefano and Andrea D'Alpaos (2015). "On funneling of tidal channels". In: *Journal of Geophysical Research: Earth Surface* 120.3, pp. 433–452. DOI: 10.1002/2014JF003203.

Lanzoni, Stefano and Giovanni Seminara (1998). "On tide propagation in convergent estuaries". In: *Journal of Geophysical Research: Oceans* 103.C13, pp. 30793–30812. DOI: 10.1029/1998JC900015.

Lanzoni, Stefano and Giovanni Seminara (2002). "Long-term evolution and morphodynamic equilibrium of tidal channels". In: *Journal of Geophysical Research* 107.C1, pp. 1–13. DOI: 10.1029/2000JC000468.

Lanzoni, Stefano, Annunziato Siviglia, Alessandro Frascati, and Giovanni Seminara (2006). "Long waves in erodible channels and morphodynamic influence". In: *Water Resources Research* 42.SUPPL. Pp. 1–15. DOI: 10.1029/2006WR004916.

Lauer, J. Wesley and Gary Parker (2008). "Net local removal of floodplain sediment by river meander migration". In: *Geomorphology* 96.1-2, pp. 123–149. DOI: 10.1016/j.geomorph.2007.08.003.

Lawrence, D. S. L., John R.L. Allen, and G. M. Havelock (2004). "Salt marsh morphodynamics: An investigation of tidal flows and marsh channel equi-

librium". In: *Journal of Coastal Research* 20.1, pp. 301–316. DOI: 10.2112/1551-5036(2004)20[301:SMMAIO]2.0.CO;2.

Lay, David C. (2000). *Linear Algebra and its applications*. Addison-We. New York. DOI: 10.1017/CBO9781107415324.004.

Lazarus, Eli D. and Scott Armstrong (2015). "Self-organized pattern formation in coastal barrier washover deposits". In: *Geology* 43.4, pp. 363–366. DOI: 10.1130/G36329.1.

Lazarus, Eli D. and José Antonio Constantine (2013). "Generic theory for channel sinuosity." In: *Proceedings of the National Academy of Sciences of the United States of America* 110.21, pp. 8447–52. DOI: 10.1073/pnas.1214074110.

Le Coz, J., M. Michalková, A. Hauet, M. Comaj, G. Dramais, K. Holubová, H. Piégay, and A. Paquier (2010). "Morphodynamics of the exit of a cutoff meander: Experimental findings from field and laboratory studies". In: *Earth Surface Processes and Landforms* 35.3, pp. 249–261. DOI: 10.1002/esp.1896.

Le Coz, J., G. Pierrefeu, and A. Paquier (2008). "Evaluation of river discharges monitored by a fixed side-looking Doppler profiler". In: *Water Resources Research* 46.4. DOI: 10.1029/2008WR006967.

Lee, Kyutae, Hao Che Ho, Muste Marian, and Chun Hung Wu (2014). "Uncertainty in open channel discharge measurements acquired with StreamPro ADCP". In: *Journal of Hydrology* 509, pp. 101–114. DOI: 10.1016/j.jhydrol.2013.11.031.

Leonardi, Nicoletta, Neil K. Ganju, and Sergio Fagherazzi (2015). "A linear relationship between wave power and erosion determines salt-marsh resilience to violent storms and hurricanes". In: *Proceedings of the National Academy of Sciences* 113.1, pp. 64–68. DOI: 10.1073/pnas.1510095112.

Leopold, Luna B., J. N. Collins, and L. M. Collins (1993). "Hydrology of some tidal channels in estuarine marshland near San Francisco". In: *Catena* 20.5, pp. 469–493. DOI: 10.1016/0341-8162(93)90043-O.

Leopold, Luna B. and W.B. Langbein (1966). "River Meanders". In: *Scientific American* 71.June 1966, pp. 60–70.

Leopold, Luna B. and Gordon M. Wolman (1957). "River Channel Patterns: Barided, Meandering and Straight". In: *USGS Professional Paper* B.282.

Leopold, Luna B. and Gordon M. Wolman (1960). "River Meanders". In: *Geological Society of America Bulletin* 71.6, pp. 769–793. DOI: 10.1130/0016-7606(1960)71.

Leopold, Luna B., M. Gordon Wolman, and John P. Miller (1964). *Fluvial processes in geomorphology / Luna B. Leopold, M. Gordon Wolman, John P. Miller*. W. H. Freeman San Francisco, p. 522.

Lewin, John (1972). "Late-stage meander growth". In: *Nature* 240, p. 116.

Lewin, John (1976). "Initiation of bedforms and meanders in coarse-grained sediment". In: *Geological Society of America Bulletin* 87, pp. 281–285.

Liaghat, A., K. Mohammadi, and M. Rahmanshahi (2014). "3D investigation of flow hydraulic in U shape meander bends with constant, decreasing and increasing width". In: *Journal of River Engineering* 2.3, pp. 1–11.

Luchi, Rossella, Guido Zolezzi, and Marco Tubino (2011). "Bend theory of river meanders with spatial width variations". In: *Journal of Fluid Mechanics* 681, 311–339\nM3 –10.1017/jfm.2011.200. DOI: 10.1017/jfm.2011.200.

Mancero-Mosquera, I., M. Gacic, and A. Mazzoldi (2010). "The effect of wind on the residual current velocities in the inlets of Venice lagoon". In: *Continental Shelf Research* 30.8, pp. 915–923. DOI: 10.1016/j.csr.2010.02.011.

Marani, Marco, Enrica Belluco, Andrea D'Alpaos, Andrea Defina, Stefano Lanzoni, and Andrea Rinaldo (2003). "On the drainage density of tidal networks". In: *Water Resources Research* 39.2, n/a–n/a. DOI: 10.1029/2001WR001051.

Marani, Marco, Stefano Lanzoni, Sonia Silvestri, and Andrea Rinaldo (2004). *Tidal landforms, patterns of halophytic vegetation and the fate of the lagoon of Venice*. DOI: 10.1016/j.jmarsys.2004.05.012.

Marani, Marco, Stefano Lanzoni, Diego Zandolin, Giovanni Seminara, and Andrea Rinaldo (2002). "Tidal meanders". In: *Water Resources Research* 38.11. DOI: 10.1029/2001WR000404.

Marciano, Raffaele, Zheng Bing Wang, Anneke Hibma, Huib J. de Vriend, and Andrea Defina (2005). "Modeling of channel patterns in short tidal basins". In: *Journal of Geophysical Research: Earth Surface* 110.1, pp. 1–13. DOI: 10.1029/2003JF000092.

Mariotti, G., S. Fagherazzi, P. Wiberg, K. McGlathery, L. Carniello, and A. Defina (2010). "Influence of storm surges and sea level on shallow tidal basin erosive processes". In: *Journal of Geophysical Research - Oceans* 115. DOI: doi:10.1029/2009JC005892.

Martin, John, Ben Sheets, Chris Paola, and David Hoyal (2009). "Influence of steady base-level rise on channel mobility, shoreline migration, and scaling properties of a cohesive experimental delta". In: *Journal of Geophysical Research: Solid Earth* 114.3, F03017. DOI: 10.1029/2008JF001142.

Martini, P., L. Carniello, and C. Avanzi (2004). "Two dimensional modelling of flood flows and suspended sediment transport: the case of Brenta river, Veneto (Italy)". In: *Natural Hazards and Earth System Sciences* 4.1, pp. 165–181.

Matthes, Gerard H. (1941). "Basic aspects of stream-meanders". In: *Eos, Transactions American Geophysical Union* 22.3, pp. 632–636. DOI: 10.1029/TR022i003p00632.

Mel, Riccardo, Daniele Pietro Viero, Luca Carniello, Andrea Defina, and Luigi D'Alpaos (2014). "Simplified methods for real-time prediction of storm surge uncertainty: The city of Venice case study". In: *Advances in Water Resources* 71, pp. 177–185. DOI: 10.1016/j.advwatres.2014.06.014.

Millar, Robert G. (2000). "Influence of bank vegetation on alluvial channel patterns". In: *Water Resources Research* 36.4, pp. 1109–1118. DOI: 10.1029/1999WR900346.

Montgomery, David R. and William E. Dietrich (1989). "Source areas, drainage density, and channel initiation". In: *Water Resources Research* 25.8, pp. 1907–1918. DOI: 10.1029/WR025i008p01907.

Motta, Davide, Eddy J. Langendoen, Jorge D. Abad, and Marcelo H. García (2014). "Modification of meander migration by bank failures". In: *Journal of Geophysical Research: Earth Surface* 119.5, pp. 1026–1042. DOI: 10.1002/2013JF002952.

Mudd, Simon M. (2011). "The life and death of salt marshes in response to anthropogenic disturbance of sediment supply Simon". In: *Geology* 39.5, pp. 511–512. DOI: 10.1130/focus052011.1.

Mudd, Simon M., Mikaël Attal, David T. Milodowski, Stuart W D Grieve, and Declan A. Valters (2014). "A statistical framework to quantify spatial variation in channel gradients using the integral method of channel profile analysis". In: *Journal of Geophysical Research: Earth Surface* 119.2, pp. 138–152. DOI: 10.1002/2013JF002981.

Mudd, Simon M., Andrea D'Alpaos, and James T. Morris (2010). "How does vegetation affect sedimentation on tidal marshes? Investigating particle capture and hydrodynamic controls on biologically mediated sedimentation". In: *Journal of Geophysical Research: Earth Surface* 115.3, F03029. DOI: 10.1029/2009JF001566.

Murray, A. Brad (2013). "Contrasting the Goals, Strategies, and Predictions Associated with Simplified Numerical Models and Detailed Simulations". In: *Prediction in Geomorphology*. American Geophysical Union, pp. 151–165. DOI: 10.1029/135GM11.

Murray, A. Brad and Chris Paola (2003). "Modelling the effect of vegetation on channel pattern in bedload rivers". In: *Earth Surface Processes and Landforms* 28.2, pp. 131–143. DOI: 10.1002/esp.428.

Myrick, Robert M. and Luna B. Leopold (1963). "Hydraulic geometry of a small tidal estuary". In: *USGS Professional Paper* B.422, pp. 1–18. DOI: 10.1016/0011-7471(65)91477-4.

Nanson, Gerald C. and Edward J. Hickin (1986). "A statistical analyisis of bank erosion and channel migration in western canada". In: *GSA Bulletin* 97, pp. 497–504. DOI: 10.1130/0016-7606(1986)97<497:ASAOBE>2.0.CO;2.

Nanson, Rachel A. (2010). "Flow fields in tightly curving meander bends of low width-depth ratio". In: *Earth Surface Processes and Landforms* 35.2, pp. 119–135. DOI: 10.1002/esp.1878.

Nepf, Heidi and Marco Ghisalberti (2008). "Flow and transport in channels with submerged vegetation". In: *Acta Geophysica* 56.3, pp. 753–777. DOI: 10.2478/s11600-008-0017-y.

Nepf, Heidi, Jeffrey Rominger, and Lijun Zong (2013). "Coherent Flow Structures in Vegetated Channels". In: *Coherent Flow Structures at Earth's Surface*. John Wiley and Sons, Ltd, pp. 135–147. DOI: 10.1002/9781118527221.ch9.

Nihei, Yasuo and Akira Kimizu (2008). "A new monitoring system for river discharge with horizontal acoustic Doppler current profiler measurements and river flow simulation". In: *Water Resource Research* 44.4, n/a–n/a. DOI: 10.1029/2008WR006970.

O'Neill, Michael P. and Athol D. Abrahams (1986). "Objective identification of meanders and bends". In: *Journal of Hydrology* 83.3-4, pp. 337–353. DOI: 10.1016/0022-1694(86)90160-5.

Onken, Reiner and Rolf Riethmuller (2010). "Determination of the freshwater budget of tidal flats from measurements near a tidal inlet". In: *Continental Shelf Research* 30.8, pp. 924–933. DOI: 10.1016/j.csr.2010.02.004.

Paola, Chris, Jim Mullin, Chris Ellis, David C. Mohrig, John B. Swenson, Gary Parker, Tom Hickson, Lincoln Pratson, James Syvitski, Ben Sheets, and Nikki Strong (2001). "Experimental Stratigraphy". In: *GSA Today* 5173.5, pp. 4–9. DOI: 10.1130/1052-5173(2001)011<0004.

Paola, Chris, Kyle Straub, David Mohrig, and Liam Reinhardt (2009). "The "unreasonable effectiveness" of stratigraphic and geomorphic experiments". In: *Earth-Science Reviews* 97.1-4, pp. 1–43. DOI: 10.1016/j.earscirev.2009.05.003.

Parker, G., Y. Shimizu, G. V. Wilkerson, E. C. Eke, J. D. Abad, J. W. Lauer, C. Paola, W. E. Dietrich, and V. R. Voller (2010). "A new framework for modeling the migration of meandering rivers". In: *Earth Surface Processes and Landforms* 36.1, pp. 70–86. DOI: 10.1002/esp.2113.

Parker, Gary (1976). "On the cause and characteristic scales of meandering and braiding in rivers". In: *Journal of Fluid Mechanics* 76.03, p. 457. DOI: 10.1017/S0022112076000748.

Parker, Gary (1986). "On the time development of meander bends". In: *Journal of Fluid Mechanics* 162.-1, pp. 139–156. DOI: 10.1017/S0022112086001970.

Parker, Gary, Panayiotis Diplas, and Juichiro Akiyama (1983). "Meander bends of High Amplitude". In: *Journal of Hydraulic Engineering* 109.10, pp. 1323–1337.

Parker, Gary, Chris Paola, Kelin X. Whipple, David Mohrig, Carlos M. Toro-Escobar, Marty Halverson, and Timoth W. Skoglund (1998). "Alluvial Fans Formed by Channelized Fluvial and Sheet Flow. II: Application". In: *Journal of Hydraulic Engineering* 124.10, pp. 996–1004. DOI: 10.1061/(ASCE)0733-9429(1998)124:10(996).

Parker, Gary, Kenji Sawai, and Syunsuke Ikeda (1982). "Bend theory of river meanders. Part 2. Nonlinear deformation of finite-amplitude bends". In: *Journal of Fluid Mechanics* 115, pp. 303–314. DOI: 10.1017/S0022112082000767.

Parsons, Dan R., Robert I. Ferguson, Stuart N. Lane, and Richard J. Hardy (2004). "Flow structures in meander bends with recirculation zones : implications for bend movements". In: *River Flow*. Ed. by Greco, Carravetta, and Della Morte. Taylor & Francis, pp. 49–57.

Parsons, Dan R., P. R. Jackson, John A. Czuba, F. L. Engel, Bruce L. Rhoads, K. A. Oberg, James L. Best, D. S. Mueller, K. K. Johnson, and J. D. Riley (2013). "Velocity Mapping Toolbox (VMT): A processing and visualization suite for moving-vessel ADCP measurements". In: *Earth Surface Processes and Landforms* 38.11, pp. 1244–1260. DOI: 10.1002/esp.3367.

Passalacqua, Paola, Tien Do Trung, Efi Foufoula-Georgiou, Guillermo Sapiro, and William E. Dietrich (2010). "A geometric framework for channel network extraction from lidar: Nonlinear diffusion and geodesic paths". In: *Journal of Geophysical Research* 115.F1, pp. 1–18. DOI: 10.1029/2009JF001254.

Perucca, E., C. Camporeale, and L. Ridolfi (2007). "Significance of the riparian vegetation dynamics on meandering river morphodynamics". In: *Water Resources Research* 43.3. DOI: 10.1029/2006WR005234.

Pestrong, Raymond (1965). "The development of drainage patterns on tidal marshes". PhD thesis. Stanford University publications, Stanford, Calif.: School of Earth Sciences, Stanford University.

Pestrong, Raymond (1972). "Tidal-flat sedimentation at cooley landing, Southwest San Francisco bay". In: *Sedimentary Geology* 8, pp. 251–288. DOI: 10.1016/0037-0738(72)90044-9.

Pethick, J. S. (1980). "Velocity surges and asymmetry in tidal channels". In: *Estuarine and Coastal Marine Science* 11.3, pp. 331–345. DOI: 10.1016/S0302-3524(80)80087-9.

Pittaluga, M. Bolla, G. Nobile, and Giovanni Seminara (2009). "A nonlinear model for river meandering". In: *Water Resources Research* 45.4, pp. 1–22. DOI: 10.1029/2008WR007298.

Postma, H. (1961). "Suspended matter and Secchi disc visibility in coastal waters". In: *Netherlands Journal of Sea Research* 1.3, pp. 359–390. DOI: 10.1016/0077-7579(61)90009-6.

Prandtl, L. (1952). *Essentials of Fluid Dynamics*. Macmillan. New York.

Priestas, A. M. and Sergio Fagherazzi (2011). "Morphology and hydrodynamics of wave-cut gullies". In: *Geomorphology* 131.1-2, pp. 1–13. DOI: 10.1016/j.geomorph.2011.04.004.

Quraishy, Mohamed S. (1944). "The origin of curves in rivers". In: *Current Science* 13.02, pp. 36–39.

Ranwell, D.S. (1972). *Ecology of salt marshes and sand dunes*. Chapman and Hall.

Rennie, C. D., F. Rainville, and S. Kashyap (2007). "Improved Estimation of ADCP Apparent Bed-Load Velocity Using a Real-Time Kalman Filter". In: *Journal of Hydraulic Engineering* 133.12, pp. 1337–1344. DOI: 10.1061/(ASCE)0733-9429(2007)133:12(1337).

Rieu, Ruben, Sytze van Heteren, Ad J. F. Van der Spek, and Poppe L. De Boer (2005). "Development and preservation of a Mid-Holocene tidal-channel network offshore the Western Netherlands". In: *Journal of Sedimentary Research* 75.3, pp. 409–419. DOI: 10.21110/jsr.2005.032.

Rinaldo, Andrea, Sergio Fagherazzi, Stefano Lanzoni, Marco Marani, and William E. Dietrich (1999a). "Tidal networks 2. Watershed delineation and comparative network morphology". In: *Water Resources Research* 35.12, pp. 3905–3917. DOI: 10.1029/1999WR900237.

Rinaldo, Andrea, Sergio Fagherazzi, Stefano Lanzoni, Marco Marani, and William E. Dietrich (1999b). "Tidal networks 3. Landscape-forming discharges and studies in empirical geomorphic relationships". In: *Water Resources Research* 35.12, pp. 3919–3929. DOI: 10.1029/1999WR900238.

Rinaldo, Andrea, Ignacio Rodriguez-Iturbe, and Riccardo Rigon (1998). "CHANNEL NETWORKS". In: *Annual Review of Earth and Planetary Sciences* 26.1, pp. 289–327.

Rodriguez-Iturbe, Ignacio and Andrea Rinaldo (1997). *Fractal River Networks: Chance and SelfOrganization*. Cambridge University press, New York.

Roner, M., A. D'Alpaos, M. Ghinassi, M. Marani, S. Silvestri, E. Franceschinis, and N. Realdon (2016). "Spatial variation of salt-marsh organic and inorganic deposition and organic carbon accumulation: Inferences from the Venice lagoon, Italy". In: *Advances in Water Resources* 93, Part B, pp. 276–287. DOI: http://dx.doi.org/10.1016/j.advwatres.2015.11.011.

Rozovskii, I.L. (1957). *Flow of Water in Bends of Open Channels (in Russian)*. Acad. of Sci. of the Ukrainian SSR. (English translation, Isr. Program for Sci. Transl., Jerusalem, 1961.) Kiev.

Sassi, M. G., A. J F Hoitink, and B. Vermeulen (2012). "Impact of sound attenuation by suspended sediment on ADCP backscatter calibrations". In: *Water Resources Research* 48.9. DOI: 10.1029/2012WR012008.

Schnauder, I. and A. N. Sukhodolov (2012). "Flow in a tightly curving meander bend: Effects of seasonal changes in aquatic macrophyte cover". In: *Earth Surface Processes and Landforms* 37.11, pp. 1142–1157. DOI: 10.1002/esp.3234.

Schumm, S. A. (1963). "Sinuosity of alluvial rivers on the great plains". In: *Bulletin of the Geological Society of America* 74.9, pp. 1089–1100. DOI: 10.1130/0016-7606(1963)74[1089:SOAROT]2.0.CO;2.

Schuttelaars, H.M. and H.E. De Swart (1997). "An Idealized Long-Term Morphodynamic Model of a Tidal Embayment". In: *Eur. J. Mech., B/Fluids* 15, pp. 55–80.

Schuttelaars, H.M. and H.E. de Swart (2000). "Multiple morphodynamic equilibria in tidal embayments". In: *Journal of Geophysical Research* 105.C10, pp. 24, 105–24, 118.

Seminara, Giovanni (2006). "Meanders". In: *Journal of Fluid Mechanics* 554.-1, p. 271. DOI: 10.1017/S0022112006008925.

Seminara, Giovanni, Stefano Lanzoni, Nicoletta Tambroni, and Marco Toffolon (2010). "How long are tidal channels?" In: *Journal of Fluid Mechanics* 643.2005, p. 479. DOI: 10.1017/S0022112009992308.

Seminara, Giovanni and Marco Tubino (1992). "Weakly nonlinear theory of regular meanders". In: *Journal of Fluid Mechanics* 244, pp. 257–288. DOI: 10.1017/S0022112092003069.

Seminara, Giovanni and Marco Tubino (2001). "Sand bars in tidal channels. Part 1. Free bars". In: *Journal of fluid mechanincs* 440, pp. 49–74.

Seminara, Giovanni, Guido Zolezzi, Marco Tubino, and Dino Zardi (2001). "Downstream and upstream influence in river meandering. Part 2. Planimetric development". In: *Journal of Fluid Mechanics* 438, pp. 213–230. DOI: 10.1017/S0022112001004281.

Smith, Charles E. (1998). "Modeling high sinuosity meanders in a small flume". In: *Geomorphology* 25.1-2, pp. 19–30. DOI: 10.1016/S0169-555X(98)00029-4.

Smith, Derald G., Stephen M. Hubbard, Dale A. Leckie, and Milovan Fustic (2009). "Counter point bar deposits: lithofacies and reservoir significance in the meandering modern Peace River and ancient McMurray Formation, Alberta, Canada". In: *Sedimentology* 56.6, pp. 1655–1669. DOI: 10.1111/j.1365-3091.2009.01050.x.

Smith, J. Dungan and S. R. Mclean (1984). "A Model for Flow in Meandering Streams". In: *Water Resources Research* 20.9, pp. 1301–1315. DOI: 10.1029/WR020i009p01301.

Solari, Luca, Giovanni Seminara, Stefano Lanzoni, Marco Marani, and Andrea Rinaldo (2002). "Sand bars in tidal channels Part 2. Tidal meanders". In: *J. Fluid Mech.* 451.January, pp. 203–238. DOI: 10.1017/S0022112001006565.

Soulsby, R. L. (1997). *Dynamics of marine sands. A manual for practical applications.* London: Thomas Telford Ed.

Stefanon, Luana, Luca Carniello, Andrea D'Alpaos, and Stefano Lanzoni (2010). "Experimental analysis of tidal network growth and development". In: *Continental Shelf Research* 30.8, pp. 950–962. DOI: 10.1016/j.csr.2009.08.018.

Stefanon, Luana, Luca Carniello, Andrea D'Alpaos, and Andrea Rinaldo (2012). "Signatures of sea level changes on tidal geomorphology: Experiments on network incision and retreat". In: *Geophysical Research Letters* 39.12, pp. 1–6. DOI: 10.1029/2012GL051953.

Stevenson, J. C., J.E. Rooth, K.L. Sundberg, and M.S. Kearney (2000). "The Health and Long Term Stability of Natural and Restored Marshes in Chesapeake Bay". In: *Concepts and Controversies in Tidal Marsh Ecology*. Ed. by Michael P. Weinstein and Daniel A. Kreeger. Dordrecht: Springer Netherlands, pp. 709–735. DOI: 10.1007/0-306-47534-0_31.

Stoesser, Thorsten, Richard McSherry, and Bruno Fraga (2015). "Secondary currents and turbulence over a non-uniformly roughened open-channel bed". In: *Water (Switzerland)* 7.9, pp. 4896–4913. DOI: 10.3390/w7094896.

Stolum, Hans Henrik (1998). "Planform geometry and dynamics of meandering rivers". In: *Bulletin of the Geological Society of America* 110.11, pp. 1485–1498. DOI: 10.1130/0016-7606(1998)110<1485:PGADOM>2.3.CO;2.

Stolum, H.H. (1996). "River Meandering as a Self-Organization Process". In: *Science* 271.5256, pp. 1710–1713. DOI: 10.1126/science.271.5256.1710.

Strahler, Arthur N. (1957). "Quantitative analysis of watershed geomorphology". In: *Eos, Transactions American Geophysical Union* 38.6, pp. 913–920. DOI: 10.1029/TR038i006p00913.

Sullivan, Jessica Chassereau, Raymond Torres, Alfred Garrett, Jackson Blanton, Clark Alexander, Michael Robinson, Trent Moore, Julie Amft, and David Hayes (2015). "Complexity in salt marsh circulation for a semienclosed basin". In: *Journal of Geophysical Research F: Earth Surface* 120.10, pp. 1973–1989. DOI: 10.1002/2014JF003365.

Symonds, Andrew M. and Michael B. Collins (2007). "The establishment and degeneration of a temporary creek system in response to managed coastal realignment: The Wash, UK". In: *Earth Surface Processes and Landforms* 32.12, pp. 1783–1796. DOI: 10.1002/esp.1495.

Tal, M. and C. Paola (2007). "Dynamic single-thread channels maintained by the interaction of flow and vegetation". In: *Geology* 35, p. 347. DOI: 10.1130/G23260A.1.

Tal, Michal, Karen Gran, A. Brad Murray, Chris Paola, and D. Murray Hicks (2004). "Riparian Vegetation as a Primary Control on Channel Characteristics in Multi-Thread Rivers". In: *Riparian Vegetation and Fluvial Geomorphology*. Ed. by S.J. Bennet and A. Simon. American Geophysical Union, pp. 43–58. DOI: 10.1029/008WSA04.

Tal, Michal and Chris Paola (2010). "Effects of vegetation on channel morphodynamics: results and insights from laboratory experiments". In: *Earth Surface Processes and Landforms* 35.9, pp. 1014–1028. DOI: 10.1002/esp.1908.

Tambroni, N., M. Bolla Pittaluga, and G. Seminara (2005). "Laboratory observations of the morphodynamic evolution of tidal channels and tidal inlets". In: *Journal of Geophysical Research: Earth Surface* 110.4. DOI: 10.1029/2004JF000243.

Tambroni, N., J. Figueiredo da Silva, R. W. Duck, S. J. McLelland, C. Venier, and S. Lanzoni (2016). "Experimental investigation of the impact of macroalgal mats on the wave and current dynamics". In: *Advances in Water Resources* 93, pp. 326–335. DOI: 10.1016/j.advwatres.2015.09.010.

Tambroni, Nico and G. Seminara (2006). "Are inlets responsible for the morphological degradation of Venice Lagoon?" In: *Journal of Geophysical Research: Earth Surface* 111.3, pp. 1–19. DOI: 10.1029/2005JF000334.

Tarboton, David G. (1997). "A new method for the determination of flow directions and upslope areas in grid digital elevation models". In: *Water Resources Research* 33.2, pp. 309–319.

Tarboton, David G., Rafael L. Bras, and Ignacio Rodriguez-Iturbe (1991). "On the extraction of channel networks from digital elevation data". In: *Hydrological Processes* 5.1, pp. 81–100. DOI: 10.1002/hyp.3360050107.

Taylor Perron, J. and Sergio Fagherazzi (2012). "The legacy of initial conditions in landscape evolution". In: *Earth Surface Processes and Landforms* 37.1, pp. 52–63. DOI: 10.1002/esp.2205.

Temmerman, Stijn, T. J. Bouma, G. Govers, Zheng Bing Wang, M. B. de Vries, and P. M J Herman (2005). "Impact of vegetation on flow routing and sedimentation patterns: Three-dimensional modeling for a tidal marsh". In: *Journal of Geophysical Research: Earth Surface* 110.4, pp. 1–18. DOI: 10.1029/2005JF000301.

Termini, D. (2004). "Flow in meandering bends". In: *River Flow*. Ed. by Greco, Carravetta, and Della Morte. Taylor & Francis, pp. 109–117.

Termini, Donatella (2013). "Effect of Vegetation on Fluvial Erosion Processes: Experimental Analysis in a Laboratory Flume". In: *Procedia Environmental Sciences* 19, pp. 904–911. DOI: 10.1016/j.proenv.2013.06.100.

Termini, Donatella (2016). "Experimental analysis of the effect of vegetation on flow and bed shear stress distribution in high-curvature bends". In: *Geomorphology* 274, pp. 1–10. DOI: 10.1016/j.geomorph.2016.08.031.

Thomas, Richard G, Derald G Smith, James M Wood, M John Visser, E Anne Calverley-Range, and Emlyn H Koster (1987). "Inclined heterolithic stratification - terminology, description, interpretation and significance".

In: *Sedimentary Geology* 53.September, pp. 123–179. DOI: 10.1016/S0037-0738(87)80006-4.

Thorne, Colin R. (1991). "Bank Erosion and meander migration of the Red and Mississippi Rivers , USA". In: *Proceedings of the Vienna Symposium*. 201. Vienna: IAHS, pp. 301–313.

Thorne, Peter D. and Daniel M. Hanes (2002). "A review of acoustic measurement of small-scale sediment processes". In: *Continental Shelf Research* 22.4, pp. 603–632. DOI: 10.1016/S0278-4343(01)00101-7.

Tiffany, Joseph B. and George A. Nelson (1939). "Studies of meandering of model-streams". In: *Eos, Transactions American Geophysical Union* 20.4, pp. 644–649. DOI: 10.1029/TR020i004p00644.

Toffolon, Marco and Stefano Lanzoni (2010). "Morphological equilibrium of short channels dissecting the tidal flats of coastal lagoons". In: *Journal of Geophysical Research: Earth Surface* 115.F4. DOI: 10.1029/2010JF001673.

Tornqvist, Torbjorn E., Chris Paola, Gary Parker, Kam-biu Liu, David C. Mohrig, John M. Holbrook, and Robert R. Twilley (2007). "Response to comment on "Wetland sedimentation from Hurricanes Katrina and Rita"". In: *Science* 316.5822. DOI: 10.1126/science.1136869.

Van Ledden, M., Z.B. Wang, H. Winterwerp, and H. De Vriend (2004). "Sand-mud morphodynamics in a short tidal basin". In: *Ocean Dynamics* 54, pp. 385–391. DOI: 10.1007/s10236-003-0050-y.

Van Maanen, B., Giovanni Coco, and K. R. Bryan (2013). "Modelling the effects of tidal range and initial bathymetry on the morphological evolution of tidal embayments". In: *Geomorphology* 191, pp. 23–34. DOI: 10.1016/j.geomorph.2013.02.023.

Vautard, R. and M. Ghil (1989). "Singular spectrum analysis in nonlinear dynamics, with applications to paleoclimatic time series". In: *Physica D: Nonlinear Phenomena* 35.3, pp. 395–424. DOI: 10.1016/0167-2789(89)90077-8.

Vermuelen, B., M.G. Sassi, and A.J.F. Hoitink (2014). "Improved flow velocity estimates frommoving-boat ADCP measurements". In: *Water Resources Research* 50, pp. 1–11. DOI: 10.1002/2013WR015152.

Vlaswinkel, Brigitte M. and Alessandro Cantelli (2011). "Geometric characteristics and evolution of a tidal channel network in experimental setting". In: *Earth Surface Processes and Landforms* 36.6, pp. 739–752. DOI: 10.1002/esp.2099.

Whitehouse, R. J. S., P. Bassoullet, K. R. Dyer, H. J. Mitchener, and W. Roberts (2000). "The influence of bedforms on flow and sediment transport over intertidal mudflats". In: *Continental Shelf Research*, pp. 1099–1124. DOI: 10.1016/S0278-4343(00)00014-5.

Whiting, Peter J. and William E. Dietrich (1993). "Experimental constraints on bar migration through bends: Implications for meander wavelength selection". In: *Water Resources Research* 29.4, pp. 1091–1102. DOI: 10.1029/92WR02356.

Williams, Garnett P. (1986). "River meanders and channel size". In: *Journal of Hydrology* 88.1-2, pp. 147–164. DOI: 10.1016/0022-1694(86)90202-7.

Willis, B. J. and H. Tang (2010). "Three-Dimensional Connectivity of Point-Bar Deposits". In: *Journal of Sedimentary Research* 80.5, pp. 440–454. DOI: 10.2110/jsr.2010.046.

Young, I.R. and L.A. Verhagen (1996). "The growth of fetch-limited waves in water of finite depth. Part 1: Total energy and peak frequency". In: *Coastal Engineering* 29.1-2, pp. 47–78.

Zarzuelo, Carmen, Andrea D'Alpaos, Luca Carniello, Miguel Ortega-Sánchez, M. Diez-Minguito, Alvise Finotello, and Miguel Losada (2015a). "Modeling sand-mud transport in a tidally- dominated bay : Cádiz (Spain)". In: *XXIV Congress on Differetial Equations and Application*.

Zarzuelo, Carmen, Manuel Díez-Minguito, Miguel Ortega-Sánchez, Alejandro López-Ruiz, and Miguel Losada (2015b). "Hydrodynamics response to planned human interventions in a highly altered embayment: The example of the Bay of Cádiz (Spain)". In: *Estuarine, Coastal and Shelf Science* 167.July 2015, pp. 75–85. DOI: 10.1016/j.ecss.2015.07.010.

Zecchin, M., L. Baradello, G. Brancolini, F. Donda, F. Rizzetto, and L. Tosi (2008). "Sequence stratigraphy based on high-resolution seismic profiles in the late Pleistocene and Holocene deposits of the Venice area". In: *Marine Geology* 253.3–4, pp. 185–198. DOI: http://dx.doi.org/10.1016/j.margeo.2008.05.010.

Zhou, Zeng, Maitane Olabarrieta, Luana Stefanon, Andrea D'Alpaos, Luca Carniello, and Giovanni Coco (2014). "A comparative study of physical and numerical modeling of tidal network ontogeny". In: *Journal of Geophysical Research: Earth Surface* 119.APRIL, pp. 892–912. DOI: 10.1002/2014JF003092.Received.

Zinger, Jessica A., Bruce L. Rhoads, James L. Best, and Kevin K. Johnson (2013). "Flow structure and channel morphodynamics of meander bend chute cutoffs: A case study of the Wabash River, USA". In: *Journal of Geo-*

physical Research: Atmospheres 118.4, pp. 2468–2487. DOI: 10.1002/jgrf.20155.

Zolezzi, Guido, Rossella Luchi, and Marco Tubino (2012). "Modeling morphodynamic processes in meandering rivers with spatial width variations". In: *Reviews of Geophysics* 50.4, pp. 1–24. DOI: 10.1029/2012RG000392.

Zolezzi, Guido and Giovanni Seminara (2001). "Dowstream and upstream influence in river meandering. Part 1. General theory and application to overdeepening". In: *Journal of Fluid Mechanics* 438.July 2001, pp. 183–211.

A | APPENDIX

TIDAL MEANDER MIGRATION AND DYNAMICS: A CASE STUDY FROM THE VENICE LAGOON

D'Alpaos, Andrea[1], Massimiliano Ghinassi[1], Alvise Finotello[1], Lara Brivio[1], Luca Giorgio Bellucci[2] and Marco Marani[3,4]

[1]Dept. of Geosciences, University of Padova, via G.Gradenigo 6, Padova, PD I-35131, Italy

[2]Consiglio Nazionale delle Ricerche, Istituto di Scienze Marine, via Gobetti 101, Bologna, BO I-40129, Italy

[3]Dept. ICEA, University of Padova, via Loredan 20, Padova, PD I-35131, Italy

[4]Nicholas School of Environment, Duke University, Durham, NC 27708

Abstract

Meandering patterns are universal features of tidal landscapes and exert a critical influence on the dynamics of tidal channel networks and on the stratigraphy of the intertidal platforms they dissect. Despite their importance in landscape evolution and their ubiquity, tidal meanders have received less attention when compared to their fluvial counterparts. To improve current understanding of tidal meander migration and its possible stratigraphic implications, we have analyzed a sequence of aerial photographs and satellite images (from 1938 to present) of a meandering tidal channel in the Venice Lagoon, which experienced multiple cutoff events during its evolution. Our results show that tidal meander migration rates per unit width display values similar to those characterizing their fluvial relatives. Detailed high-resolution geomorphological, sedimentological, and geochronological analyses have been carried out in detail for an abandoned, 13 m in diameter meander bend which experienced one of these cutoffs. Aerial photographs before and after the cutoff event have been used to infer a minimum velocity of migration (about 0.10 m/yr). Well-cores have also been collected along a transect crossing through the neck of the meander in order to evaluate changes in grain size, sedimentation rates across the cutoff event, and gain further insight into the velocity of migration of meander bends. The spatial distribution of sedimentary facies (pointbar sand, oxbowlake, and salt-marsh mud), grain size analyses, and ^{210}Pb and ^{137}Cs chronologies highlighted that meander cutoff occurred progressively around 70 years before present

with a velocity of migration of about 0.25 m/year. The effectiveness of the methods used and the high spatial and temporal resolution of the data call for further investigations and analyses of the type proposed herein, furthermore highlighting the potentiality of the study area as modern analogue for ancient tidal deposits.

Introduction

Salt-marsh landscapes are commonly dissected by networks of meandering tidal channels that exert a strong control on the ecomorphodynamic evolution of these landscapes, facilitating the exchange of water, sediments and nutrients (D'Alpaos et al., 2005; Hughes, 2012; Coco et al., 2013). In spite of their prominence and wide occurrence, the characteristics and dynamics of meanders shaped by the periodically reversing tidal flows lack the detailed inspection that has been devoted to their fluvial relatives (e.g., Leopold and Wolman, 1960; Ikeda and Parker, 1989; Seminara, 2006; Zolezzi et al., 2012; Hooke, 2013). A handful of papers, in fact, exists that analyzed the planimetric shape, morphometric characteristics, and morphodynamic evolution of tidal meanders. Marani et al. (2002) studied the geometrical properties of tidal meanders through field observations and modelling interpretation; Solari et al. (2002) developed the first 3D model capable to predict the flow field and bed topography in weakly meandering tidal channels; Fagherazzi et al. (2004) coupled field observations and numerical modelling to analyze the effects of bidirectional flows on planform meander configuration and migration; Hood (2006) highlighted the role of deposition processes on tidal meander formation; Garotta et al. (2007) set up a laboratory experiment for a tidal meander, emphasizing along-channel changes in the relationship between bar–pool patterns and channel curvature. The effects of sediment cohesion and vegetation growth on tidal meander dynamics have also been analyzed (Garofalo, 1980; Gabet, 1998; Kleinhans et al. 2009) suggesting that the presence of highly cohesive soils on channel bed and banks and the stabilizing effect of marsh vegetation on the banks, hinder tidal meanders from being characterized by the dynamic behavior which distinguishes their fluvial counterparts and contribute to their reputation of being quite stable landscape features. The depositional architecture of tidal meander bends has also been somewhat neglected (Choi and Jo, 2015) compared to the attention devoted to the fluvial realm (e.g, Allen, 1965; Bridge et al., 1986) and has mainly been approached using facies models (Barwis, 1978; de Mowbray, 1983; Choi et al., 2004; Choi, 2011) which assume the stratal geometries of tidal deposits to show marked similarities with those of their fluvial counterparts (Jackson, 1976; Brierley, 1991). A relevant question, with theoretical and practical implications, is whether

or not morphodynamic and architectural models, mediated from the study of fluvial meanders, can be applied to tidal ones. The question arises from the observation that several different processes sculpt tidal and fluvial meanders. The existence of periodically reversing flows in tidal settings probably stands out most. In addition, in tidal channels landscape-forming discharges and strong flow velocities occur when tidal levels are just above (during the flood phase) or below (during ebb) the elevation of the marsh platform, whereas in rivers, high water levels and water depths are generally a proxy for large discharges. Moreover, while rivers experience flood events characterized by high discharges which overlap to slowly varying discharges through the year, and high flow velocities can be maintained for relatively long time during floods (days), tidal channels are characterized by highly variable discharges during a tidal period (hours) but are generally shaped by water fluxes that vary in a defined range of possible values. If, one the one hand, the signatures of these different processes can hardly be unraveled by the analysis of tidal meander planform configuration (e.g., Marani et al., 2002; Solari et al., 2002), on the other hand, a recent detailed scrutiny of the internal architecture and sedimentary features of a tidal meander bend (Brivio et al., 2016) emphasized the existence of relevant differences imprinted in the sedimentary record, such as the absence of crevasse splay deposits, the development of elongated pool zones, the overall symmetric distribution of sediment grain size along the landward and seaward sides of the bend, and the observed spoon-shaped geometry of the bar-top mud, resulting from the coupled effects of lateral migration and vertical aggradation (Brivio et al., 2016).

In addition, it is worth recalling that the occurrence of ecological and geomorphological processes that shape tidal landscapes (e.g., D'Alpaos et al., 2012) which act at overlapping spatial and temporal scales (Feola et al., 2005) has challenged our capability of providing predictive numerical and experimental models of tidal-landscape dynamics (D'Alpaos et al., 2007; van Maanen et al., 2011; Vlaswinkel and Cantelli, 2011; Stefanon et al., 2012; Zhou et al., 2014), accounting for the effect of tidal meandering, thus calling for further research efforts. Towards the goal of improving current understanding of the intertwined evolution of salt-marsh platforms and tidal channels cutting through them, and in particular of the dynamics of tidal meandering patterns, the present study investigates the morphodynamic evolution of a meandering tidal channel in a salt marsh of the Northern Venice Lagoon (Italy; Figure A.1), which experienced various neck cutoffs along its reach (e.g., Hooke, 2004). Along this meandering channel, we focus in particular on an abandoned meander bend, which experienced one of these cutoffs, using an multidisciplinary approach which combines different complementary analyses deriving from i)

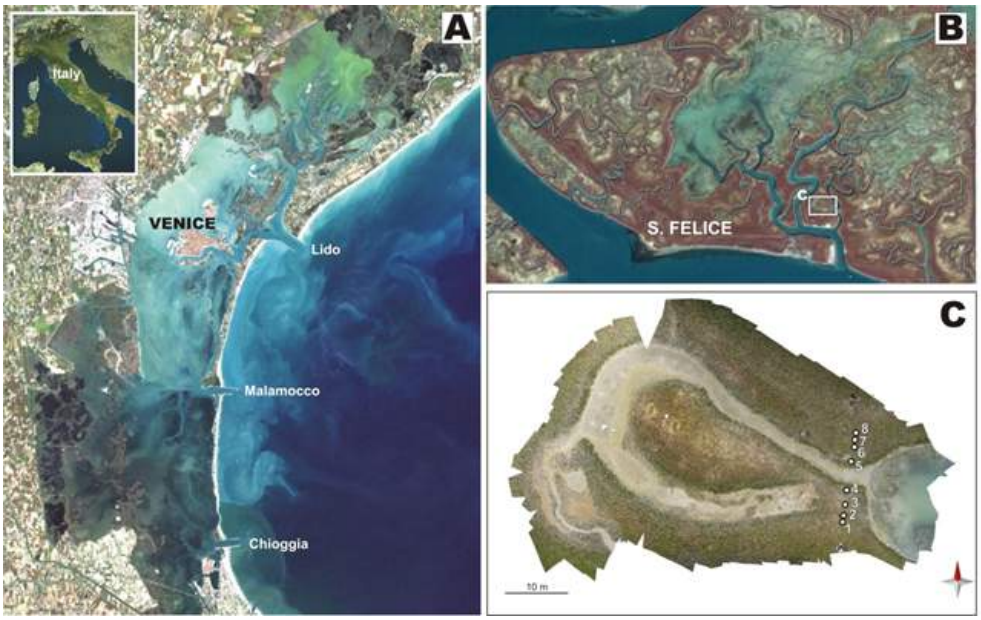

Figure A.1: Geographic location of the study site. (A) Location of the Venice Lagoon in the Mediterranean Sea. (B) Location of study site, the San Felice salt marsh, in the northern part of the Venice Lagoon. (C) Image showing the abandoned meander loop, studied in detail herein. The location of the 8 sedimentary cores recovered from the study site is also shown.

field observations; ii) mathematical modelling; and iii) sedimentary analyses. The aim of this paper is twofold. We first describe, through remote-sensing observations and modeling interpretation, tidal meander migration and evolution, a widely-examined issue in the fluvial landscape (Hickin and Nanson 1975, 1984; Hooke, 1984; Lagasse et al., 2004; Frascati and Lanzoni, 2009, 2010; Parker et al., 2011; Eke et al., 2014) that has however escaped detailed scrutiny in the tidal realm. Second, through the analysis of closely spaced sedimentary cores and the dating of significant sedimentary surfaces across the neck of the meander loop after the cutoff, we provide a new methodology to determine meander migration rates in the absence of high-temporal resolution aerial photographs.

Geological setting

The Venice Lagoon

The Venice Lagoon (Figure A.1A), located in the north- western Adriatic Sea, is the largest Mediterranean shallow water body, with an area of about 550 km^2 (length and width of the tidal basin are about 50 km and 10 km, respectively, see Figure A.1A) and a mean water depth of 1.0-1.5 m. The tidal regime is semidiurnal and microtidal, with an average range of about 1.0 m and maximum water

excursions at the inlets of ±0.75 m around mean sea level (hereinafter MSL), which can suddenly be increased by meteorological forcing (Carniello et al., 2016). The lagoon is separated from the Adriatic Sea by two narrow land strips about 0.5 km wide, while three inlets (Lido, Malamocco, and Chioggia) grant communication and active water exchange between the lagoon and the sea (Figure A.1A).The Venice Lagoon is hosted in the coastal sector of the Venetian Plain foreland basin (Massari et al., 2009). During the early Pleistocene, this basin experienced a change from turbiditic to shallow marine deposition (Massari et al., 2004), that allowed the accumulation of ca. 750 m of shallowing-upward deposits. During Last Glacial Maximum (LGM), the Brenta river megafan occupied most of the present day Venice area (Fontana et al., 2014). The Venice Lagoon formed as a consequence of the Holocene transgression, which promoted flooding of the LGM alluvial plain with formation of lagoon – estuarine – barrier systems in the Northern epicontinental Adriatic shelf (Zecchin et al., 2009).

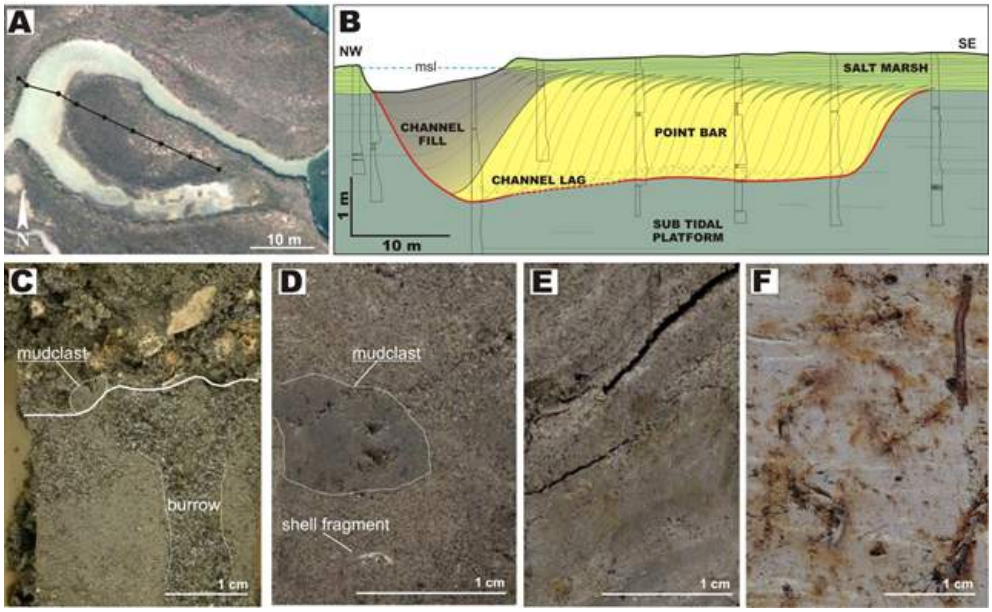

Figure A.2: Sedimentological log transect and sedimentary features of point bar and salt marsh deposits. (A) Location of the stratigraphic sections across the studied point bar. (B) Sedimentological log transect parallel to the point bar axis, showing the progressive channelward thickening of the bar deposits. (C) Shell-rich channel lag deposits. (D) Lower point bar massive sand deposits, with shell fragments and mud clasts. (E) Laminated, sandy upper bar deposits. (F) Oxidized, salt marsh mud

The study site

The study site is located in the San Felice salt marsh (Figure A.1B), in the northern part of the Venice lagoon, which represents one of the

most naturally preserved portions of the Lagoon (Marani et al., 2003; Rizzetto and Tosi, 2011, 2012). The marsh is characterized by an average elevation of about 0.26 m above MSL and is mainly colonized by four halophytic species: Spartina maritima, Limonium narbonense, Sarcocornia fruticosa and Juncus spp. (Marani et al., 2006). The San Felice salt marsh is considered to be a stable marsh (Rizzetto and Tosi, 2011; Roner at al., 2016) whose accretion rate of about 3 mm/yr (Day et al., 1998) is on average in equilibrium with the forcing rate of relative sea level rise of about 3 mm/yr (Carbognin et al., 2004; Strozzi et al., 2013). The present study focuses on point bar deposits associated with an abandoned meander loop oriented NW-SE (Figure A.1C), that was formed by a 6 m wide channel cutting through the salt marsh. The meander loop is characterized by a "simple symmetrical planform" (sensu, Hooke, 2013) and by a radius of curvature of about 13 m (Figure A.1C). Stratigraphic architecture and sedimentological features of the point bar associated with the study bend have been recently highlighted by Brivio et al. (2016). The point bar body deposits (Figure A.2A and B) overlay sub-tidal platform mud and sand, and are paved by a shell-rich, channel lag sand (Figure A.2C). Point bar deposits show an overall fining upward trend, defined by grey-bluish fine sand sediments grading into sandy mud. Lower bar deposits are commonly massive with scattered mudclasts in the lower bar (Figure A.2D), whereas, in the upper bar, traces of the primary lamination are locally well-preserved (Figure A.2E). Channel-fill deposits consist of massive, dark grey-bluish, organic-rich mud with rare shells in life position. Bar deposits are capped by oxidized salt-marsh mud (Figure A.2F), that is characterized by the occurrence of abundant roots and a pervasive horizontal lamination. The upper bar deposits and overlying channel-fill mud are the goal of the present study.

Material and Methods

Remoste sensing data

We analyzed a long historical record of high-resolution aerial photographs and satellite images (acquired in 1938, 1955, 1968, 1978, 1987, 1995, 2006, and 2012 see Figure A.3) of tidal channels dissecting the San Felice saltmarsh, in the Venice Lagoon. All images were georeferenced to an accuracy of ± 0.1 m. Channel banks were firstly manually digitized in a Geographic Information System (GIS) environment and were approximated through broken lines, i.e., using a suitable number of straight segments (Figure A.3), later used to compare channel planform characteristics and changes, and to compute meander migration rates.

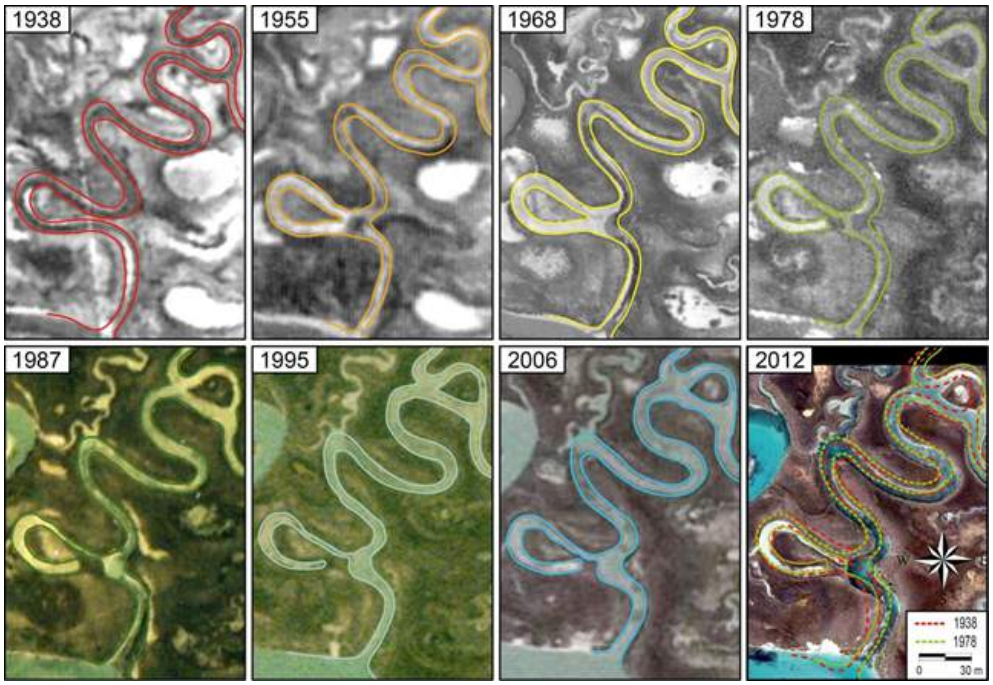

Figure A.3: Temporal evolution of the considered meandering channel cutting through the San Felice salt marsh in the Venice Lagoon. The planimetric configuration of the channel is overlapped to aerial photographs (1938-2006) and satellite images (2012) at different years. Image resolution (pixel size in meters) is as follows: 1938 (0.90 m); 1955 (1.00 m); 1968 (0.65 m); 1978 (0.92 m); 1987 (0.89 m); 1995 (0.90 m); 2006 (0.70 m); 2012 (0.25 m).

Analysis of meander migration

Meander migration rates were determined through the analysis of a sequence of aerial photographs at different times. A first approach considers the Best Fitting Circle (BFC) method (e.g., Lagasse et al., 2004), according to which the studied meander bends are described by a series of delineation points, and the center and radius of the best-fitting circle are determined (Figure A.4A). The comparison of two different planform configurations at different times allows one to compute the rate of migration of channel bends, together with meander wavelength, amplitude, and width. A second approach, that can be used when neck-cutoff events occur along a meandering channel, consists in measuring distance between the two neighboring concave banks, that are progressively getting closer, at different instants during the evolution. If Δx_1 is the distance at time t_1 and Δx_2 is the distance at time t_2, the migration rate can be computed as $m = (\Delta x_1 - \Delta x_2)/(t_2 - t_1)$ (Figure A.4 B-D).

Sedimentary cores

A total of eight sedimentary cores were recovered intruding vertical PVC pipes in the deposits along a NNE-SSW trending transect (Figure A.1C). Specifically, five and three cores were recovered from in-channel (2 – 6 in Figure A.1C) and bar-top (1, 7 and 8 in Figure A.1C) areas, respectively. PVC pipes were 8 cm in diameter and penetrated the study deposits about 1 m causing compaction of the sampled sediment. In order to evaluate compaction, supplementary cores were recovered in the immediacy of each main coring site using a Ejikelkamp hand auger, that allows one to recover uncompacted cores, 3 cm in diameter. Retrieving of larger cores was required in order to collect an appropriate volume of sediment suitable for chronological analyses (see Section 3.4). If not differently specified, de-compacted thicknesses are used here in the text. Cores were studied following the basic principles of facies analyses, highlighting vertical changes in sediment texture and color. Grain size analyses were carried out on core 4 (Figure A.1C) within the neck of the cutoff later encroached by vegetation, in order to provide a quantitative estimation of the decrease in sand content at the transition between bar and overlying channel-fill deposits. Grain size analysis was carried out through a Mastersizer 2000 (Version 5.40, MALVERN INSTRUMENTS), that measures the size of particles by laser diffraction quantifying the intensity of light scattered as a laser beam passes through the dispersed particulate sample.

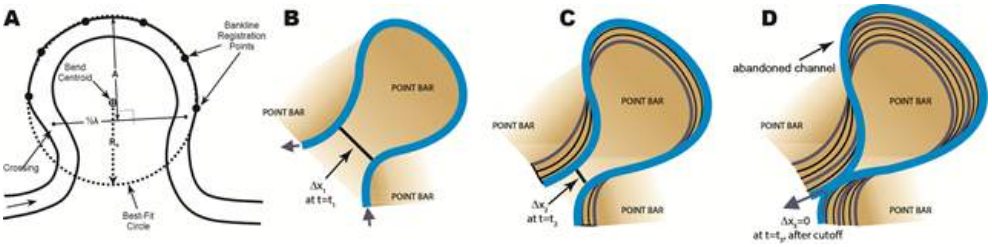

Figure A.4: Analysis of meander migration. (A) Sketch of the Best Fitting Circle (BFC) method (adapted from Lagasse et al., 2004). (B) Proposed methodology that can be used, in particular, when neck-cutoff events occur along a meandering channel. Distances between the two neighboring concave banks ($\Delta x1$; $\Delta x2$; and $\Delta x3$) at different times (t_1; t_2; and t_3, respectively) during the evolution can be used to determine the minimum migration rate as $m = (\Delta x_i - \Delta x_{i+1})/(t_{i+1} - t_i)$.

Geochronological Analysis

The chronology of core 4 was estimated by ^{210}Pb and ^{137}Cs profiles. The analyses were carried out following the procedures reported in Bellucci et al. (2007), to which we refer the interested reader for a detailed description of the methods, briefly summarized here for the

sake of clarity. Alpha spectrometry of ^{210}Pb was used for total ^{210}Pb determinations, assuming secular equilibrium between the two isotopes. Supported ^{210}Pb activities were obtained from constant values at depth in the core, where ^{210}Pb and ^{226}Ra were considered to be in radioactive equilibrium. Excess ^{210}Pb was calculated by subtracting the supported ^{210}Pb activity from the total. ^{210}Cs activities were measured via gamma spectrometry to validate the ^{210}Pb-derived chronology, using coaxial intrinsic germanium detectors.

Multidisciplinary approach to determine meander migration rates

Meander migration rates can be determined on the basis of the procedures above described (Section "Analysis of meander migration" in "Material and Method"). However, an alternative procedure to determine meander bend migration, that can be applied after their demise due to neck cutoff formation, is proposed and described below (Figure A.5). After the neck cutoff event, the meander bend is progressively abandoned by the tidal currents, causing tractional sedimentation of sand to be progressively replaced by mud fallout (Figure A.5, right panel). The sedimentological analysis of sediment cores along the neck cutoff, allows one to determine the stratigraphic interval that testifies the onset of channel abandonment. Dating of that surface through ^{210}Pb and ^{137}Cs chronometers allows one to determine when the cutoff occurred. Such a procedure is particularly useful when historical records of aerial photographs lack high-temporal resolution.

Results and discussion

Channel planform dynamics and meander migration rates through remote sensing and modeling interpretation

We first analyzed the temporal evolution of the planimetric shape of a tidal meandering channel cutting through the study area (Figure A.3). This channel is a tributary of a larger channel from which it departs with an almost rectilinear path, that becomes more sinuous towards the inner portion of the marsh. The considered channel was about 5.5 m wide in 1938 (Figure A.6A,C) and the Cartesian length (straight line between the end points of the channel path) of the channel portion shown in the images of Figure A.3 was about 150 m. Some of the meanders along the channel were already quite tortuous in 1938: absolute value of the curvature was about 0.1 m-1 (Figure A.6B, see also Marani et al., 2002 for computational details), while the average sinuosity was about 2.25 (Figure A.6B). A first neck cutoff event (hereinafter named as south cutoff) occurred between 1938 and 1955, due to the progressive narrowing of the meander neck until two neighboring concave banks of the meander come into contact allowing tidal

currents to shape a shorter path and bypass the meander loop. The meander bend was therefore abandoned by the tidal flows and an oxbow lake formed. Sediment infill within the oxbow lake and across the former neck was likely enhanced due to differential erosion and deposition (e.g., Stefanon et al., 2012; Hood, 2010) and by vegetation encroachment on the former meander limbs and neck, further enhancing soil formation (Figure A.3, images from 1968 to present). The cutoff induced "important processes of geomorphic change" (Mosley, 1975), limiting the spatial evolution of the meandering channel and leading to and reducing planform geometrical complexity (Camporeale et al., 2008): as an example, sinuosity decreased from 2.25 to about 1.75, whereas channel width slightly increased. A second cutoff event occurred between 1968 and 1978 (hereinafter named as north cutoff), although in this case sedimentation across the neck and eventual vegetation colonization have not been observed (yet), and the cutoff has not been sealed off the tidal channel. Channel sinuosity further decreased to about 1.5, remaining almost constant in the following years. Figure A.6 provides a detailed description of changes in local channel width (Figure A.6A) and curvature (Figure A.6B) together with average channel width (Figure A.6C) and reach sinuosity (Figure A.6D).

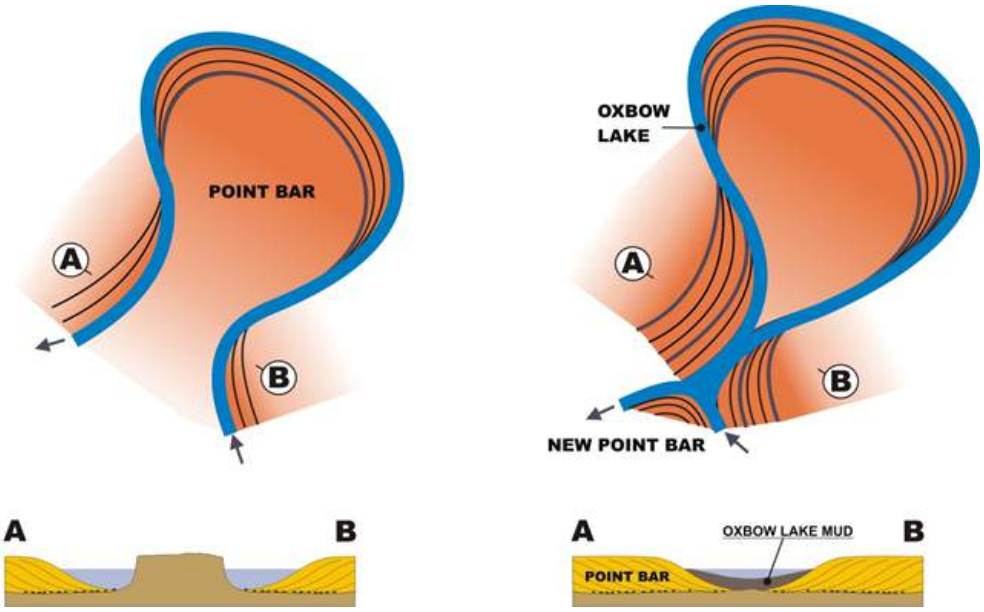

Figure A.5: Evolution of an expansional point-bar. Once the cutoff has occurred and oxbow lake forms in which muddy deposits start to accumulate above sandy point-bar clinoforms. Sedimentological analysis of sediment cores along the neck cutoff allows one to determine the stratigraphic interval testifying the onset of channel abandonment, whose dating through ^{210}Pb and ^{137}Cs chronometers makes it possible to determine when the cutoff occurred.

An interesting issue, both for theoretical and practical reasons, concerns the analysis and estimation of the lateral migration rate of tidal

meanders (Finotello et al., submitted). Figure A.7A shows lateral migration rates as a function of channel radius of curvature, for the meander bends of the study channel reach, computed with the BFC method and by considering changes in the width of a meander neck (distance between the two concave bends) at two consecutive configurations before the cutoff event (Section 3.2). As an example, the distance between the bends of the north cutoff in 1938, 1955, 1968 (note that the cutoff had already occurred in 1978) was equal to 4.65 m, 3.32 m, and 1.65 m, providing rates of migration for the different periods equal to 0.08 m/year, 0.13 m/year, and 0.17 m/year, respectively. The migration rates of the considered bends display values in the range 0.04-0.17 m/yr, that are consistent with those determined by other studies in tidal landscapes (Garofalo, 1980; Gabet, 1988) but are smaller than those observed for fluvial meanders (e.g., Hickin and Nanson 1975, 1984; Hooke, 1984; Lagasse et al., 2004). However, when conveniently scaled by local channel width, migration rates per unit width of tidal meanders are of the same magnitude of those characterizing fluvial ones. Figure A.7B, in fact, shows migration rates per unit width plotted as a function of the dimensionless radius of curvature, in the range 0.5-2.5%. These values nicely fit within values obtained by Lagasse et al. (2004) from a total of 89 rivers, as well as with those reported by Hooke et al. (2013), and are also consistent with those obtained by Finotello et al. (submitted) for 250 tidal bends in the Venice lagoon, whose envelope curve is shown in Figure A.7C together with other envelope curves for a couple of rivers, reported by Hook (2013). These findings challenge the reputation of tidal meanders of being quite stable tidal landscape features characterized by imperceptible changes. In addition, maximum migration rates per unit width and dimensionless channel curvature display a non-linear relationship as typically observed for fluvial patterns, thus suggesting that bend curvature crucially drives meander migration also in tidal landscapes.

Sedimentary cores

Sedimentary cores recovered from the bar top areas (cores 1, 7 and 8 in Figure A.8E) show an overall fining-upward grain size trend from fine sand to mud. The sandy lower part of these cores is mainly massive, although local relict of a primary, sub-horizontal lamination can be locally detected (Figure A.8A). Bivalves in life position have been locally recovered (Figure A.8A), whereas inarticulated shells or shell fragments are uncommon. In the uppermost part of this sandy interval, local occurrence of millimetric muddy laminae highlights plane-parallel stratifications. The upper muddy interval is up to 15 cm thick and consists of horizontally-laminated, mottled mud, with a variable amount of fine to very fine sand (Figure A.8A). Mud is mas-

sive and locally rich in plant debris. Sand forms 1-2 mm thick horizontal laminae, which are characterized by good grain-size sorting. Roots, wood fragments and bioturbation are common. The fining-upward grain size trend recorded in cores 1, 7 and 8 testifies the gradual transition from point bar (i.e. the lower sandy interval) to salt-marsh deposits (i.e. the upper muddy deposits interval, see also Brivio et al., 2016). The occurrence of horizontal lamination in the bar deposits suggests they accumulated in the upper part of the bar, that was characterized by a flat topography. Dominance of sand in this interval indicates that mud, accumulated during slack water phases, was successively removed by both ebb and flood currents. The sporadic muddy laminae reflect probably exceptional accumulations as during spring tides. Overlying salt-marsh mud (e.g. Allen, 2000) accumulated therefore, in the highest portion of the intertidal zone that is commonly affected by subaerial exposure, as indicated by a diffuse sediment mottling. Mud deposition occurred during high-water slack. Sandy laminae formed at high tide conditions during storm events, when wind-induced waves suspended mud and remobilized sand under tractional conditions (Choi and Jo, 2015). Textural sorting of sandy laminae and absence of a muddy matrix strongly support this hypothesis. A progressive upward transition from fine sand to mud (Figure A.8F) characterize also cores recovered from channel-fill deposits (cores 2 – 6 in Figure A.8E). The lower sandy part of these cores represents the lateral extent of the point bar sand detected in cores 1, 7 and 8, and no significant lateral change in grain size or sedimentary facies have been detected. Point bar sand grades upward into a massive dark mud (Figure A.8D), through a progressive increase in organic matter content and a decrease in definition of laminae (Figure A.8 B and C). Mud-rich deposits overlying point bar sand show a maximum thickness of about 50 cm, and locally, their uppermost part is characterized by mottling. Grain size analyses carried out on 22 samples from core 4 (ranging from sample n.22 just below the surface to sample n. 1 at the bottom of the core, the spacing between samples being equal to 4cm) show that deposits overlying the point –bar sand are characterized by a marked decrease in sand content (Figure A.8F). Horizontally-laminated deposits accumulated above the point bar sand settled down in the abandoned channel after its cutoff (Choi et al., 2013). The progressive, upward decrease in the sandy fraction (Figure A.8F) suggests that the channel was not abruptly deactivated, and water flowed along the bend just after the cutoff event. After the final abandonment, mud settling caused a progressive infill of the channel, that was completed by accumulation of the organic-rich mud. Local presence of mottling heralds colonization from salt-marsh halophytic vegetation and an incipient salt-marsh deposition.

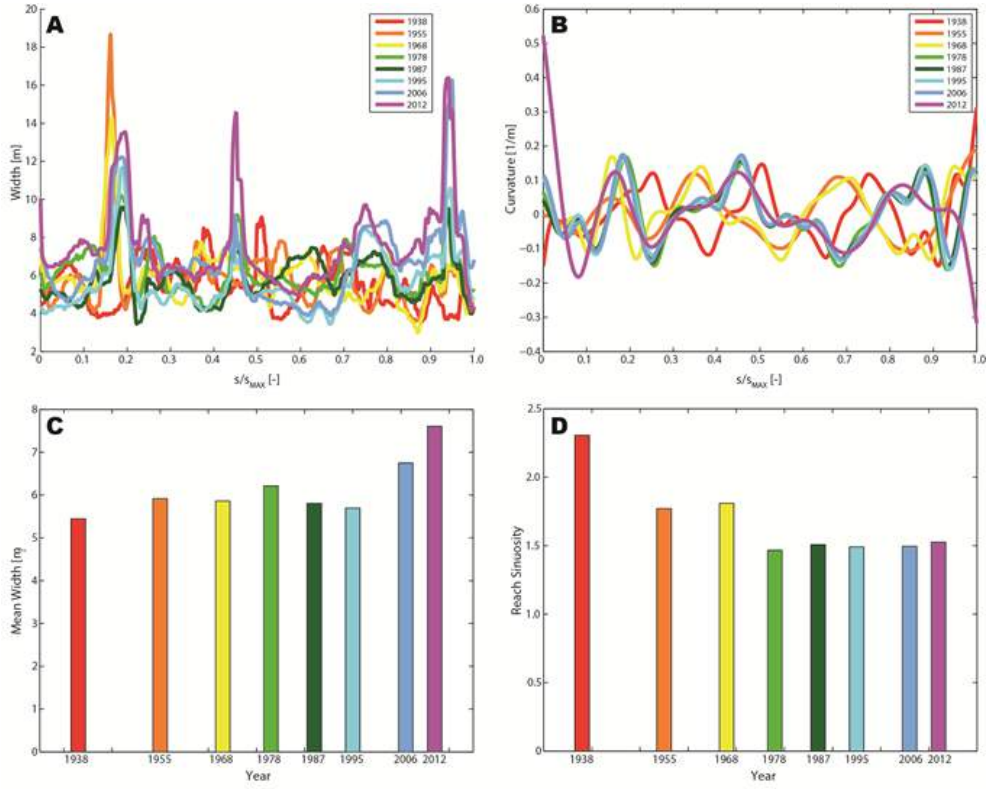

Figure A.6: Spatial evolution of channel width (A) channel curvature (B) along the curvilinear coordinate s originating at channel inlet, made dimensionless with the maximum coordinate s_{MAX} at different years; average channel width (C) and sinuosity (D) at different years.

Geochronological analysis

^{210}Pb shows a generally decreasing profile, with an isolated peak at 20 cm depth, and reaching the equilibrium at 60 cm depth (Figure A.8G). The Constant Flux–Constant Sedimentation (CF–CS) model for the unsupported ^{210}Pb supply was used to calculate the sedimentation rate (Appleby, 2001). A significant linear correlation between the logarithm of ^{210}Pbxs concentrations and depth was found and a mean sedimentation rate of 0.7 cm/y was obtained. The ^{137}Cs activity profile shows a peak at 20 cm corresponding to the fallout from the Chernobyl accident in 1986 (Figure A.8G). The presence of low but detectable activities of ^{137}Cs at depth in the core, below the ^{210}Pb equilibrium depth, is probably due to ^{137}Cs mobilization and migration in the sediment. Despite this uncertainty, the Chernobyl peak confirms the chronology based on the ^{210}Pb model, providing consistent ages for the same level.

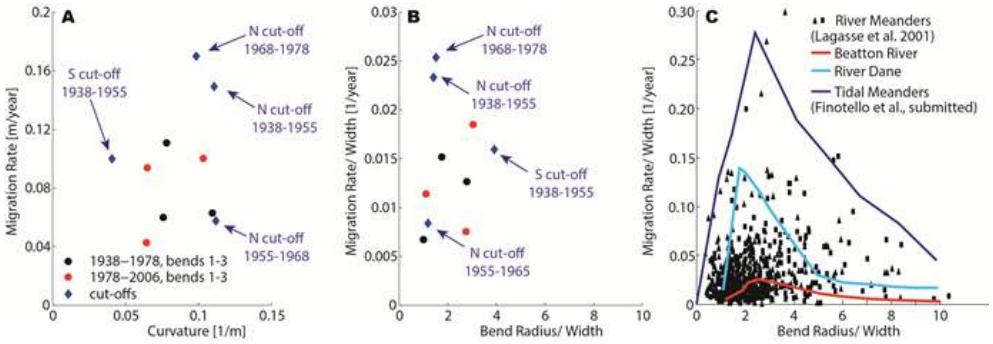

Figure A.7: (A) Migration rates as a function of bend curvature characterized through the BFC method. (B) Migration rates per unit width versus the dimensionless radius of curvature. (C) Migration rates per unit width, versus the dimensionless radius of curvature for a few fluvial systems compared to tidal ones.

Multidisciplinary approach to determine meander migration rates

Sedimentological analyses coupled with the analysis of grain size distribution allow one to determine the depth of the sample in correspondence of which the cutoff initiates. After the neck cutoff event, the meander bend is progressively abandoned by the tidal currents whose capability of transporting sand decreases, causing the accumulation of silt deposits. The decrease in the percentage of sand volume in the upper point-bar and abandoned channel deposits (see in Figure A.8F the decrease in sand content in correspondence of sample 9 at a depth of 52 cm below the surface) documents the occurrence of the cutoff event. However, it is worthwhile noting that sedimentological and grain size analyses highlight that meander cutoff occurred progressively (see the continuous decrease in grain size from sample 9 to sample 13 at a depth of 36 cm, in Figure A.8F). The final abandonment of the channel corresponds to the minimum sand content (samples 13 to 22, at the surface). ^{210}Pb and ^{137}Cs chronometers suggest that the cutoff (sample 9) occurred in 1945 and that, after cutoff initiation, mud accumulated at a rate of about 7.0-7.5 mm/yr. The distance between the two neighboring concave banks leading to the south cutoff (Figure A.3) was about 1.70 m in 1938. If the cutoff occurred in 1945, the migration rate of the two bends computed through the proposed method reveals to be equal to 0.25 m/yr, which is larger than the minimum velocity of migration of 0.10 m/yr computed by comparing images in 1938 and 1955. The new methodology to determine meander migration rates leading to a cutoff event is particularly effective in the absence of high-temporal resolution aerial photographs

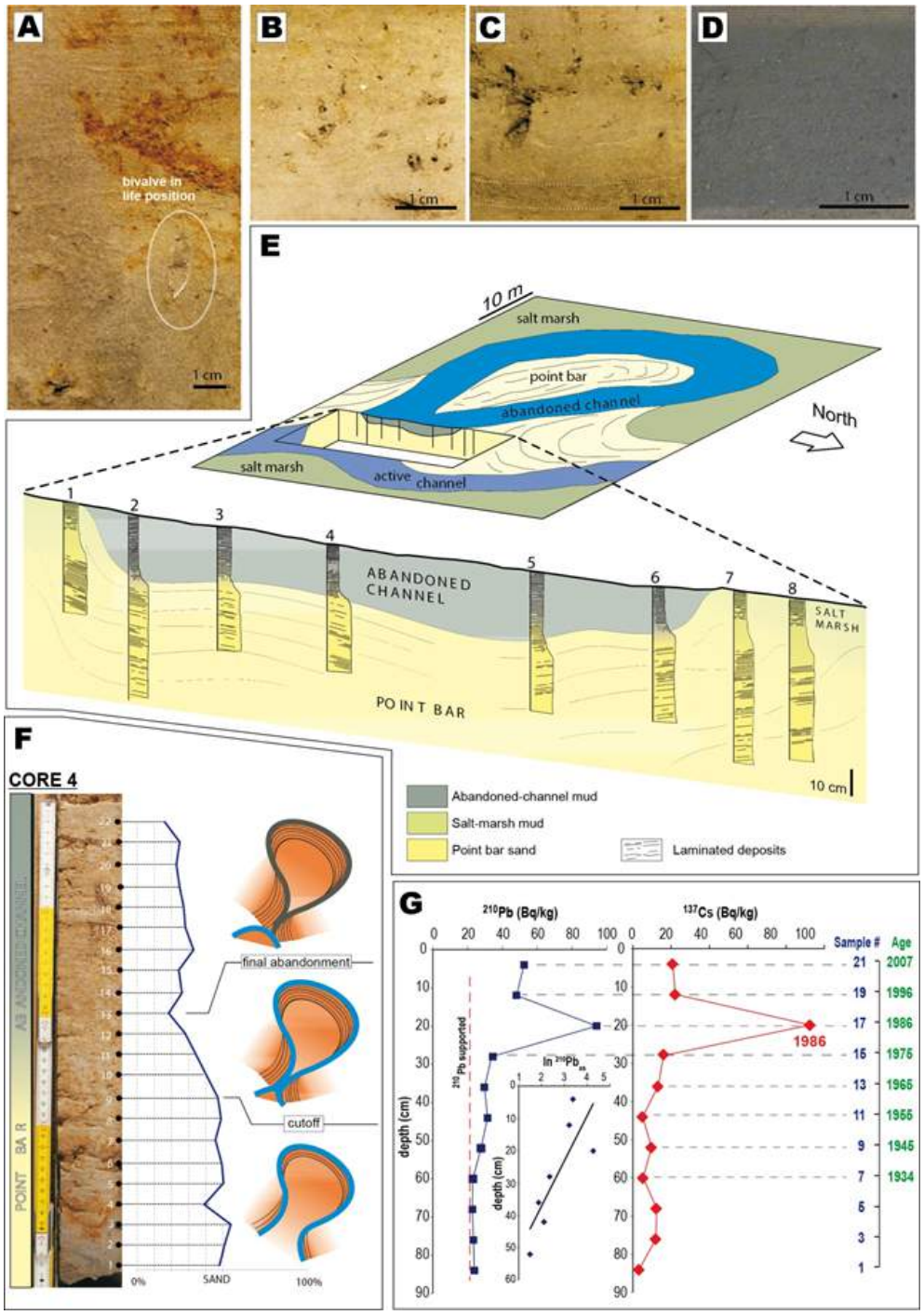

Figure A.8: Upper point bar laminated sand with a bivalve shell in life position. B - C) Laminated muddy silt (B) and mud (C) forming the lower and middle part of abandoned channel succession, respectively. Dark laminae in C are characterized by a higher content in organic matter. D) Massive, organic-rich mud forming the uppermost part of abandoned channel deposits. E) Spatial distribution and thickness of point-bar, salt-marsh and abandoned-channel deposits defined through integration between sedimentary cores and present-day morphology of the study bar. F) Sand percentage (volume) in the upper point-bar and abandoned channel deposits. The cutoff event is documented by the onset of decrease in sand content (sample 9), whereas the final abandonment of the channel corresponds to the minimum sand content (samples 13 to 22). G) Total ^{210}Pb and ^{137}Cs activity vs. depth in core 4, across the meander neck cutoff. The correlation between the logarithm of ^{210}Pbxs concentrations and depth is also shown, together with the ages of the different soil samples shown in inset F.

Conclusions

The geomorphological, geochronological, and sedimentological analyses presented herein are applicable to tidal meandering channels developed in microtidal salt-marsh systems. Nonetheless, the adopted multidisciplinary approach provides insights into tidal meander dynamics and migration rates that are of general interest. The main conclusions of this paper can be summarized as follows.

1. Tidal meanders display modes of migration similar to those which characterize their fluvial cousins. Values of the dimensional migration rates of the considered tidal meanders range between 0.05 m/yr and 0.2 m/yr. However, when conveniently scaled by local channel width, migration rates of tidal meanders are of the same magnitude of fluvial ones, thus challenging the paradigm of tidal channels as quite stable landscape features.

2. The considered meandering channel, that is about 6 m wide, has been characterized by multiple neck cutoff events, about 150m apart, in the last 60 years. These events are indeed quite frequent in the study area and represent a signature of the dynamic nature of tidal channels. In the study bend, the spatial distribution of sedimentary facies, grain size analyses, and ^{210}Pb and ^{210}Cs chronometers highlighted that channel abandonment occurred progressively. Nevertheless, the neck cutoff event lead to important geomorphic changes which not only affected network complexity, but also influenced the ecogeomorphic evolution of the adjacent marsh platform. Mud accumulated within the abandoned reach at a rate of about 7.0 ± 1.5 mm/yr , which doubles the rate of vertical accretion of the salt marsh surface.

3. A new methodology is presented to determine tidal meander migration rates when neck cutoff occurs. The analysis of aerial photos allows one to determine the velocity of migration of the two bends that come into contact. Although avoiding possible errors related to image georeferentiation, this procedure provides the minimum velocity of migration, depending on the temporal resolution of the images compared to the real occurrence of the cutoff event. The applied methodology allows one to detect the age of the cutoff event dating (through ^{210}Pb and ^{137}Cs chronometers) the onset fine-grained deposits accumulation within the channel. Once the age of the cutoff is known, the actual velocity of migration can be computed.

Towards the goal of developing models of tidal-landscape evolution accounting for tidal meander inception and growth, future research

will expand the analyses carried out herein to include a variety of meandering tidal channels from different places worldwide.

References for Appendix A

Appleby, P.G., 2001. Chronostratigraphic techniques in recent sediments. In: Last, W.M., Smol, P.M. (Eds.), Tracking Environmental Change using Lake Sediments, Vol. 1: Basin Analysis, Coring, and Chronological Techniques. Kluwer Academic, pp. 171–203.
- Allen, J.R.L., 1965. A review of the origin and characteristics of recent alluvial sediments: Sedimentology, 5,. 89-191.
- Allen, J.R.L., 2000. Morphodynamics of Holocene salt marshes: a review sketch from the Atlantic and Southern North Sea coasts of Europe. Quaternary Sci. Rev. 19, 1155–1231.
- Barwis, J.H., 1978. Sedimentology of some South Carolina tidal creek point bars and a comparison with their fluvial counterparts. In: Miall, A.D. (Ed.), Fluvial Sedimentology. Canadian Society of Petroleum Geologists Memoir 5, pp. 129–160 (Calgary).
- Bellucci, L.G., Frignani, M., Cochran, J.K., Albertazzi, S., Zaggia, L., Cecconi, G., 2007. ^{210}Pb and ^{137}Cs as chronometers for salt marsh accretion in the Venice Lagoon − Links to flooding frequency and climate change. J. Environ. Radioact., 97, 85-102.
- Bridge, J.S., Smith, N.D., Trent, F., Gabel, S.L., and Bernstein, P., 1986. Sedimentology and morphology of a low-sinuosity river: Calamus River, Nebraska Sand Hills. Sedimentology, 33, 851-870.
- Brierley, G.J. 1991. Bar sedimentology of the Squamish River, British Columbia: definition and application of morphostratigraphic units. J. Sediment. Res. 61, 211-225.
- Brivio, L., Ghinassi, M., D'Alpaos, A., Finotello, A., Fontana, A., Roner, M., Howes, N., 2016. Aggradation and lateral migration shaping geometry of a tidal point bar: An example from salt marshes of the Northern Venice Lagoon (Italy). Sed. Geol., 343, 141–155.
- Camporeale, C., Perucca, E., Ridolfi, L. 2008. Significance of cutoff in meandering river dynamics. J. Geophys. Res. 113, F01001, doi:10.1029/2006JF000694
- Carbognin, L., Teatini, P., Tosi, L., 2004.
-Eustacy and land subsidence in the Venice lagoon at the beginning of the new millennium. J. Mar. Syst., 51, 345–53. Carniello, L., D'Alpaos, A., Botter, G., Rinaldo, A., 2016. Statistical characterization of spatio temporal sediment dynamics in the Venice lagoon. J. Geophys. Res. Earth Surf. 121, 1049–1064.
- Choi, K.S., Dalrymple, R.W., Chun, S.S., Kim, S.P., 2004. Sedimentology of modern, inclined heterolithic stratification (IHS) in the macrotidal Han River delta, Korea. J. Sediment. Res. 74, 677–689.
- Choi, K.S., 2011. External controls on the architecture of inclined heterolithic stratification (IHS) of macrotidal Sukmo channel: wave versus rainfall. Mar. Geol. 285, 17–28.
- Choi, K.S., Jo, J.H., 2015. Morphodynamics of tidal channels in the open coast macrotidal flat, southern Ganghwa island in Gyeonggi Bay, west coast of Korea. J. Sediment. Res., 85, 582–595.
- Coco, G., Zhou, Z., van Maanen, B., Olabarrieta, M., Tinoco, R., 2013. Morphodynamics of tidal networks: Advances and challenges. Mar. Geol. 346, 1–16, doi:10.1016/j.margeo.2013.08.005.
- D'Alpaos, A., Lanzoni, S., Marani, M., Fagherazzi, S., Rinaldo, A., 2005. Tidal network ontogeny: channel initiation and early development. J. Geophys. Res.110, doi:10.1029/2004JF000182.
- D'Alpaos, A., Lanzoni, S., Marani, M., Rinaldo, A., 2007. Landscape evolution in tidal embayments: modeling the interplay of erosion, sedimentation, and vegetation dynamics. J. Geophys. Res., 112, F01008. http://dx.doi.org/10.1029/2006JF000537.
- D'Alpaos, A., Da Lio, C., Marani, M., 2012. Biogeomorphology of tidal landforms: physical and biological processes shaping the tidal landscape. Ecohydrology, 5, 550–562.
- Day, J.W., Rismondo, A., Scarton, F., Are, D., Cecconi, G. 1998. Relative sea level rise and Venice lagoon wetlands. J. Coast. Conserv. 4,27–34.
- De Mowbray, T., 1983. The genesis of lateral accretion deposits in recent intertidal mudflat channels, Solway Firth, Scotland. Sedimentology 30, 425–435.
- Eke, E., Parker, G., Shimizu, Y., 2014. Numerical modeling of erosional and depositional

bank processes in migrating river bends with self-formed width: Morphodynamics of bar push and bank pull. J. Geophys. Res. 119 (7), 1455-1483.
- Fagherazzi, S., Gabet, E.J., Furbish, D.J. 2004. The effect of bidirectional flow on tidal channel planforms. Earth Surf. Proc. Land. 29(3), 295–309.
- Feola, A., Belluco, E., D'Alpaos, A., Lanzoni, S., Marani, M., Rinaldo, A., 2005. A geomorphic study of lagoonal landforms. Water Resour. Res. 41, W06019, doi:10.1029/2004WR003811.
- Finotello, A., Lanzoni, S., Ghinassi, M., Marani, M., Rinaldo, A., and D'Alpaos, A. 2016. Sustained migration rates of tidal meanders challange current understanding on morphodynamic - Submitted
- Fontana, A., Mozzi, P., Marchetti, M., 2014. Alluvial fans and megafans along the southern side of the Alps. Sed. Geol. 301, 150–171.
- Frascati, A., Lanzoni, S., 2009. Morphodynamic regime and long-term evolution of meandering rivers, J. Geophys. Res., 114, F02002, doi:10.1029/2008JF001101.
- Frascati, A., Lanzoni, S., 2010. Long river meandering as a part of chaotic dynamics? A contribution from mathematical modelling, Earth Surf. Proc. Land. 35, 791-802, doi:10.1002/esp.1974.
- Gabet, E.J., 1998. Lateral migration and bank erosion in a salt marsh tidal channel in San Francisco Bay, California. Estuaries 21, 745–753.
- Garofalo, D., 1980. The influence of wetland vegetation on tidal stream channel migration and morphology. Estuaries 3, 258–270.
- Garotta, V., Rummel, A., Seminara, G. 2007. Long-term morphodynamics and hydrodynamics of tidal meandering channels. Proceedings of the 5th IAHR Symposium on River, Coastal and Estuarine Morphodynamics. 105,163–168.
- Hickin, E.J., Nanson, G.C. 1975. The character of channel migration on the Beatton River, Northeast British Columbia, Canada. Geol. Soc. Am. Bull. 86(4), 487–494.
- Hickin, E.J., Nanson, G.C. 1984. Lateral Migration Rates of River Bends. J. Hydraul. Eng. Asce 110,1557–1567. Hood, W.G., 2010. Tidal channel meander formation by depositional rather than erosional processes: examples from the prograding Skagit River Delta (Washington, USA). Earth Surf. Proc. Land. 35, 319–330, doi:10.1029/2001WR000404.
- Hooke, J.M., 1984. Changes in river meanders : a review of techniques and results of analyses. Progr. Phys. Geog. 8(4), 473–508.
- Hooke, J.M., 2004. Cutoffs galore!: occurrence and causes of multiple cutoffs on a meandering river. Geomorphology, 61, 225–238.
- Hooke, J.M., 2013. River meandering. In: Shroder, J.F. (Ed.)Treatise on Geomorphology vol. 9. Academic Press, San Diego (California, United States), pp. 260–288.
- Hughes, Z.J., 2012. Tidal channels on tidal flats and marshes. In: Davis Jr., R.A., Dalrymple, R.W. (Eds.), Principles of Tidal Sedimentology. Springer, Netherlands, pp. 269–300.
- Ikeda, S., Parker, G., 1989. River Meandering, Water Resources Monograph, 12.
- Jackson, R.G. 1976. Depositional Model of Point Bars in the Lower Wabash River. J. Sediment. Petrol. 46(3), 579-594. Kleinhans, M., Schuurman, F., Wiecher, B., Markies, H. 2009. Meandering channel dynamics in highly cohesive sediment on an intertidal mud flat in the Westerschelde estuary, the Netherlands. Geomorphology 105, 261–276.
- Lagasse, P.F., Spitz, W.J., Zevenbergen, L.W. 2004. Handbook for predicting stream meander migration, 107 pages. Leopold, L.B., Wolman, G.M. 1960. River Meanders. Geol. Soc. Am. Bull. 71(6), 769–793.
- Marani, M., Lanzoni, S., Zandolin, D., Seminara, G., Rinaldo, A., 2002. Tidal meanders. Water Resour. Res. 38, 1225, doi:10.1029/2001WR000404.
- Marani, M., Belluco, E., D'Alpaos, A., Defina, A., Lanzoni, S., Rinaldo, A., 2003. On the drainage density of tidal networks. Water Resour. Res. 39, 1040, doi:10.1029/2001WR001051.
- Marani, M., Belluco, E., Ferrari, S., Silvestri, S., D'Alpaos, A., Lanzoni, S., Feola, A., Rinaldo, A., 2006. Analysis, synthesis and modelling of high-resolution observations of saltmarsh eco-geomorphological patterns in the Venice lagoon. Estuar. Coast. Shelf S., 69 (3–4), 414–426.
- Massari, F., Rio, D., Barbero, R.S., Asioli, A., Capraro, L., Fornaciari, E., Vergerio, P.P., 2004. The environment of Venice area in the past two million years. Palaeogeogr. Palaeocl. 202, 273–308.
- Massari, F., Grandesso, P., Stefani, C., Jobstraibizer, P.G., 2009. A small polyhistory foreland basin evolving in a context of oblique convergence: the Venetian basin (Chattian to Recent, Southern Alps, Italy). In: Allen, P.A., Homewood, P. (Eds.), Foreland Basins. Blackwell Sci-

entific, Oxford, pp. 141–168.
- Mosley, M., 1975. Meander cutoffs on the River Bollin, Cheshire, in July 1973. Rev. Geomorphol. Dyn., 24, 21–32.
- Parker, G., Shimizu, Y., Wilkerson, G.V., Eke, E.C., Abad, J.D., Lauer, J.W., Paola, C., Dietrich, W.E., Voller, V.R., 2011. A new framework for modeling the migration of meandering rivers. Earth Surf. Proc. Land. 36 (1), 70-86.
- Rizzetto, F., Tosi, L., 2011. Aptitude of modern salt marshes to counteract relative sea-level rise, Venice Lagoon (Italy). Geology 39, 755–758.
- Rizzetto, F., Tosi, L., 2012. Rapid response of tidal channel networks to sea-level variations (Venice Lagoon, Italy). Global Planet. Change 92, 191–197.
- Roner, M., D'Alpaos, A., Ghinassi, M., Marani, M., Silvestri, S., Franceschinis, E., Realdon, N., 2016. Spatial variation of salt-marsh organic and inorganic deposition and organic carbon accumulation: Inferences from the Venice lagoon, Italy. Adv. Water Resour. 93, 276–287.
- Seminara, G. 2006. Meanders. J. Fluid Mech. 554, 271-297.
- Solari, L., Seminara, G., Lanzoni, S., Marani, M., Rinaldo, A., 2002. Sand bars in tidal channels, part two, Tidal meanders. J. Fluid Mech. 451, 203–238.
- Stefanon, L., Carniello, L., D'Alpaos, A., Rinaldo, A., 2012. Signatures of sea level changes on tidal geomorphology: Experiments on network incision and retreat. Geophys. Res. Lett., 39, L12402, doi:10.1029/2012GL051953.
- Strozzi, T., Teatini, P., Tosi, L., Wegmüller, U., Werner, C., 2013. Land subsidence of natural transitional environments by satellite radar interferometry on artificial reflectors. J. Geophys. Res. 118:1177–1791.
- van Maanen, B., Coco, G., Bryan, K., 2013. Modelling the effects of tidal range and initial bathymetry on the morphological evolution of tidal embayments. Geomorphology 191, 23–34, doi:10.1016/j.geomorph.2013.02.023.
- Vlaswinkel, B.M., Cantelli, A. 2011. Geometric characteristics and evolution of a tidal channel network in experimental setting, Earth Surf. Proc. Land. 36(6), 739–752, doi:10.1002/esp.2099.
- Zecchin, M., Brancolini, G., Tosi, L., Rizzetto, F., Caffau, M., Baradello, L., 2009. Anatomy of the Holocene succession of the southern Venice lagoon revealed by very high-resolution seismic data. Cont. Shelf Res. 29, 1343–1359.
- Zhou, Z., Olabarrieta, M., Stefanon, L., D'Alpaos, A., Carniello, L., Coco, G. 2014. A comparative study of physical and numerical modeling of tidal network ontogeny. J. Geophys. Res. Earth Surface 119, doi:10.1002/2014JF003092.
- Zolezzi, G., Luchi, R., Tubino, M. 2012. Modeling morphodynamic processes in meandering rivers with spatial width variations. Rev. Geophys. 50, RG4005, doi:10.1029/2012RG000392.

B | APPENDIX

MORPHODYNAMIC EVOLUTION AND STRATAL ARCHITECTURE OF TRANSLATING TIDAL POINT BARS: INFERENCES FROM THE NORTHERN VENICE LAGOON (ITALY)

Ghinassi, Massimiliano[1], Andrea D'Alpaos[1], Andrea Gasparotto[1], Luca Carniello[2], Lara Brivio[1], Alvise Finotello[1], Marcella Roner[1], Erica Franceschinis[3], Nicola Realdon[3] and Nick Howes[4]

[1]Dept. of Geosciences, University of Padova, via G.Gradenigo 6, Padova, PD I-35131, Italy

[2]Dept. ICEA, University of Padova, via Loredan 20, Padova, PD I-35131, Italy

[3]Dept. of Pharmaceutical and Pharmacological Sciences, University of Padova, via Marzolo 5, Padova, PD-I35121, Italy

[4]Shell Technology Ceneter Houston, 3333 Highway 6 South Houston, TX 77082-3101, USA

Abstract

Tidal channels those commonly develop sinuous bends and form complex networks draining lagoons and estuaries. Widespread distribution of tidal meanders in modern coasts contrasts with their limited documentation in the fossil record, where the influence of fluvial processes on sedimentation is always questionable. The sedimentary products of tidal bends evolution are therefore poorly known, and specific facies models for tidal point bars are still missing. The present study contributes aims at improving our understanding of tidal 3 meanders through a multidisciplinary study approach that combines analyses of historical aerial photos, measurements of in-channel flow velocity, high-resolution facies analyses on sedimentary cores, and 3D architectural modeling. The study channel (15-12 m wide and 2-3 m deep) drains a saltmarsh area located in the NE sector of the microtidal Venice Lagoon (Italy). Historical photos show that during the past 77 years the bar translated seaward about 15 m without changing significantly its planform geometry. Our Results show that the study bend formed on a non-vegetated mud flat that was progressively colonized by halophytic vegetation. Seaward translation occurred under aggradational conditions, with a 3 migration rate of 20-30 cm/yr, and was promoted by the occurrence of cohesive, poorly erodible outer bank deposits, as occurs in fluvial bends cut in cohesive mud. Translation of the channel bend promoted erosion and deposition along

the landward and seaward side of the bar, respectively. The opposing and offset tidal currents provides a peculiar grain size distribution within the bar. During the flood stage, sand sedimentation occurs in the upper part of the bar, where the maximum flow velocity is located occurs. During the ebb stage, the bar experiences the secondary helical flow that accumulates sand at the toe of the bar. Lateral stacking of flood and ebb deposits caused the formation of coarsening- and fining- upward sedimentary packages, respectively.

Introduction

It has long been recognized that the variability of sedimentary and stratal patterns characterizing meandering river deposits is strictly connected with different types of channel planform transformations (e.g. Jackson, 1976; Willis, 1989; 1993; Bridge, 2003; Willis and Tang, 2010). Studies on modern rivers show that the evolution of channel bends can be depicted in terms of three basic modes of transformation (Fig. B.1-A), namely: expansion, translation and rotation (Daniel, 1971; Jackson, 1976) which can also occur in combination. Expansion increases the channel-bend sinuosity, while the bend apex migrates away along the channel-bend axis. Translation maintains the channel sinuosity, while the bend apex 6 migrates downstream transverse to the channel-bend bend axis. Rotation, which commonly occurs in combination with translation or expansion, increases meander-bend asymmetry through the migration of the bend apex away from bend axis. Sedimentological studies linking fluvial bend transformations with related sedimentary products (e.g. Smith et al., 2009; 2011; Willis, 1993; Willis and Tang, 2010; Ghinassi and Ielpi, 2015) highlight that point bars generated by different planform behaviors differ in terms of stratal architecture, grain size distribution and sedimentary facies patterns. Tidal meanders have not received a similar attention, and little is known about their 6 modes of planform transformations and related sedimentary products. The morphodynamic evolution of branching and meandering tidal channels is controlled by a strong interaction between intertwined processes such as those related to tidal asymmetry, changes in the tidal prism, sediment texture, sediment supply, and vegetation cover (Garofalo, 1980; Dalrymple et al., 1991; Gabet, 1998; Fenies and Faugères, 1998; Marani et al., 2002; Lanzoni and Seminara, 2002; Solari et al., 2002; Fagherazzi et al., 2004; D'Alpaos et al., 2005; Garotta et al., 2006). Despite the complex interaction between different processes which act at overlapping spatial and temporal scales, tidal meanders are commonly assumed to increase their sinuosity in time through a progressive migration of the bend apex along the channel- bend axis. Accordingly, their internal stratal architecture and sedimentary facies distribution (San-

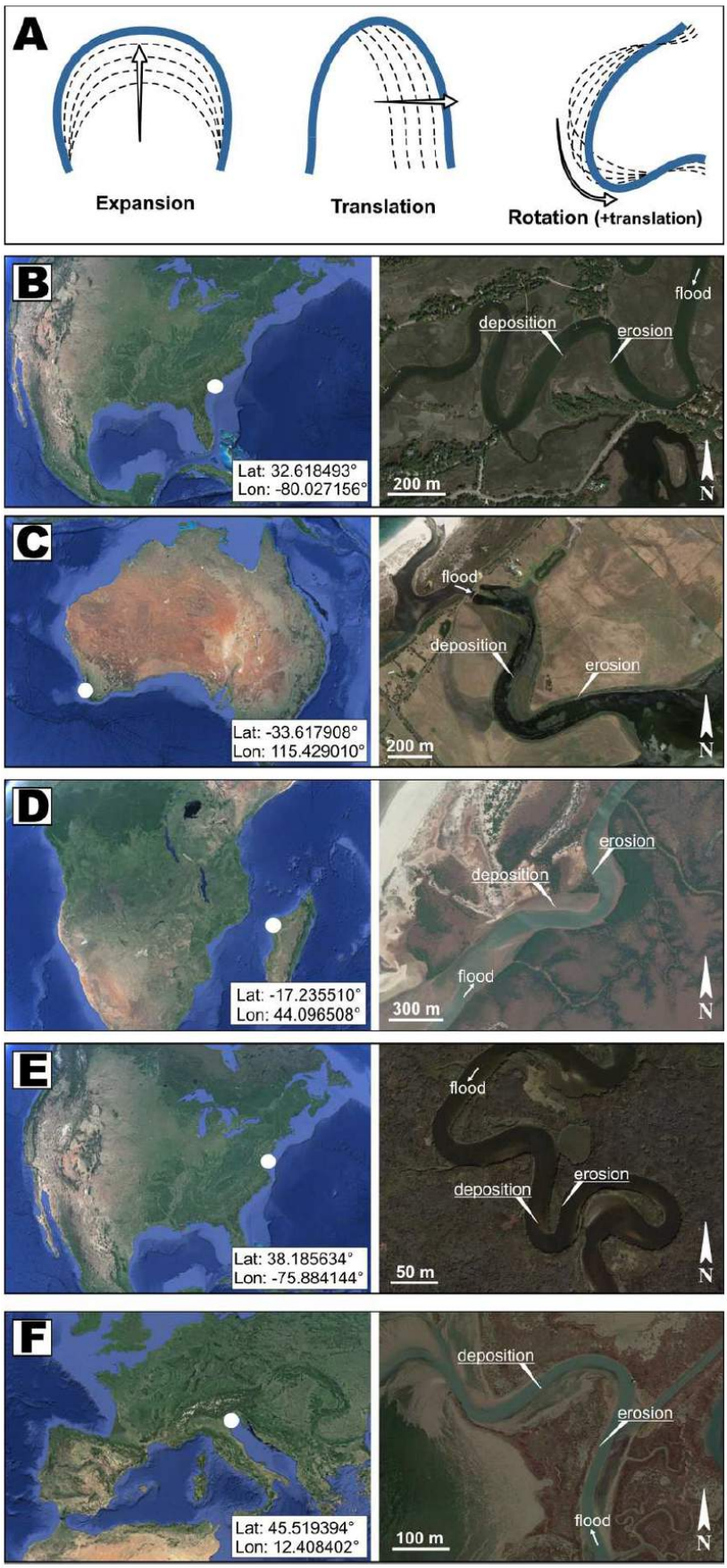

Figure B.1: (A) Planform modes of meander-bend evolution. (B - F) Google©Earth satellite views of translating tidal meander bends located in different sites. Coordinates are from Google©Earth.

tos and Rossetti, 2006; Díez-Canseco et al., 2014) is mainly analyzed following the classical facies model developed for expanding fluvial bends (Allen 1963; McGowen and Garner, 1970; Brice, 1974; Jackson, 1976; Nanson, 1980). Therefore, beyond acknowledging occurrence of bidirectional paleoflow indicators, along with high mud content and degree of bioturbation (Barwis, 1978), tidal point bar deposits are expected to show a fining upward- grain size trend (Santos and Rossetti, 2006; Díez-Canseco et al., 2014) and well-developed inclined heterolithic stratification (Thomas et al., 1989). Although these features undoubtedly typify tidal point bars, a view of branching and 8 meandering tidal networks through freely-distributed satellite images highlights that planform evolution of tidal point bars can also strongly differ from classical expansion, and bar translation commonly occurs in tidal realms (B.1, B - F). It arises, therefore, that translating tidal bars are poorly known in terms of their morphodynamic evolution and related sedimentary products. In order to provide a first insight to the understanding of these bars, from this two-way perspective, this work focuses on a translating tidal point bar located in the Northern part of the Venice Lagoon, Italy (Fig. B.2). Our analyses are the result of a multidisciplinary approach that combines analyses of historical aerial photos, 9 measurements of cross-sectional flow velocity profiles, high-resolution facies analyses on sedimentary cores, and 3D architectural modeling. The aims of this study are threefold: i) characterizing the morphodynamics of a translating tidal point bar; ii) assessing the governing forcing which trigger meander translation; iii) analyzing different patterns of sediment distribution along the accreting side of the bar. We deem our results will bear important consequences for the morphodynamic evolution of tidal landscapes, will contribute at improving tidal facies models, and finally will find applications in paleoenvironmental reconstruction for subsurface exploration.

Geomorphological setting

The Venice Lagoon is the largest Mediterranean brackish water body and is located in the northern sector of the Adriatic Sea (Fig. B.2A). The Lagoon, about 50 km long and 10 km wide, is connected to the Adriatic Sea through three inlets (Lido, Malamocco and Chioggia; Fig. B.2B), and is characterized by an average water depth of about 1.0-1.5 m. The tidal range is about 1.0 m and astronomical tidal peak oscillations are about 0.75 m (D'Alpaos et al., 2013) around Mean Sea Level (MSL). The Venice Lagoon is located in the coastal sector of the Venetian Plain foreland basin, which formed since the Late Oligocene (Massari et al., 2009) between the Apennine and South-Alpine chains. The Pleistocene infill of this basin consists of turbiditic deposits grading upward into coastal sediments (Massari et al., 2004),

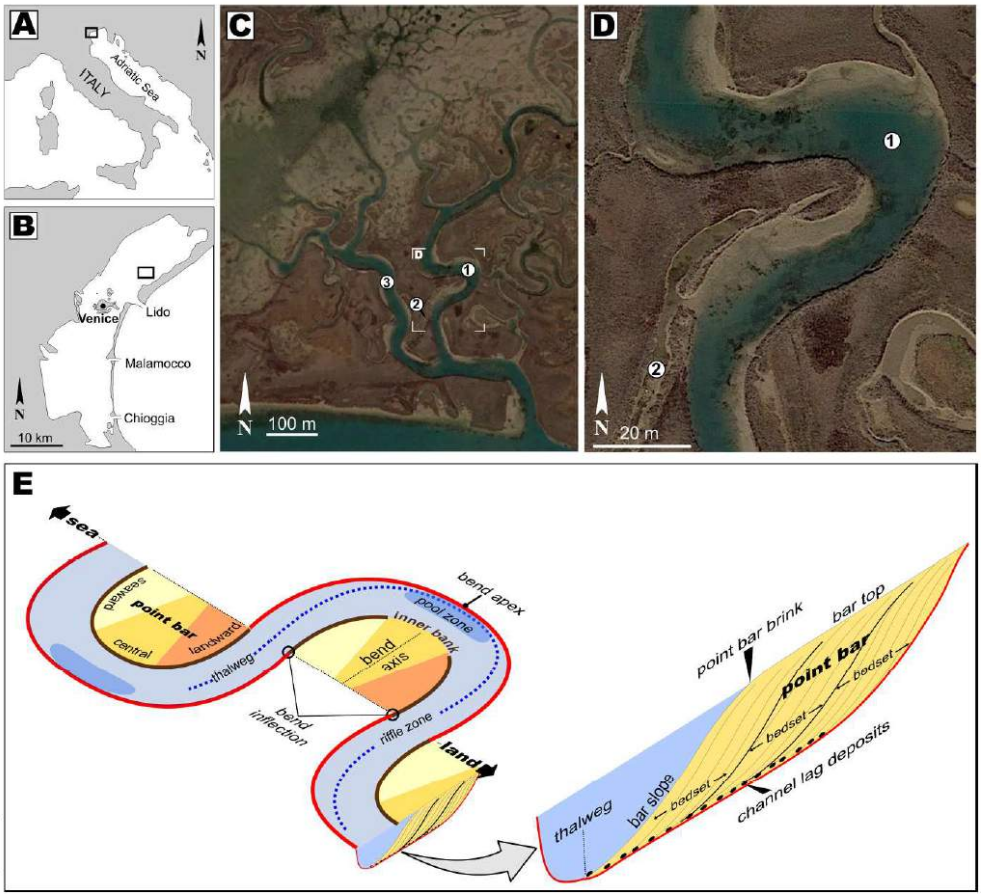

Figure B.2: (A) Location of the study site in the Adriatic sea. (B) Position of the study channel in the Venice Lagoon. (C) Channel network draining the study area. The study channel is indicated by number 1. (D) Close view of the study meander bend. (E) Descriptive terminology for meander-bend morphology and point-bar deposits.

which consist of alternating continental and shallow marine deposits accumulated under control of glacio-eustatic fluctuations (Kent et al., 2002). During Last Glacial Maximum, the Venice area experienced alluvial sedimentation in the distal reaches of the Brenta River megafan (Fontana et al., 2014). The Holocene transgression, which triggered paralic deposition in the Northern Adriatic areas, promoted the formation of the Venice Lagoon since about 7500 yrs BP (Zecchin et al., 2009). The study channel is located in the eastern sector of the lagoon (Fig. B.2B), where the Holocene deposits consist of lagoonal mud and sand up to 14 m thick (Canali et al., 2007). This area is the most naturally preserved portion of the Venice Lagoon (Marani et al., 2003) and hosts a dense network of branching and sinuous channels, which decrease in cross-sectional area as moving landward (Fig. B.2C). The two main channels draining the study area are numbered as 1 (aim of the present work) and 3 in Figure B.2C. Channels 1 and 3 are similar in size and almost NW-SE trending. They merge southward into a

single channel and were also connected by a mud-filled abandoned channel, numbered as 2 in Figure B.2C. The study channel, 15-20 m wide (Fig. B.2D), is located in the upper part of the intertidal zone and cuts through a salt-marsh platform encroached by a mosaic of halophytic vegetation species such as Limonium narbonense , Juncus maritimus, and Salicornia veneta. The meander bend shows a "simple asymmetric" planform (Fig. B.3A) (sensu Brice,1974) and its axis trends ENE- 1 WSW. It has a radius of curvature of about 17 m and varies in depth from 3.0 to 2.0 m in the channel pool and riffle zone, respectively (Fig. B.3B).

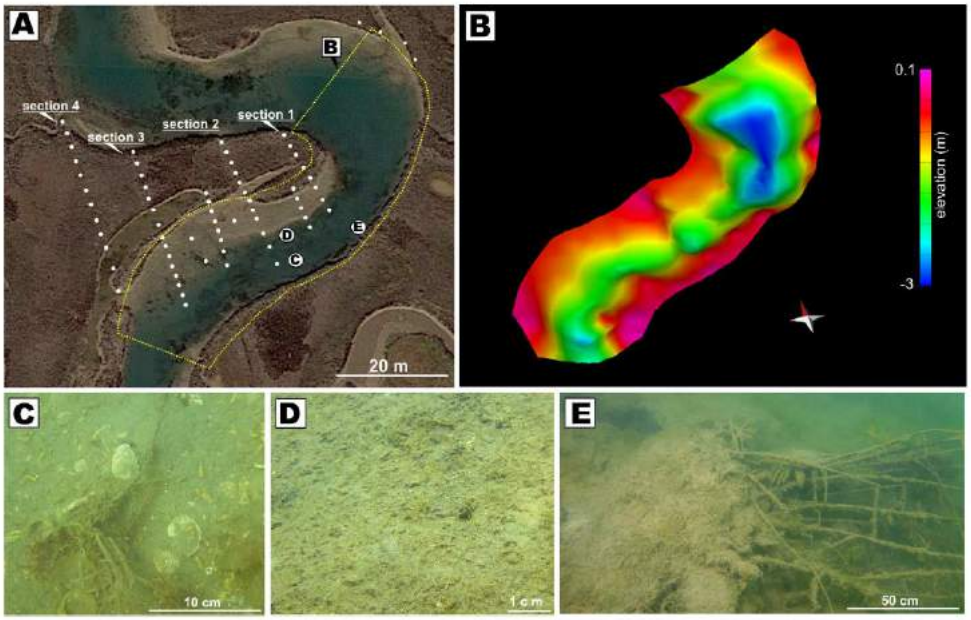

Figure B.3: (A) Location of coring sites. Cores from sections 1 – 4 are showed and correlated in Figure 9. (B) Bathymetric map of the seaward side of the meander bend. (C) Shell-rich sand from the thalweg zone. Location of the photo is shown in inset A. (D) Bioturbated depositional interface in the SE part of section 2. Location of the photo is shown in inset A. (E) Collapsed block at the toe of the outer bank. Location of the photo is shown in inset A.

Methods

Bar morphology: remote sensing and ADCP measurements

Aerial photos were used for monitoring the planform changes of the study bend since 1938. Photos were georeferenced using ArcGIS 10 (Esri) and successively superimposed in order to evaluate the lateral shifts of the channel margins. The overall planform evolution of the study bend was reconstructed along the past 77 years by analyzing four available aerial photos dating 1938, 1968, 1978 and 2015

respectively (see Fig. B.4A). Particular attention was devoted to the relationship between the meander migration and the evolution of the neighboring channel network over the past 47 years (Fig. B.4 B and C). The flow field along the entire channel bend (Fig. B.3A) as well as the bathymetry were measured using a SonTek River Surveyor M9 system, which is a robust and highly accurate Acoustic Doppler Current Profiler (ADCP) system specifically designed to measure flow discharge, 3D current profile, water depth, and bathymetry from a moving or stationary vessel.

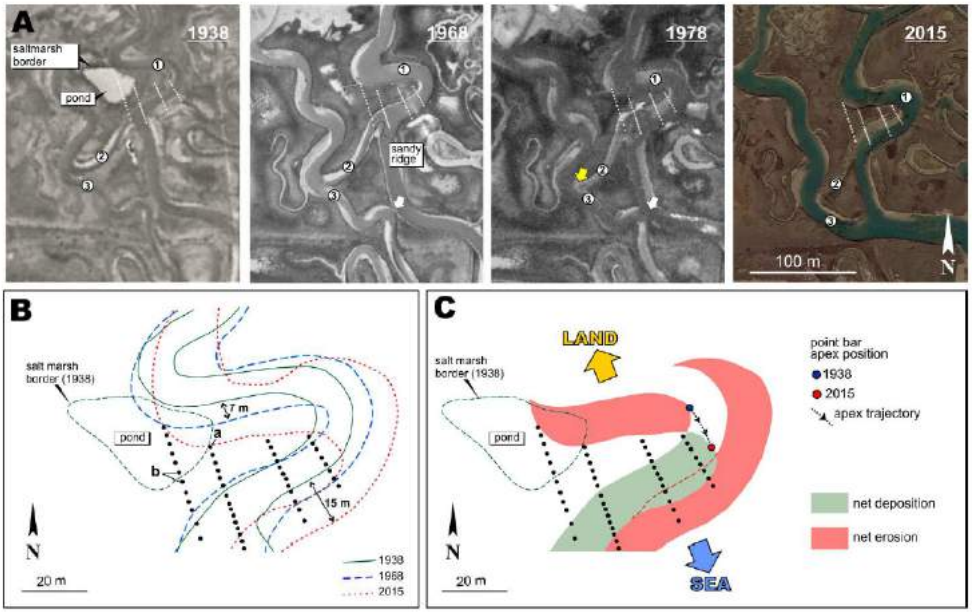

Figure B.4: (A) Evolution of the tidal network in the study area since 1938. White arrow points to the piracy where channel 1 merged with channel 3. Yellow arrow indicates deposits those dammed channel 2 causing its definitive abandonment. (B) Successive channel margins showing channel migration (1938-2015). Letters "a" and "b" indicates cores located at the boundaries of vegetation cover in 1938. (C) Areas affected by erosion and deposition over the past 77 years.

The M9 ADCP is a nine-beam system with two sets of four profiling beams (each set having its own frequency). Thanks to the use of multiple acoustic frequencies, the M9 ADCP automatically adjusts the vertical cell size moving from shallow to deep water in order to optimize performance and resolution. The velocity profiling range spans from 0.2 to 30 m. An additional 0.5-MHz vertical acoustic beam (echo sounder) provides water depth data together with a precise bathymetric survey. The presence of and integrated Differential Global Positioning System (DGPS) provides a sub meter precision in positioning data collected by the M9 ADCP. The SonTek M9 ADCP has been recently tested and validated by the USGS Office of Surface Water (Boldt and Oberg, 2015). The georeferenced bend bathymetry provided by the

ADCP vertical beam (Fig. B.3B) was integrated on the basis of direct underwater snorkeling observations (Fig. B.3C - E).

Bar sedimentology: sedimentary cores and 3D modelling

A total of 63 cores were recovered on the bar top and adjacent channel, whereas 4 additional cores were recovered from the outer bank zone (Fig. B.3A). The position of the cores was georeferenced using differential GPS TOPCON GR-3 receivers – dual frequency (L1/L2) and dual constellation (NavStar/Glonass) with integrated Tx/Rx UHF radio. Cores were recovered using an Ejikelkamp hand auger, through a gouge sampler with a length of 1 m and a diameter of 30 mm. Coring depth spans from 1 to 3 m. Collected cores were kept humid in PVC liners and successively cut longitudinally, photographed and logged. Core logging was carried out following the basic principles of facies analyses, emphasizing sediment grain size and color, presence of sedimentary structures, vertical grain-size trends, degree of bioturbation and occurrence of plant and/or shell remains. Integration between core location and related sedimentary features allowed us to define different types of deposits that will be described and discussed in the following section.

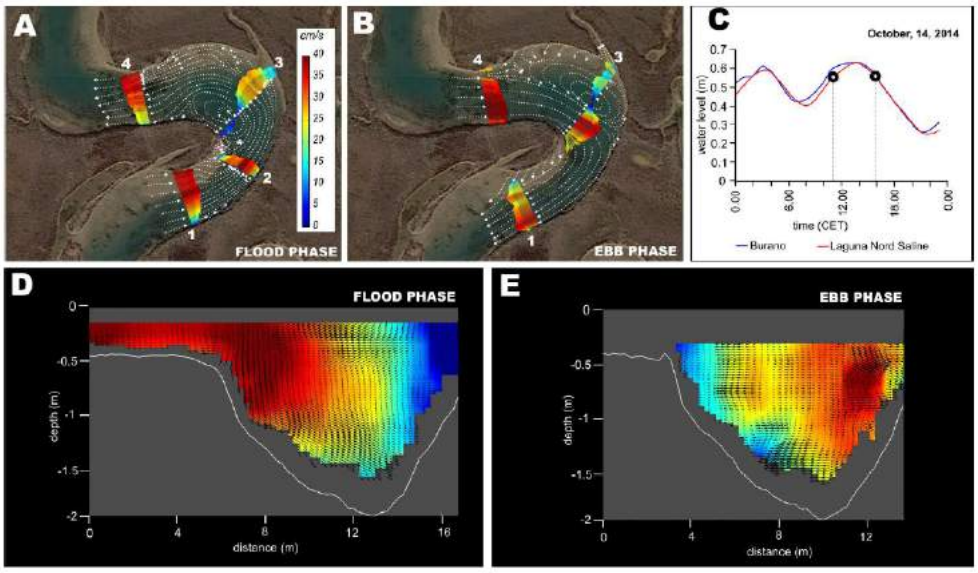

Figure B.5: Velocity distribution along the study bend. (A) and (B): Plan-view 825 of depth averaged velocities for the surveyed sections. Velocity magnitude is represented by both color scale and vector lengths. Dotted lines stand for possible depth-averaged flow trajectories. (C) Water level recorded from two gauge stations ("Burano" and "Laguna Nord Saline") close to the study site indicating the two instants when the ADCP measurements were collected. (D)and (E): Cross-sectional view of section1 during ebb and flood phases. Colors indicates Rozovskii primary velocity magnitude, whereas vectors stand for bot direction and intensity of Rozovskii secondary velocity.

Vertical and lateral changes in sediment grain size were highlighted analysing 183 sediment samples selected from different parts of the bar. Grain size analysis was carried out through a Mastersizer 2000 (Version 5.40, MALVERN INSTRUMENTS). The Mastersizer measures the size of particles by laser diffraction quantifying the intensity of light scattered as a laser beam passes through the dispersed particulate sample. These data are then analyzed to calculate the size of particles that created the scattering pattern. Study cores were correlated along 2D sections (see Fig. B.3A) which, once placed in a virtual space, enabled us to define a 3D model of bed stratigraphy using the MoveTM 2014.2 software. Architectural modeling was limited to the portion of the bar accumulated over the past 47 years. Terminology used in the present work to indicate different parts of channel bend and related bar is shown in Figure B.2E.

Results

Planform Evolution

Comparison between georeferenced 1938-1968 aerial photos (Fig. B.4A) shows that channels 1 – 3 did not change significantly their planform configuration. During the early 70's, channel 1 pirated channel 3 (white arrow in Fig. B.4A), causing a deactivation of the portion of channel 3 located seaward of the piracy site. This network reorganization promoted sediment accumulation at the confluence between channel 2 and 3 (yellow arrow in Fig. B.4A), which was consequently dammed and filled with mud. Differently, after the piracy event, channel 1 significantly increased its width seaward of the piracy site (Fig. B.4A). Since 1938, the planform evolution of the study bar was characterized by a progressive seaward shifting that moved the point bar apex along a trajectory transverse to the bar axis (Fig. B.4B and C).

Over the past 77 years, the landward and seaward sides of the bar shifted of about 15 m (Fig. B.4B), allowing the bar to maintain an overall asymmetric profile. Bar top areas were covered by halophytic vegetation since 1968, whereas a wide unvegetated area (i.e. pond) occupied the innermost part of the bar in 1938 (Fig. B.4A). Aerial photos show that the drainage reorganization, occurred during the early 70's, caused a significant change in seaward migration rate of the study bar. Specifically, between 1938 and 1968 the landward side of the bar shifted faster than the seaward one that almost did not migrate and occupying the same position and pivoting around the bend inflection point (Fig. B.4B). During this time span the landward side of the bar migrated ca. 7 m, with a rate of about 20 cm/yr. Differently, after the piracy event, the migration rate of the seaward side of the bar shifted ca. 15 m (Fig. B.4B), with an average migration

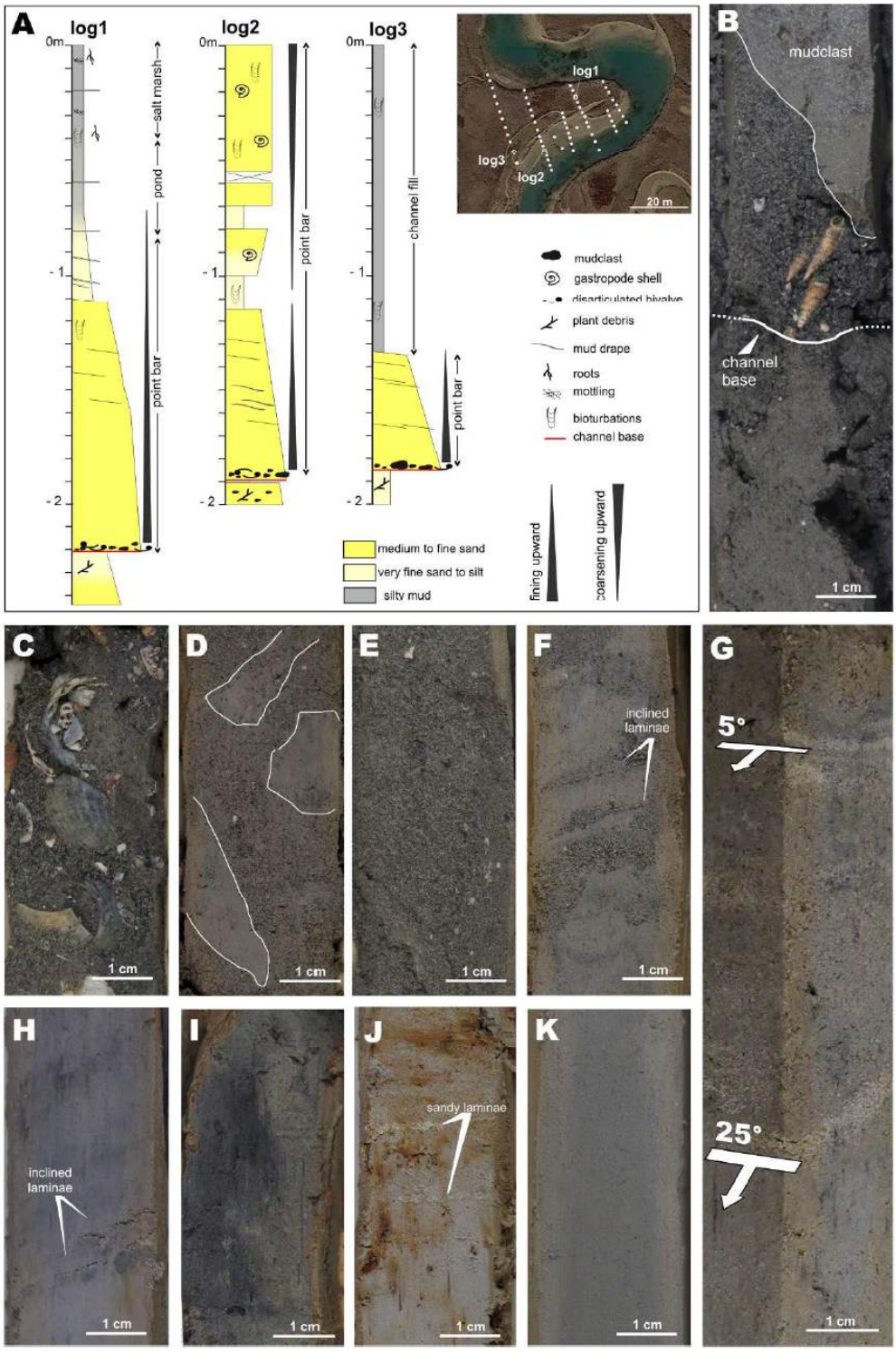

Figure B.6: (A) Sedimentological logs across point bar deposits characterized by different vertical grain-size trends. (B) Shell-rich channel lag sand with a pebble-sized mudclast. (C) Channel lag sand with abundant disarticulated and fragmented bivalves (Cerastoderma edule). (D) Massive sand with isolated pebble-sized mudclasts in the lower part of bar deposits. (E)Massive sandy bar deposits. (F – G) Heterolithic bar deposits consisting of silt with a variable amount of inclined sandy laminae. Note the upward decrease in dip angle of sandy laminae shown in G. (H) silty bar deposits with inclined laminae of well-sorted, fine to very fine sand. (I) Organic-rich massive pond mud. (J) Oxidized salt marsh mud containing laminae of well- sorted fine sand. (K) dark, massive channel-fill mud.

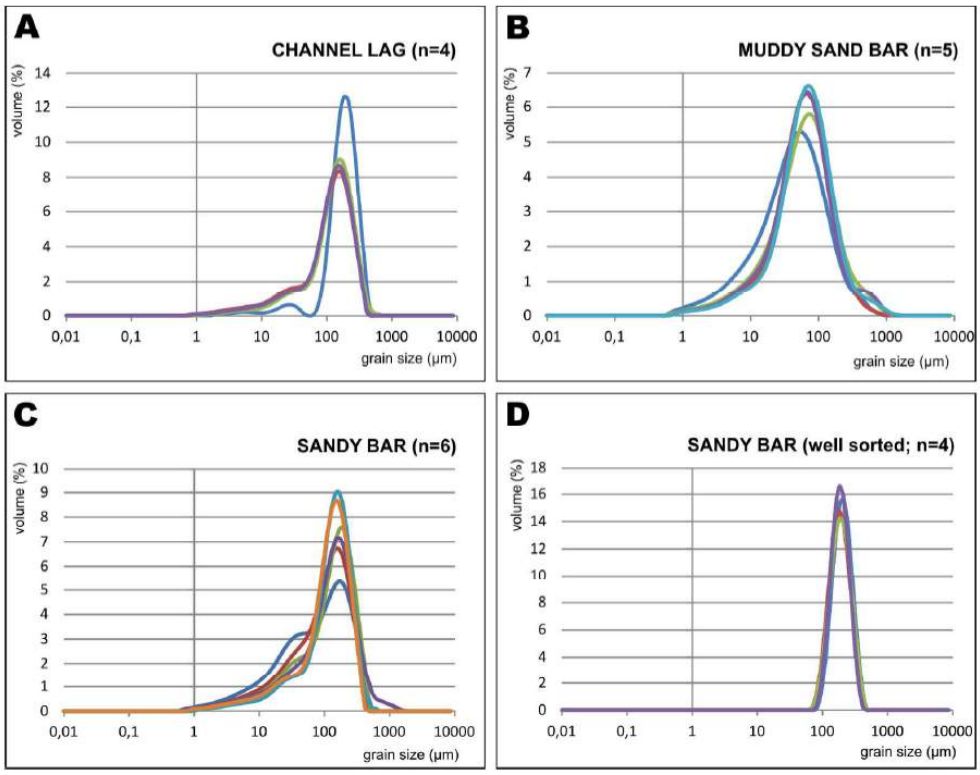

Figure B.7: Grain size of channel lag and bar deposits. (A) Channel lag. (B) Muddy sand bar deposits. (C) Sandy bar deposits. (D) Mud-free sandy bar deposits.

rate of about 30 cm/yr. Because of this migration, the confluence zone between channel 1 and 2 was progressively covered by deposits accumulated along the seaward side of the bar (Fig. B.4A and B).

Velocity Distributions

Flow velocity profiles collected using the SonTek River Surveyor M9 ADCP at different cross sections along the channel bend (Fig. B.5) allowed us to identify the main characteristics of the hydrodynamic flow field. Data were collected at 4 cross sections during the flood phase (Fig. B.5A) and at 3 of the same cross sections during the subsequent ebb phase (Fig. B.5B). Plotting the 2D depth-averaged velocity vectors across each section enabled us to reconstruct the 2D flow patterns along the bend (dashed stream lines in Fig. B.5A and B). These patterns display quite different features during the flood phase and the ebb phase. More precisely, during the flood phase flow velocities are high (ca. 40 cm/s) along the seaward side of the bar (section 1) due to the presence of a meander bend seaward of the considered section 1 (see Fig. B.2C and D). Moving landward, the flux tends to concentrate along the outer bank (sections 2,3 and 4), whereas quite a large eddy was observed to form close to the point bar apex (section

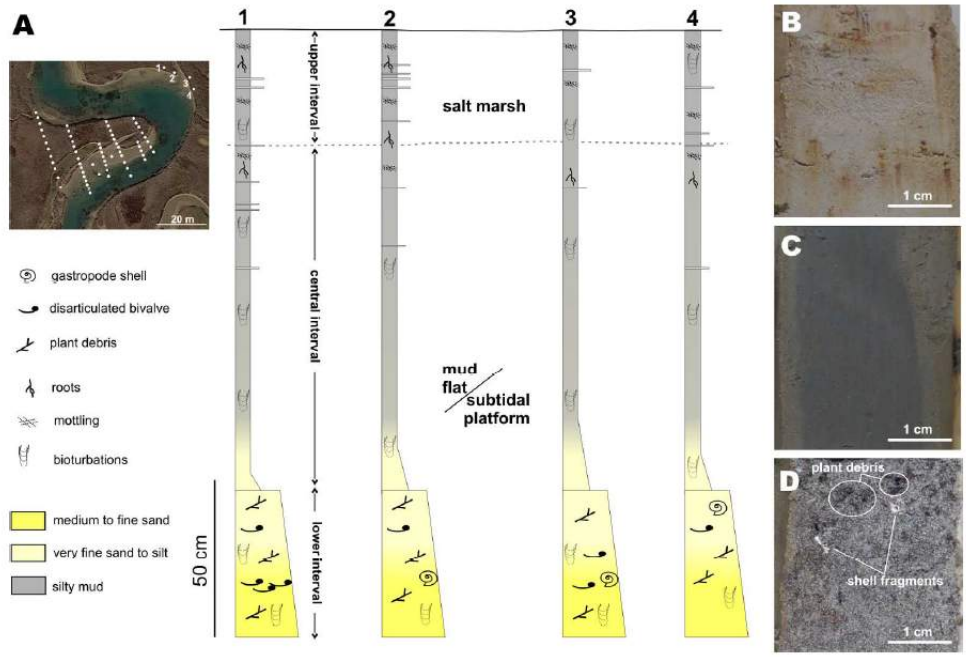

Figure B.8: (A) Sedimentological logs across outer bank deposits. (B) Oxidized salt marsh mud. (C – D) Massive mud (C) and sand (D) accumulated in mud flat/subtidal platform depositional setting.

3). During the ebb phase, on the contrary, the flux is almost uniform across section 4 while, moving seaward, it tends to concentrate along the point bar apex (section 3) and toward the outer (southern) bank at section 1. A large eddy recirculates the flow in the outer part of the bend upstream (landward) of the point bar apex, between section 3 and 4. Figure B.5D and E provide the 2D vertical flow patterns during the flood and the ebb phase, respectively, across section 1 which is located in the middle of the area where cores were recovered. Interestingly, as we shall discuss in the following, the cross-sectional flow pattern adds useful information for understanding the sedimentological evolution of the study meander bend. In Fig. B.5D and E colours represent the primary velocity (Rozovskii definition, see Lane et al. 2001), while arrows represent the secondary flow vectors.

A well- established counter clockwise secondary current clearly characterizes the flood phase (Fig. B.5D) with water flowing toward the inner bank in the upper part of the cross section and toward the outer bank in the lower part of the cross section. Flow velocity displays higher values in the upper part of the bar and it slows down moving toward the center of the channel. During the ebb phase (Fig. B.5E) a clockwise secondary current is observed which is characterized by water fluxes toward the outer bank in the upper part of the cross section and toward the inner bank in the lower part of the cross section.

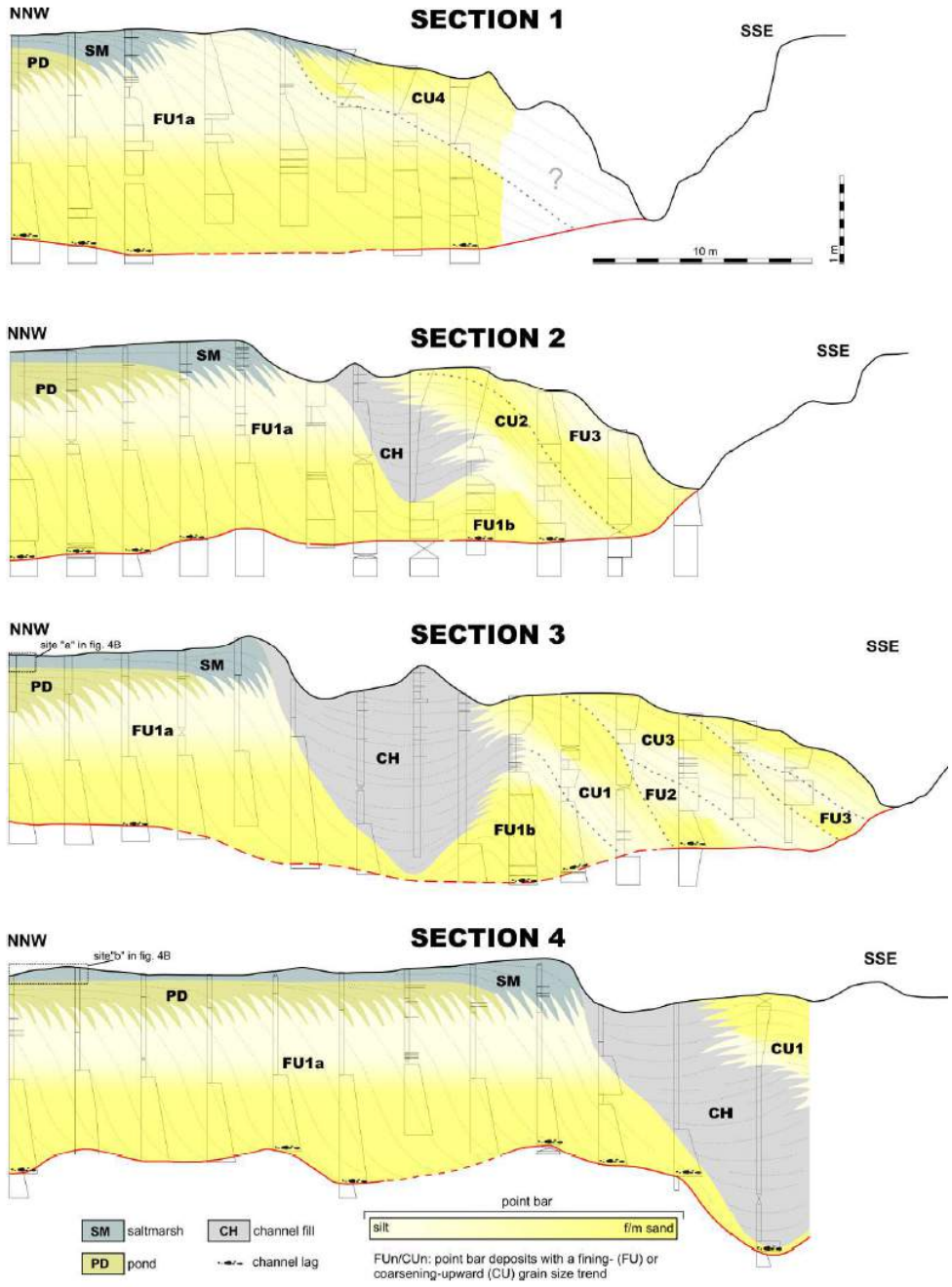

Figure B.9: Stratigraphic cross sections across bar deposits (see Figure B.1 for location).

In this case, flow velocity displays higher values in the center of the channel and lower values when climbing the seaward side of the bar.

Core Data

CHANNEL LAG DEPOSITS Channel-lag deposits occur at a core depth spanning between 1.8 and 2.3 m. They are 5-10 cm thick (Fig. B.6A)

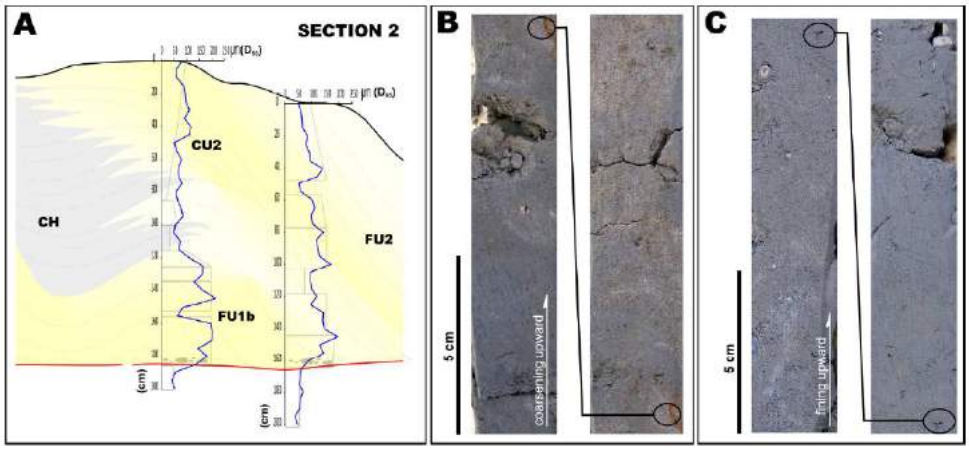

Figure B.10: (A) Vertical grain size (D50) trends in point bar deposits of section 2. (B-C) Coarsening- and fining-upward grain size trend in cores recovered from the seaward side of the bar.

and consist of massive grey-bluish fine to medium sand (Fig. B.7A) draping an erosional surface cut onto plant-debris rich sand. This latter sand is clearly visible also in cores recovered from overbank areas (Fig. B.8) and is described and interpreted further in the text. Channel lag sand contains abundant shells and shell fragments (Fig. B.6B and C) and mud clasts (Fig. B.6B) that are up to 6 cm in diameter. Locally, vertical cylindrical burrows cut through the sand and the underlying deposits.

These deposits accumulated in the deeper part of the channel, where currents exerted the maximum bottom shear stress (cf. Barwis and Hayes, 1979; Terwindt, 1988). This process causes winnowing of the fine-grained deposits and accumulation of coarse particles including shell fragments (Fig. B.3C). Pebble-sized mudclasts derived from fragmentation of blocks collapsed from the flanks of the channel (cf. Terwindt, 1988).

POINT BAR DEPOSITS Point bar deposits are found in all the cores located within the meander loop and appear to be up to 1.9 m thick (Fig. B.6A). They cover the channel-lag sand and are overlain by salt marsh, channel-fill of pond deposits. Bar deposits consist of sand or sandy silt (Fig. B.7B and C). Sandy deposits commonly contain a limited amount of mud, that can be locally concentrated in millimetric laminae. Sandy deposits appear mainly massive (Fig. B.6E) or faintly laminated, although the reduced diameter of cores and intense bioturbation prevent from detecting specific sedimentary structures. These deposits are locally well-sorted and deprived of muddy fraction (Fig. B.7D). Shells and shell fragments are not common, although they can be locally concentrated in 1-3 cm thick layers. Where sandy deposits occur close to the boundary with the channel lag sand, they include

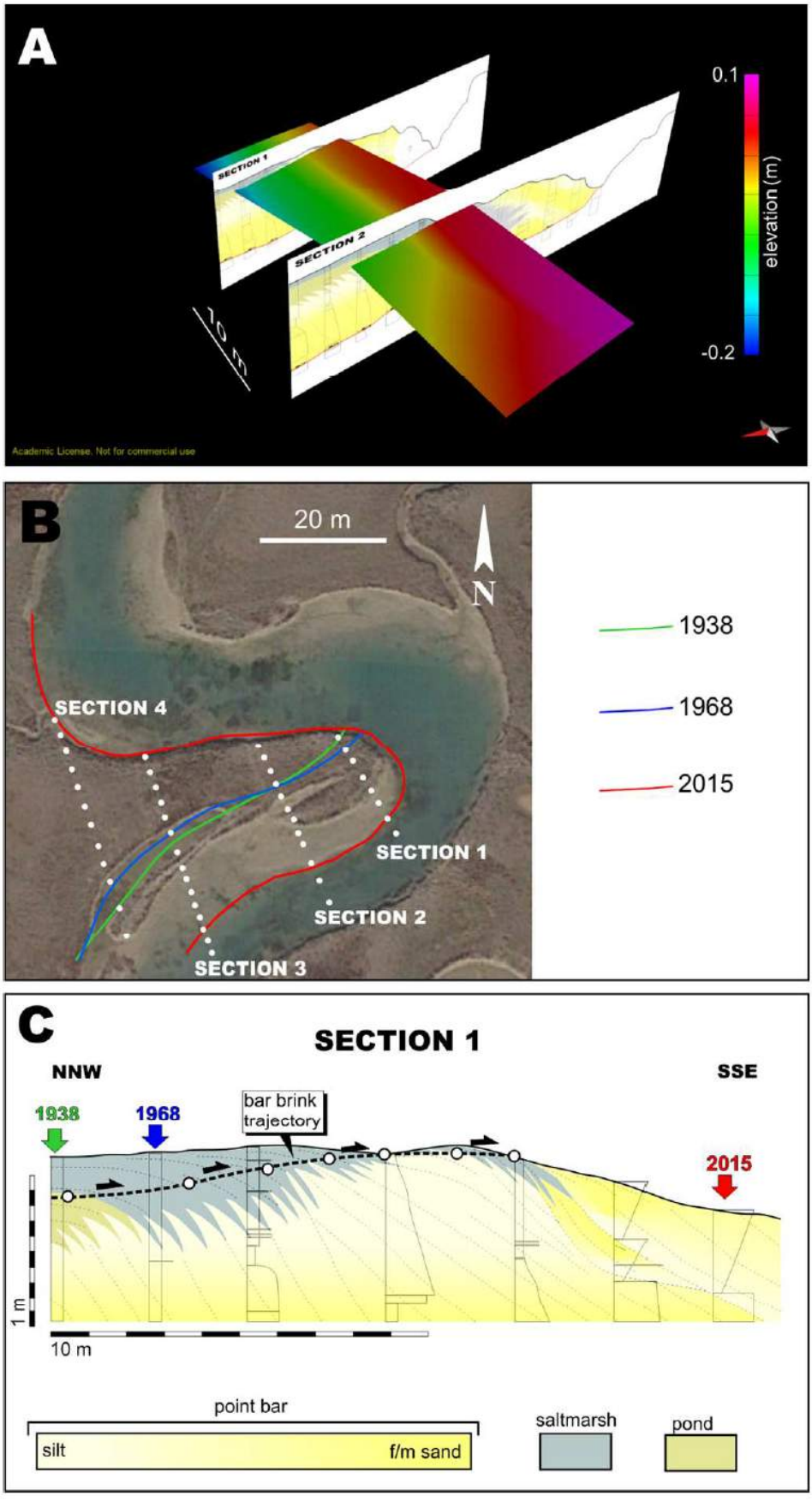

Figure B.11: (A) 3D model showing spatial orientation of the surface flooring salt marsh deposits. (B) Location of successive channel margins along the seaward side of the bar (1938-2015). (C) Close view of Section 1 showing trajectory defined by the bar brink during shift of the channel bank occurred between 1938 and 2015.

scattered, pebble-sized mudclasts (Fig. B.7D). Sandy silt deposits consist of greyish massive, silt with a variable amount of very fine to fine sand (Fig. B.7B). These deposits show an inclined heterolitic stratification, with laminae dipping at between 5° and 15° (Fig. B.6F). Where the silty fraction is dominant, inclined laminae consist of well-sorted, fine to very-fine sand (Fig. B.6H). Inclination of laminae decrease moving upward in the bar (Fig. B.6G). Bar deposits are bioturbated, although bioturbation is more concentrated in the finer-grained intervals. Sandy and sandy silt deposits are organized into define different vertical grain size trends, those range from a fining- to fining – coarsening-upward (Fig. B.6A, B.9 and B.10). Despite these grain-size changes are well visible in the cores (Fig. B.10B and C), they appear as subtle changes in the D50 curves (Fig. B.10A), as consequence of the relatively low sediment textural sorting (Fig. B.7B and C). These sediments accumulated in a point bar setting (cf. Rieu et al., 2005; Santos and Rossetti, 2006) following the lateral shift of the main channel bend (Fig. B.4). Sandy deposits were accumulated where tidal fluxes and the related bottom shear stresses where high enough to remove the muddy fraction, thus allowing local concentration of shells and shell fragments. Local occurrence of millimetric muddy laminae suggests that ebb and flood currents removed the majority of the fine-grained deposits settled on the bar during slack water phases, possibly during exceptional conditions such as during spring tides (Jablonski and Dalrymple, 2016). Sandy silt accumulated in areas of reduced bottom shear stress, where fallout from suspension was the dominant sedimentary processes. Where muddy deposits occur in the upper part of the bar, millimetric laminae of well-sorted sand are thought to be formed during storm events, when salt marshes and bar top were deprived of mud by wave winnowing (Green and Coco, 2007; Fruergaard et al., 2011; Carniello et al., 2011; Green and Coco, 2014; Choi and Jo, 2015). The upward decrease in inclination of lamination, that is documented both in sandy silt and muddy deposits, reflects the flattening of the bar morphology moving from bar slope to bar top.

POND DEPOSITS Pond deposits occur in the cores located on the bar top and are up to 15 – 25 cm thick. They are sandwiched between point-bar and salt-marsh sediments, and consist of massive, organic-rich dark mud (Fig. B.6I). They can locally contain wood fragments or bivalves (Cerastoderma glaucum) in life position, or even roots from the overlying salt-marsh deposits. Transition toward the salt-marsh deposits occurs through a gradual change in color and increase in root elements. Pond deposits formed in a protected area in the middle-lower part of the intertidal zone, where low elevation above the mean sea level prevented growth of halophytic vegetation and soil oxidation (Silvestri et al., 2005; Roner et al., 2016). Mud settled from suspension

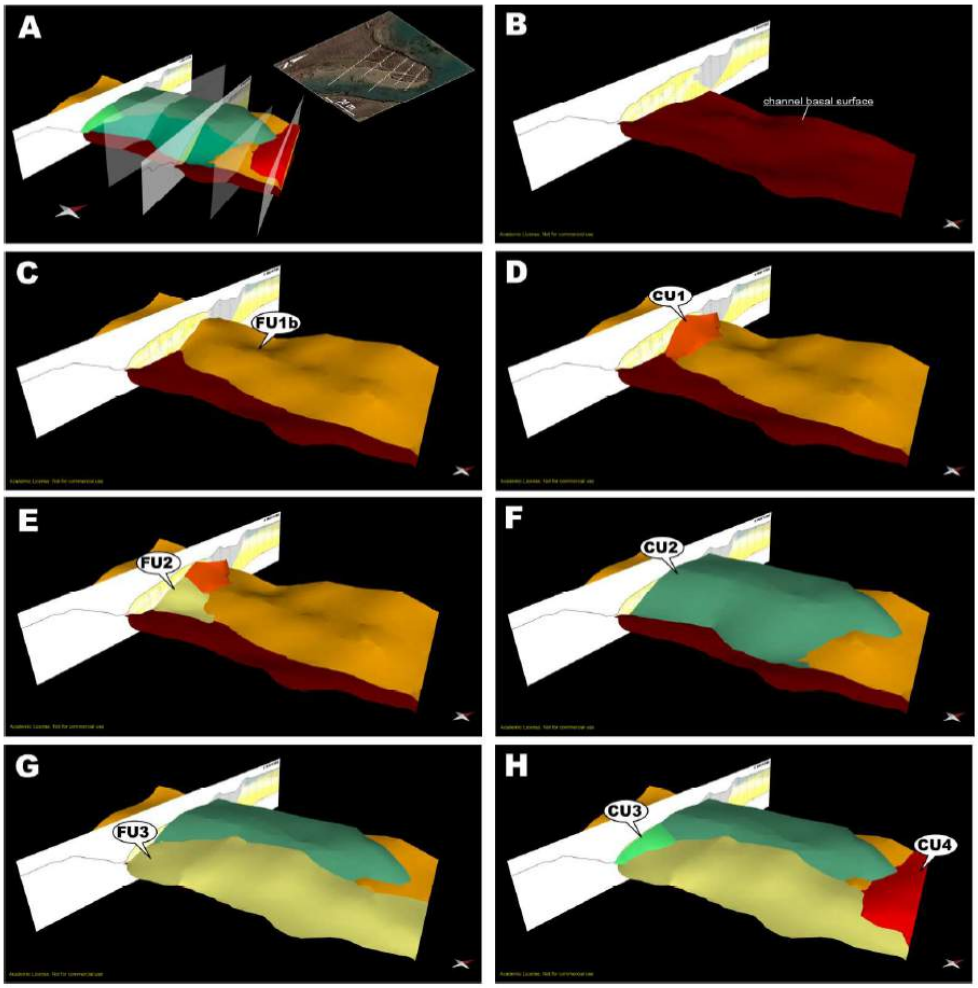

Figure B.12: (A) Tridimensional reconstruction of bar architecture. (B) Geometry of the channel basal surface, flooring point bar deposits. (C – H) Spatial distribution and geometries of different FU and CU packages accumulated on the seaward side of the bar between 1938 and 2015.

(cf. Davis, 2012), probably during high water slack at the end of the flood phase.

SALT MARSH DEPOSITS Salt-marsh deposits occur just below the vegetated bar top surface and are widespread in the bar top zone. They are up to 30 cm thick, and consist of a horizontally- laminated, brownish, mottled mud, with a of fine to very fine sand (Fig. B.6J). Plant debris and organic matter are seldom present within dark, 1-2 mm thick, muddy laminae. In situ roots and bioturbation are common. Sand is concentrated within 1-3 mm thick horizontal laminae (Fig. B.6J), which show a remarkable grain-size sorting. Salt-marsh deposits accreted due to the joint contribution of mud settling and direct capture di vegetation (e.g., Allen, 2000; D'Alpaos et al., 2007; Mudd et al., 2010) and organic matter deposition (e.g., Nyman et al., 2006; Roner

et al., 2016 ;). Oxidations and widespread rooting account for sedimentation in the upper part of the intertidal zone, that is completely flooded only during spring high tides and storm events (Silvestri et al., 2005, D'Alpaos et al., 2013). Organic-rich muddy laminae point to slightly reductive conditions, due to the presence of stagnant water in small ponds. Mud deposited mainly during high water slacks, at the transition between flood and ebb tide. Textural sorting of sandy laminae, suggest they were generated at high tide conditions during storm events, when wind-induced waves winnowed the salt marsh surface (Moeller et al., 1999), suspending mud and concentrating coarser particles (Choi and Jo, 2015).

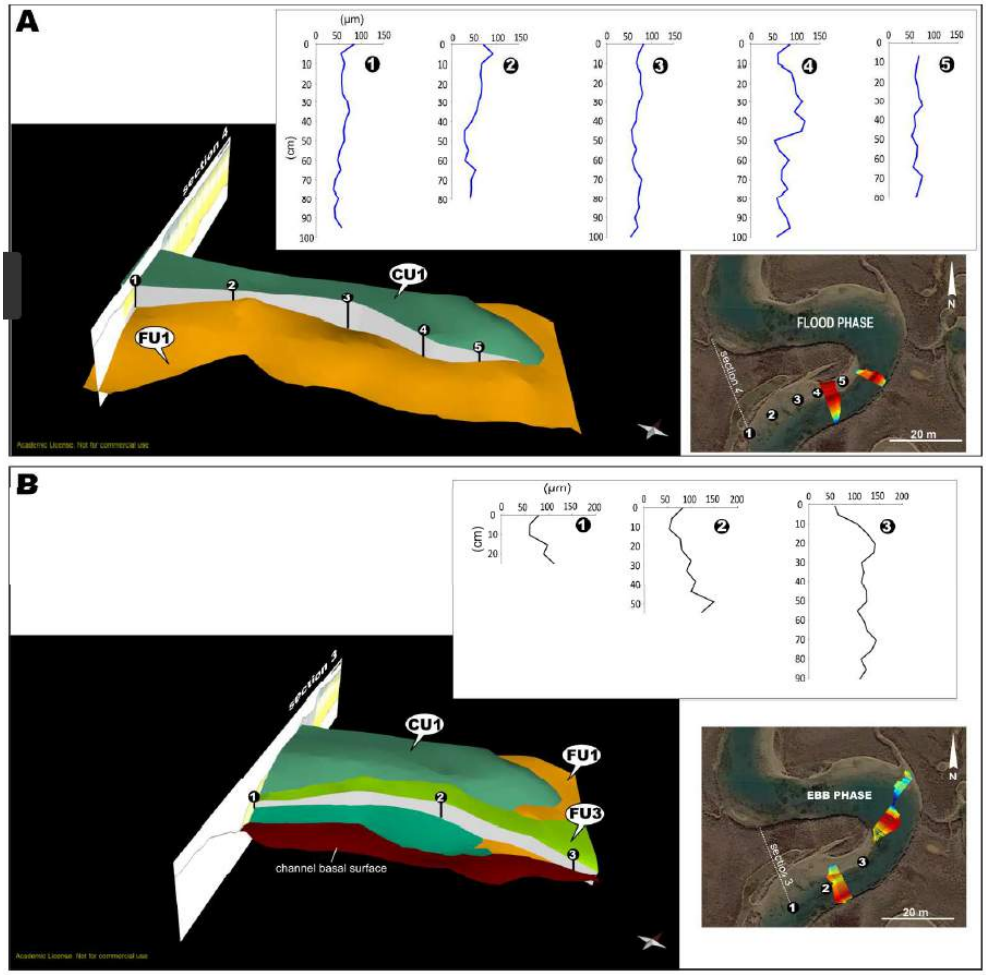

Figure B.13: (A) Along-strike changes in grainsize for package CU1. (B) Along-strike changes in grainsize for package FU3.

CHANNEL–FILL DEPOSITS Channel-fill deposits occur in all the cores distributed along the planform profile of channel 2. They are up to 2.2 m thick and consist of dark, massive mud (Fig. B.6K) with dispersed bivalves in life position. In places, close to the top of the de-

posits, they can be either sandier or characterized by mottling and root traces. Location and sedimentary features of these deposits suggest that they mainly settled down in channel 2 after its deactivation. We deem their structureless texture to be the result of intense bioturbation (cf. Davis, 2012). The presence of a sandy fraction in the upper part of the channel-fill suggests that the latest stage of infill was locally associated to an increase in clastic input, that possibly occurred under tractional conditions. Differently, the local presence of mottling and roots points to local subaerial exposure, that heralds colonization from salt-marsh halophytic vegetation.

OUTER BANK DEPOSITS The four cores recovered from the overbank zone (Fig. B.8A) show that stratigraphy of this area is characterized by three vertically stacked, tabular intervals. The upper interval is about 35 cm thick and is made of horizontally-laminated, brownish, mottled mud (Fig. B.8B). 3 Mud is commonly rooted and contains both 1-3 mm thick, organic-rich laminae and 1-2 mm thick layers of well-sorted, fine sand. The central interval is about 110-120 cm thick and consists of massive, bioturbated mud (Fig. B.8C), that contains isolated, 1-3 mm thick layer consisting of well-sorted, fine sand. The lower interval is at least 50 cm thick and is made of medium sand grading upward into silty mud. The sandy portion is made of massive sandy deposits with subordinate muddy layers. Sand is medium to fine in grain size and contains sparse shells and shell fragments (Fig. B.8D). Plant debris is common and locally form 1-5 mm thick layers. Sand is massive, due to the intense bioturbation, although traces of a primary plane-parallel stratification can be locally detected. Mud is mainly massive and contains scattered shells and wood fragments. Mottled mud of the upper interval is interpreted as to be formed in a salt-marsh setting, given its marked similarity with oxidized mud capping the study point bar. Deposits of the central interval settled down from suspension in a low-energy environment, and could be consistent with the presence of a former tidal flat/subtidal platform or an abandoned channel setting. The occurrence of laminae of well-sorted, mud-free sand points to an open environment occasionally affected by winnowing of the depositional interface. This reconstruction would be consistent with a tidal flat/subtidal platform area affected by wind-induced storm events. The sandy beds of the lower interval were originated in a tidal flat/subtidal platform area, where wave winnowing deprived the lagoon floor of fine- grained deposits (e.g., Carniello et al., 2009). A contribute to deposition of this sandy interval could also have been provided either by riverine flood flows, that entered the lagoon during main storm events (D'Alpaos, 2010), or washover events from the barrier. 3 Muddy layers formed under fair-

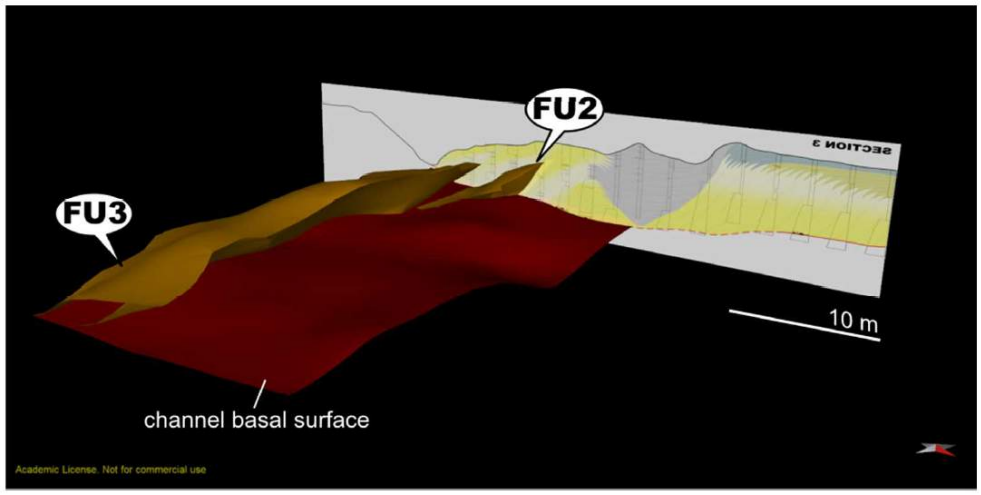

Figure B.14: Spatial distribution and geometry of fining-upward sedimentary packages accumulated on the seaward side of the bar between 1938 and 2015.

weather conditions, especially after storm events, when suspended mud settled down to the bottom.

Stratal architecture

The 3D model obtained from spatial interpolation of differently oriented sections (Fig. B.9,B.11 and B.12A) reveals the internal architecture of the study bar. The base of the bar body is represented by the surface flooring the channel lag deposits, that appears as an uneven horizontal surface (Fig. B.9 and B.12B). Above this surface, a muddy channel fill (CH) separates two main fining-upward sandy packages (e.g. Section 3 in Figure B.9). These packages are named here FU1a and FU1b, and are located NNW and SSE of the CH deposits, respectively. Comparison between the location of the cores and historical photos (Fig. B.4A and B) shows that CH mud fits with the infill of channel 2, and that the FU1a package corresponds to the older deposits of the study bar. FU1b deposits fit with the sandy ridge separating channel 3 from channel 2 before the latter was deactivated (see the 1968 image in Figure B.4A). A number of coarsening- and fining-upward accretionary packages (FU2 – 3 and CU1 - 4), cover FU1b along the seaward side of the bar (Fig. B.9 and B.12). Finally, point bar deposits are capped by pond (PD) and salt-marsh (SM) mud (Fig. B.9). Two main features of the bar deposits will be shown here in detail: i) spatial geometry of the surface flooring the salt-marsh mud (Fig. B.9 and B.11); ii) architecture and grain-size distribution of packages FU2 – 3 and CU1 – 4 (Fig. B.9, B.10 and B.12 – B.14). The surface flooring the salt marsh deposits gently dips toward NE (Fig. B.11A), highlighting that maximum thickness of these deposits

occurs in the NNW reach of Section 1 (Fig. B.11C). Sections transverse to the bar axis (Fig. B.9), show that salt-marsh deposits thin toward the seaward side of the bar and pinch out in correspondence of the current edge of the marsh. Inclination of the basal surface of salt-marsh deposits is well-visible in the point bar apex zone, where the maximum bar shift occurred since 1938 (Fig. B.5B and C). In this area, positioning of 1938 and 1968 bar edge on the present day morphology (Fig. B.11B) shows that the bar brink shifted seaward following a rising trajectory (Fig. B.11C), that tends to flat down after 1968. The coarsening- and fining-upward packages accumulated above FU1 appear as lens- shaped units characterized by a variable geometry, thickness and textural features. Along-dip sections (Fig. B.9) show that coarsening-upward packages are commonly developed along the whole bar slope (e.g. CU1 in Section3 of Figure B.9), whereas fining-upward packages are more common in the middle-lower part of the slope (e.g. CU1 in Section3 of Figure B.9). Along-strike extent of CU/FU packages is variable (Fig. B.12), since they can be locally (e.g 4-5 m of CU1; Fig. B.12D) or largely developed (e.g 25-30 m of FU2; Fig. B.12G). CU packages tend to fine and thin both downdip (Fig. B.9) and toward the bend apex (core 1 to 5 in Fig. B.13A). FU packages fine and thin updip (Fig. B.9) and toward the bend inflection (core 3 to 1 in Fig. B.13B). Volumetric distribution of CU and FU packages shows that CU deposits (CU1 – 4) are more abundant than FU ones (FU2 – 3), those consist of two blade-shaped bodies striking parallel to the bend axis and pinching out updip and toward the bend apex (Fig. B.14)

Discussion

Bar development, aggradation and migration rates

Time and mode of bar development and evolution can be addressed coupling sedimentological analyses, historical photos (1938-2015) and the characterization of the flow field The occurrence of pond mud over the oldest bar deposits (i.e. those located in the NNW part of sections 1 – 4) suggests that the bar developed where the tidal fluxes and the low elevations of the surface, prevented halophytic vegetation growth on the bar top (i.e. lower part of the intertidal zone). Greening of the bar top started when sediment advected from the channel to the marsh platform and direct spillover from the channel (cf. Mariotti and Fagherazzi, 2012) formed channel levees and those were colonized by halophytic vegetation, that progressively expanded toward the inner part of the bar. This reconstruction is supported by bar configuration showed by the 1938 aerial photo (Fig. B.5A), where a remnant of a non-vegetated pond was still preserved in the innermost part of the

bar (i.e. section 3 and 4 area). Similarity between the maximum thickness of bar-top and overbank salt-marsh mud suggests that vegetation encroachment of the platform occurred simultaneously in those areas. Integration between the 1938 aerial photo and core data from section 4 allowed us to estimate an average aggradation rate for salt-marsh deposits. Specifically, the 1938 aerial photo shows that two coring sites (sites a and b in Figure B.5B) were located at the border of the pond located in the bar top area. In these sites, salt-marsh deposits are about 20 cm thick (Fig. B.9) indicating a salt marsh aggradation rate of ca. 2.5-3.0 mm/yr. This aggradation rate is consistent with values obtained in the San Felice area by Bellucci et al., (2007), Rizzetto and Tosi, (2011), and Roner et al., (2016). Aggradation of salt marshes during bar migration (cf. De Mowbray, 1983) is documented also by the rising trajectory depicted by the bar brink (Fig. B.11C). Aggradation of the salt marsh, which keeps pace with the rate of relative sea-level rise through organic and inorganic accumulation (Morris et al., 2002; D'Alpaos et al., 2007; Mudd et al., 2010), causes a rise of channel banks. Rising of the channel banks allows the accommodation of an increased tidal prism, and a progressive thickening of bar deposits in the direction of channel shifting (cf. Brivio et al., submitted). Historical aerial photos also show that the rate of channel lateral shifting increased over the past 77 years. Specifically, the abrupt increase in the migration rate occurred during the early 70's can be ascribed to an increase in water discharge due to the above described piracy event and subsequent merging of channels 1 and 3 (Fig. B.4A). This change in the migration rate is also documented by flattening of the bar brink trajectory (Fig. B.11C), which points to an increase in the ratio between lateral and vertical migration rate of the brink. These changes highlight the strong sensitivity of tidal channels to the reorganization of the tidal network and emphasize that the evolution of single tidal meandering channel cannot be addressed without considering the evolution of the of the surrounding areas. Overall, current meandering patterns in the tidal landscape retain the signatures of processes which act at larger spatial scales. Nevertheless, migration rates measured here are consistent with those obtained by recent works on meandering channels of the Venice Lagoon (Finotello et al., 2015) and by other studies on salt-marsh systems (Garofalo, 1980; Gabet, 1998).

Linking morphodynamics with sedimentary patterns (1968–2015)

FORCING ON PLANFORM EVOLUTION Planform changes affecting the study channel over the past 47 years caused a progressive shift of the point-bar apex along a trajectory that was almost transverse to the bend axis (cf. Fig. B.4C). Such an evolution is consistent with a translation planform evolution (Fig. B.1A) and challenges the classical "expansional" (sensu Jackson, 1976) planform behaviour of tidal meander

bends (Hughes, 2012). Similar processes are documented in other sites of the Venice Lagoon (Fig. B.1F) and in other lagoons worldwide (Fig. B.1B – E), pointing to a common incidence of these processes in tidal networks. Translation of point bars is widely documented in fluvial setting (Sundborg, 1956; Nanson, 1980; Nanson and Page, 1983; Hickin, 1986; Smith et al., 2009; Nicoll and Hickin, 2010), where the point-bar apex migrates downstream following a trajectory that is transverse to the channel-bend axis. Translation (or "downstream migration" sensu Smith et al., 2009) causes erosion and deposition in the upstream and downstream side of the bar, respectively, and produces point-bar deposits well documented in the stratigraphic record (Willis, 1993; Makaske and Andweerts, 2005; Fustic, 2007; Smith et al., 2009; Ghinassi et al., 2014; Ghinassi et al., 2013; Durkin et al., 2015). The study bar shows a marked asymmetric cross-sectional profile, due to dominance of erosive processes along its landward side. Accordingly, the preserved bar body is expected to be represented by deposits accumulated along its seaward side (i.e. seaward-dipping beds). Downstream migration of fluvial point bars occurs where meander belts are confined within valley flanks, or where outer banks undercut poorly erodible muddy channel fills or floodplain deposits (Smith et al., 2009; Nicoll and Hickin, 2010; Smith et al., 2011; Ielpi and Ghinassi, 2014; Ghinassi and Ielpi, 2015; Ghinassi et al., 2016). The presence of cohesive mud along the outer bank of the study bend (Fig. B.7) points to a strong similarity with the latter case, and suggests that scarce erodibility of the outer bank prevents migration of the point bar apex along the bend axis. Moreover, the outer bank resistance to erosion in a tidal channel is not challenged by intense flood events which typify their fluvial counterparts. Accumulation of collapsed blocks of mud at the toe of the outer bank (Fig. B.2E) is a further element that hinders retreat of the bank (Gabet, 1998).

FLOW DISTRIBUTION AND SEDIMENTARY PROCESSES Flow distribution varies significantly along a meander bend. In the upstream part of the bend, flow is mainly directed toward the outer bank (Dietrich and Smith, 1983; Frothingham and Rhoads, 2003; Kasvi et al., 2013) and promotes transport of larger particles near the inner bank across the zone of maximum curvature (Dietrich and Smith, 1984; Frothingham and Rhoads 2003). In the central part, the outward-moving surficial flow is forced downward (Rozovskii, 1957; Hooke, 1975), triggering a secondary helical current which moves inwards and upwards over the point-bar face (Dietrich et al., 1979; Dietrich and 4 Whiting, 1989; Termini and Piraino, 2011). This secondary flow is fully developed in the downstream part of the bend (Hooke, 1975; Dietrich et al., 1979; Dietrich and Smith, 1984), where finer-grained particles are transported towards the inner bank and coarser-grained sediment, that is largely

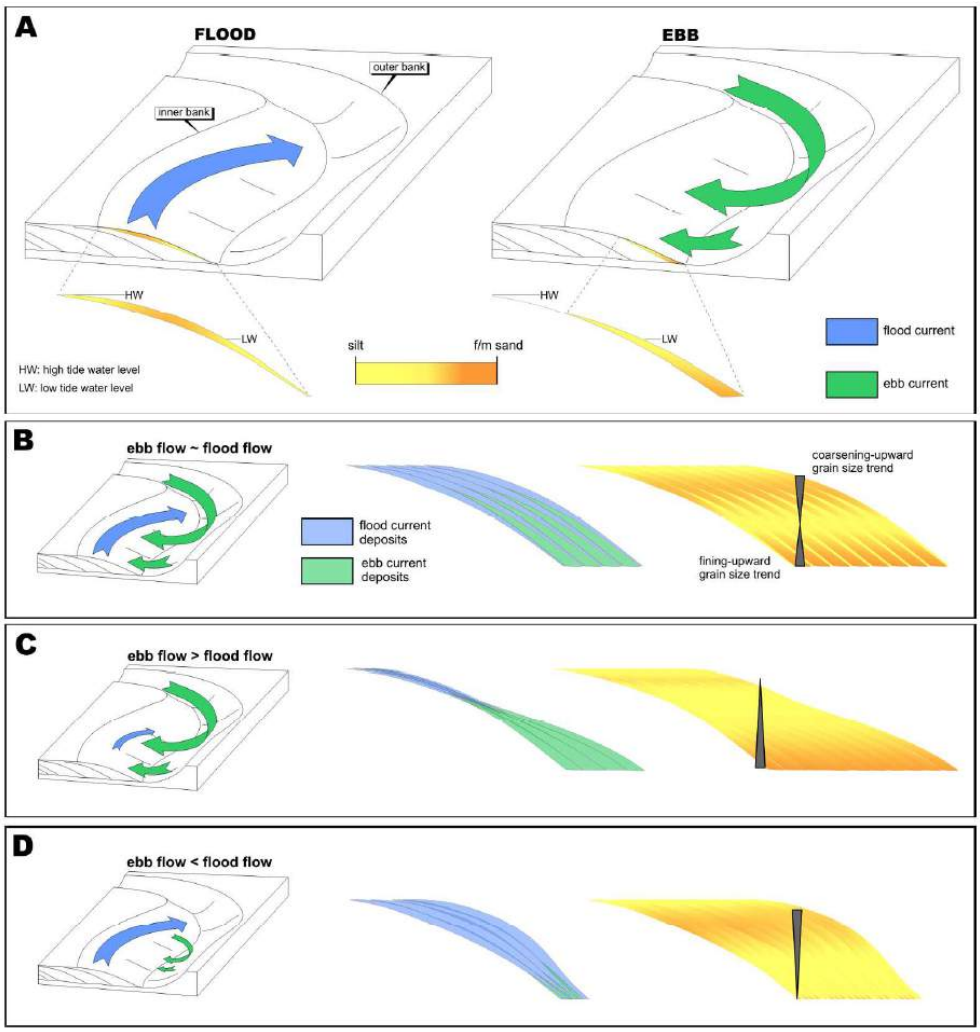

Figure B.15: (A) Block diagrams showing linkage between tidal currents and sediment grain-size distribution on the bar. (B – D) Vertical grain-size trends developing in bar deposits as consequence of similarity between flood and ebb currents: comparable ebb and flood currents (B), prevalence of ebb currents (C) and prevalence of flood currents (D).

affected by the gravity force, accumulates in the deeper parts of the channel (Dietrich et al., 1979). In fluvial setting, this flow pattern develops a clear downstream-fining grain size trend (Jackson, 1976), that is well-developed in downstream- migrating point bars (Smith et al., 2011; Ghinassi and Ielpi, 2015; Durkin et al., 2015). This flow configuration is also experienced by tidal meanders, although the differential paths of the high-velocity streamlines during a tidal cycle (Mutti et al., 1985; Choi et al., 2004; Fagherazzi et al., 2004; Dalrymple and Choi, 2007; Li et al. 2008; Hughes, 2012; Choi and Jo., 2015) allow the same side of the bar (e.g. seaward side) to cyclically experience both the outward-directed flow (e.g. flood flow) and the secondary helical current (e.g. ebb flow). These opposing and offset currents, highlighted

by Fenies and Faugères (1998) showing orientation of bedforms along a point bar of the Arcachon Lagoon (SW France), contribute to explain the sedimentary features of the study bar. Specifically, although flow indicators (i.e. sedimentary structures) were not detected, the configuration of these currents fits with different patterns of grain size distribution. During the flood stage, the maximum flow velocity is located along the inner bank of the study side of the bar (line 1 in Figure B.5A). This velocity distribution accounts for the occurrence of sandy deposits in the upper part of the bar succession (Fig. B.15A), that has been observed also by previous studies (cf. Choi et al., 2004; Pearson and Gingras, 2006). Consistently, downdip fining of grain size is consistent with the presence of weaker flows in the thalweg and along the outer bank zone (line 1 in Figure B.5A). In the bend apex zone, deflection of the flood maximum velocity zone toward the outer bank (line 2 in Figure B.3A) agrees with fining of these sandy deposits toward the bend apex (Fig. B.13A). During the ebb phase, the seaward side of the bar experiences the effects of the secondary helical flow (Fig. B.15A), with the maximum flow velocity located along the outer bank (line 1 in Figure B.3B). Such a configuration fits with accumulation of sandy deposits at the toe of the bar. Consistently, updip decrease in sand content agrees with waning of the secondary current moving from the thalweg to the bar top (Dietrich and Whiting, 1989; Termini and Piraino, 2011). At the ebb phase, high streamwise velocities in the bar apex zone (line in Figure B.3B) account for mobilization of sand, that was transported from the thalweg to the bar top originating coarsening-upward deposits of package CU4 (section 1 of Figure B.9). Progressive seaward shift of the channel allowed this flow configuration to build up the bar succession. Specifically, lateral stacking of deposits associated with flood and ebb currents developed coarsening- and fining-upward packages, respectively (Fig. B.15B – D). Nevertheless, the variable proportion between flood- and ebb-related deposits in different sections points to local prevalence of one of the two currents (Fig. B.15C and D), although the overall dominance of coarsening-upward packages indicates that sediment distribution over the past 47 years was mainly controlled by flood flows.

Conclusions

An asymmetric tidal meander bend located in the northern part of the Venice Lagoon has been studied through integration between analyses of historical aerial photos, measurements of flow velocity patterns, high-resolution facies analyses and 3D architectural modeling. Results stemmed out from this work provided new insights to understanding the link between the morphodynamic evolution of tidal

point bars and the related sedimentary products. The main results of the paper can be summarized as follows:

- The study bend formed on an un-vegetated mud flat, that was progressively colonized by halophytic vegetation. Over the past 77 years, although the migration rate increased as consequence of local drainage network reorganization, the channel shifted with a rate of 20-30 cm/yr, which is comparable with data obtained for channel bends developed in salt marshes. Channel migration occurred under aggradational conditions, as documented by the rising trajectory defined by the shift of the bar brink in sections parallel to the direction of channel migration.
- Over the past 47 years, the channel planform evolution was characterized by translation, since the channel shifted seaward without increasing its sinuosity and maintaining its planform profile. This process was triggered by the occurrence of a cohesive, poorly-erodible outer bank that prevented expansion of the bend as predicted by classical models. Blocks of mud collapsed from the outer bank contributed to armor the toe of the bank, increasing its resistance to erosion.
- The occurrence of opposing and offset tidal currents contribute to develop a peculiar grain size distribution along seaward side of the bar. During the flood stage, the maximum flow velocity is located along the inner bank of the bar, contributing to sand sedimentation in the upper part of the bar. During the ebb stage, the bar experiences the effects of the secondary helical flow that concentrates the sandy deposits at the toe of the bar slope. Progressive shift of the channel causes lateral stacking of flood and ebb deposits that developed coarsening- and fining-upward sedimentary packages, respectively.

References for Appendix B

Allen, J.R.L. (1963) The classification of cross-stratified units with notes on their origin. Sedimentology, 2, 93-114.

- Allen, J.R.L. (2000) Morphodynamics of Holocene salt marshes: a review sketch from the Atlantic and Southern North Sea coasts of Europe. Quatern. Sci. Rev., 19, 1155-1231.

- Barwis, J.H., 1978. Sedimentology of some South Carolina tidal creek point bars and a comparison with their fluvial counterparts. In: Fluvial sedimentology (Miall, A.D. Ed.),. Canadian Society of Petroleum Geologists Memoir 5, Calgary, pp. 129-160.

- Barwis, J.H. and Hayes, M.O. (1979) Regional patterns of modern barrier island and tidal inlet deposits as applied to paleoenvironmental studies. In: Carboniferous Depositional Environments in the Appalachian Region: Columbia, South Carolina, Carolina Coal Group (Eds. J.C. Ferm and J.C. Horne), University of South Carolina Columbia, SC, pp. 472-508.

- Bellucci, L.G., Frignani, M., Cochran, J.K., Albertazzi, S., Zaggia, L., Cecconi, G. and Hopkins, H. (2007) 210Pb and 137Cs as chronometers for salt marsh accretion in the Venice Lagoon– links to flooding frequency and climate change. Journal of Environmental Radioactivity, 97, 85-102.

- Boldt, J.A. and Oberg, K.A. (2015) Validation of streamflow measurements made with M9 and RiverRay Acoustic Doppler Current Profilers. J. Hydraul. Eng., 04015054, doi: 10.1061/(ASCE)HY.1943-7900.0001087
- Brice, J.C. (1974) Evolution of meander loops. Geol. Soc. Am. Bull., 85, 581-586.
-Bridge, J.S. (2003) Rivers and Floodplains. Blackwell Scientific Publications, Oxford, 491 pp.
- Canali, G., Capraro, L., Donnici, S., Rizzetto, F., Serandrei-Barbero, R. and Tosi, L. (2007) Vegetational and environmental changes in the eastern Venetian coastal plain (Northern Italy) over the past 80,000 years. Palaeogeogr. Palaeoclimatol. Palaeoecol., 253, 300-316.
- Carniello, L., Defina, A. and D'Alpaos, L. (2009) Morphological evolution of the Venice Lagoon: evidence from the past and trend for the future. J. Geophys. Res.-Earth Surface, 114, F04002, doi:10.1029/2008JF001157.
- Carniello, L., D'Alpaos, A. and Defina, A (2011) Modeling wind waves and tidal flows in shallow micro-tidal basins. Estuar. Coast. Shelf. Sci., 92, 263-276.
- Choi, K.S. and Jo, J. H. (2015) Morphodynamics of tidal channels in the open coast macrotidal flat, southern Ganghwa island in Gyeonggi Bay, west coast of Korea. J. Sed. Res., 85, 582-595.
- Choi, K.S., Dalrymple, R.W., Chun, S.S. and Kim, S.P. (2004) Sedimentology of modern, inclined heterolithic stratification (IHS) in the macrotidal Han River delta, Korea. J. Sed. Res., 74, 677-689.
- D'Alpaos, A., Lanzoni, S., Marani, M., Fagherazzi, S. and Rinaldo, A. (2005) Tidal network ontogeny: Channel initiation and early development. J. Geophys. Res., 110, F02001, doi:10.1029/2004JF000182.
- D'Alpaos, A., S. Lanzoni, M. Marani, and A. Rinaldo (2007), Landscape evolution in tidal embayments: Modeling the interplay of erosion, sedimentation, and vegetation dynamics, J. Geophys. Res., 112, F01008
- D'Alpaos, A., Lanzoni, S., Marani, M. and Rinaldo, A. (2007) Landscape evolution in tidal embayments: modeling the interplay of erosion, sedimentation, and vegetation dynamics. J. Geophys. Res.-Earth Surface, 112, F01008, doi:10.1029/2006JF000537.
- D'Alpaos, A., Carniello, L. and Rinaldo, A. (2013) Statistical mechanics of wind wave- induced erosion in shallow tidal basins: Inferences from the Venice Lagoon. Geophys. Res. Lett., 40, 3402-3407, doi:10.1002/grl.50666.
- D'Alpaos, L. (2010), Fatti e misfatti di idraulica lagunare, Ist. Veneto di Sci. Lett. e Arti, Venice, Italy.
- Dalrymple, R.W. and Choi, K.S. (2007) Morphologic and facies trends through the fluvial-marine transition in tide-dominated depositional systems: a systematic framework for environmental and sequence-stratigraphic interpretation. Earth-Sci. Rev., 81, 135-174.
- Dalrymple, R.W., Makino, Y. and Zaitlin, B.A. (1991) Temporal and spatial patterns of rhythmite deposition on mud flats in the macrotidal Cobequid Bay-Salmon River estuary. Bay of Fundy, Canada. Clastic Tidal Sedimentology - Memoir 16, 137-160.
- Daniel, J.F. (1971) Channel movement of meandering Indiana streams. US Geol. Surv. Prof. Pap., 732-A, 18 pp.
- Davis Jr, R.A. (2012) Tidal signatures and their preservation potential in stratigraphic sequences. In: Principles of tidal sedimentology (Eds R.A. Davis Jr and R.W. Dalrymple), pp. 35-55. Springer, Netherlands.
- De Mowbray, T. (1983) The genesis of lateral accretion deposits in recent intertidal mudflat channels, Solway Firth, Scotland. Sedimentology, 30, 425-435.
- Dietrich, W.E. and Smith, J.D. (1983) Influence of the point bar on flow through curved channels. Water Resour. Res., 19, 1173-1192.
- Dietrich, W.E. and Smith, J.D. (1984) Processes controlling the equilibrium bed morphology in river meanders. Rivers '83: Proceedings of a Specialty Conference on River Meandering. American Society of Civil Engineers, 759-769.
- Dietrich, W.E. and Whiting, P.J. (1989) Boundary shear stress and sediment transport in river meanders of sand and gravel. In: River Meandering (Eds S. Ikeda and G. Parker). American Geophysical Union, Water Resources Monograph 12, 1-50.
- Dietrich, W.E., Smith, J.D. and Dunne, T. (1979) Flow and sediment transport in a sand bedded meander. J. Geol., 87, 305-315.
- Díez-Canseco, D., Arz, J.A., Benito, M.I., Díaz-Molina, M. and Arenillas, I. (2014) Tidal in-

fluence in redbeds: a palaeoenvironmental and biochronostratigraphic reconstruction of the Lower Tremp Formation (South-Central Pyrenees, Spain) around the Cretaceous/Paleogene boundary. Sed. Geol., 312, 31-49.
- Durkin, P.R., Hubbard, S.M., Boyd, R.L. and Leckie, D.A. (2015) Stratigraphic Expression of Intra-Point-Bar Erosion and Rotation. J. Sed. Res., 85, 1238-1257.
- Fagherazzi, S., Gabet, E.J. and Furbish, D.J. (2004) The effect of bidirectional flow on tidal channel planforms. Earth Surf. Proc. Land., 29, 295-309.
- Fenies, H. and Faugères, J.C. (1998) Facies and geometry of tidal channel-fill deposits (Arcachon Lagoon, SW France). Mar. Geol., 150, 131-148.
- Finotello, A., D'Alpaos, A., Ghinassi, M., Lanzoni, S., Marani, M. and Rinaldo, A. (2015) Analysis of Meander Migration Rates in Tidal Landscapes. EGU General Assembly 2015. Geophysical Research Abstracts, Vol. 17, EGU2015-12723.
- Fontana, A., Mozzi, P. and Marchetti, M. (2014) Alluvial fans and megafans along the southern side of the Alps. Sed. Geol., 301, 150-171.
- Frothingham, K.M. and Rhoads, B.L. (2003) Three-dimensional flow structure and channel change in an asymmetrical compound meander loop, Embarras River, Illinois. Earth Surf. Proc. Land., 28, 625-644.
- Fruergaard, M., Andersen, T.J., Nielsen, L.H., Madsen, A.T., Johannessen, P.N., Murray, A.S., Kirkegaard, L. and Pejrup, M. (2011) Punctuated sediment record resulting from channel migration in a shallow sand-dominated micro-tidal lagoon, Northern Wadden Sea, Denmark. Mar. Geol., 280, 91-104.
- Fustic, M. (2007) Stratigraphic dip analysis a novel application for detailed geological modeling of point bars and predicting bitumen grade, McMurray Formation, Muskeg River 6 Mine, Northeast Alberta. Natural Resources Research, 16, 31-43.
- Gabet, E.J. (1998) Lateral migration and bank erosion in a salt marsh tidal channel in San Francisco Bay, California. Estuaries, 21,745-753.
- Garofalo, D. (1980) The influence of wetland vegetation on tidal stream channel migration and morphology. Estuaries, 3, 258-270.
- Garotta, V., Pittaluga, M.B. and Seminara, G. (2006) On the migration of tidal free bars. Phys. Fluids, 18, 096601.
- Ghinassi, M. and Ielpi, A. (2015) Stratal Architecture and Morphodynamics of Downstream-6 Migrating Fluvial Point Bars (Jurassic Scalby Formation, UK). J. Sed. Res., 85, 1123-1137.
- Ghinassi, M., Billi, P., Libsekal, Y., Papini, M. and Rook, L. (2013) Inferring fluvial morphodynamics and overbank flow control from 3D outcrop sections of a Pleistocene point bar, Dandiero Basin, Eritrea. J. Sed. Res., 83, 1066-1084.
- Ghinassi, M., Nemec, W., Aldinucci, M., Nehyba, S., Özaksoy, V. and Fidolini, F. (2014) Plan-form evolution of ancient meandering rivers reconstructed from longitudinal outcrop sections. Sedimentology, 61, 952-977.
- Ghinassi, M., Ielpi, A., Aldinucci, M., and Fustic, M. (2016). Downstream-migrating fluvial point bars in the rock record. Sedimentary Geology, 334, 66-96.
- Green, M.O. and Coco, G. (2007) Sediment transport on an estuarine intertidal flat: measurements and conceptual model of waves, rainfall and exchanges with a tidal creek. Estuar. Coast. Shelf. Sci., 72, 553–569.
- Green, M. O., and Coco G. (2014) Review of wave-driven sediment resuspension and transport in estuaries. Rev. Geophys., 52, 77–117, doi:10.1002/2013RG000437.
- Hickin, E.J. (1986) Concave-bank benches in the floodplains of Muskwa and Fort Nelson Rivers, British Columbia. The Canadian Geographer, 30, 111-122.
- Hooke, R. (1975) Distribution of sediment transport and shear stress in a meander bend. J. Geol., 83, 543-565.
- Hughes, Z.J. (2012) Tidal Channels on Tidal Flats and Marshes. In: Principles of tidal sedimentology (Eds R.A. Davis Jr and R.W. Dalrymple), pp. 269-300. Springer, Netherlands.
- Ielpi, A. and Ghinassi, M. (2014) Planform architecture, stratigraphic signature and morphodynamics of an exhumed Jurassic meander plain (Scalby Formation, Yorkshire, UK). Sedimentology, 61, 1923-1960.
- Jablonski, B.V. and Dalrymple, R.W. (2016) Recognition of strong seasonality and climatic cyclicity in an ancient, fluvially dominated, tidally influenced point bar: Middle McMurray Formation, Lower Steepbank River, north-eastern Alberta, Canada. Sedimentology, 63, 552-

585, doi: 10.1111/sed.12228.
- Jackson, R.G. (1976) Depositional model of point bars in the lower Wabash River. J. Sed. Petrol., 46, 579-594.
- Kasvi, E., Vaaja, M., Alho, P., Hyyppä, H., Hyyppä, J., Kaartinen, H. and Kukko, A. (2013) 7 Morphological changes on meander point bars associated with flow structure at different discharges. Earth Surf. Proc. Land., 38, 577-590.
- Kent, D.V., Rio, D., Massari, F., Kukla, G. and Lanci, L. (2002) Emergence of Venice in the Pleistocene. Quatern. Sci. Rev., 21, 1719-1727.
- Lane, S. N., K. F. Bradbrook, K. S. Richards, P. M. Biron, and A. G. Roy (2000), Secondary circulation cells in river channel confluences : measurement artefacts or coherent flow structures ?, Hydrol. Process., 14(June 1998), 2047 – 2071
- Lanzoni, S. and Seminara, G. (2002) Long-term evolution and morphodynamic equilibrium of tidal channels. J. Geophys. Res.– Oceans, 107, C1, 3001, 10.1029/2000JC000468.
- Li, C., Chen, C., Guadagnoli, D. and Georgiou, I. (2008) Geometry induced residual eddies in estuaries with curved channels observations and modeling studies. J. Geophys. Res., 113, C01005, doi:10.1029/2006JC004031.
- Makaske, B. and Andweerts, H.J.T. (2005) Muddy lateral accretion and low stream power in a sub-recent confined channel belt, Rhine–Meuse delta, central Netherlands. Sedimentology, 52, 651-668. Marani, M., Lanzoni, S., Zandolin, D., Seminara, G. and Rinaldo, A. (2002) Tidal meanders. 7 Water Resour. Res., 38, 1225, doi:10.1029/2001WR000404.
- Marani, M., Belluco, E., D'Alpaos, A., Defina, A., Lanzoni, S. and Rinaldo, A. (2003) On the drainage density of tidal networks. Water Resour. Res., 39, 1040, doi:10.1029/2001WR001051.
- Mariotti, G., and S. Fagherazzi (2012), Channels-tidal flat sediment exchange: The channel
- spillover mechanism, J. Geophys. Res., 117, C03032, doi:10.1029/2011JC007378
- Massari, F., Rio, D., Barbero, R.S., Asioli, A., Capraro, L., Fornaciari, E. and Vergerio, P.P. (2004) The environment of Venice area in the past two million years. Palaeogeogr. Palaeoclimatol. Palaeoecol., 202, 273-308.
- Massari, F., Grandesso, P., Stefani, C. and Jobstraibizer, P.G. (2009) A small polyhistory foreland basin evolving in a context of oblique convergence: the Venetian basin (Chattian to Recent, Southern Alps, Italy). In: Foreland basins (Eds P.A. Allen and P. Homewood), pp. 141- 168. Blackwell Scientific, Oxford
-. McGowen, J.H. and Garner, L.E. (1970) Physiographic features and stratification types of coarse-grained point bars: modern and ancient examples. Sedimentology, 14, 77-111.
- Moeller, I., Spencer, T., French, J.R., Leggett, D.J. and Dixon, M. (1999). Wave transformation over salt marshes: a field and numerical modeling study from North Norfolk, England. Estuar. Coast. Shelf. Sci., 49, 411-425.
- Morris, J.T., Sundareshwar, P.V., Nietch, C.T., Kjerfve, B. and Cahoon, D.R. (2002) Responses of coastal wetlands to rising sea level. Ecology, 83, 2869-2877.
- Mudd, S.M., D'Alpaos, A. and Morris, J.T. (2010) How does vegetation affect sedimentation on tidal marshes? Investigating particle capture and hydrodynamic controls on biologically mediated sedimentation. J. Geophys. Res.- Earth Surface, 115, F03029, doi:10.1029/2009JF001566.
- Mutti, E., Rosell, J., Allen, G.P., Fonnesu, F. and Sgavetti, M. (1985) The Eocene Baronia tide dominated delta-shelf system in the Ager Basin. In: Excursion Guidebook, 6th European Regional Meeting (Eds M.D. Mila and J. Rosell), pp. 579-600. International Association of Sedimentologists, Lleida, Spain.
- Nanson, G.C. (1980) Point bar and floodplain formation of the meandering Beatton River, northeastern British Columbia, Canada. Sedimentology, 27, 3-29.
- Nanson, G.C. and Page, K. (1983) Lateral accretion of fine-grained concave benches associated with meandering rivers. In: Modern and Ancient Fluvial Systems (Eds J.D. Collinson and J. Lewin), Int. Assoc. Sedimentol. Spec. Publ., 6, 133-143.
- Nicoll, T.J. and Hickin, E.J. (2010) Planform geometry and channel migration of confined meandering rivers on the Canadian prairies. Geomorphology, 116, 37-47.
- Nyman, J. A., R. J. Walters, R. D. Delaune, and W. H. Patrick (2006), Marsh vertical accretion via vegetative growth, Estuarine Coastal Shelf Sci., 69, 370–380.
- Pearson, N.J. and Gingras, M.K. (2006) An ichnological and sedimentological facies model for muddy point-bar deposits. J. Sed. Res., 76, 771-782.
- Rieu, R., Van Heteren, S., Van der Spek, A.J.F. and De Boer, P.L. (2005) Development and

preservation of a mid-Holocene tidal-channel network offshore the western Netherlands. J. Sed. Res., 75, 409-419.
- Rizzetto, F. and Tosi, L. (2011) Aptitude of modern salt marshes to counteract relative sea-level rise, Venice Lagoon (Italy). Geology, 39, 755-758.
- Rozovskiĭ, I.L. (1957) Flow of water in bends of open channels. Academy of Sciences of the Ukrainian SSR, Kiev, 233 pp.
- Santos, A.E.de A. and Rossetti, D.de F. (2006) Depositional model of the Ipixuna formation (late Cretaceous-early Tertiary), Rio Capim area, Northern Brazil. Latin American Journal of Sedimentology and Basin Analysis, 13, 101-117. Silvestri, S. , Defina, A. , and Marani, M . Tidal regime, salinity and salt marsh plant zonation. Estuar Coast Shelf Sci, 62, 119–30.
- Smith, D.G., Hubbard, S., Leckie, D. and Fustic, M. (2009) Counter point bars in modern meandering rivers: recognition of morphology, lithofacies and reservoir significance, examples from Peace River, AB, Canada. Sedimentology, 56, 1655-1669.
- Smith, D.G., Hubbard, S.M., Lavigne, J., Leckie, D.A. and Fustic, M. (2011) Stratigraphy of counter-point-bar and eddy-accretion deposits in low-energy meander belts of the Peace-Athabasca Delta, northeast Alberta, Canada. In: From River to Rock Record: The Preservation of Fluvial Sediments and Their Subsequent Interpretation (Eds S.K. Davidson, S. Leleu and C.P. North), SEPM Spec. Publ., 97, 143-152.
- Solari, L., Seminara, G., Lanzoni, S., Marani, M. and Rinaldo, A. (2002) Sand bars in tidal channels, part two, Tidal meanders. J. Fluid Mech., 451, 203-238.
- Sundborg, A. (1956) The River Klaralven: a study of fluvial processes. Geografiska Annaler, 38, 238-316.
- Termini, D. and Piraino, M. (2011) Experimental analysis of cross-sectional flow motion in a large amplitude meandering bend. Earth Surf. Proc. Land., 36, 244-256.
- Terwindt, J.H.J. (1988) Palaeo-tidal reconstructions of inshore tidal depositional environments. In: Tide-influenced sedimentary environments and facies (Eds R.L. de Boer, A. van Gelder and S.D. Nio), pp. 233-263. Reidel, Dordrecht.
- Thomas, R.G., Smith, D.G., Wood, J.M., Visser, J., Calverley-Range, E.A. and Koster, E.H. (1987) Inclined heterolithic stratification -Terminology, description, interpretation and significance. Sed. Geol., 53, 123-179.
- Willis, B.J. (1989) Paleochannel reconstructions from point bar deposits: a three- dimensional perspective. Sedimentology, 36, 757-766.
- Willis, B.J. (1993) Bedding geometry of ancient point bar deposits. In: Alluvial Sedimentation (Eds M. Marzo and C. Puigdefabregas). Int. Assoc. Sedimentol. Spec. Publ., 17, 101-114. Willis, J.B. and Tang, H. (2010) Three-dimensional connectivity of point-bar deposits. J. Sed. Res., 80, 440-454.
- Zecchin, M., Brancolini, G., Tosi, L., Rizzetto, F., Caffau, M. and Baradello, L. (2009) Anatomy of the Holocene succession of the southern Venice lagoon revealed by very high- resolution seismic data. Cont. Shelf Res., 29, 1343-1359.

C | APPENDIX

OBSERVATIONAL STRATAL ARCHITECTURE CHALLENGES CURRENT UNDERSTANDING OF TIDAL MEANDER MORPHODYNAMICS

Brivio, Lara[1], Massimiliano Ghinassi[1], Andrea D'Alpaos[1], Alvise Finotello[1], Luca Carniello[2], Marco Marani[2,3], Alessandro Cantelli[4] and Nick Howes[4]

[1]Dept. of Geosciences, University of Padova, via G.Gradenigo 6, Padova, PD I-35131, Italy

[2]Dept. ICEA, University of Padova, via Loredan 20, Padova, PD I-35131, Italy

[3]Nicholas School of Environment, Duke University, Durham, NC 27708

[4]Shell Technology Ceneter Houston, 3333 Highway 6 South Houston, TX 77082-3101, USA

Abstract

Meandering channel network exert a fundamental control on hydrodynamic and morphodynamic processes within tidal landscapes. However, the planform evolution of tidal meanders is currently inferred via observations and models of their fluvial counterparts. The present study addresses in tidal landscapes, the internal architecture and morphodynamic evolution of a tidal meander bend in the Venice Lagoon (Italy), through an approach integrating three-dimensional high-resolution geophysical investigations, bathymetric field surveys, aerial photographs, and numerical modeling. We find that lateral tributaries influence sedimentation patterns within the meander bend in such a way that their effects remain imprinted in the sedimentary record of meander deposits. We also find that the evolution of tidal channels is punctuated by abrupt changes in channel dynamics, that contrast with the predictable and monotonous rise and fall of the tides. Meander dynamics inferred from depositional architectures challenge current assessments of tidal meander morphodynamics. The critical role exerted by lateral tributaries on tidal meander migration, emerges in response to evolving landforming processes operating on comparable timescales. Key differences with fluvial meanders emerge. Specifically, the concept that meander wavelength and radial progression stem from free migrating modes excited by bottom or flow instabilities is insufficient to explain tidal meander evolution, as evidenced by its stratigraphic record. A more complex set of forcings, including the influence of lateral tributaries, must be invoked.

Significance

Sinuous channels are ubiquitous features of tidal landscapes and contribute to the distribution of water, sediments and nutrients in these landscapes. However, little is known about their morphodynamic evolution and related sedimentary products, and these meandering channels are commonly studied following theories developed for their fluvial counterparts. Here we show that tidal meander evolution differs from that of fluvial ones and distinctive features characterize deposits formed in tidal bends. Specifically, we highlight the role of minor tributaries that allow sediment accumulation where traditional models predict erosion. This bears important consequences for the management of tidal landscapes and interpretation of tidal channel deposits in the fossil record.

Significance

A longstanding question in geomorphology is whether the morphology of a particular landscape is in balance with its current environmental forcings or if it contains distinct relict signatures of past ones. Clear examples of these two end-member cases exist (Rinaldo et al.,1995), but in contexts where the rates of change of the forcings are comparable with (the inverse of) adaptation timescales of physical or biological processes, the identification of equilibrium/disequilibrium features is not straightforward. Branching and meandering tidal channels, the essential circulation system of lagoons and estuaries, form the pathway for tidal currents to propagate and distribute clastic sediments and nutrients (e.g. Hughes, 2012; Coco et al., 2013), thus providing a primary control on tidal landscape ecomorphodynamics (Fagherazzi et al., 2012). Although meandering patterns are ubiquitous features of the tidal landscape, very few studies have analyzed their planimetric shape, morphometric characteristics, and their morphodynamic evolution (Gabet, 1998; Marani et al., 2002; Solari et al., 2002; Fagherazzi et al., 2004). The depositional architecture of tidal meander bends has received even less attention, and is commonly approached using facies models (Barwis, 1978; De Mowbray, 1983; Choi and Jo, 2015) developed from the comparison with their fluvial counterparts (Jackson, 1976; Brierley, 1991), and by assuming that the abundance of mud and bidirectional flows represent the main differences with the fluvial realm (e.g. Thomas et al., 1987). Quantifying the sediment transport dynamics in tidal channel bends and its impact on meander-bend architecture is a fundamental step towards an improved understanding of the role of tidal channels in the ecomorphodynamic evolution of lagoonal and estuarine systems. The present study addresses, for the first time in tidal landscapes, the internal ar-

chitecture and morphodynamic evolution of a tidal meander bend in the Venice Lagoon (Italy, Figure C.1) by coupling three-dimensional, high-resolution geophysical investigations with geomorphological information from bathymetric field surveys, aerial photographs and numerical modeling. Theoretical investigations (Marani et al., 2002; Solari et al., 2002; Fagherazzi et al., 2004) posit that locally the relevant dynamics follows from bend assessments for fluvial meanders (Seminara, 2006). Specifically, field evidence (Marani et al., 2002) shows that tidal meanders develop a characteristic spatial wavelength of about 10-15 channel widths, an observation that is consistent across channels of different widths, varying up to two orders of magnitude. This suggests that the mechanism of meander evolution is controlled by processes acting at the scale of a few channel widths. This observation has motivated notable attempts to interpret the above process on the basis of a planimetric instability theory, of the type established for fluvial meandering (Ikeda et al., 1981; Parker et al., 2011). Here we show, on the contrary, that sediment pulses delivered to the main channel through lateral tributaries, substantially influence meander evolution, by promoting the formation of atypical sedimentary bodies with sediment accumulation along the outer bank, where erosion is expected for fluvial meanders. This results from a concurrent evolution of the sediment supply and landforming discharges, tied to an ever-changing competition for relevant tidal prisms driving channel morphologies, co-evolving with RSL changes and the related ecological adaptations. Typical characteristic timescales are argued to be comparable, thus leading tidal landforms to a perennial transient state whose imprintings are long-lived. Landforms in equilibrium with the current forcing and relict features are argued to perennially coexist in the tidal landscape.

Geomorphological setting

We analyzed a meander bend of the Gaggian Channel, located in the Northern, and best naturally preserved, part of the Venice Lagoon (Figure C.1A). The Venice Lagoon, which formed over the last 7500 years covering alluvial Late Pleistocene deposits locally known as Caranto (Zecchin et al., 2008), is the largest Mediterranean brackish water body, with an area of about 550 km2. It is connected to the Adriatic Sea through three inlets (Lido, Malamocco and Chioggia) and is subjected to a semidiurnal tidal regime, with an average tidal range of about 1.0 m and peak tidal amplitudes of about 0.75 m around Mean Sea Level (MSL). The study site is a 900 m long meander bend, which develops around a point bar with a mean radius of curvature of about 200 m (Figure C.1B). The channel is about 100 m wide, up to 8 m deep and receives tributaries, on both the inner and the outer banks. We focus specifically on the two main tributaries along

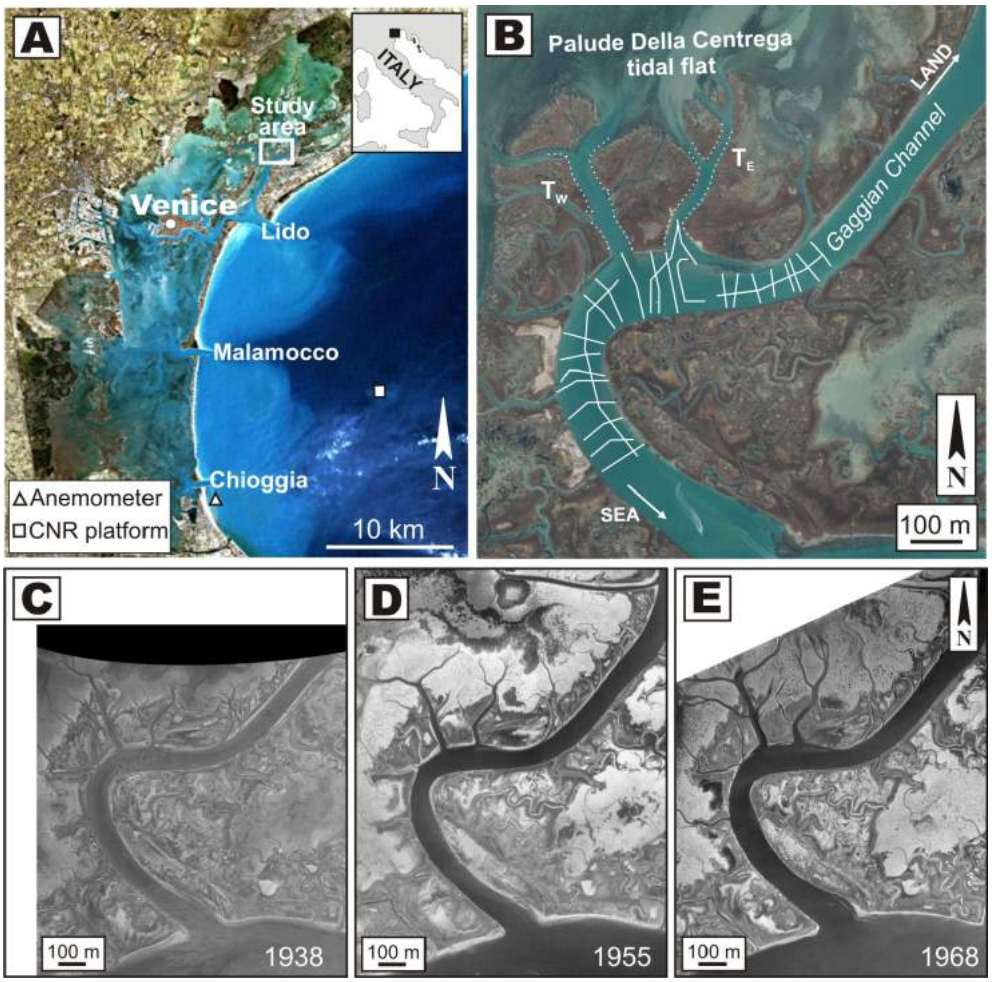

Figure C.1: The study site. (A) Geographic location of the study area, in northeastern portion of the Venice Lagoon, Italy. (B) Satellite image (2012) of the Gaggian channel showing the acquisition scheme of sub bottom profiles (white lines). (C – E) Digitalized orthophotos of the Gaggian channel in: 1938 (C), spatial resolution of 600 dpi (1pixel = 0.897 m); 1955 (D), resolution of 600 dpi (1pixel = 1.124 m); 1968 (E), resolution of 600 dpi (1pixel = 0.599 m).

the outer bank, named hereafter as TW (Western Tributary) and TE (Eastern Tributary), which enter the Gaggian channel near the bend apex and connect it with the Palude della Centrega tidal flat to the North (Figure C.1B). Medium to coarse-grained sand is common in the deepest part of the Gaggian channel, whereas fine-grained silty sand occurs in shallower areas and along the thalweg of the TW and TE tributaries. The TW and TE tributaries, which are about 40 and 30 m wide and 3.6 and 3.0 m deep, respectively, branch northward into a number of minor channels which cut through the 0.55 m deep Palude della Centrega tidal flat. Historical aerial photos (Figure C.1C, D, E) show that between 1938 and 1968 the TW and TE tributaries were narrower than they are today and used to drain a salt marsh platform,

thus conveying smaller water and sediment fluxes into the Gaggian channel compared to modern conditions.

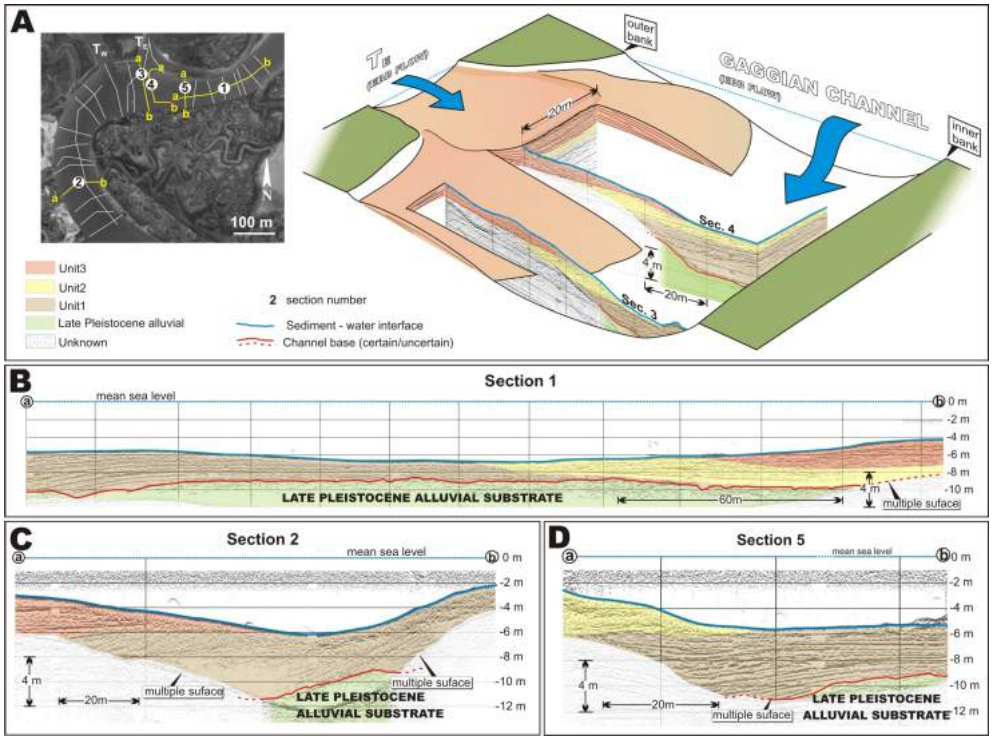

Figure C.2: Interpretation of the most representative seismic sections. (A) Sections 3 and 4 in a sketch depicting the lobe fed by the TE tributary. (B) Longitudinal section along the landward portion of the Gaggian channel showing ebb-oriented inclined deposits of Unit 1. (C) Inclined deposits of Unit 1, dipping 10-20° toward the outer bank, overlain by deposits of Unit 3. (D) Inclined deposits of Unit 1 and 2 dipping toward the outer bank, together with minor erosive truncations and gravitative deformations.

Results of Geophysical Investigations

Geophysical data (Figure C.2) show that the basal erosive surface of the Gaggian channel deposits locally occurs between 7 and 12 m below MSL, and overlies alluvial Late Pleistocene deposits. In-channel deposits are split into three sedimentary Units (hereafter called Unit 1, 2 and 3) by two distinctive and laterally extensive surfaces (Figure C.2), which show streamwise changes from erosive to depositional features.

Unit 1 overlies the channel basal surface and reaches 6 m in thickness along the seaward side of the inner bank, whereas it becomes thinner in the landward side (Figure C.2B). Unit 1 consists of inclined deposits dipping 10 – 20° toward the outer bank (Figure C.2C, D), as commonly expected in channel bends. Minor erosive truncations

and gravitational deformations occur in the central and upper portion of the inclined beds (Figure C.2D). Unit 1 developed during the first stage of meander bend evolution, when sedimentation occurred along the inner bank due to the occurrence of a bend-apex helicoidal flow, as usually expected for fluvial patterns (Seminara, 2006). The thickness of deposits of Unit 1 is relatively constant along the bar, although its asymmetric planform profile suggests dominance of ebb currents. Unit 2 mainly occurs in the landward side of the bend, where it erosionally overlies Unit 1 and locally the Caranto deposits, reaching the maximum thickness of about 4 m. Inclined beds dip toward the outer bank at about 10 – 15^{O} and show minor internal truncations (Figure C.2A, D). Locally, the basal surface of this Unit is characterized by 1.0 – 1.5 m deep scours, which are filled with cross-stratified deposits fed by seaward-directed flows. Unit 2 testifies the seaward propagation of a sediment wave, which mainly accreted above Unit 1 along the landward side of the inner bank. Cross-stratified deposits agree with dominance of ebb currents (see Figure 3.8 in chapter 3.2). The erosive nature of the basal surface suggests an increase in the landscape forming water discharge, which heralded the propagation of the aforementioned sediment wave. Finally, Unit 3 which is up to 3.5 m thick, is erosively based and is distributed along the outer bank of the meander bend. Beds dip at about 10^{O} toward the inner bank (see Section 3 and 4 in Figure C.2A) and define two lobes at the outlet of the TW and TE tributaries. The proximal part of these lobes includes channelized deposits (see Section 4 in Figure C.2A). The surface capping Unit 3 defines the present-day bend morphology, which is characterized by the erosion of the inner bank, where deposits of Unit 1 are exposed on the channel bottom (see Section 3 in Figure C.2A). Unit 3 documents the onset of accumulation at the outlets of the TW and TE tributaries, which fed two main sedimentary lobes in the Gaggian channel. Accumulation of these lobes likely promoted a migration of tidal currents towards the inner bank of the main channel, triggering its erosion.

Discussion and conclusions

Unit 1 to 3 document the occurrence of three distinct stages of meander bend evolution, named as Stage 1 (older) to 3 (younger) in Figure C.3. These stages are characterized by a transition from inner to outer bank accumulation. During the first and second stages of bend evolution, sediments were mainly stored along the inner bank (Figure C.3A, B). During the third stage of bend evolution (Figure C.3C), the occurrence of sedimentation along the outer bank and erosion along the inner bank is the dominant morphodynamic feature. These atypical sedimentary patterns are associated to the development of

the lobes at the outlets of the TW and TE tributaries (Figure C.3C), which suddenly delivered to the main channel an amount of sediment that exceeded its maximum sediment transport capacity. This abrupt increase in sediment supply from the TW and TE tributaries was triggered by increasing sediment erosion over the Palude della Centrega tidal flat, which is connected to the Gaggian Channel by the TW and TE tributaries. The Venice Lagoon experienced a strong erosional trend over the last century (Carniello et al., 2009), which led to an increase in the average water depth of about 0.60 m in the Palude della Centrega tidal flat (see Figure C.5). The positive feedback between tidal flat deepening and wind-wave induced erosion (Fagherazzi et al., 2006) results in high values of the suspended sediment concentration during storm events. The sediment suspended by wind waves in the Palude della Centrega tidal flat was therefore routed into the Gaggian channel (Figure C.3F) by the ebb currents, which increased flow velocity and the related sediment transport capability (see Figure 3.8 in chapter 3.2) triggering erosion and bypass along the tributaries. Mutually evasive currents, documented in tidal bends, contribute to storing sediment along the outer bank (Hughes, 2012; Li et al., 2008). The effect of these currents here is however overwhelmed by the sediment supply of lateral tributaries as emphasized by the development of lobate units at the outlet of the tributaries (Figure C.3C), which causes a shift of the pool scour toward the inner bank zone.

The analysis of aerial photographs and the results of numerical modelling (see the Material and Methods for details), confirms the above scenario (Figure C.4). A comparison of the 1938 and 2007 channel planforms and bathymetries (Figure C.4A, B) indicates that the Gaggian Channel and the two lateral tributaries experienced an increase in their width and depth. This was due to the increase in the tidal prisms shaping their cross sections (D'Alpaos et al., 2010), triggered by the vertical erosion of the tidal flat surfaces drained by these channels due to wind-wave induced erosion processes (Carniello et al., 2009). When the model is forced with the same tidal levels and wind velocities and directions for both configurations (Figure C.4C), results show that both hydrodynamics and sediment transport processes experienced important changes (Figure C.4D-I). The erosion of the landward tidal flat and salt marsh surfaces led to an increase in the landscape-forming discharges (Figure C.4D, E), whereas the amount of mud (Figure C.4F, G) and sand (Figure C.4H, I) routed towards the main channel along the two tributaries largely increased, yielding two lobate structures at the confluences. Interestingly, although discharges routed through the Gaggian Channel experienced a 60The occurrence of erosively-bounded sedimentary Units emphasizes that tidal channels evolve under the control of significant changes in local

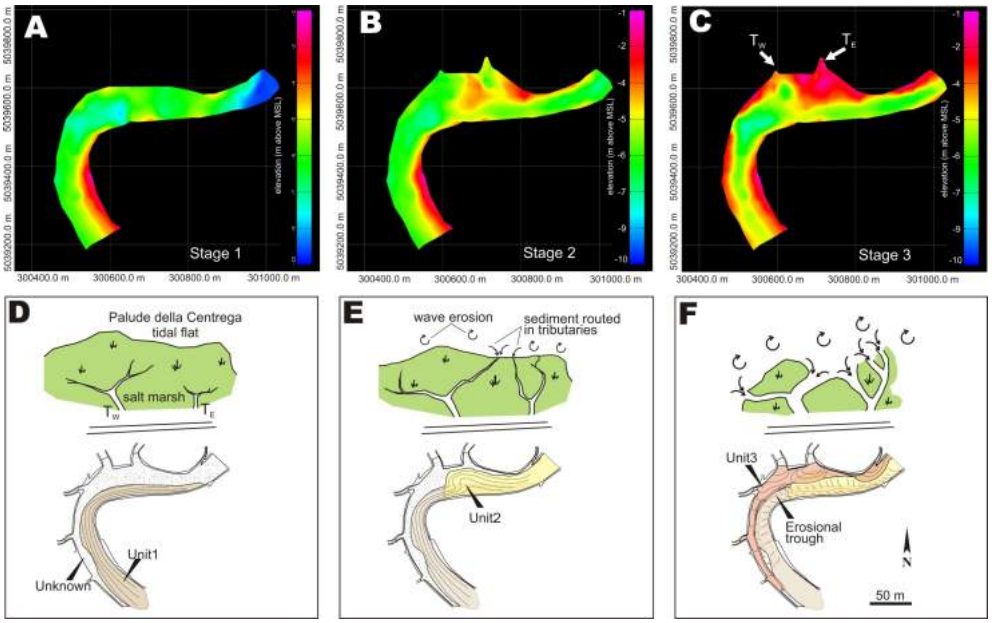

Figure C.3: Morphological evolution of the Gaggian channel. (A - C) Top morphologies of Unit 1 to 3 as they emerge from the spatial interpolation of seismic profiles obtained through a kriging procedure. Panels A – C highlight the development of lobes at the tributary outlets and the related deposition patterns along the outer bank. (D – F) Conceptual model portraying the three stages of the Gaggian channel evolution. (D) TW and TE tributaries do not receive sediment from the Palude della Centrega tidal flat and the Gaggian channel bend is dominated by inner bank deposition. (E) Ongoing inner bank sedimentation, which is mainly concentrated along the landward side of the inner bank. (F) Sediments resuspended by wind waves in the Palude della Centrega are routed into the Gaggian channel through the TW and TE tributaries causing accumulation along the outer bank

hydrodynamics, which apparently contrast with the predictability of channel discharge dictated by specific ranges of tidal excursion. The evolution of the tributary network plays a key role in driving the above described morphodynamic changes. Although tidal and fluvial meanders seem to be characterized by a similar planform morphology (Marani et al., 2002; Solari et al., 2002), the governing mechanisms, documented by the Gaggian stratigraphic record, lead to the establishment of sediment patterns which differ in the two considered cases. Accumulation in the outer bank zone is observed in tidal bends thanks to mutually evasive currents (Hughes, 2012) but is locally overwhelmed by the discharge from lateral tributaries, that can produce confluence bars. Differently from fluvial confluence bars (Biron et al., 1993), which are commonly removed during flood events, tidal confluence bars are much more likely preserved in the stratigraphic record. Our results suggest that tidal meander bends are commonly affected by abrupt variations in sediment and water discharge, which trigger

alternation between growth and degradation of channel bars as a result of evolutionary timescales subsumed by variations in the tidal prism, an effective proxy of landscape morphology. We show that lateral tributaries exert a critical role on tidal meander evolution because they control the amount of water and sediment provided to the main channel. When the sediment discharge of tributaries at the outer bank exceeds the sediment transport capability of the main channel, sediment accumulation at the outlet of tributary channels forms prograding lobate units. This causes flux concentration against and erosion of the inner bank, where both fluvial and tidal classical facies models predict deposition. Overall, we find that current landforms in the tidal landscape bear the signatures of processes occurring at larger spatial scales, prompting alternating sediment production and dissipation, watershed capture and migration, channel advancement and retreat, salt marsh and tidal flat construction and reflected in varying evolutions of tidal meanders. Our main results call for a paradigm shift in the theory of tidal meanders and in the interpretation of tidal geomorphology from theories derived from their fluvial counterparts (Barwis, 1978; De Mowbray, 1983; Choi and Jo, 2015) to new approaches specifically developed for tidal landscapes.

Material and methods

Geophysical data

In April 2011 two longitudinal sub-bottom profiles and 25 transverse profiles were collected within the Gaggian channel (Figure C.1-B). These profiles were acquired by using a Innomar SES – 2000 Compact, a parametric sub-bottom profiler, equipped with a SES 2000 transducer. During the acquisition, low frequencies were used to investigate the subsurface architectures. An 8 kHz frequency was used and varied locally in the range of 5-10 kHz in order to increase the penetration (5 kHz) of the signal and to improve the resolution (10 kHz). Data processing was carried out by means of SES Innomar software, using a signal velocity of 1509 m/s determined on the basis of contemporary temperature and salinity measurements. Position data were recorded through GPS (two TOPCON GR-3 receivers – dual frequency (L1/L2) and dual constellation (NavStar/Glonass), with integrated Tx/Rx UHF radio were used) and processed through the Geo Office software (Leica). The main bounding surfaces separating different sedimentary units were defined on the basis of onlap, downlap, and toplap geometries. The Move 2013.1TM software was used to correlate interpreted seismic sections through a kriging procedure, with the goal of defining the paleo-morphology of the meander bend at different depositional stages.

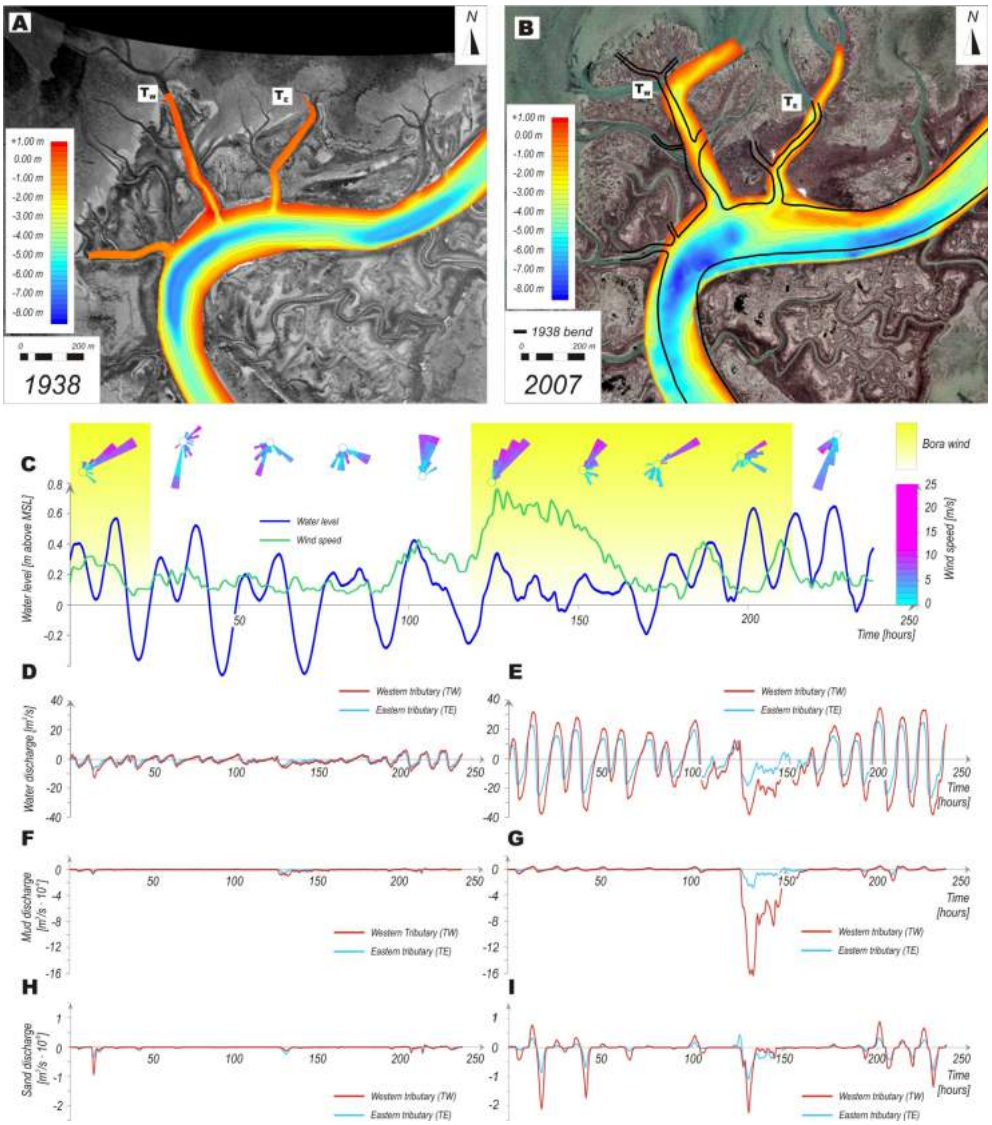

Figure C.4: Results of the numerical model. (A, B) Orthophotos of the Gaggian channel configuration in 1938/2007 over which bathymetric surveys of 1930/2012, respectively, are overlapped. (C) Observed water levels and wind velocities and directions used to force the sediment transport model. Water (D,E), mud (F,G), and sand (H,I) discharges through the TW (red line) and TE (light blue line) tributaries computed for the 1938/2007 configurations, respectively.

Mathematical modelling

A series of aerial photographs (Figure C.1-B, C, D, E) and bathymetric data, obtained from the 1932 and 2013 bathymetries (see, Carniello et al., 2009 for details), were used to determine morphological changes of the Gaggian channel and its lateral tributaries. A numerical morphodynamic model was used to analyze changes in water and sediment fluxes occurred along the considered bend. The model describes tidal and wave hydrodynamics and sediment transport processes to

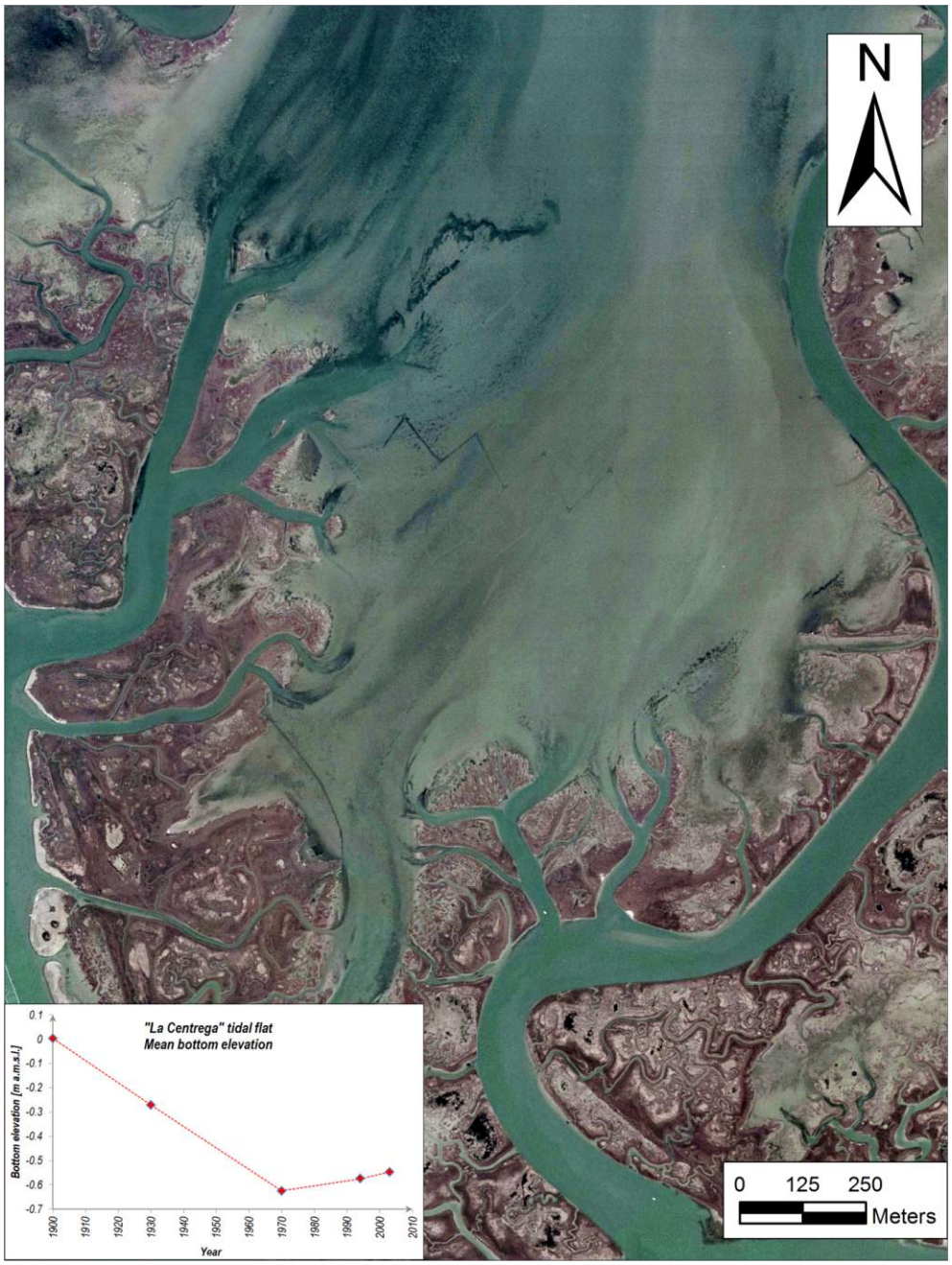

Figure C.5: Orthophoto of the Gaggian channel in 2007 and evolution in time (inset) of the average bottom elevation of the Palude della Centrega tidal flat, which is drained by TW and TE tributaries.

determine the related bed evolution in shallow tidal basins (Carniello et al., 2012, the reader is referred to the original paper for full derivations). A hydrodynamic model, which solves the 2D shallow water equations (see, D'Alpaos and Defina, 2007) is fully coupled to a wind-wave model (Carniello et al., 2011) that solves the wave-action conservation equation parameterized using the zero-order moment of the wave action spectrum in the frequency domain. Tidal currents

and wind waves determine the hydrodynamic field used to solve an advection-diffusion equation and the related sediment resuspension, transport, and deposition that control bed evolution accounting for the simultaneous presence of both cohesive (mud) and non-cohesive (sand) sediments (Carniello et al., 2012). Numerical simulations were carried out on different computational grids representing the Venice Lagoon in its 1932 and present configurations. In all simulations, the model was forced by using 30 days (from 11/16/2005 to 12/16/2005) of hourly tidal levels measured at the CNR Oceanographic Platform, located in the Adriatic Sea in front of the Venice Lagoon, and wind velocities and directions observed at the Chioggia anemometric station (Figure C.1A).

References for Appendix C

1. Rinaldo A, Dietrich WE, Rigon R, Vogel GK, Rodrlguez-Lturbe I (1995) Geomorphological signatures of varying climate. Nature 374(6523):632–635.
2. Hughes ZJ (2012) Tidal Channels on Tidal Flats and Marshes. Principles of Tidal Sedimentology, eds Davis Jr. RA, Dalrymple RW (Springer, Dordrecht Heidelberg London New York), pp. 269–300.
3. Coco G, Zhou Z, van Maanen B, Olabarrieta M, Tinoco R, Townend I (2013) Morphodynamics of tidal networks: Advances and challenges. Mar Geol 346:1–16.
4. Fagherazzi S, et al. (2012) Numerical models of salt marsh evolution: ecological, geomorphic, and climatic factors. Rev Geophys 50(1):RG1002.
5. Gabet EJ (1998) Lateral migration and bank erosion in a salt marsh tidal channel in San Francisco Bay, California. Estuaries 21(4B):745–753.
6. Marani M, Lanzoni S, Zandolin D, Seminara G, Rinaldo A (2002) Tidal meanders. Water Resour Res 38(11):1225.
7. Solari L, Seminara G, Lanzoni S, Marani M, Rinaldo A (2002) Sand bars in tidal channels, part two, Tidal meanders. J Fluid Mech 451:203–238.
8. Fagherazzi S, Gabet EJ, Furbish DJ (2004) The effect of bidirectional flow on tidal channel planforms. Earth Surf Process Landforms 29:295–309.
9. Barwis JH (1978) Sedimentology of some South Carolina tidal creek point bars and a comparison with their fluvial counterparts. Fluvial sedimentology, Canadian Society of Petroleum Geologists Memoir 5, eds Miall AD(Canadian Society Petroleum Geologists, Calgary), pp. 129–160.
10. De Mowbray T (1983) The genesis of lateral accretion deposits in recent intertidal mudflat channels, Solway Firth, Scotland. Sedimentology 30:425–435.
11. Choi K, Jo JH (2015) Morphodynamics of Tidal Channels In the Open Coast Macrotidal Flat, Southern Ganghwa Island In Gyeonggi Bay, West Coast of Korea. J Sed Res 85(6):582–595.
12. Jackson RG (1976) Depositional Model of Point Bars in the Lower Wabash River. J Sed Petrol 46(3):579–594.
13. Brierley GJ (1991) Bar sedimentology of the Squamish River, British Columbia: definition and application of morphostratigraphic units. J Sed Res 61:211–225.
14. Thomas RG, Smith DG, Wood JM, Visser J, Calverley-Range EA, Koster EH (1987) Inclined heterolithic stratification -Terminology, description, interpretation and significance. Sed Geol 53:123–179.
15. Seminara G (2006) Meanders. J Fluid Mech 554:271–297.
16. Ikeda S, Parker G, Sawai K (1981) Bend theory of river meanders. 1. Linear development. J Fluid Mech 112:363–377.
17. Parker G, Shimizu Y, Wilkerson GV, Eke EC, Abad JD, Lauer JW, Paola C, Dietrich WE, Voller VR (2011) A new framework for modeling the migration of meandering rivers. Earth

Surf Process Landforms 36:70–86.
18. Zecchin M, Baradello L, Brancolini G, Donda F, Rizzetto F, Tosi L (2008) Sequence stratigraphy based on high-resolution seismic profiles in the late Pleistocene and Holocene deposits of the Venice area. Mar Geol 253:185–198.
19. Carniello L, Defina A, D'Alpaos L (2009) Morphological evolution of the Venice Lagoon: evidence from the past and trend for the future. J Geophys Res – Earth Surface 114:F04002.
20. Fagherazzi S, Carniello L, D'Alpaos L, Defina A (2006) Critical bifurcation of shallow microtidal landforms in tidal flats and salt marshes. Proc Natl Acad Sci USA 103(22): 8337–8341.
21. Li C, Chen C, Guadagnoli D, Georgiou IY (2008) Geometry induced residual eddies in estuaries with curved channels: Observations and modeling studies. J Geophys Res 113:C01005.
22. Biron P, Roy AG, Best JL, Boyer CJ (1993) Bed morphology and sedimentology at the confluence of unequal depth channels. Geomorphology 8:115–129.
23. D'Alpaos A, Lanzoni S, Marani M, Rinaldo A (2010) On the tidal prism–channel area relations. J Geophys Res115:F01003.
24. Carniello L, Defina A, D'Alpaos L (2012) Modeling sand-mud transport induced by tidal currents and wind waves in shallow microtidal basins: Application to the Venice Lagoon (Italy). Estuarine Coastal Shelf Sci 102–103: 105–115.
25. D'Alpaos L, Defina A (2007) Mathematical modeling of tidal hydrodynamics in shallow lagoons: A review of open issues and applications to the Venice lagoon. Comput Geosci 33:476–496.
26. Carniello L, D'Alpaos A, Defina A (2011) Modeling wind waves and tidal flows in shallow micro-tidal basins. Estuarine Coastal Shelf Sci 92(2):263–276.

I hereby declare that this submission is my own work and that, to the best of my knowledge and belief, it contains no material previously published or written by another person or material which has to a substantial extent been accepted for the award of any other degree or diploma at any university or other institute of higher learning, except where due acknowledgement has been made in the text.

Padova, janaury 2016

_____

Alvise Finotello